

VOLUME 82

APRIL 6, 1978

NUMBER 7

JPCHAx

THE JOURNAL OF

PHYSICAL

CHEMISTRY



PUBLISHED BIWEEKLY BY THE AMERICAN CHEMICAL SOCIETY

THE JOURNAL OF PHYSICAL CHEMISTRY

BRYCE CRAWFORD, Jr., Editor
STEPHEN PRAGER, Associate Editor
ROBERT W. CARR, Jr., C. ALDEN MEAD, Assistant Editors

EDITORIAL BOARD: C. A. ANGELL (1978-1982), F. C. ANSON (1974-1978), V. A. BLOOMFIELD (1974-1978), J. R. BOLTON (1976-1980), L. M. DORFMAN (1974-1978), W. E. FALCONER (1977-1978), H. L. FRIEDMAN (1975-1979), H. L. FRISCH (1976-1980), W. A. GODDARD (1976-1980), E. J. HART (1975-1979), W. J. KAUZMANN (1974-1978), R. L. KAY (1977-1981), L. KEVAN (1978-1982), D. W. McCLURE (1974-1978), K. MYSELS (1977-1981), R. M. NOYES (1978-1982), R. G. PARR (1977-1979), J. PERI (1978-1982), W. B. PERSON (1976-1980), J. C. POLANYI (1976-1980), J. PRAUSNITZ (1978-1982), S. A. RICE (1976-1980), D. SETSER (1978-1980), W. A. STEELE (1976-1980), J. B. STOTHERS (1974-1978), F. A. VAN-CATLEDGE (1977-1981)

Published by the
AMERICAN CHEMICAL SOCIETY
BOOKS AND JOURNALS DIVISION
D. H. Michael Bowen, Director; Marjorie Laflin, Assistant to the Director

Editorial Department: Charles R. Bertsch, Head; Marianne C. Brogan, Associate Head; Joseph E. Yurvati, Assistant Editor

Magazine and Production Department: Bacil Guiley, Head

Research and Development Department: Seldon W. Terrant, Head

Advertising Office: Centcom, Ltd., 25 Sylvan Road South, Westport, Conn. 06880.

© Copyright, 1978, by the American Chemical Society. **Permission** of the American Chemical Society is granted for libraries and other users to make reprographic copies for use beyond that permitted by Sections 107 or 108 of the U.S. Copyright Law, provided that, for all articles bearing an article code, the copying organization pay the stated per-copy fee through the Copyright Clearance Center, Inc. For further information write to Office of the Director, Books and Journals Division at the ACS Washington address.

Published biweekly by the American Chemical Society at 20th and Northampton Sts., Easton, Pennsylvania 18042. Second class postage paid at Washington, D.C. and at additional mailing offices.

Editorial Information

Instructions for authors are printed in the first issue of each volume. Please conform to these instructions when submitting manuscripts.

Manuscripts for publication should be submitted to *The Journal of Physical Chemistry*, Department of Chemistry, University of Minnesota, 207 Pleasant St. S.E., Minneapolis, Minn. 55455. Correspondence regarding **accepted papers and proofs** should be directed to the Editorial Department at the address below.

Page charges of \$60.00 per page may be paid for papers published in this journal. Payment does not affect acceptance or scheduling of papers.

Bulk reprints or photocopies of individual articles are available. For information write to Business Operations, Books, and Journals Division at the ACS Washington address.

The American Chemical Society and its Editors assume no responsibility for the statements and opinions advanced by contributors.

Subscription and Business Information

1978 subscription prices, printed or microfiche, including postage. Microfiche by air mail; printed by surface mail. Printed edition air mail or air freight rates available from Membership & Subscription Services at the address below.

	U.S.	Foreign
Members	\$24.00	\$34.00
Nonmembers	96.00	106.00
Supplementary material (available in microfiche only)	20.00	36.00

New and renewal subscriptions should be sent with payment to the Office of the Controller at the ACS Washington address.

Changes of address must include both old and new addresses with ZIP code and a recent mailing label. Send all address changes to Membership & Subscription Services. Please allow six weeks for change to become effective.

Claims for missing numbers will not be allowed if loss was due to failure of notice of change of address to be received in the time specified; if claim is dated (a) North America—more than 90 days beyond issue date, (b) all other foreign—more than 1 year beyond issue date; or if the reason given is "missing from files". Hard copy claims are handled by Membership & Subscription Services.

Microfilm editions of all ACS primary publications, by single volume or entire back issue collection, are available. For additional microfilm (and microfiche) information, contact Microforms Program at the ACS Washington address or call (202) 872-4554.

To order **single issues or back volumes**, printed or microfiche, contact Special Issues Sales at the ACS Washington address, or call (202) 872-4365. Current year single issue \$4.75. Prior year single issue \$5.00. Back volume \$126.00. Foreign postage additional.

Supplementary material mentioned in the journal appears in the microfiche edition. Papers containing supplementary material are noted in the Table of Contents with a ■. See Supplementary Material notice at end of article for number of pages. Orders over 20 pages are available only on 24× microfiche. Orders must state photocopy or microfiche. Full bibliographic citation including names of all authors and prepayment are required. Prices are subject to change.

	U.S.	Foreign
Microfiche	\$3.00	\$4.00
Photocopy		
1-8 pages	5.50	7.00
9-20 pages	6.50	8.00

Single microfiche or paper copies of Supplementary Material may be ordered from Business Operations, Books and Journals Division at the ACS Washington address, or call (202) 872-4559.

American Chemical Society
1155 16th Street, N.W.
Washington, D.C. 20036
(202) 872-4600

Editorial Department
American Chemical Society
P.O. Box 3330
Columbus, Ohio 43210
(614) 421-6940 ext 3171

Membership & Subscription Services
American Chemical Society
P.O. Box 3337
Columbus, Ohio 43210
(614) 421-7230

Volume 82, Number 7 April 6, 1978

JPCHAx 82(7) 753-846 (1978)

ISSN 0022-3654

Gas-Phase Photolysis of Ethylcyclopropane at 147.0 and 123.6 nm ... Encarnacion Lopez and Richard D. Doepker*	753
A Pulse Radiolysis Study of Aqueous Cyanamide Solutions ... I. G. Draganić,* Z. D. Draganić, and K. Sehested	757
Reactions of Iodine with Olefins. 5. The Systematics of Electrophilic High Energy Iodine in Gaseous, High Pressure, and Liquid Isomers of Butene ... Kar-Chun To, M. E. Berg, and E. P. Rack*	761
Tunneling Reactions of Trapped Electrons with Added Electron Acceptors in Alcohol Glasses at 77 K ... John R. Miller	767
An Ultrasonic Absorption Investigation of Lanthanide Chloride Complexation in Aqueous Methanol ... Herbert B. Silber,* David Boulter, and Timothy White	775 ■
Behavior of Ruthenium in Fluoride-Volatility Processes. 3. Thermal Decomposition of RuOF ₄ ... Tsutomu Sakurai* and Akira Takahashi	780
The Apparent Molal Volumes and Adiabatic Compressibilities of Aqueous Amino Acids at 25 °C ... Frank J. Millero,* Antonio Lo Surdo, and Charles Shin	784 ■
Standard Thermodynamics of Transfer. Uses and Misuses ... A. Ben-Naim	792
Statistical Mechanical Theory of Nonionic Micelles ... A. Wulf	804
Effect of Organic Additives on Micellar Systems Studied by Positron Annihilation Techniques ... Yan-ching Jean and Hans J. Ache*	811
The Interaction of Rare Gas Atoms with Graphitized Carbon Black ... William A. Steele	817 ■
Raman Spectroscopic Study of Chloroform and Carbon Tetrachloride in 69% Dipalmitoyl Lecithin-31% Water Multilayers ... Bernard J. Bulkin* and Nehama Yellin	821
Crystal-Field Calculations with Trigonal Bipyramidal Symmetry Potential. 2. Weak-Field Matrices at Nonzero Spin-Orbit Coupling for a d ^{3,7} Configuration ... F. Palacio	825 ■
Crystal-Field Calculations with Trigonal Bipyramidal Symmetry Potential. 3. d ^{4,6} Configurations ... F. Palacio	830 ■
Crystal-Field Calculations with Trigonal Bipyramidal Symmetry Potential. 4. d ⁵ Configuration ... F. Palacio	837 ■

COMMUNICATIONS TO THE EDITOR

Modification of Benzophenone Phosphorescence by Molecular Complexation. A Reversible Process ... R. Snyder and A. C. Testa*	842
The Infrared Spectrum of Adsorbed Carbon Monoxide on a Platinum Surface in the Presence of High Pressure Gas-Phase Carbon Monoxide ... William G. Golden, Douglas S. Dunn, and John Overend*	843

Infrared Spectra and Structure of the Argon-Matrix Isolated HF_2^- Anion **Bruce S. Ault** 844

■ Supplementary and/or miniprint material for this paper is available separately (consult the masthead page for ordering information); it will also appear following the paper in the microfilm edition of this journal.

* In papers with more than one author, the asterisk indicates the name of the author to whom inquiries about the paper should be addressed.

AUTHOR INDEX

Ache, H. J., 811	Dunn, D. S., 843	Overend J., 843	Snyder, R., 842
Ault, B. S., 844			Steele, W. A., 817
Ben-Naim, A., 792	Golden, W. G., 843	Palacio, F., 825, 830, 837	Takahashi, A., 780
Berg, M. E., 761	Jean, Y., 811	Rack, E. P., 761	Testa, A. C., 842
Bouler, D., 775	Lopez, E., 753		To, K.-C., 761
Bulkin, B. J., 821	Lo Surdo, A., 784	Sakurai, T., 780	White, T., 775
Doepker, R. D., 753	Miller, J. R., 767	Sehested, K., 757	Wulf, A., 804
Draganić, I. G., 757	Millero, F. J., 784	Shin, C., 784	Yellin, N., 821
Draganić, Z. D., 757		Silber, H. B., 775	

THE JOURNAL OF PHYSICAL CHEMISTRY

Registered in U. S. Patent Office © Copyright, 1978, by the American Chemical Society

VOLUME 82, NUMBER 7 APRIL 6, 1978

Gas-Phase Photolysis of Ethylcyclopropane at 147.0 and 123.6 nm

Encarnacion Lopez and Richard D. Doepker*

Department of Chemistry, University of Miami, Coral Gables, Florida 33124 (Received September 6, 1977)

Publication costs assisted by the University of Miami

The photolysis of ethylcyclopropane has been studied using xenon (147.0 nm) and krypton (123.6 nm) resonance radiation. The major products observed were 1-butene, ethylene, hydrogen, 1,3-butadiene, propylene, allene, acetylene, and propyne, in order of decreasing importance. Radical scavengers, NO and O₂ as well as radical interceptors H₂S, D₂S, and HI, were used to determine the relative importance of radical and molecular processes. Nine primary reaction channels have been identified, and quantum yields for each channel determined and assigned. The most predominate primary reaction channel was found to be the elimination of methylene from the cyclopropane ring, producing a stable 1-butene fragment. No further secondary decomposition nor isomerization of the 1-butene fragment was observed. Although ionization was observed at 123.6 nm (ionization efficiency = 0.12) no evidence could be found for charge transfer process with NO, nor could any product be identified as originating exclusively from an ion-molecule reaction channel.

Introduction

Several years ago, a program was undertaken in this laboratory, to examine the primary and secondary reaction channels of the neutral excited (8.4 and 10.0 eV) substituted cyclopropane molecules. Initial studies have been reported for methylcyclopropane² and methylenecyclopropane.² In continuing this program, ethylcyclopropane (ECP, reported here), vinylcyclopropane,^{3a} 1,1-dimethylcyclopropane,^{3b} and *cis*- and *trans*-1,2-dimethylcyclopropane^{3b} have been or are being investigated.

Only cyclopropane has been extensively investigated,⁴⁻⁷ although *cis*-1,2-dimethylcyclopropane⁸ and 1,1-dimethylcyclopropane⁹ have been examined with regard to the formation of the methylene radical. Of major concern in these latter studies is the relative importance of the methylene elimination process from the photoexcited state and/or the chemical reactivity of the resulting methylene radical. Recently Collin⁹ has reviewed the photochemistry of the substituted cyclopropanes.

Experimental Section

Materials. Ethylcyclopropane (K & K Laboratories) was purified by means of vapor chromatography with a 25-ft., 30% squalane on Chromosorb P column, followed by a

second purification utilizing a 6-ft. phenyl isocyanate on Porasil C column. The purity of the resulting material was better than 99.8%. Purification of other materials used has been described elsewhere.^{1,2}

Irradiation and Analysis. The vacuum ultraviolet photolysis of ECP was investigated at room temperature (25 °C) in a standard static system using a 600-cm² reaction vessel and a "gettered" xenon (147.0 nm) or krypton (123.6 nm) resonance lamp. Analysis was performed by vapor chromatography (25-ft. squalane at 60 °C, 6-ft. *n*-octane/Porasil C, and phenyl isocyanate/Porasil C) and mass spectrometry (CEC 21-103C) as reported earlier.²

The chemical actinometers used at 147.0 nm were cyclobutene ($\Phi_{C_4H_6} = 0.23$)¹⁰ and cyclopentene ($\Phi_{C_5H_8} = 0.24$),¹¹ while at 123.6 nm only cyclopentene ($\Phi_{C_5H_8} = 0.19$)¹¹ was employed.

Results

The quantum yields of the major products of the photolysis of ECP at 147.0 and 123.6 nm reported in Tables I and II, respectively, are representative data collected under varying experimental conditions. In addition to these data, the following observations and control should be reported.

TABLE I: Quantum Yields for the 147.0-nm Photolysis of Ethylcyclopropane

P, Torr	1.0	40.0	1.0	20.0	1.0	1.0	1.0	1.0
Additive, Torr	None	None	0.05 NO	1.0 NO	0.05 NO 110 N ₂	0.1 HI	0.08 HI 110 N ₂	0.15 H ₂ S
H ₂	0.19	Nd ^a	0.20	0.19	Nd	Nd	Nd	Nd
CH ₄	0.05	0.03	0.01	0.01	0.01	0.65	0.66	0.60
C ₂ H ₂	0.03	0.03	0.03	0.03	0.03	0.03	0.03	0.03
C ₂ H ₄	0.29	0.28	0.28	0.28	0.28	0.40	0.41	0.38
C ₂ H ₆	0.10	0.08				0.07	0.08	0.07
C ₃ H ₆	0.08	0.09	0.06	0.06	0.06	0.19	0.19	0.08
C ₃ H ₈ ^b	0.02	0.02				0.01		
C ₃ H ₄ ^b	0.01	0.01	0.01	0.01	0.01	0.01	0.01	0.01
C ₃ H ₄ ^c	0.07	0.06	0.06	0.07	0.06	0.06	0.06	0.06
C ₄ H ₈ -1	0.35	0.33	0.32	0.31	0.32	0.37	0.39	0.32
C ₄ H ₆ -1,3	0.14	0.13	0.17	0.18	0.17	0.15	0.16	0.04

^a Not determined. ^b Methylacetylene. ^c Allene.

TABLE II: Quantum Yields for the 123.6-nm Photolysis of Ethylcyclopropane

ECP, Torr	1.0	1.0	1.0	20.0	1.0	1.0	1.0	1.0
Additive, Torr	None	156 N ₂	0.05 NO	1.0 NO	0.05 NO 105 N ₂	0.08 HI	0.08 HI 105 N ₂	0.15 H ₂ S
H ₂	0.21	Nd	0.18	0.19	Nd	Nd	Nd	Nd
CH ₄	0.06	0.04	0.01	0.01	0.01	0.49	0.50	0.48
C ₂ H ₂	0.03	0.04	0.03	0.03	0.02	0.03	0.03	0.03
C ₂ H ₄	0.27	0.28	0.25	0.26	0.24	0.32	0.31	0.29
C ₂ H ₆	0.09	0.07				0.06	0.07	0.06
C ₃ H ₆	0.08	0.07	0.07	0.07	0.08	0.24	0.22	0.09
C ₂ H ₈	0.03	0.02				0.01		
C ₃ H ₄	0.03	0.03	0.03	0.03	0.03	0.03	0.03	0.03
C ₃ H ₄	0.06	0.07	0.06	0.06	0.05	0.06	0.06	0.07
C ₄ H ₈ -1	0.32	0.33	0.31	0.30	0.29	0.35	0.35	0.30
C ₄ H ₆ -1,3	0.07	0.06	0.09	0.08	0.09	0.09	0.08	0.02

(1) Irradiation times were selected so as to hold the conversion below 0.05% for those experiments where quantum yields were obtained, except for those cases where hydrogen yields were to be analyzed through mass spectrometry. Conversions of nearly 0.3% were required for sufficient hydrogen production. When radical scavengers (NO or O₂) were present, all products, with the possible exception of 1,3-butadiene, appeared to be independent of irradiation time over a range of approximately 0.02–0.2% conversion.

(2) Although considerable effort was expended, C₆ products observed even in the presence of radical scavengers could not be quantitatively determined, nor positively identified due primarily to parent molecule tailing. The sum of the quantum yields of the observed compounds was estimated to be less than 0.2 at both wavelengths. No strong pressure dependence was observed for these products.

(3) No C₅ compounds were observed in the presence of radical scavengers. Vinylcyclopropane, with a quantum yield of 0.02 or greater, should have been observed if formed. In the absence of radical scavengers, small amounts of C₅ were observed, with a total quantum yield of nearly 0.05.

(4) Extensive use of radical interceptors, H₂S(D₂S)¹² and HI,¹³ was employed in this investigation. HI was found to be a more effective radical interceptor than H₂S, as suggested by Ausloos.¹¹ Increasing the concentration of HI from 3 to 15% revealed that the optimum concentration of HI for radical interception is between 5 and 10% (8% normally used). This corresponds to the maximum in radical yields vs. HI concentration curve. H₂S, on the other hand, required nearly 15% addition to obtain similar effects. Nonradical products were unaffected by the addition of HI, while 1,3-butadiene was reduced in the presence of H₂S. The reason for this anomalous result is unclear. When D₂S (15%) was used, stable products were isolated and determined through mass spectrometry. For

a 2 Torr ECP (15% D₂S) at 147.0 nm the results showed H₂:HD:D₃ = 36:51:13; CH₃D:CH₄ = 64:36; C₂H₅D:C₂H₆ = 57:43; C₂H₃D:C₂H₄ = 16:84; 1-C₄H₇D:1-C₄H₈ = 4:96; and 1,3-C₄H₅D:1,3-C₄H₆ = 100:0. Results of a similar experiment at 123.6 nm were H₂:HD:D₂ = 31:55:14; CH₃D:CH₄ = 70:30; C₂H₅D:C₂H₆ = 64:36; C₂H₃D:C₂H₄ = 20:80; 1-C₄H₇D:1-C₄H₈ = 12:88; and 1,3-C₄H₅D:1,3-C₄H₆ = 100:0.

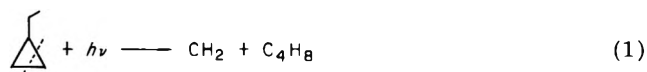
(5) The ionization energy of ECP was 9.50 eV as determined by Lossing.¹⁴ At 123.6 nm (10.0 eV), ionization occurs with the formation of the parent ion. The ionization efficiency was determined to be 0.12 at this wavelength (assuming the ionization efficiency of cyclopentene = 0.16.^{11,15} Examination of product yields vs. applied collector voltage gave no indication of the presence of ion-molecule reactions. The methods used were the same as reported earlier.¹¹ When 10% NO replaced the 5% O₂ as a radical scavenger, no changes in product quantum yields were observed (ionization energy NO < ionization energy of ECP).

Discussion

The observed products presented in this report result from the primary decomposition of the photoexcited molecule, from the decomposition of resulting primary fragments, and from radical reactions. The use of NO or O₂ radical scavengers eliminates the latter reactions except for those involving hot radicals or methylene. The ability to distinguish between primary decomposition of the photoexcited molecule and the decomposition of resulting primary fragments requires either a competitive kinetic titration or deactivation process. The latter usually involves an evaluation of the quantum yields vs. total pressure with respect to selected photolysis products.

From the results presented in Tables I and II it can be seen that the quantum yields of the unsaturated products appear independent of pressure and generally insensitive to the presence or absence of additives under the experimental conditions followed in this investigation.

Formation of 1-Butene. The elimination of methylene from the cyclopropane ring would result in a C_4H_8 fragment structurally identical to 1-butene (reaction 1). At



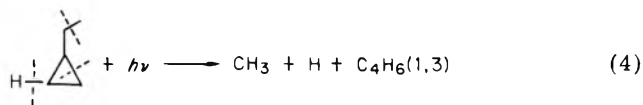
147.0 nm, this process is exothermic by nearly 100 kcal/mol, and 136 kcal/mol exothermic for 123.6-nm photons. If this excess energy were partitioned predominantly on the C_4H_8 fragment, secondary decomposition could result according to reactions 2 and 3.¹⁶ Reactions 2 and 3 require



in excess of 100 and 72 kcal/mol, respectively. It is highly unlikely that either reaction occurs at 147.0 nm, but it is more difficult to rule them out at 123.6 nm. The absence of any observable pressure effect on the quantum yield of 1-butene at 123.6 nm though would prohibit a stepwise elimination channel resulting in the further fragmentation of the excited butene.

The quantum yield of 1-butene in the presence of radical scavengers would be a direct measure of the primary reaction channel 1, assuming the absence of any secondary decomposition of the butene fragment. Therefore $\phi_1 = 0.32$ and 0.31 at 147.0 and 123.6 nm, respectively. It is interesting to note that this quantum yield corresponds well with a value of 0.32 at 147.0 nm for methylcyclopropane¹⁷ and 0.33 at 147.0 nm for 1,1-dimethylcyclopropane.^{3b} The fate of the eliminated methylene radical is somewhat in doubt. Insertion of the methylene into ECP is considerably exothermic. The resulting substituted ECP excited molecule would be expected to isomerize to a variety of "hexenes" through ring opening processes.

Formation of 1,3-Butadiene. The most probable reaction channel leading to the formation of 1,3-butadiene involves the elimination of the terminal methyl group, 1-2 carbon cleavage of the cyclopropane ring, and the elimination of a 3-carbon hydrogen. Since, again, no pressure effect was observed in the formation of 1,3-butadiene, nor does the addition of additives (other than H_2S) affect the total quantum yield, it is not possible to determine the order of the bond cleavages involved. Thus the primary reaction channel is assumed to be a concerted process within the time frame of the collision interval (reaction 4).

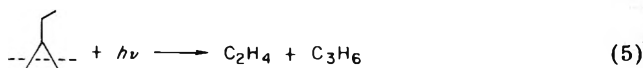


Reaction 4 is exothermic by 82 and 118 kcal/mol for 147.0 and 123.6 nm, respectively. Although further decomposition is energetically possible, the absence of a pressure dependence would seem to render the reaction unlikely, especially in view of the necessary distribution of excess energy that would be required.

If it can be assumed that reaction 4 represents the sole process leading to the formation of 1,3-butadiene, then the primary quantum yield of reaction channel 4 is equal to the quantum yield of 1,3-butadiene $\phi_4 = \Phi_{C_4H_6}$; $\phi_4 = 0.17$ and 0.09 at 147.0 and 123.6 nm, respectively. It should be noted that 1,3-butadiene is decreased in the presence of H_2S , but not when HI is used as a radical interceptor. Similar effects have been observed previously in this laboratory as well as by Collin and Perrine.¹⁸ Presumably, this is due to the rapid addition of HS to 1,3-butenes forming a resonance-stabilized C_4H_6SH radical.

Formation of Propylene. Considering the observed cleavage of many cyclic hydrocarbons, ECP may be ex-

pected to dissociate directly into ethylene and propylene (reaction 5). This process is highly exothermic, 177 and

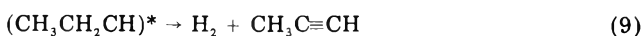


213 kcal/mol with the 147.0- and 123.6-nm radiation, respectively. If a major part of this excess energy were to reside in the "ethylene" fragment, processes 6-8 would be expected.¹³ Again the absence of a pressure effect on the

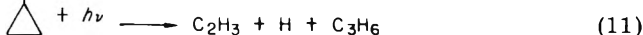


formation of ethylene eliminates reaction 8, and would require that reactions 6 and 7 be occurring nearly simultaneously with the propylene formation, that is within the framework of the collision interval associated with the pressures utilized in this study.

If, on the other hand, the distribution of excess energy were concentrated on the propylene fragment, methylacetylene might be expected to be produced (reaction 9).

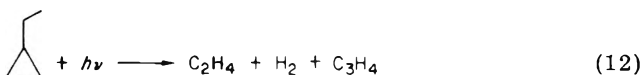


With regards to the formation of propylene, a concerted process combining reaction 5 with reactions 6 and 7 would result in the formation of propylene (reactions 10 and 11).



The quantum yields of propylene formation (in the presence of NO) are reported as 0.06 and 0.07 for the xenon and krypton photolyses, respectively. The quantum yield of reaction 10 may be assigned from the reported quantum yield of acetylene, (i.e., $\phi_{10} = \Phi_{C_2H_2}$), $\phi_{10} = 0.03$ for both wavelengths. Thus, the evaluation of reaction channel 11 can be obtained by $\phi_{11} = (\Phi_{C_3H_6} - \Phi_{C_2H_2})$ or $\phi_{11} = 0.03$ at 147.0 nm and 0.04 at 123.6 nm.

Formation of Methylacetylene and Allene. The reaction channel leading to the formation of methylacetylene is related to the secondary decomposition of propylene, reaction 9. Again no pressure effects are observed for either propylene or methylacetylene formation and a "concerted" process is in order (reaction 12). The




quantum yield assignment for this reaction channel is based on the methylacetylene yields of 0.01 and 0.03 at 147.0 and 123.6 nm, respectively.

Allene would not be expected from the reaction channel 12 due to the structure of the "propylene" fragment. On the other hand, the elimination of the whole ethyl fragment would result in the formation of a "hot" cyclopropyl radical which would undergo a 2-3 carbon cleavage with or without hydrogen atom elimination (reactions 13-15).



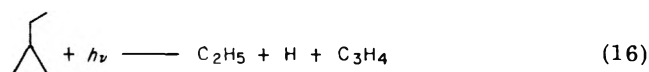
Reaction 13 is exothermic by some 102 or 138 kcal/mol depending upon the wavelength used. Sufficient energy is therefore available for the production of allene since the

TABLE III: Quantum Yield for the Primary Reaction Channels in the Vacuum-UV Photolysis of Ethylcyclopropane

	147.0	123.6	123.6 ^a
 + $h\nu$			
$\xrightarrow{1}$ CH ₂ + C ₄ H ₈	0.32	0.31	0.35
$\xrightarrow{4}$ CH ₃ + H + C ₄ H ₆ (1,3)	0.17	0.09	0.10
$\xrightarrow{10}$ C ₂ H ₂ + H ₂ + C ₃ H ₂	0.03	0.03	0.03
$\xrightarrow{11}$ C ₂ H ₃ + H + C ₃ H ₆	0.03	0.04	0.05
$\xrightarrow{12}$ C ₂ H ₄ + H ₂ + C ₃ H ₄ ^b	0.01	0.03	0.03
$\xrightarrow{16}$ C ₂ H ₅ + H + C ₃ H ₄ ^c	0.06	0.06	0.07
$\xrightarrow{17}$ C ₂ H ₄ + H + C ₃ H ₅	0.16	0.18	0.20
$\xrightarrow{18}$ CH ₃ + C ₂ H ₄ + C ₂ H ₃	0.11	0.04	0.05
$\xrightarrow{19}$ CH ₃ + C ₄ H ₇	0.05	0.05	0.06
Total	0.94	0.83	0.94

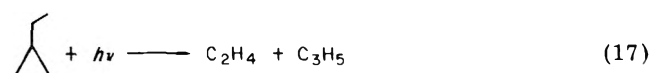
^a Corrected to exclude ionization. ^b Methylacetylene. ^c Allene.

overall process requires approximately 124 kcal/mol (reaction 16). If, therefore, reaction 16 is the only process

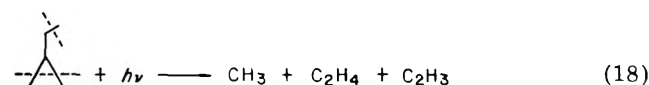


involving the formation of allene, $\phi_{16} = \Phi_{\text{C}_3\text{H}_4(\text{allene})} = 0.06$ at both wavelengths. With respect to this assignment, it would be expected that the $\Phi_{\text{C}_2\text{H}_5}$ formation equal $\Phi_{\text{C}_3\text{H}_4}$. It may be seen in Tables I and II that the quantum yields of C₂H₆ (in the presence of HI or H₂S) are within the expected experimental uncertainties of these values.

Formation of Ethylene. As previously cited, ethylene is formed in conjunction with the formation of methylacetylene, reaction 12; but this reaction channel only accounts for a small fraction of the ethylene observed. Two additional sources of ethylene might be expected. Considering reaction 13, with the excess energy favoring the ethyl radical, a hydrogen atom may be eliminated. The resulting reaction channel would produce ethylene, a hydrogen atom, and an allyl radical (reaction 17). In



addition, ethylene formation may be accounted for by a process similar to reaction 4, in that, through a methyl radical elimination and two C-C bond cleavages, ethylene may be formed (reaction 18). Assignment of values to ϕ_{17}

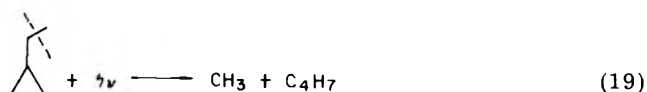


and ϕ_{18} would not be possible without a measure of either $\Phi_{\text{C}_2\text{H}_3}$ or $\Phi_{\text{C}_3\text{H}_5}$ since both H₂S and HI appear nearly quantitatively to intercept vinyl radicals^{12,13,19} and both lead to nearly the same value, i.e. [$\Phi_{\text{C}_2\text{H}_3} = \Phi_{\text{C}_3\text{H}_4}$ (with HI or H₂S) - $\Phi_{\text{C}_3\text{H}_4}$ (with NO)]. $\Phi_{\text{C}_2\text{H}_3}$ is assigned values of 0.12 and 0.07. Recalling that reaction 11 required a vinyl quantum yield of 0.03 and 0.04 for 147.0 and 123.6 nm, respectively, then $\phi_{18} = 0.09$ and 0.03 for the two wavelengths in question.

Considering the total $\Phi_{\text{C}_3\text{H}_4} = 0.28$ at 147.0 nm, the $\phi_{17} = (0.28 - \phi_{12} - \phi_{18}) = (0.28 - 0.01 - 0.09) = 0.18$ at 123.6 nm $\phi_{17} = (0.25 - 0.03 - 0.03) = 0.19$. The direct titration of the allyl radical by HI produces $\Phi_{\text{C}_3\text{H}_5} = 0.13$ and 0.15. This would seem to indicate that HI intercepted approximately 75% of the allyl radical, based on the assumption that the vinyl radical was quantitatively intercepted. In reality, one must assume that neither the vinyl nor the allyl radical is quantitatively intercepted but will

account for around 80–90% of these radical species present. With this in mind, the assumed values of reaction channels 17 and 18 should reflect approximately an 85% efficiency. Thus, $\phi_{17} = 0.16$ and $\phi_{18} = 0.11$ at 147.0 nm and $\phi_{17} = 0.18$ and $\phi_{18} = 0.04$ at 123.6 nm.

Other Primary Reaction Channels. Although H₂S has been generally accepted as a quantitative interceptor for methyl radicals (and methylene), it can be seen that the quantum yield of methane is further increased in the presence of HI. If it can be assumed that HI is nearly a quantitative interceptor for methyl radical, $\Phi_{\text{CH}_3} = 0.65$ and 0.49, at 147.0 and 123.6 nm, respectively. Considering the mechanism proposed at 147.0 nm, $\Phi_{\text{CH}_3} = \phi_1 + \phi_4 + \phi_{18} = 0.60$ (assuming the methylene abstracts from HI, as opposed to inserting into the ethylcyclopropane ring in the presence of HI). At 123.6 nm, the mechanism predicts $\Phi_{\text{CH}_3} = 0.44$. This would seem to indicate another reaction channel for the production of CH₃/CH₂. A second hint to the possible reaction channel may be found in the observed increase in 1-butene in the presence of HI, indicating the presence of a C₄H₇ species. A value for $\Phi_{\text{C}_4\text{H}_7} = 0.06$ can be obtained at 147.9 nm and 0.04 at 123.6 nm. Since both the excess Φ_{CH_3} and the value of $\Phi_{\text{C}_4\text{H}_7}$ are equal, within experimental error, it would seem acceptable to assume that both are formed in the same reaction channel (reaction 19). ϕ_{19} may be calculated from the methane



yields as approximately 0.05 at both wavelengths.

It must be emphasized though, that the measurement of the CH₃/CH₂ radical yields by HI titration must be considered a minimum value for the CH₂ yield. Although the presence of HI did substantially reduce the C₆ products, still small amounts were observed indicating the incomplete interception of all the methylene present.

Summary and Conclusion

The vacuum photolysis of ethylcyclopropane may be described in terms of nine primary reaction channels. These are given in Table III. It must be noted that the above mechanism gives $\Phi_{\text{H}} = 0.42$ and $\Phi_{\text{H}_2} = 0.04$ at 147.0 nm; while at 123.6 nm $\Phi_{\text{H}} = 0.37$ and $\Phi_{\text{H}_2} = 0.06$, which are not in particularly good agreement with the reported $\Phi_{\text{H}_2} = 0.20$ at both wavelengths. It must be recalled though that the results of the D₂S experiments indicate predominate production of H atoms. This, coupled with the need of long irradiation times, would be expected to produce apparent hydrogen yields which are below the true

value due to the buildup of unsaturated species during the photolysis process.

Acknowledgment. The authors acknowledge the National Science Foundation which aided in the support of this investigation in the early years of effort through Grant No. NSF-GP-20878. The authors also thank Dr. Guy Collin for timely correspondence.

References and Notes

- (1) R. D. Doepker, *J. Phys. Chem.*, **73**, 3219 (1969).
- (2) K. L. Hill and R. D. Doepker, *J. Phys. Chem.*, **76**, 3153 (1972).
- (3) (a) E. Lopez and R. D. Doepker, manuscript in preparation; (b) J. B. Binkewicz and R. D. Doepker, in preparation; (c) T. S. Pendleton and R. D. Doepker, study in progress.
- (4) C. L. Currie, H. O. Okabe, and J. R. McNesby, *J. Phys. Chem.*, **67**, 1494 (1963).
- (5) A. A. Scala and P. Ausloos, *J. Chem. Phys.*, **49**, 2282 (1968).
- (6) K. Shibuya, K. Ohi, and J. Tanaka, *Bull. Chem. Soc. Jpn.*, **48**, 1974 (1975).
- (7) A. Dhingra and R. D. Koob, *J. Phys. Chem.*, **74**, 4490 (1970).
- (8) K. Dees and R. D. Koob, *J. Phys. Chem.*, **77**, 759 (1973).
- (9) G. J. Collin, *J. Chim. Phys.*, **74**, 302 (1977).
- (10) A. Deleon and R. D. Doepker, *J. Phys. Chem.*, **75**, 3656 (1971).
- (11) C. K. Tu and R. D. Doepker, *J. Photochem.*, **3**, 13 (1974-1975).
- (12) P. Ausloos and S. Lias, *J. Chem. Phys.*, **44**, 521 (1966).
- (13) P. Ausloos, R. E. Rebert, and S. Lias, *J. Photochem.*, **2**, 267 (1973-1974).
- (14) F. P. Lossing, *Can. J. Chem.*, **50**, 3973 (1972).
- (15) R. Leasleux, S. Searles, L. Wayne Sieck, and P. Ausloos, *J. Chem. Phys.*, **54**, 3411 (1971).
- (16) F. P. Lossing, D. G. Maroden, and J. B. Farmer, *Can. J. Chem.*, **34**, 701 (1956).
- (17) R. D. Doepker, unpublished results.
- (18) G. J. Collin and P. M. Perrin, *Can. J. Chem.*, **50**, 2400 (1972).
- (19) G. J. Collin, P. M. Perrin, and C. M. Gaucher, *Can. J. Chem.*, **50**, 239 (1972).

A Pulse Radiolysis Study of Aqueous Cyanamide Solutions

I. G. Draganić,^{*1} Z. D. Draganić,[†] and K. Sehested

Accelerator Department, Risø National Laboratory, DK-4000 Roskilde, Denmark (Received October 19, 1977)

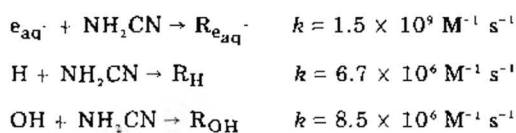
Publication costs assisted by Risø National Laboratory

The radiolysis of oxygen-free, aqueous solutions of cyanamide was studied by fast kinetic spectrophotometry. Computer simulation of the reaction mechanisms was used to evaluate the experimental data. Four different species are identified: (1) the radical anion $(\text{NH}_2\text{CN})^\cdot$ absorbing light in the UV with $\lambda_{\text{max}} < 240$ nm and $\epsilon_{240} = 1500 \text{ M}^{-1} \text{ cm}^{-1}$; the disappearance is a second-order process with $2k = 1.3 \times 10^9 \text{ M}^{-1} \text{ s}^{-1}$; (2) the hydrogen adduct, $\text{NH}_2\text{C}(\text{H})=\dot{\text{N}}$ (or $\text{NH}_2\dot{\text{C}}=\text{NH}$), with $\lambda_{\text{max}} 300$ nm and $\epsilon_{300} = 150 \text{ M}^{-1} \text{ cm}^{-1}$ decaying by second-order kinetics with $2k = 3.1 \times 10^8 \text{ M}^{-1} \text{ s}^{-1}$; (3) the hydroxyl radical preferentially adds to the cyano group, $\text{NH}_2\text{C}(\text{OH})=\dot{\text{N}}$ (or $\text{NH}_2\dot{\text{C}}=\text{NOH}$). This species rearranges in the submicrosecond scale to $\text{NH}_2\text{C}(\text{O})\text{NH}$ ($\lambda_{\text{max}} 325$ nm and $\epsilon_{325} = 1900 \text{ M}^{-1} \text{ cm}^{-1}$) and disappears by a second-order process with $2k = 6.3 \times 10^8 \text{ M}^{-1} \text{ s}^{-1}$; (4) It is estimated that about 10% of OH radicals attack the substituent group and by H abstraction produce the $\dot{\text{N}}\text{HCN}$ radical ($\lambda_{\text{max}} 370$ nm and $\epsilon_{370} = 1800 \text{ M}^{-1} \text{ cm}^{-1}$); it disappears by a pseudo-first-order process attributed to a hydrolysis reaction. At increasing acidities, protonation of this radical takes place, $\text{NHCN} + \text{H}^+ \rightarrow \text{NH}_2\text{CN}$; the protonated form decays faster and absorbs more strongly. In a cyanamide solution containing $\text{S}_2\text{O}_8^{2-}$, the SO_4^\cdot radicals react with cyanamide, $k = 1 \times 10^8 \text{ M}^{-1} \text{ s}^{-1}$, producing $\text{NH}_2\text{CN}^\cdot$ radicals. The dependence of the optical density at 325 nm on the dose rate and solute concentration are quantitatively consistent with the assumption that the OH radicals react with the $\text{NH}_2\text{C}(\text{O})\text{NH}$ species with $k = 4 \times 10^8 \text{ M}^{-1} \text{ s}^{-1}$. It is concluded that the cyano group in cyanamide, a N-cyano compound, is the main point of attack by e_{aq}^\cdot , H, and OH as was the case with previously studied nitriles with a C-cyano group and various cyanides.

Introduction

Recent investigations¹ of the radiolysis of simple RCN compounds have suggested that the cyano group is the main target of attack by the primary free radicals from irradiated water. The substituent R was CH_3 , C_2H_5 , CH_2CN , or $(\text{CH}_2)_2\text{CN}$, and they were found mainly to influence the amount of a given chemical change.¹ All these nitriles contained the $\text{>C}\equiv\text{N}$ group.

The present work concerns the early stages of the radiolysis of cyanamide, H_2NCN . This compound represents another type of nitriles, the N-cyano compounds. No published data on the radiolytic behavior of $\text{>N}\text{--}\text{C}\equiv\text{N}$ compounds in aqueous solutions are available. A recent study of the γ radiolysis of aqueous cyanamide solutions² gives the following rate constants for the primary reactions



$\text{R}_{\text{eq}}^\cdot$, R_{H} , and R_{OH} are the short-lived intermediates. Their absorption spectra and kinetic behavior under various experimental conditions are the subject of the present study. The experimental data were obtained by fast kinetic spectrophotometry, and computer calculations were used to determine concentrations of the intermediates and to derive rate constants which could not be obtained directly from experiments.

Experimental Section

Irradiations. The pulse radiolysis system is described elsewhere.³ Relative dosimetry of the 10-MeV electron pulses was carried out by means of a setup registering the current induced in a coil surrounding the electron beam.

¹ Permanent address: Laboratory of Radiation Chemistry, Boris Kidric Institute of Nuclear Science, P.O. Box 522, Beograd 11001, Yugoslavia.

The absolute dose was measured with a hexacyanoferrate(II) dosimeter, in which $G(e_{aq}^- + OH^-) = 5.25$ and $\epsilon_{420}[Fe(CN)_6^{3-}] = 1000 \text{ M}^{-1} \text{ cm}^{-1}$ were used. The dosimeter solution was $1 \times 10^{-3} \text{ M}$.

Solutions. All samples were prepared in fresh, triple-distilled water and deoxygenated by bubbling argon through it for at least 30 min. The cyanamide was a Fluka product, mp 44–46 °C, with 2% boric acid as stabilizer. A Merck product without stabilizer, mp 43–46 °C, was used in some experiments without affecting the results. In preparing strongly acid samples $HClO_4$ was added to deaerated neutral solutions before irradiations.

Computer Simulation. The reaction mechanism was analyzed by computer simulation. When the fitted rate constants were derived, a sequence of reactions was selected so that only one parameter had a dominant influence on the experimentally observed rate of chemical changes.

Computer-calculated concentrations of the reactive intermediates were used for the determination of molar extinction coefficients. The contributions from various short-lived species were taken into account, when the calculated values were fitted to the experimental data at different times after the pulse, usually up to about 15 μs .

In the reaction model, the following reactions of primary radicals in pure irradiated water were considered:



The rate constants for reactions 1–7 were taken from ref 4–6. The values of G_{OH} , G_H , and $G_{e_{aq}^-}$ were taken according to the reactivities of solutes from ref 7.

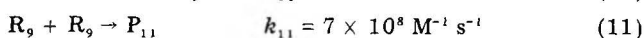
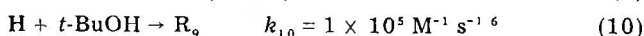
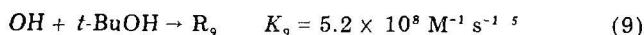
The computations were performed on the Burroughs B 6700 computer at Risø, using a B 6700 extended algol program language and a program developed for kinetic studies in radiation chemistry by Lang Rasmussen.⁸

Results and Discussion

Reaction of the Hydrated Electron with Cyanamide. No hydrogen is produced by the reaction of the hydrated electron with cyanamide.² Also, the measured rate constant² of this reaction satisfies Taft's empirical relation, which was previously found to be valid for a series of $e_{aq}^- + RCN$ reactions.¹ This supports the assumption of e_{aq}^- addition to the cyano group



Figure 1 summarizes the transient absorptions observed 1 μs after the pulse in deoxygenated cyanamide solutions. Besides the addition product from reaction 8 the transient spectrum in Figure 1a also includes the contributions of unscavenged OH radicals and the product from the reaction of cyanamide with hydroxyl radicals. When *tert*-butyl alcohol (*t*-BuOH) is present in the solution (0.2 M), hydroxyl radicals are efficiently removed by reaction



9 and the absorption in Figure 1b is thus due to the radical

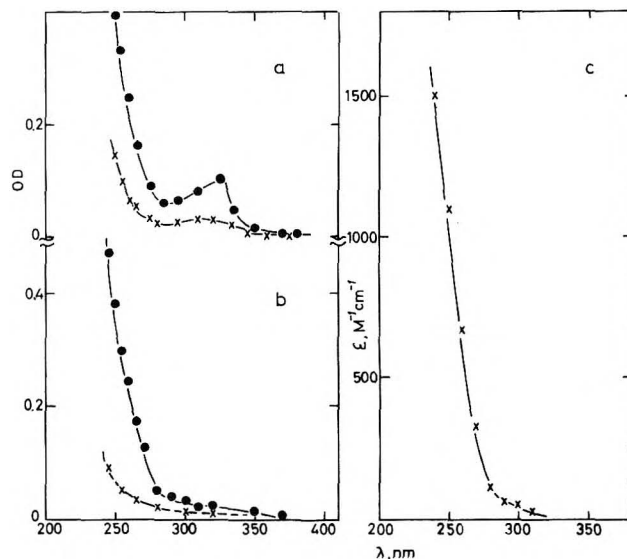
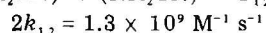


Figure 1. The absorption spectra of the transients in aqueous solutions of cyanamide ($2.5 \times 10^{-2} \text{ M}$), pH 5, 20 krd. (a) Argon saturated solution: ●, 1 μs after the pulse; x, 35 μs after the pulse. (b) ●, 0.2 M *t*-BuOH added to the cyanamide solution; x, 0.2 M *t*-BuOH. (c) Molar extinction coefficients of the $(NH_2CN)^-$ radical anion.

anion, $(NH_2CN)^-$, and the *tert*-butyl radical, R_9 . Scavenging of the hydrated electrons by N_2O leads to a decrease of the absorption in the UV region and supports the assumption that the product of reaction 8, the radical anion, is the species absorbing with $\lambda_{max} < 240 \text{ nm}$.

The spectrum of the radical anion, $(NH_2CN)^-$, shows no maximum absorption, but a monotonous increase in the UV region. The spectrum is shown in Figure 1c. When the experimental data from Ar-saturated cyanamide solutions were used for the calculations of the molar extinction coefficients, the reactions of the hydroxyl radical (eq 15–16, 20–21) were also taken into account besides reactions 1–8 and 12–13. The spectral contributions of $(NH_2CN)^- + (NH_2CN)^- \rightarrow P_{12}$ (12)



the hydroxyl radicals were calculated by using published data on the OH radical spectrum.⁹ The computations resulted in a disappearance rate of $(NH_2CN)^-$ following second-order kinetics.

The molar extinction coefficients can also be calculated from the experimental data in Figure 1b. In these computations, reactions 9–11 were also taken into account; it was assumed that the R_9 species does not interfere with the reaction scheme proposed for pure cyanamide solutions. The measured extinctions were corrected for the contribution of the R_9 species. The molar extinction coefficients for R_9 were determined in separate experiments using 0.2 M *t*-BuOH. The results obtained for the ϵ values for the $(NH_2CN)^-$ radical anion and for k_{12} agree with those calculated from pure cyanamide solutions. This supports the assumption that the R_9 species disappears by reaction 11 only.

Reaction of the Hydrogen Atom with Cyanamide. Figure 2 shows the transient absorptions in acid cyanamide solutions. The hydrated electrons are converted to H atoms by reaction 1. This conversion is practically complete in solutions containing 0.5 M $HClO_4$ and 0.1 M NH_2CN . In acid solutions we have also $NH_2CN + H^+ \rightarrow NH_3^+CN$. The pK is 1.1¹⁰ and the studied solutions contain both the protonated and unprotonated species. We used only unprotonated forms in eq 13 and 14 because of scarce information on the acidity influence on H atom reactions.

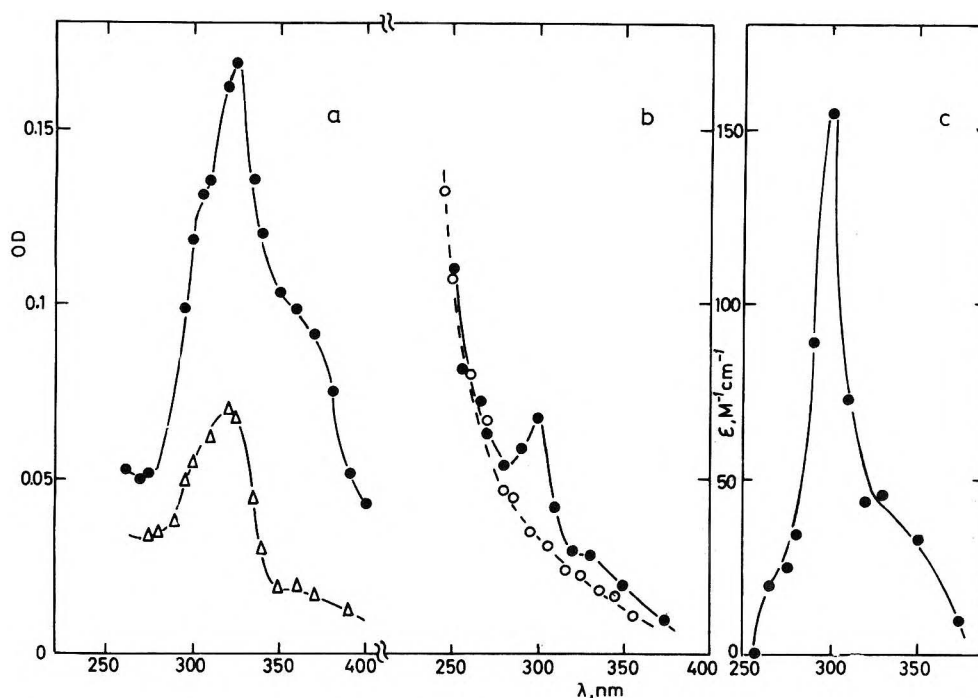
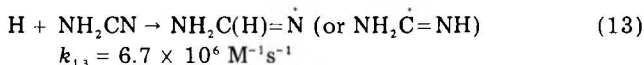


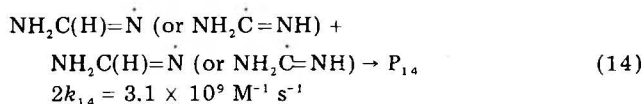
Figure 2. The absorption spectra of the transients in acid solutions (0.5 M HClO_4) of cyanamide (0.1 M), 20 krd. (a) \bullet , immediately after the pulse; Δ , 25 μs after the pulse. (b) \bullet , 0.5 M *t*-BuOH added to the cyanamide solution; \circ , 0.5 M *t*-BuOH in 0.5 M HClO_4 . (c) Molar extinction coefficients of H atom adduct of cyanamide.

In Figure 2a the transient absorption is due to the products of the cyanamide reactions with the hydroxyl radical and the species produced by the H atom

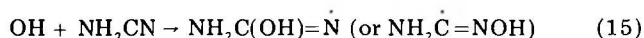


The value of k_{13} was derived from competition experiments in γ radiolysis.² These experiments showed that no hydrogen is produced by reaction 13, and suggested that the H atom adds to the cyano group. When *t*-BuOH is present in the solution the hydroxyl radicals are removed by reaction 9, and the resulting absorption appears to have a λ_{max} of 300 nm (Figure 2b). This spectrum is assigned to the H atom adduct produced in reaction 13. Figure 2c shows the absorption spectrum and molar extinction coefficients derived from experimental data similar to those in Figure 2b. In the computation of the concentrations of the radical intermediates reactions 14–16 and 20–21 are taken into account in addition to reactions 1–13.

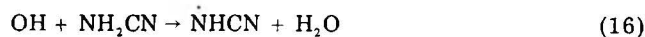
A fast second-order decay process was observed for the radical produced by reaction 13. By assuming that the *tert*-butyl radical does not interfere, as was the case with the disappearance of $(\text{NH}_2\text{CN})^-$ by reaction 12, the decay is attributed to



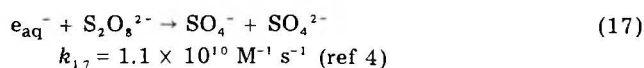
Reactions of the Hydroxyl Radical with Cyanamide. Transient absorptions similar to those in Figure 1a are obtained when solutions of different cyanamide concentrations (up to 1 M), at pH 5, were exposed to radiation at various doses per pulse (up to 25 krd). Kinetic analysis shows that two species are produced by the reaction of OH radicals with cyanamide. One decays by a second-order process, and absorbs light with a λ_{max} of 325 nm. Its origin is attributed to the addition reaction



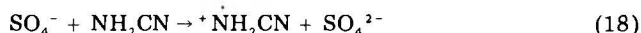
A considerably weaker absorption with λ_{max} of 370 nm, which disappears through a pseudo-first-order process, is attributed to the abstraction reaction



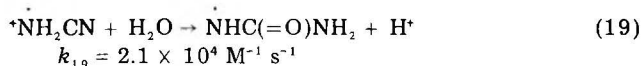
Aqueous Solutions of $\text{NH}_2\text{CN} + \text{S}_2\text{O}_8^{2-}$. Evidence supporting the abstraction reaction (eq 16) is obtained by irradiating aqueous solutions of cyanamide containing persulfate (pH \sim 5). The hydrated electron reacts efficiently with the persulfate



forming the sulfate radical anion. This radical anion is known to react by a direct oxidative electron transfer forming a radical cation.^{11–13} The resulting spectrum shown in Figure 3 is similar to that in Figure 2a. The extinction at 325 nm corresponds roughly to that in N_2O saturated solution. The contribution from the species produced by the hydrated electron is ascribed to the sequence of reaction 17 and



The rate constant for reaction 18 was calculated as $k_{18} = 1 \times 10^8 \text{ M}^{-1}\text{s}^{-1}$. Besides reactions 1–8 and 12–22, the dimerization reaction of the sulfate radical ion with $k = 8.8 \times 10^8 \text{ M}^{-1}\text{s}^{-1}$ (ref 11) was taken into account in the computer simulations. The radical cation produced in reaction 18 disappears by a pseudo-first-order process with a half-life of 0.6 μs . The decay is ascribed to a hydrolysis reaction followed by a deprotonation



The Structure of the OH Adduct of Cyanamide. The experiments with the cyanamide solutions containing persulfate revealed some insight into the form of the free radical produced in reaction 15. The decay of the radical cation $\dot{\text{N}}\text{NH}_2\text{CN}$ (eq 19) leads to an increase of absorption

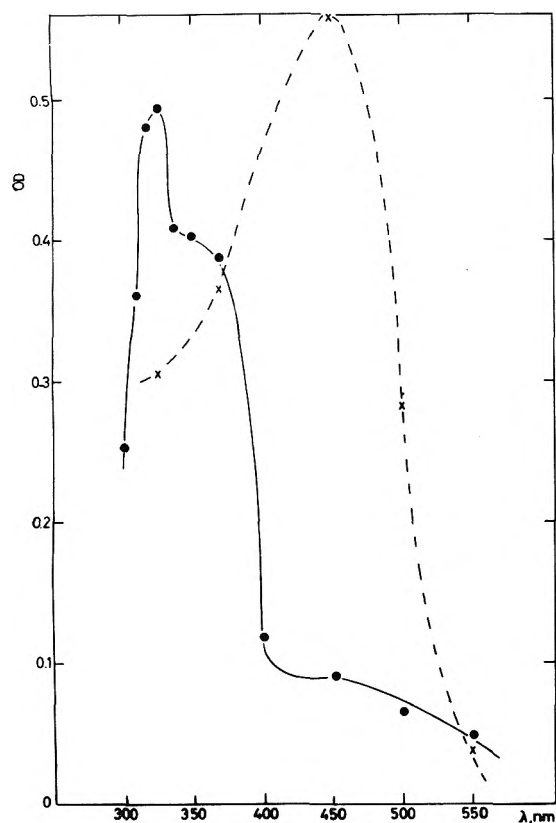
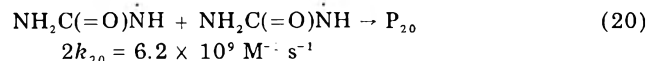


Figure 3. The transient absorptions in aqueous solution, pH 5, argon saturated: ●, NH_2CN (0.1 M) + $\text{S}_2\text{O}_8^{2-}$ (0.1 M); x, $\text{S}_2\text{O}_8^{2-}$ (0.1 M). 0.5 μs after the pulse, 26.7 krd.

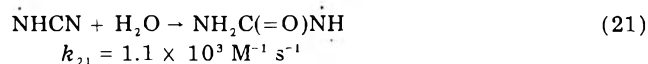
at 325 nm. A possible explanation is that the radical produced in reaction 19 has a spectrum similar to that of the species produced in reaction 15. It seems more likely, however, that the OH adduct of cyanamide (eq 15) undergoes a rearrangement on the submicrosecond scale, $\text{NH}_2\text{C}(\text{OH})=\dot{\text{N}}$ (or $\text{NH}_2\dot{\text{C}}=\text{NOH}$) \rightarrow $\text{NH}_2\text{C}(\text{O})\dot{\text{N}}\text{H}$, and that the absorption with a λ_{max} of 325 nm is due to $\text{NH}_2\text{C}(\text{O})\dot{\text{N}}\text{H}$ radicals only.

The Rate Constants of the Reactions of OH Radicals with Cyanamide and the Decays of Species Produced in Reactions 15 and 16. The values of k_{15} and k_{16} cannot be obtained experimentally by the techniques used in this work, but a reliable estimate is, however, possible. Based on the experimentally obtained overall rate constant $k(\text{OH} + \text{NH}_2\text{CN}) = 8.5 \times 10^6 \text{ M}^{-1} \text{ s}^{-1}$ (ref 2) and on the kinetic behavior of the products from reactions 15 and 16, a reasonable assumption is $k_{16}/k_{15} = 0.1$, which gives $k_{15} = 7.7 \times 10^6 \text{ M}^{-1} \text{ s}^{-1}$ and $k_{16} = 0.77 \times 10^6 \text{ M}^{-1} \text{ s}^{-1}$. These values were used in computer calculations.

The decay of the $\text{NH}_2\text{C}(\text{O})\dot{\text{N}}\text{H}$ radical was found to obey second-order kinetics and at pH 5



A pseudo-first-order process was found for the decay of the radical produced in reaction 16. This was observed at 370 nm. At pH 5



Acid Solutions of Cyanamide. The transient spectra observed at various acidities (0.01–1 M HClO_4) are similar to those shown in Figure 2a. It should be noted, however, that the absorption increases with acidity, as shown for the optical densities at 325 and 370 nm in Figure 4a. This increase is larger for the NHCN species. Its half-life also

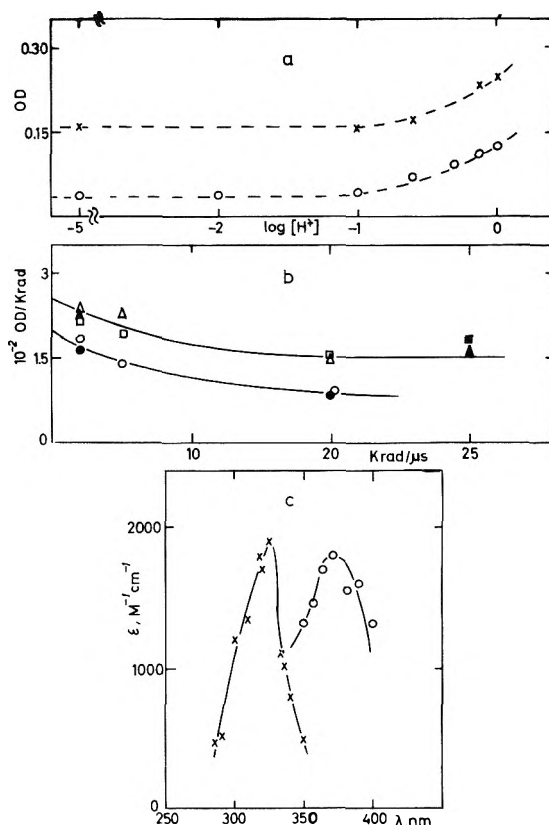
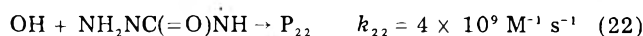


Figure 4. (a) The influence of acid concentration (HClO_4) on the transient absorption at 325 (upper curve) and 370 nm (lower curve). Cyanamide concentration 0.1 M, 20 krd. (b) The influence of the dose rate (1.8–25 krd in 1- μs pulse) on the transient absorptions at 325 nm measured at different concentrations of NH_2CN : □, 1 M NH_2CN , pH 5; ■, 1 M NH_2CN + 0.5 M HClO_4 ; △, 0.5 M NH_2CN , pH 5; ▲, 0.5 M NH_2CN + 0.5 M HClO_4 ; ○, 0.1 M NH_2CN , pH 5; ●, 0.1 M NH_2CN + 0.5 M HClO_4 ; for comparison the plotted OD values for 0.5 M perchloric acid solutions are $0.91 \text{ OD}_{\text{meas}}$. (c) The absorption spectra of $\text{NH}_2\text{C}(\text{O})\dot{\text{N}}\text{H}$ (λ_{max} 325 nm) and NHCN (λ_{max} 370 nm).

strongly depends on the acidity: it decreases from 11 μs at pH 5 down to 2 μs in the presence of 1 M HClO_4 . These findings suggest a protonation of the radical $\text{NHCN} + \text{H}^+ \rightarrow {}^+\text{NH}_2\text{CN}$. The radical cation undergoes faster hydrolysis, which also may be seen from a comparison of k_{19} and k_{21} . A protonation of the radical produced in reaction 15, $\text{NH}_2\text{C}(\text{O})\dot{\text{N}}\text{H} + \text{H}^+ \rightarrow \text{NH}_2\text{C}(\text{O})^+\dot{\text{N}}\text{H}_2$, may explain the increase of the optical density at 325 nm, as well as a lower value of $2k_{20} = 4.6 \times 10^9 \text{ M}^{-1} \text{ s}^{-1}$ measured in the presence of 0.5 M HClO_4 .

Figure 4a shows that the pK of the transients formed in reactions 15 and 16 are shifted toward acidities higher than the pK value of solute itself, which is reported as 1.1.¹⁰ More work would be required for a better understanding of the acidity influence but the hydrolysis of cyanamide makes the interpretation of measurements difficult.

Reaction of OH with $\text{NH}_2\text{C}(\text{O})\dot{\text{N}}\text{H}$. The optical density at 325 nm depends both on the cyanamide concentration and on the dose rate as shown in Figure 4b. This dependence was observed both in neutral and acid media and with other solute concentrations as well. These variations in the hydroxyl radical adduct yield cannot be explained solely by an incomplete scavenging of the OH radicals, but must partly be attributed to a fast reaction of OH radicals with the radical adduct.



The rate constant for reaction 22 was derived by computer calculations, fitting reactions 1–8, 12–16, and 20–22 to the experimental values.

The Molar Extinction Coefficients for $H_2NC(=O)NH$ and $HNCN$. Figure 4c summarizes the absorption spectra and the molar extinction coefficients for the radicals produced by the reaction of hydroxyl radicals with cyanamide. They are mainly derived from the experimental data obtained with 4.6–20 krd per pulse and with 0.5 M NH_2CN solutions (pH 5). For the computations of the free radical concentrations, the reaction scheme included reactions 1–8, 12–16, and 20–22.

Concluding Remarks

(1) The results obtained in this work offer a fairly complete picture of the early stages of the radiolysis of NH_2CN in aqueous solutions at pH 5. When the proposed reaction scheme is used in computer simulation of the reaction mechanism, the computed rate curves agree with the experimental ones within 15%. This is considered a fair agreement because of the large range of experimental conditions under which the testing was carried out (1.85–26.7 krd/pulse, 0.025–1 M NH_2CN).

(2) This study shows that the cyano group in NH_2CN is the main point of attack by hydroxyl radical, hydrogen atom, and hydrated electron, as was the case for the $>C-CN$ molecules and various cyanides previously studied.

Acknowledgment. We thank the operator staff of the accelerator for their skillful assistance and O. Lang Rasmussen for supplying the computer program and performing the computations. We are also indebted to J. Holcman and E. Bjergbakke for many valuable discussions during the work.

References and Notes

- (1) I. Draganić, Z. Draganić, Lj. Petković, and A. Nikolić, *J. Am. Chem. Soc.*, **95**, 7193 (1973).
- (2) Z. D. Draganić, I. G. Draganić, and S. Jovanovic, submitted for publication.
- (3) K. Sehested, H. Corfitzen, H. C. Christensen, and E. J. Hart, *J. Phys. Chem.*, **79**, 310 (1975).
- (4) M. Anbar, M. Bambenek, and A. B. Ross, *Natl. Stand. Ref. Data Ser., Natl. Bur. Stand.*, No. 43 (1973).
- (5) L. M. Dorfman and G. E. Adams, *Natl. Stand. Ref. Data Ser., Natl. Bur. Stand.*, No. 46 (1973).
- (6) M. Anbar, Farhataziz, and A. B. Ross, *Natl. Stand. Ref. Data Ser., Natl. Bur. Stand.*, No. 51 (1975).
- (7) Z. D. Draganić and I. G. Draganić, *J. Phys. Chem.*, **77**, 765 (1973).
- (8) O. Lang Rasmussen, to be submitted for publication.
- (9) S. O. Nielsen, B. D. Michael, and E. J. Hart, *J. Phys. Chem.*, **80**, 2482 (1976).
- (10) S. Soloway and A. Lipschitz, *J. Org. Chem.*, **23**, 613 (1958).
- (11) E. Hayon, A. Treinin, and J. Wilf, *J. Am. Chem. Soc.*, **94**, 47 (1972).
- (12) P. Neta, V. Madhavan, H. Zemel, and R. W. Fessenden, *J. Am. Chem. Soc.*, **99**, 163 (1977).
- (13) J. Holcman and K. Sehested, *J. Phys. Chem.*, **80**, 1642 (1976).

Reactions of Iodine with Olefins. 5. The Systematics of Electrophilic High Energy Iodine in Gaseous, High Pressure, and Liquid Isomers of Butene¹

Kar-Chun To, M. E. Berg, E. P. Rack*

Department of Chemistry, University of Nebraska, Lincoln, Nebraska 68588

General Medical Research, V. A. Hospital, Omaha, Nebraska 68105 (Received October 26, 1977)

Publication costs assisted by the U.S. Department of Energy

Reactions of high energy iodine with isomers of butene were studied in gaseous, high pressure, and condensed phase conditions, with rare gas additives and in the presence and absence of radical scavengers (I_2 and O_2). It was found that the *trans*-butene-2 system behaves as a hot system while *cis*-butene-2 and methylpropene (isobutylene) are dominated by I_2 -dependent ion-molecule reactions. The diverse and complex nature of the reactions cannot be explained by simple chemical and physical parameters. Comparison with other π -bond systems demonstrates the preferential attack of iodine at the double bond and results in the characterization of general traits common to these systems.

Introduction

Reactions of iodine-128 have been observed with alkane,^{2,3} alkene,^{4–8} and alkyne⁹ systems and it has been found to react via high energy, photochemical, and ion-molecule product formation routes. Unlike tritium and light halogens activated by nuclear transformations, iodine shows higher selectivity in olefinic systems, preferring electrophilic attack at or near the double bond. This attack often leads to the formation of a reaction complex which then further reacts via available mechanistic routes; e.g. decomposition, stabilization, abstraction, elimination, or biomolecular combination.

It has been recently reported that radiative neutron capture activated iodine-128 in reaction with butene-1

leads to the formation of six labeled organic products, many formed by complexation reactions.⁸ Greater than 70% of the total organic product yield formed at 1 atm was the result of attack at or near the double bond. This paper reports on the study of (n, γ)-activated ^{128}I with isomers of C_4H_8 throughout the gas to condensed phase transition, providing a probe of new reaction channels of high energy electrophilic iodine and demonstrating their dependence on molecular environment, experimental variations unavailable to other techniques.

Experimental Section

Materials. Research-grade xenon, helium, and krypton were obtained from Matheson Chemical Co. with stated purities of 99.995 mol % and were used without further purification. *cis*-Butene-2, *trans*-butene-2, methylpropene (Philips Petroleum Co. research grade with 99.94 mol %

* Address correspondence to this author at the Department of Chemistry, University of Nebraska.

purity), and trifluoroiodomethane (Pierce Chemical Co.) were used after repeated degassing on the vacuum line. Iodine was sublimed from a mixture of Mallinkrodt reagent grade I_2 , Baker reagent grade potassium iodide, and calcium oxide.

Preparation of Reaction System. A description of the techniques used to produce gaseous and condensed phase samples has recently been reported.^{10,11} High pressure gaseous samples were prepared by freezing 0.2 ± 0.01 Torr of iodine and 5 Torr of CF_3I into the ampoule followed by the measured quantity of butene. Rare gas additives used in 1-atm samples were filled in the customary manner.¹⁰

Liquid samples were prepared by first freezing known quantities of iodine (5.15×10^{-5} mole fraction) into the ampoule followed by a known quantity of butene.

All samples were filled in a dark room, wrapped in aluminum foil, and stored in liquid nitrogen until just prior to irradiation to prevent photoinduced reactions.

Neutron Irradiation. All irradiations were performed in the Omaha, Nebraska V.A. Hospital Triga reactor at a thermal neutron flux of 1.1×10^{11} neutrons $cm^{-2} s^{-1}$, and an accompanying γ ray flux of 3×10^{17} eV $g^{-1} min^{-1}$. The samples were irradiated from 0.5 to 30 min and extrapolated to zero irradiation time for correction of radiation damage. The liquid phase samples were irradiated at room temperature, immersed in ice water or dry ice. The density of the reaction mixture was determined by the method of Willard and Rice¹² and compared to literature values.^{13,14} To minimize thermal reactions of I_2 with butene, temperatures greater than room temperature were not attempted.

Extraction Procedure. After irradiation, the ampoules were broken in a separatory funnel containing 5 mL each of $CCl_4 + I_2$ and 0.5 M Na_2SO_4 solution. The organic and inorganic phases (3 mL each) were counted in an Ortec single channel analyzer employing a 3×3 in. NaI(Tl) detector. The samples containing xenon moderator were counted on a Harshaw 12.2% efficient Ge(Li) detector interfaced with a Nuclear Data 2400 1024-channel analyzer.

Radiogas Chromatographic Separations of the Activated Mixtures. The radiogas chromatograph used in this research has been previously described in detail.^{10,11} The column used was a 3-mSS coil containing 5% by weight di-(2-ethylhexyl) sebacate on 50/60 mesh firebrick. Linear temperature programming from 25 to 130 $^{\circ}C$ was employed for gaseous samples together with a mixture of known carrier composition which was simultaneously injected into the helium stream. Liquid phase samples were directly injected into the chromatograph by employing the preinjection freeze-controlled-thaw technique.¹⁰

Individual organic product yields were determined by triplicate radiogas chromatographic runs. Integration of the chromatograms gave relative yields which were normalized to the total organic product yield to give the absolute individual organic yields (IOPY)¹⁵ for a particular mole fraction additive. A radiation dose curve as established for each sample condition by evaluating yields for 0.5-, 1.0-, 2.0-, 5.0-, 10.0-, 15.0-, 20.0-, and 30.0-min irradiations. Extrapolation to zero irradiation time produced TOPY¹⁵ and IOPY values corrected for radiolytic contributions.

All the products reported in this paper showed a decrease in yield (with the exception of i - C_4H_9I in the methylpropene system) with increase in irradiation time. Butyl iodides were also observed in the *cis*-butene-2 and *trans*-butene-2 systems. However, their yields extrapolated to zero at zero time of irradiation. No attempt was made

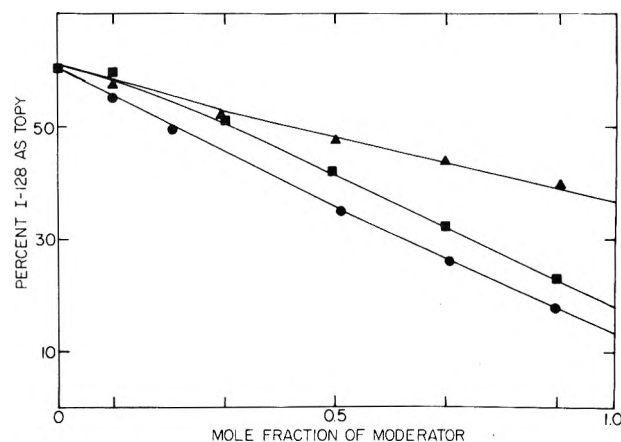


Figure 1. Effect of rare gas additives on total organic product yield at 1 atm (*cis*-butene-2); helium (●); krypton (■); xenon (▲).

to analyze the inorganic products $H^{128}I$ produced by abstraction or $^{128}I-I$ by thermal exchange with the scavenger due to the rapid exchange between I_2 and HI .

Results and Discussion

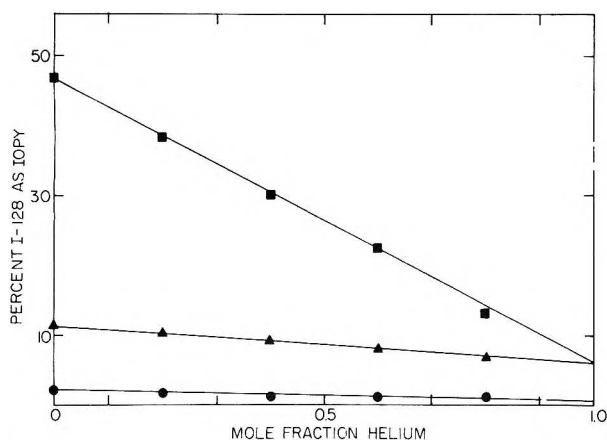
The characteristics of radiative-neutron capture iodine-128 have been reported.⁹ The translational spectrum of ^{128}I ranges from 0 to 194 eV with a most probable value of 152 eV.¹⁶ Greater than 50% of the iodine born via the (n, γ) process are charged and at least 25% is in excited electronic states.^{17,18} The isomers of butene have several characteristics that make them ideally suitable for study. They are experimentally easy to work with and provide π bond and multiple σ bond sites for iodine attack. More importantly, butene-1, methylpropene, *cis*-butene-2, and *trans*-butene-2 have the same molecular weight, a narrow range of ionization potentials (a range of 0.6 eV),¹⁹ and many other properties that show only minor variations in the series. The only major variation in the series is structural.

The *cis*-Butene-2 System. The total organic product yield of iodine-128 with *cis*-butene-2 in the 1-atm unmoderated system is found to be $60.5 \pm 2.2\%$. Three products are observed: CH_3I (47.0%), C_2H_5I (11.5%), and C_2H_5I (2.0%). O_2 is often added to systems as a radical scavenger; however, at 0.1 mole fraction O_2 additive the organic product yield is $59.0 \pm 2.0\%$, equal within experimental error, to that of the I_2 scavenged 1-atm system. Both O_2 and I_2 are radical scavengers. In all systems containing oxygen additive, I_2 was also present. Even if the O_2 and I_2 reaction rates with radicals are different as we may expect, we would expect the addition of 10 mole % O_2 to the system would be sufficient to scavenge a significant radical population. Therefore, since the addition of O_2 has no effect on the organic product yield, we suggest there are no major product formation routes that are radical in nature in the *cis*-butene-2 system.

The removal of I_2 from the reaction system has a more profound effect. Unlike "normal" systems where I_2 acts as a radical scavenger, the total organic product yield is reduced to $29.9 \pm 3.5\%$, the major reduction being in the CH_3I (to 19.7%) and the complete suppression of C_2H_5I . This is similar to the $^{128}I-C_2H_4$ system,⁷ where Pettijohn and Rack found ion-molecule reactions to occur that were dependent on the formation of $^{128}I-I^+$ as the initiation step of the reaction mechanism. Pettijohn and Rack also reported an inverse trend in moderator behavior, not normally associated with hot reactions. As can be seen in Figure 1, a similar trend occurs in the ^{128}I -*cis*-butene-2 system where moderation occurs in the order $Xe < Kr <$

TABLE I: Total and Individual Organic Product Yields for the *cis*-Butene-2-Iodine-128 System

ρ , g cm ⁻³	λ/σ	TOPY	CH ₃ I	C ₂ H ₃ I	C ₂ H ₅ I
0.002 (1 atm)	12.65	60.5 ± 2.2	47.0	11.5	2.0
0.007 (3 atm)	8.74	53.4 ± 1.1	42.4	11.0	
0.62 (liq, 23 °C)	1.95	45.2 ± 3.3	33.9	11.3	
0.64 (liq, 0 °C)	1.92	50.3 ± 2.0	21.4	28.9	
0.73 (liq, -78 °C)	1.85	53.2 ± 2.0	33.0	20.2	
Absence of I ₂ at 1 atm		29.9 ± 3.5	19.7	10.2	
10 mole % O ₂ at 1 atm		59.0 ± 2.0			

Figure 2. Effect of mole fraction helium on individual organic product yields at 1 atm (*cis*-butene-2): CH₃I (■); C₂H₃I (▲); C₂H₅I (●).

He. Important to the development of a proposed reaction scheme, which is consistent with the experimental data, is the postulation of an ion-molecule mechanism whose basic premise is that ¹²⁸I ions will exchange atoms with I₂ originally proposed by Pettijohn and Rack⁷ for iodine-128 reactions with ethylene and propylene (¹²⁸I⁺ + I₂ → ¹²⁸II⁺ + I) rather than simply charge transfer (¹²⁸I⁺ + I₂ → ¹²⁸I + I₂⁺). While we would expect charge exchange rather than the proposed ion-molecule mechanism, the only possible explanation that is consistent with the I₂-dependent data is the postulation of the iodine ion-molecule formation route.

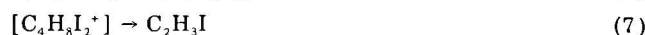
Figure 2 shows the individual organic product yields as a function of the mole fraction of helium. Ethyl iodide is completely suppressed at unit mole fraction He while the CH₃I product shows the greatest sensitivity. The IOPYs of C₂H₅I and C₂H₃I extrapolate to 0% at 0.2 and 0.4 mole fraction Kr, respectively. The C₂H₃I yield extrapolates to 0% at 0.6 mole fraction Xe while the C₂H₅I yield is completely suppressed in the presence of 0.2 mole fraction Xe. At unit mole fraction of Kr and Xe, the CH₃I yields are 17.0 and 37.8%, respectively.

Summarized in Table I is the variation of total and individual organic product yields with density. The total organic product yield decreases with increasing density reaching a minimum and then increasing. This is similar to the behavior of the major product, CH₃I. This decrease followed by an increase in product yield of CH₃I and the dependence of CH₃I formation on I₂ cannot be adequately explained by one reaction channel. It is apparent that more than one product formation route is involved in the formation of the CH₃I product. Similar density behavior has been reported by Loberg et al. for ¹²³I with CH₄ where ion-molecule reactions were found to predominate.²⁰

Vinyl iodide exhibits only minor dependence on I₂ and has an approximately constant yield from the 1-atm gas point into the liquid state. Only at higher liquid densities does a product yield increase occur suggesting that vinyl iodide is formed via a hot mechanism which enhances in

the liquid state. The complete disappearance of C₂H₅I in the absence of I₂ and in high pressure gaseous and liquid phase samples and the minor yield observed at 1 atm suggests that ethyl iodide is formed via a reaction intermediate that requires considerable rearrangement and which has a lifetime long compared to the collision frequency in systems at larger pressures than 1 atm.

Consistent with these observations we propose the following reaction scheme:²²



Reactions involving ¹²⁸I may be either direct (1-4) or proceeding via the formation of I₂ (5) in reactions similar to those proposed by Pettijohn and Rack. For all the butenes, the ionization potentials are lower than that of I⁺ so charge exchange is possible. Ion-molecule reactions involving I⁺ directly with butene molecules cannot be dismissed on charge exchange arguments alone.

Methyl iodide may be formed by attack at a terminal methyl group (1), decomposition of a reaction intermediate or an I₂ ion-molecule reaction. Vinyl iodide may be formed via a reaction intermediate or from I₂-dependent ion-molecule reactions while ethyl iodide is solely the results of I₂-dependent reactions. The I₂-dependent ion-molecule reactions are similar to those proposed by Pettijohn and Rack.⁷ The initiation step involves the reaction of ¹²⁸I with I₂ to form ¹²⁸I-I⁺ (5). This reaction must be the limiting step in I₂ ion-molecule reaction since the lower mole fraction of I₂ in high pressure gaseous and liquid phase samples shows an initial decrease in organic product yields. The I₂⁺ then reacts with a *cis*-butene-2 molecule to form a reaction complex which further reacts to form products.²³ We cannot experimentally determine whether this complex reacts alone or in combination with another C₄H₈ molecule ([C₄H₈I₂]⁺ + C₄H₈ → products), but the presence of C₂H₅I at 1 atm suggests the occurrence of complex rearrangements which cannot be explained by the complex reacting alone.

Vinyl iodide shows little dependence on I₂ and most likely proceeds through a reaction intermediate (2). The formation of this intermediate by cleavage of the π bond would appear radical in nature, but O₂-additive data suggest no radical reactions. The reaction intermediate may be very short-lived (lifetime less than the collision frequency), proceeding via hydrogen migration to form the observed products. It should be noted that CH₃I is a decomposition product of this intermediate which, al-

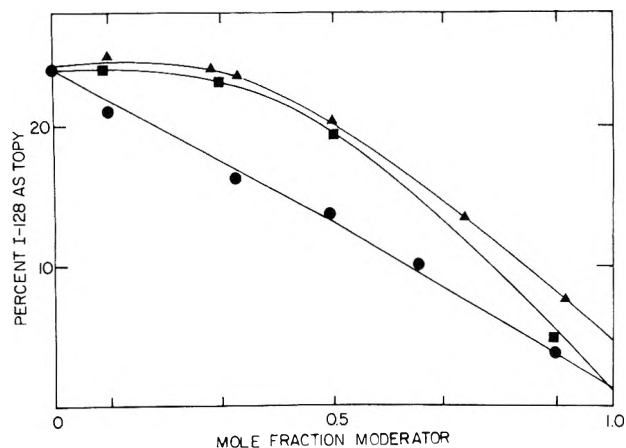


Figure 3. Effect of rare gas additives on total organic product yield at 1 atm (*trans*-butene-2): helium (●); krypton (■); xenon (▲).

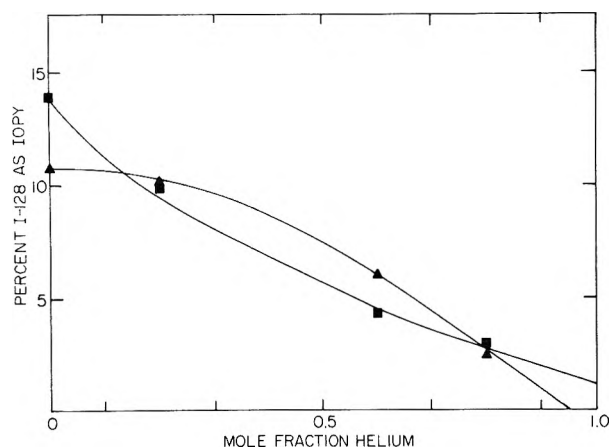


Figure 4. Effect of mole fraction helium on individual organic product yields at 1 atm (*trans*-butene-2): CH₃I (■); C₂H₅I (▲).

though decreasing with increasing pressure as observed, cannot explain the increase of CH₃I yield in the highest density condensed phases. The proposed reaction intermediate (2), while involving only internal migrations, is sensitive to the molecular environment. This sensitivity is most likely the result of nonreactive stabilizing collisions with the vibrationally excited product.

The *trans*-Butene-2 System. Iodine-128 is organically bound in the 1-atm *trans*-butene-2 system to the extent of $23.8 \pm 0.4\%$ and, as seen in Figure 3, exhibits the same moderator trend (Xe < Kr < He) as observed in the *cis*-butene-2 system. No reduction in total organic product yield is observed in the presence of 10 mol % O₂; however, counter to the *cis*-butene-2 system, an increase in organic yield (to $29.9 \pm 3.5\%$) is observed in the absence of I₂. It is apparent that, contrary to the moderator data, no I₂-dependent ion-molecule reactions occur. Figure 4 shows the variation of vinyl iodide and methyl iodide yields with mole fraction of He. The methyl and vinyl iodide yields decrease with increase mole fraction of the rare gas additives Kr and Xe with vinyl iodide showing "normal" behavior (He < Kr < Xe) and inverted behavior for methyl iodide.

This apparently paradoxical problem of moderator trends is resolved by noting the gas to condensed phase transition data (Table II). The vinyl iodide yield increases throughout the entire gas to condensed phase transition showing hot reaction and enhancement. The methyl iodide yield decreases and disappears in the condensed phase. The anomalous behavior observed under moderated 1-atm conditions is the result of CH₃I being formed via a decomposition reaction.

TABLE II: Total and Individual Organic Product Yields for the *trans*-Butene-2-Iodine System

ρ , g cm ⁻³	λ/σ	TOPY	CH ₃ I	C ₂ H ₅ I
0.002 (1 atm)	15.04	23.8 ± 0.4	13.6	10.2
0.007 (3 atm)	7.85	36.2 ± 1.5	9.4	26.8
0.60 (liq, 23 °C)	1.77	37.9 ± 2.1		37.9
0.63 (liq, 0 °C)	1.75	42.3 ± 1.3		42.3
0.71 (liq, -78 °C)	1.68	43.8 ± 0.4		43.8
Absence of I ₂ at 1 atm		29.9 ± 3.5		
10 mol % O ₂ at 1 atm		23.7 ± 1.4		

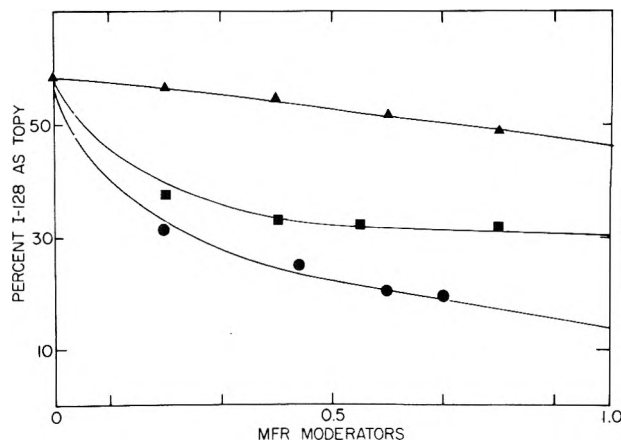


Figure 5. Effect on rare gas additives on total organic product yields at 1 atm (methylpropene): helium (●); krypton (■); xenon (▲).

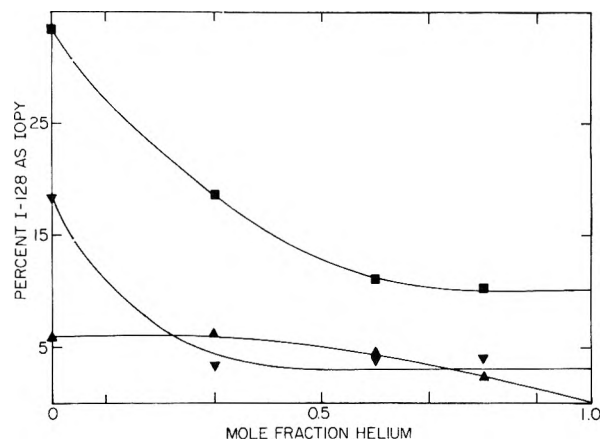


Figure 6. Effect of mole fraction helium on individual organic product yields at 1 atm (methylpropene): CH₃I (■); C₂H₅I (▼); *i*-C₄H₉I (▲).

trans-Butene-2 would appear to proceed via a short-lived reaction intermediate analogous to the *cis*-butene-2 reactions (2-4):

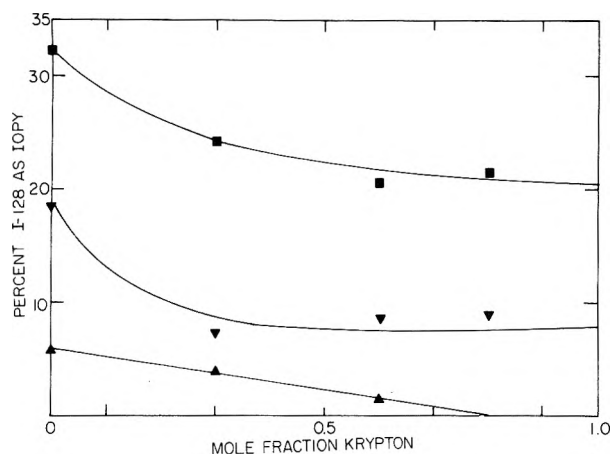
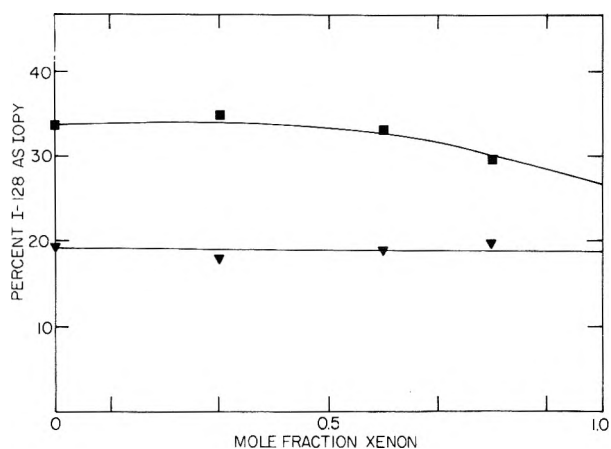


while it may be tempting to ascribe part of the CH₃I yield to direct attack by I at a terminal CH₃ group, this would result in a product whose yield should increase or remain constant throughout the gas to condensed phase transition. Only a decomposition mode would show the negative pressure dependence observed.

The Methylpropene System. Presented in Figures 5-8 are the effects of rare gas additives on the total and individual organic product yields of the iodine-128-methylpropene system.²¹ An inverse moderator trend is again observed where Xe < Kr < He. Three organic products are observed in the 1-atm unmoderated system:

TABLE III: Total and Individual Organic Product Yields for the Methylpropene-Iodine-128 System

ρ , g cm ⁻³	λ/σ	TOPY	CH ₃ I	C ₂ H ₅ I	<i>i</i> -C ₄ H ₉ I
0.002 (1 atm)	15.66	58.4 ± 1.2	33.8	18.7	5.9
0.007 (3 atm)	10.86	54.7 ± 3.7	32.8	17.7	4.2
0.59 (liq, 23 °C)	2.46	26.7 ± 1.1	11.2	12.3	3.2
0.62 (liq, 0 °C)	2.43	32.5 ± 2.3	24.4	6.5	1.6
0.70 (liq, -78 °C)	2.33	46.2 ± 0.7	41.1	5.1	
Absence of I ₂ at 1 atm		26.2 ± 2.3	25.4	0.4	0.4
10 mol % O ₂ at 1 atm		45.1 ± 2.8			

Figure 7. Effect of mole fraction krypton on individual organic product yields at 1 atm (methylpropene): CH₃I (■); C₂H₅I (▼); *i*-C₄H₉I (▲).Figure 8. Effect of mole fraction xenon on individual organic product yields at 1 atm (methylpropene): CH₃I (■); C₂H₅I (▼).

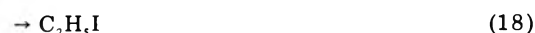
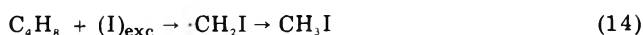
viz., CH₃I (33.8%); C₂H₅I (18.7%); and *i*-C₄H₉I (5.9%), summing to a total organic product yield of 58.4 ± 1.2%. The removal of I₂ at 1 atm results in a reduction of yield to 26.2 ± 2.3%, again suggesting the presence of I₂ dependent ion-molecule reactions. Only trace quantities, approximately equal to zero within the limits of error, are found for ethyl iodide and isobutyl iodide suggesting that they are formed entirely by these I₂ sensitive reaction channels. The addition of 0.1 mole fraction of O₂ also suppresses the organic product yield to 45.1 ± 2.8%. Examination of Figure 5 shows that the O₂ suppression is approximately equal to that expected by kinetic energy moderation (the point falls between the Kr and He curves) but, since kinetic theory cannot be rigorously applied to iodine systems, some doubt may exist as to the suppression being entirely due to kinetic energy moderation or a combination of moderation and radical suppression.

The data in Table III show the effect of collapsing molecular environment on the total and individual organic product yields. Similar to the *cis*-butene-2 systems there

is an initial decrease in total organic product yield with increasing density followed by an increase in yield in the condensed state. The product yield of CH₃I follows an identical trend. Ethyl- and isobutyl iodide display a decrease in yield with *i*-C₄H₉I disappearing in the highest density system.

This decrease in C₂H₅I and *i*-C₄H₉I yields is suggestive of decomposition reactions, but, as strictly the result of I₂-dependent reactions, cannot be the result of the decomposition of a short-lived reaction intermediate, as in *trans*-butene-2 (hot reaction), or from a persistent reaction complex as in acetylene or butene-1 systems.^{8,9} Furthermore, the decomposition of an I₂-dependent complex of the type [C₄H₈I₂]⁺ is not feasible since the *i*-C₄H₉I product would be the result of a stabilization reaction and the C₂H₅I product can only be formed via extensive rearrangement, most probably requiring a second methylpropene molecule. The decrease in yield of these two products must be the result of kinetic and/or dynamic restrictions which are functions of molecular environment. For example, in the formation of the reaction initiator ¹²⁸I⁺, the use of a constant quantity of I₂ in the gaseous and high pressure samples results in a decrease in the mole fraction of I₂, reducing the relative concentration of the reactant. Additionally, if directed attack on an olefinic molecule is a necessity for the formation of an I₂-olefin complex (it appears that attack at the double bond is required), the interposition of nonreacting molecules between the I₂⁺ and the ultimate target molecule results in the narrowing of the successful attack angle, the equivalent of a reduction in reactive cross section.

Methyl iodide is the only product which has both I₂-dependent and nondependent product formation routes. Since the O₂ additive data are inconclusive, the data do not provide sufficient evidence of a "radical" formation route for CH₃I. However, in considering possible product formation routes, we must include the radical formation routes for CH₃I in the reaction scheme. These reaction routes would show the necessary enhancement increase in the condensed phase that would result in an increase in the organic product yield. The proposed scheme is



The Systematics of Iodine-128 Attack on π -Bond Systems. From previous studies of reactions of radiative neutron capture iodine with π -bond systems^{4,5,7} it is known that iodine reactions are diverse and complex. cursory examination of these iodine- π bond systems shows no systematic trend with simple chemical or physical pa-

TABLE IV: CH₃I Organic Product Yields for the 1-atm Unmoderated System

Originating system	Total CH ₃ I yield	Direct I ₂	IM ^c	Radical	De-com-position
Ethene	10.0	8.0	2.0		
Propene	18.7	Yes ^a	Yes ^a		
Methylpropene	33.8	12.1	8.4	13.3 ^b	
1-Butene	8.6	3.0		5.6	
cis-2-Butene	47.0	19.7	27.3		
trans-2-Butene	13.8				13.8
Ethyne	0.49				0.49

^a No attempt had been made to separate the two components. ^b There may be a radical component to CH₃I formation in methylpropene or the 13.5% reduction may be the result of kinetic energy moderation on a direct product formation route. ^c Ion-molecule.

rameters. For the purpose of close examination of the reactions of iodine-128 the isomers of butene were chosen to minimize the effects of simple parameters other than structure.

By comparison with previous studies of ethene,⁷ propene,⁷ butene-1,⁸ and acetylene,⁹ the following trends become apparent: (1) for olefins through the isomers of butene, direct substitution products (I for H) only occur for straight chain olefins with terminal methylene groups, and, furthermore, substitution occurs at the π -bond site. (2) When I₂-dependent ion-molecule reactions occur, the magnitude of the I₂-dependent organic product yield is approximately equal to the I₂-independent organic yield. (3) For all π -bond systems the product CH₃I is formed, the magnitude of the yield increasing with the number of carbons. However, as can be seen in Table IV, CH₃I is formed by a variety of reaction mechanisms (hot or thermal direct, I₂-dependent ion-molecule, radical and/or decomposition) even in the same system.

Of major importance is the experimental evidence that recoil iodine is electrophilic in nature. Unlike tritium and fluorine-18, born with energies near the MeV range, radiative neutron capture activated iodine-128 displays preferential attack at or near the π bond of olefinic systems. We have observed in the isomers of butene preferential attack at or near the π bond of the following magnitudes: methyl propene, >55%; cis-butene-2, >65%; butene-1, >70%; and trans-butene-2, ~100%. These magnitudes are greater than the 25-50% predicted by nonselective attack and demonstrate the importance of chemical considerations in the prediction of high energy reactions.

While the isomers of butene were originally chosen to observe the effect of structure on the reactions of iodine, the only simple parameter which can be correlated to the product distribution is the center of mass of the butene isomers. Organic products containing four carbons are only observed for the butene-1 and the methylpropene systems. For cis- and trans-butene-2 systems only one and two carbon products are observed. This trend is not related to I₂-dependent reactions since, in both cases, one system is hot while the other is hot and ion-molecule in nature. It should be noted that in the cases of methylpropene and butene-1 the center of mass lies outside the limits of the π bond. Therefore, attack by iodine at the double bond will lead to energy transfer into rotational modes of the molecular or newly formed complex. For the butene-2 isomers the center of mass lies on the double bond or along the line bisecting the double bond (and lying in the molecular plane) such that attack by iodine at the double bond cannot generate the torsional strain possible in the

former case. Energy transfer must go primarily into translational modes or into vibrational excitation which results in π -bond scission.

While such arguments may explain the carbon chain lengths of the observed products, no simple single parameter argument can adequately describe the general lack of substitution products and the general distribution and abundances of the various products. We feel the reactions of recoil iodine with π -bond systems is the result of a composite of chemical and physical parameters, often of a subtle nature, which are intrinsic to the individual target molecules. The diversity of products suggests that while iodine is electrophilic, preferentially attacking the electron rich π bond(s), the chemical and physical nature of the target molecule ultimately determines the type of reactions and the products formed.

Summary

While the reactions of high energy iodine with olefins are complex, the following observations can be made:

- (1) There is no simple systematic trend with chemical and physical parameters. The impact and inertial models are not applicable in these systems.
- (2) I₂-dependent ion-molecule reactions may show an inverse trend with rare gas additives.
- (3) Preferential site attack by iodine occurs at the double bond for short chain olefins.
- (4) Organic products may be formed by diverse reaction channels.
- (5) For I₂-dependent ion molecule reactions the CH₃I yield increases with carbon chain length.
- (6) Collapsing molecular environment decreases the attack angle on the π bond by interposition of bath molecules.
- (7) When the center of mass is centered on, or along the line bisecting the double bond, attack at the double bond results in bond cleavage and/or molecular translation rather than rotation.

The preferential electrophilic attack by iodine on the π bond allows the use of bulb techniques as a probe of new high energy reaction channels, not easily observed by other chemical techniques.

References and Notes

- (1) This research was supported by the United States Department of Energy Contract No. EY-76-S-02-1617*000. This is ERDA document No. C00/1617-54.
- (2) E. P. Rack and A. A. Gordus, *J. Chem. Phys.*, **34**, 1855 (1961).
- (3) J. F. Horning, G. Levey, and J. E. Willard, *J. Chem. Phys.*, **20**, 1556 (1952).
- (4) R. L. Ayres, O. C. Gadeken, and E. P. Rack, *J. Phys. Chem.*, **75**, 2880 (1971).
- (5) R. L. Ayres, C. J. Michejda, and E. P. Rack, *J. Am. Chem. Soc.*, **93**, 1389 (1971).
- (6) A. Loventhal, M. Kim, and E. P. Rack, *Radiochim. Radioanal. Lett.*, **26**, 239 (1976).
- (7) R. P. Pettijohn and E. P. Rack, *J. Phys. Chem.*, **76**, 3342 (1972).
- (8) K.-C. To, M. E. Berg, and E. P. Rack, *J. Phys. Chem.*, **81**, 1239 (1977).
- (9) K.-C. To, M. E. Berg, and E. P. Rack, *J. Phys. Chem.*, **80**, 1411 (1976).
- (10) M. E. Berg, A. Loventhal, D. J. Adelman, W. M. Grauer, and E. P. Rack, *J. Phys. Chem.*, **81**, 837 (1977).
- (11) M. E. Berg, W. M. Grauer, R. W. Helton, and E. P. Rack, *J. Phys. Chem.*, **79**, 1327 (1975).
- (12) W. E. Rice and J. E. Willard, *J. Am. Chem. Soc.*, **75**, 6158 (1953).
- (13) R. C. Wackler, C. B. Linn, and A. V. Grosse, *Ind. Eng. Chem.*, **37**, 464 (1945).
- (14) Technical Committee, National Gasoline Association of America, *Ind. Eng. Chem.*, **34**, 1240 (1942).
- (15) The total organic product yield (TOPY) is the fraction of I-128 activity organically bound and is equal to OA/(OA + IA) \times 100% where OA is the activity of the organic fraction and IA is the activity of the inorganic fraction of the extracted sample after corrections for isotopic decay. Individual organic product yield (IOPY) values represent the fraction of activity chemically bound with a specific organic substrate. Integration of radiogas chromatographic peaks, corrected for isotope decay and radiolytic contributions and normalized to the TOPY value.

- are used in the assignment of these values.
- (16) M. Yoong, Y. C. Pao, and E. P. Rack, *J. Phys. Chem.*, **76**, 2685 (1972).
- (17) T. A. Carlson and R. M. White, *J. Chem. Phys.*, **44**, 4510 (1966).
- (18) S. Wexler and H. Davies, *J. Phys. Chem.*, **20**, 1688 (1952).
- (19) R. W. Kiser, "Tables of Ionization Potential", U.S. Atomic Energy Commission, Office of Technical Information, No. TID-6142, 1960.
- (20) M. D. Loberg, K. A. Krohn, and M. J. Welch, *J. Am. Chem. Soc.*, **95**, 5596 (1973).
- (21) The IOPY of $i\text{-C}_4\text{H}_9\text{I}$ in the methylpropene system was found to be 2.03% at 0.3 mole fraction of Xe and diminished to 0% at 0.6 mole fraction of Xe.
- (22) The reaction schemes proposed are not detailed definitive mechanisms but suggested routes consistent with the experimental observations; while alternate mechanisms may be proposed, it is felt that, in light of current knowledge in iodine-olefin hot atom chemistry, no unambiguous mechanistic determination can be made.
- (23) No ion cyclotron resonance experiments were made because of the small differences in ionization potential of I_2 and the isomers of butene studied.

Tunneling Reactions of Trapped Electrons with Added Electron Acceptors in Alcohol Glasses at 77 K[†]

John R. Miller

Chemistry Division, Argonne National Laboratory, Argonne, Illinois 60439 (Received September 14, 1977)

Publication costs assisted by Argonne National Laboratory

The kinetics of reactions of several electron acceptors with trapped electrons in alcohol glasses at 77 K have been studied from 10^{-7} to 10^2 s by pulse radiolysis. In EtOH glass, where the traps progressively deepen with time, weak acceptors capture only the shallowly trapped electrons present at short times. Some strong acceptors react more readily with the deeply trapped, than with the shallowly trapped electrons. The observations are qualitatively rationalized in terms of long-range electron transfer (tunneling) reactions, the rates of which depend on Franck-Condon factors for overlap with vibrational states of the products. Spectral changes of the trapped electrons, which occur with or without added acceptors, are attributed to relaxation of the solvent around the electrons. The data do not support the concept that the electrons undergo any transport processes, aside from tunneling to electron-accepting impurities, on the time scale of these experiments.

I. Introduction

This paper explores the influence of energy on electron tunneling reactions by exploiting the time dependent trap depths of solvated electrons trapped in alcohol glasses. The electron solvation process effectively "sweeps" the exothermicity of the electron transfer reaction as a function of time. The results will be interpreted in terms of the effects of nuclear restrictions (e.g., Franck-Condon factors) on electron tunneling reactions. The results also support the concept that electron solvation occurs by dipole re-orientation around a stationary trapped electron (all localized electrons will be called trapped electrons, herein, no matter what their state of solvation).

"Electron tunneling reactions" described herein are electron transfers which occur at long distances, between species separated by tens of angstroms of inert solvent. Because the rates of these reactions depend very strongly on distance (typically the rate changes by a factor of 10 for each 1.5 Å change in distance between the reactants), a huge range of rates is observed when the reactants are randomly dispersed in rigid matrices. There is much evidence for these reactions¹ including observation of tunneling reactions over as many as ten orders of magnitude in time²⁻⁶ and implication of electron tunneling in photosynthetic electron transport.⁷

The rates of tunneling reactions of trapped electrons depend strongly on the nature of the acceptor, displaying large range of rates ($>10^{10}$).² The rates seem to depend very strongly on the difference between the energy which

binds the electron to the electron donor and the electron affinity of the acceptor.²

Electrons trapped in alcohol glasses reside initially in shallow traps and absorb light in the infrared, relaxing to deeper traps which absorb in the visible.⁸⁻¹² These relaxations deepen the traps over a wide time scale from nanoseconds to minutes,¹⁰⁻¹² and have interesting effects on the kinetics of electron tunneling reactions with acceptors added to the matrix.

II. Experimental Section

All of the experimental procedures have been described in ref 11 and its supplementary material, copies of which are available from the author. Reagent grade chemicals were used without additional purification. The molar concentrations given herein are for the matrices at 77 K. The room temperature concentrations were about 17% smaller. Samples were degassed and sealed off under vacuum in quartz cells. They were immersed in liquid nitrogen at least 5 min before use.

The samples were irradiated with 4-40 ns, 5 A pulses of ca. 15-MeV electrons. The analyzing light passed through a monochromator (bandwidth ≤ 10 nm full width at half-height) and a light chopper (5% "on") before reaching the sample to reduce photobleaching. Tests both in the pure matrices and in matrices containing scavengers showed that the data were unaffected by fivefold changes in light intensity. EMI 9781R and RCA 8852 (for $\lambda > 600$ nm) photomultiplier tubes were used in five-stage configurations. Data were digitized by a Biomation 8100 transient recorder, operated under control of the Chemistry Division's Sigma 5 computer. The yields of absorbance were reproducible to only $\pm 10\%$, but the reported results

[†] Work performed under the auspices of the Division of Physical Research of the U.S. Energy Research and Development Administration.

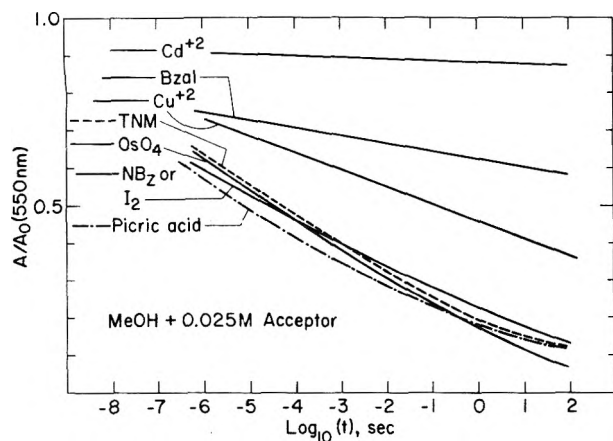


Figure 1. Reactions of trapped electrons in MeOH (+5% ethylene glycol) at 77 K. At each point in time the absorbance A in a sample containing electron acceptor is divided by the absorbance, A_0 , in a sample without added electron acceptors. The abbreviations used are listed in Table I.

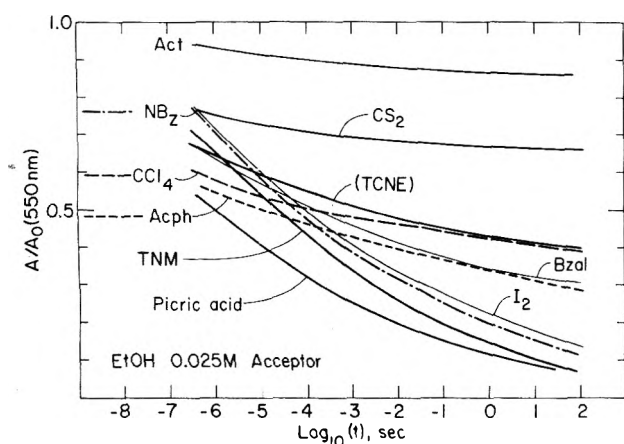


Figure 2. Reactions of trapped electrons in EtOH glass at 77 K. A and A_0 have the same meaning as in Figure 1.

are based on repeated experiments and the yields are believed to be accurate to $\pm 7\%$. The shapes of the decay curves were more reproducible.

III. Results

Spectral shifts during solvation of electrons in alcohol glasses cause the absorbance due to the electrons to grow in the visible and decay in the near-infrared. The largest growth occurs in EtOH glass, where the absorbance at 550 nm almost doubles between 10^{-7} and 10^2 s. Complete data are reported in ref 10–12. Methanol glass (which contained 5% ethylene glycol (EtG) to prevent crystallization) is unusual among alcohols in that the final (visible) absorption spectrum is almost fully formed at 10^{-8} s.¹¹ Figure 1 shows the decay of solvated electron absorbance due to several electron acceptors. To correct for the small growth of absorbance which occurs in MeOH glass without acceptors, we divide the absorbance (A) in the sample containing the acceptor by A_0 , the absorbance of MeOH glass without acceptor. This is done at each point in time. Thus we plot the fraction of solvated electrons which survive capture by the acceptor as a function of time. We use the same method in the other alcohols.

The reactions of acceptors with solvated electrons in MeOH glass (Figure 1) are very similar to reactions in aqueous glasses.^{2,3} We note especially that the several fastest reacting acceptors give almost identical decay curves. The situation in EtOH glass (Figure 2) is different. In EtOH glass the decay curves for the strong electron

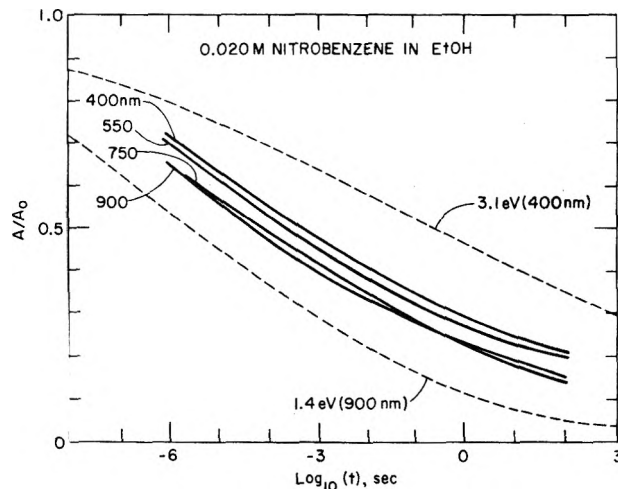


Figure 3. Decay of trapped electrons in EtOH at 77 K observed at different wavelengths as the electrons react with nitrobenzene. The stimulations, from eq 2 and 3 (dashed curves), are based on the extreme assumption that absorption at different wavelengths is due to different electrons, and that the observed photon energy is proportional to the trap depth.

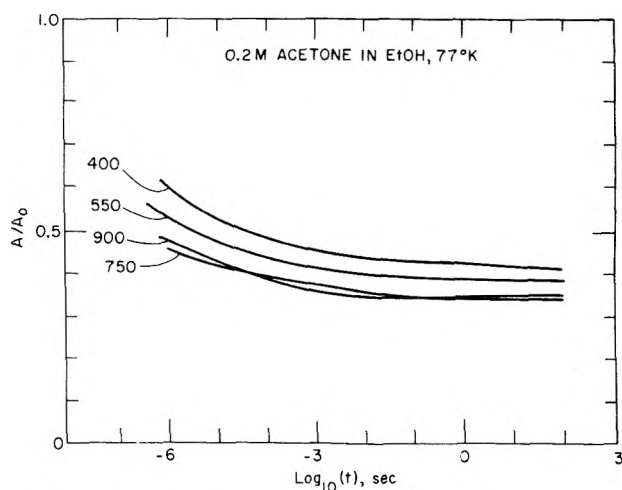


Figure 4. Decay curves at different observing wavelengths for reaction of trapped electrons in EtOH with the weak acceptor acetone.

acceptors nitrobenzene (NBz), I_2 , tetranitromethane (TNM), and picric acid are similar to each other and to the corresponding decay curves in MeOH only at long times ($t > 1$ s). At short times, when the electrons in EtOH are in shallow traps, picric acid captures a greater fraction of the electrons in EtOH than in MeOH. This is as expected, because the more shallowly trapped electrons in EtOH can tunnel further in a given period of time. However remarkably, the strong acceptors NBz, I_2 , and TNM capture fewer electrons at short times ($< 10^{-4}$ s) in EtOH than in MeOH. Apparently these strong scavengers react efficiently with deeply trapped electrons, but not as efficiently with shallowly trapped electrons. These effects can be rationalized in terms of Franck–Condon restrictions, which can slow a reaction because it is too exothermic.

Figures 1 and 2 show reactions measured at only one wavelength, at approximately the long time λ_{max} , although the spectra of the solvated electrons are broad in all matrices (≥ 1 eV at half-height) and change with time in EtOH and 2-PrOH (2-propanol) glasses. Figures 3–5 show how the decay curves are affected by the wavelength at which the absorbance is measured. There little effect of wavelength on the decay curve in EtOH (Figures 3 and 4) indicating that most of the electrons have similar trap depths at any given instant in time, even while the

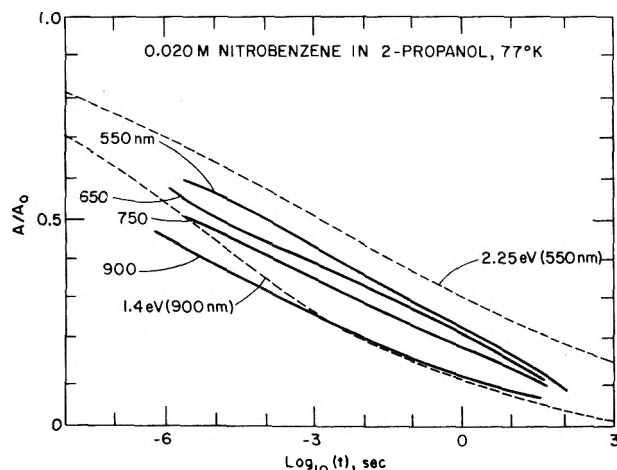


Figure 5. Decay of trapped electrons observed at different wavelengths as the electrons react with nitrobenzene in 2-PrOH glass at 77 K. The differences among the decay curves indicate that range of trap depths simultaneously present. The dashed curves have the same meaning as in Figure 3. The range of trap depths appears to be narrower than the range of photon energies in the absorption spectrum.

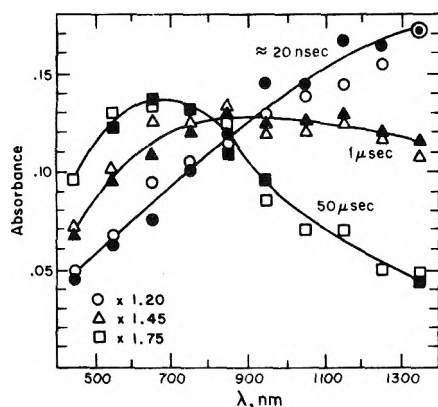


Figure 6. Data of Baxendale and Sharpe¹² replotted to demonstrate the invariance of the absorption spectrum of trapped electrons in EtOH at 77 K as benzyl chloride captures the electrons.

spectrum changes during solvation. The decay curves in 2-PrOH (Figures 5 and 7) are more sensitive to the wavelength of observation, indicating some dispersion of trap depths, with the shallower traps having red-shifted absorption spectra.

Similar data for the case of benzyl chloride have been obtained over a wider range of wavelengths.¹² Figure 6 shows data of Baxendale and Sharpe¹² replotted to show the invariance of the solvated electron's absorption spectrum as benzyl chloride (BzCl) captures electrons in EtOH glass at 77 K. Even when nearly half of the electrons have been captured by BzCl, the shape of the spectrum of e_t^- in 0.0174 M BzCl is identical, within experimental uncertainty, to the spectrum in pure EtOH. This agrees with the present results (Figures 3 and 4), which show decay curves that are nearly independent of wavelength. Baxendale and Sharpe¹² also studied the reaction of trapped electrons in 1- and 2-propanol, where the spectra¹² (not shown here) were altered as the electrons decayed. The spectral changes were greatest in 1-propanol, where the ratio of the far red absorbance (1300 nm) to the absorbance at the peak of the spectrum (~ 575 nm) decreased almost a factor of 2 at 1 s by the addition of 8.7 mM BzCl. It appears that trapped electrons are present in a fairly wide spectrum of trap depths in 1-PrOH, in contrast to EtOH.

Figure 7 shows decay curves for the weak acceptors CS₂ and phenol. As with acetone (Figure 4) these acceptors

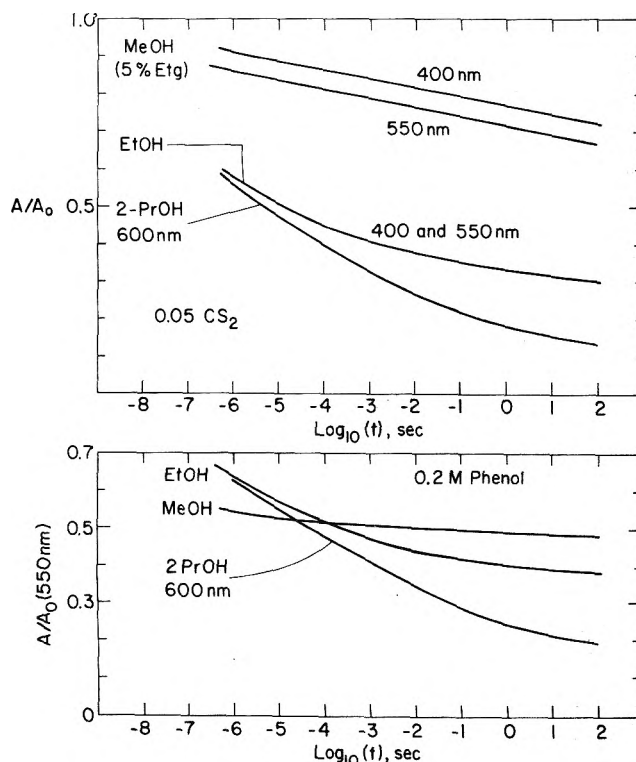


Figure 7. Decay of trapped electrons reacting with the weak acceptors (a) 0.05 M CS₂ and (b) 0.2 M phenol in alcohol glasses at 77 K. The reactions almost cease after the electrons become sufficiently solvated at $\approx 10^{-1}$ s in EtOH, $\approx 10^{-1}$ s in 2-PrOH, and $< 10^{-8}$ s in MeOH.

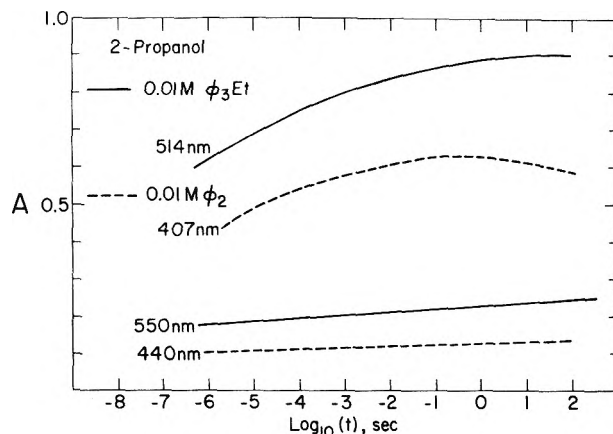


Figure 8. Growths of anions of biphenyl and triphenylethylene as these aromatic molecules capture trapped electrons in 2-PrOH at 77 K. The growths are monitored at the peaks of the anions. The figure also displays the absorbance at nearby wavelengths where the extinction coefficients of the anions are at least five times smaller, but the extinction coefficients of the trapped electrons are not greatly different.

are effective at capturing only the shallowly trapped electrons. As the traps deepen in EtOH and 2-PrOH, reaction with these acceptors slows greatly, and nearly ceases in some cases, leaving a sizeable fraction of the electrons unreacted. The remaining absorbances in these cases (e.g., acetone, CS₂, and phenol) are smaller if larger concentrations of the acceptors are used, and are readily bleached with visible light, indicating that the absorbances are due to solvated electrons.

Figure 8 shows the growths of anions of biphenyl (Ph₂) and triphenylethene (Ph₃Et) as these molecules capture solvated electrons in 2-PrOH by tunneling. The growth of Ph₂⁻ is relatively small because Ph₂ is a weak acceptor which reacts well only with the shallowly trapped electrons which are present at early times. The apparent growths of Ph₂⁻ and Ph₃Et⁻ would both be larger were it not for

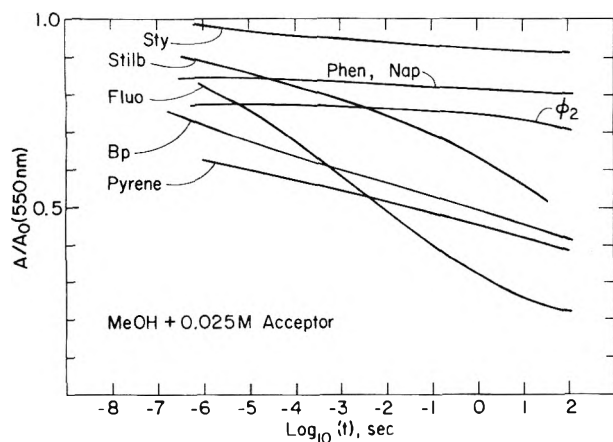


Figure 9. Decays of trapped electrons reacting with various aromatic molecules in MeOH at 77 K. The decay curves have been corrected for the growing absorbance due to anions of the aromatics. The abbreviations are given in Table I, except for biphenyl, which appears as Ph_2 there.

decay of these anions due to protonation by the solvent and transfer of the electrons to positive charge or other radiation products.⁶ Kevan reported that Ph_2^- did not grow under similar conditions,⁹ but his data covered a much narrower range of time. In the present work, the anions of pyrene and Ph_3Et were also observed to grow in EtOH glass.

Figure 9 shows reaction of several aromatic molecules with solvated electrons in MeOH glass. Most of these aromatics do not have sufficient electron affinity to react efficiently with the deeply trapped solvated electrons in MeOH glass.

Discussion

A. Literature Review and List of Conclusion to be Drawn. Solvated electrons in alcohol glasses are useful for the study of electron transfer reactions, particularly to determine the role of energy in determining the reaction rates. For this use of solvated electrons, we must understand their nature, which is in dispute. It is generally agreed⁸⁻¹² that the near-infrared spectra observed at short times ($\leq 10^{-5}$ s) in EtOH, 1-PrOH, and 2-PrOH at 77 K are due to shallowly trapped electrons, and that the spectra peaking in the visible at long times (> 1 s) are due to deeply trapped electrons. Most workers assume that the trap depths are approximately equal to the size of the absorbed quanta. It is not known whether the spectra are very broad because each electron has a broad spectrum ("homogeneous broadening"), or because many different electrons absorbing at different wavelengths combine to produce a broad spectrum ("heterogeneous broadening"). Neither is it known whether the electrons reorient solvent molecules to "dig" deeper traps, or move about "seeking" deeper, preformed traps. Walker¹³ has recently reviewed the "diggers" vs. "seekers" and homogeneous vs. heterogeneous broadening questions. The diggers-seekers question is closely related to the mechanism of reaction with solutes. Thermally activated "trap hopping"¹² and "trap to trap tunneling"¹⁴ have been suggested to explain reactions with solutes as well as spectral changes which occur in the absence of solutes. These are presently only rough concepts which have not yet led to well-defined models.^{12,14} Both of these concepts are rejected here, for the reasons given below.

It is concluded that electrons, once localized in alcohol glasses, are immobile, except for the possibility of tunneling directly to an electron acceptor added to the matrix. The rates of these tunneling reactions are controlled by

well-known principles of outer-sphere electron transfer. The reactions serve as tests of electron transfer theories with three unusual features: (1) fixed distances (no diffusion), (2) low temperature, (3) the energy of the donor state varies with time as the electrons solvate. The electrons dig deeper traps by reorienting nearby solvent molecules. This reorientation process is gradual, taking many orders of magnitude change in time to deepen the traps by about a factor of about 2. In EtOH at intermediate times, most of the electrons are at the same stage of the solvation process, and have very similar trap depths. The spectra are therefore homogeneously broadened, in the limited sense, that the breadth of the spectra are not due to different trap depths. In 1-PrOH, and to a lesser extent in 2-PrOH, a substantial range of trap depths contributes to the widths of the spectra.

The ways in which the present data and data of other workers point out to these conclusions will be described below.

B. The Nature of Electron Solvation and Reactions.

1. Evidence Against Trap Hopping Mechanisms. It is tempting to explain both the spectral shifts and electron capture by solutes in rigid alcohol glasses by one mechanism: that electrons hop into successively deeper, preexisting traps. The conceptual difficulties with such a mechanism would seem nearly to rule it out a priori, as will be discussed below. Conflicts of trap hopping mechanisms with present experimental data and data of other workers will be described first.

Figures 1-7 show that, as in aqueous glasses,² the time required to capture a given fraction of the deeply trapped electrons is longer by a factor of at least 10^8 , for many of the weak acceptors, than for the strong acceptors. This is true for several acceptors (biphenyl, naphthalene, acetone, CS_2 , CCl_4 , phenanthrene, and Cd^{2+}) which react at nearly diffusion-controlled rates with solvated electrons in liquid alcohols. The weak acceptors often react only with the shallowly trapped electrons present at short times, while strong acceptors react with deeply trapped electrons as well. The "reaction radii" for weak acceptors listed in the trap to trap tunneling model¹⁴ could not be independent of time as Buxton assumed,¹⁴ but would have to decrease to unreasonably small values, less than 1 Å, at long times ($t > 10^{-3}$ s in EtOH glass and over our whole time region in MeOH glass). Clearly the direct interaction between the trapped electron and the acceptor molecule is most important, not the rate of trap to trap hopping, which should be unaffected by the nature of the acceptor.

This is also indicated by studies at very low temperatures, where the spectral shifts are greatly slowed. The shallow, infrared absorbing electrons in EtOH, which disappear on the microsecond time scale at 77 K, are stable to at least minutes at 4 K.^{15,16} However benzyl chloride, a weak acceptor, captures electrons much more effectively at 4 K than at 77 K.¹⁸ This result is readily understood in terms of tunneling, because the shallowly trapped electrons live longer, and thus can tunnel farther at 4 K. If "trap hopping" were responsible for the spectral changes and the reactions with solutes, then these processes should not have been affected oppositely by a temperature change. The data of Higashimura and co-workers¹⁸ also provide interesting evidence that relaxation processes, which are inhibited at least for minutes at 4 K, are necessary to develop the optical absorption spectrum of the benzyl radical ($\text{Bz}\cdot$). Thus the absorbance of $\text{Bz}\cdot$ is an unreliable measure of electron capture by BzCl . This may have contributed, along with the inability of this weak acceptor to react efficiently with deeply trapped electrons, to

failures to observe growth of the absorbance of $Bz\cdot$ in pulse radiolysis experiments.^{9,12,17}

Furthermore, the present data show that reactions with strong acceptors in EtOH persist after 1 s, when the spectral changes are very slow and nearly complete. In addition in MeOH, where there is little spectral change over the entire time range (10^{-7} to 10^2 s), the reactions with strong acceptors are as rapid as those in EtOH, where large spectral shifts are occurring. A large amount of spectral shift in a given time range is not correlated with increased reactivity with solutes in that time range, providing further evidence favoring long-range tunneling over trap-hopping mechanisms.

A special example of long-range tunneling is the intermolecular electron transfer from biphenyl anions to triphenylethylene molecules in EtOH glass.⁶ Because all the trapped electrons were captured by biphenyl before 10^{-6} s, the kinetics of the intermolecular electron transfer process cannot be attributed to electrons hopping around into progressively deeper traps in the matrix. The kinetics of this intermolecular electron tunneling process⁶ were also independent of biphenyl concentration (J. Miller, unpublished results), and were very similar to those reported herein for reactions of trapped electrons with strong acceptors. Since direct, long-range tunneling occurs in intermolecular electron transfer, the hypothesis of trap to trap processes is, at best, unnecessary to explain the data on reactions of trapped electrons.

Thus the evidence is predominantly against all types of "trap hopping" mechanisms, including both "thermal excitation from shallow traps"¹² and "trap to trap tunneling".¹⁴ The experimental evidence favors trap deepening by molecular reorientation and tunneling to solutes as the causes of the kinetic spectral changes and reactions. It will be shown below that presently available electron transfer theory gives a reasonably complete account of many interesting details of the data which result from the interplay between these two kinetic processes.

It is not surprising that the experimental evidence militates against trap hopping mechanisms. To make these mechanisms at all plausible, one must make daring assumptions. Thermal excitation out of traps is unlikely unless the traps are much shallower than usually assumed. For a trap as shallow as 0.5 eV, the Boltzmann factor at 77 K is about 10^{-30} . Trap to trap tunneling requires the assumption of a special distribution of preformed traps, many of which are very deep. For both of these models, one must also assume that the polar matrix relaxes (i.e., digs a deeper trap) negligibly when an electron is localized at some site in the matrix. If a trapped electron does dig a deeper well for itself, it will be very difficult to tunnel to another preexisting trap.

2. "Dry Electron" Reactions. During preparation of this manuscript Kroh and co-workers published a letter¹⁷ indicating that solvated electrons in alcohol glasses do not decay, but that capture of "dry electrons" (unlocalized precursors of e_s^-) is the only mechanism which reduces e_s^- yields. Their conclusion was based on the observation that no decay of e_s^- occurred in the presence of weak scavengers, such as benzyl chloride. They report little decay also with 0.025 M I_2 , in which nearly all e_s^- should have been gone before the start of their experiments. Their conclusions, which are based on too limited a selection of acceptors and concentrations, are contradicted by data presented herein.

All acceptors studied here caused the yield of trapped electrons to decrease ($A/A_0 < 1.0$) by some process which occurred prior to $\approx 10^{-6}$ s, our earliest measurement. The decay curves are suggestive, in all cases, that reaction of

trapped electrons also occurs before the measurements started. In the case of weak scavengers, only shallowly trapped electrons, present in early stages of the solvation process, are involved. The data clearly require that trapped electrons disappear by reaction with added acceptors in the time region studied here, but do not require any reaction of mobile, unlocalized, "dry" electrons. It is the opinion of the present author that most of the reduction of trapped electron yield observed at $\approx 10^{-6.5}$ s is due to reactions of trapped electrons at early times, and that reactions of "dry" electrons are unimportant except at large (≈ 1 M) concentrations of acceptors.

3. The Whole Spectrum Decays as a Unit. Homogeneous Broadening. Figures 3 and 4 and Baxendale and Sharpe's data replotted in Figure 6 demonstrate strikingly that capture of trapped electrons by acceptors does not alter the shape of the absorption spectrum of trapped electrons in EtOH glass. Both tunneling and trap-hopping mechanisms predict that acceptors will capture electrons in shallower traps more rapidly. Electron acceptors are therefore expected to cause a blue shift in the absorption spectrum if the spectrum is broadened by the simultaneous presence of electrons in different trap depths. Such shifts are observed in 1-PrOH and to a lesser extent in 2-PrOH, but not in EtOH. It seems reasonable to conclude that the distribution of trap depths in EtOH is not more than half as broad as the absorption spectrum even during the trap deepening process. The same conclusion may be inferred from earlier studies of the spectral shifts in pure alcohols.¹⁰⁻¹² In 1-PrOH the spectra have two unresolved peaks,¹² suggesting that at least two types of electrons are present.

Because weak acceptors are found to react only with shallowly trapped electrons, weak acceptors should be most effective at blue shifting the absorption spectrum. Thus the failure of acetone, a weak acceptor, to cause significant spectral shifts in EtOH (Figure 4), indicates most sensitively that there is little spectral broadening due to different trap depths in EtOH at 77 K. This finding supports the validity of the ratio (A/A_0) plotting method. We are deterred, however, from concluding that the EtOH spectra are homogeneously broadened by noting the humbling complexity of transient, photobleaching data obtained by Walker and May,^{19,23} using a Q-switched ruby laser. For trapped electrons in some glasses they found transient (within a few nanoseconds) bleaching at the exciting wavelength, 694 nm, but not at shorter wavelengths as close as 633 nm. Their data would seem to be at least superficially in contradiction with the conclusion, herein, that all the electrons in EtOH are in traps of similar depths, at any given time. While there is yet no direct conflict, because May and Walker did not study EtOH, it is useful to note that at least one type of hypothesis reconciles the two types of data. The spectrum of an individual trapped electron might show sharp vibrational structure which changes with time, averaging to a smooth, very broad band over a time longer than some characteristic thermal averaging time for molecular motions of the solvent molecules nearest the electron. More realistically there would be a spectrum of averaging times. The absorption spectrum of many such electrons with similar trap depths would appear to be heterogeneously broadened when examined at short times, with pulsed light sources but homogeneously broadened when examined over periods of time longer than the characteristic averaging times for molecular motions of the solvent molecules nearest the electron. This proposal would seem able to account for the both present data and laser photobleaching data.

The failure of electron acceptors to modify the absorption spectrum in EtOH also shows that electron solvation occurs either continuously or, through many steps. If solvation occurred in one or two discrete steps, the spectrum would either show sudden changes (viewed in log time) if all electrons had the same rate constant for each step, or would be altered by electron acceptors if different electrons took greatly different times to solvate. Solvation in many steps seems unlikely to be accomplished by the trap to trap tunneling mechanism unless such tunneling can occur with very little energy loss in each step.

The data which led us to believe that most of the trapped electrons in EtOH have similar solvation histories do not exclude the possibility that a modest fraction ($\leq 20\%$) of the trapped electrons are solvated much faster than the rest. This possibility is supported by the fact that 0.017 M benzyl chloride in EtOH at 4 K removes almost all of the infrared absorption (shallowly trapped electrons) revealing a small absorption in the visible, similar to the spectrum of fully solvated electrons, and by photoshuttling between visible and infrared absorbing traps at 4 K.¹⁸ Clearly trapped electrons may be simultaneously present in a wide range of trap depths at 4 K. This may be true also at early times at 77 K, but the present data suggest that it is only a small fraction of the trapped electrons which have trap depths substantially deeper than the average.

C. *Theory for Electron Tunneling Reactions.* The complex variations of the reaction rates with time and the nature of the acceptor will be interpreted by electron tunneling reaction rates proportional to Franck-Condon factors, F . This is the same interpretation we used in aqueous glasses.² The tunneling rate W at a given distance a is

$$W = \nu_0 F \exp[-2a(2mB)^{1/2}/\hbar] \text{ s}^{-1} \quad (1)$$

where $\nu_0 \approx 10^{15} \text{ s}^{-1}$. We invert this expression to obtain the tunneling distance a (in Å) at a given time t (in s)

$$a = a_0 + 2.26(15 + \log F + \log t)B^{-1/2} \text{ Å} \quad (2)$$

where B is the binding energy for the electron on the donor (in this case a solvent trap) in eV and a_0 , which is usually about 4 Å, corrects for the finite size of the electron donor and acceptor.

Equations 1 and 2 are currently based on very recent treatments of electron transfer²⁰⁻²⁷ which employ modern radiationless transition theory to express the electron transfer rate as the product of a Franck-Condon weighted density of states (line shape) function and the square of an electron exchange matrix element (interaction energy). Implicit in eq 1 is the estimation of the interaction energy using calculations on very simple model potentials, double square wells or the H_2^+ molecule ion.²⁸ Also we use the separation to give a simple product of an averaged Franck-Condon factor and an averaged density of states for the region of interest.²⁹ It is interesting that eq 1 and 2 were first obtained from the different idea of a barrier penetration probability and an attempt frequency, with Franck-Condon factors inserted afterward.² The new treatments place the theory on a more consistent basis.

The very interesting dependence of the Franck-Condon factor on temperature,²⁰⁻²² with temperature-dependent activation energies and activationless regions, does not concern us here. We are most interested in the dependence of the rate on ΔE , the exothermicity of the reaction, at a constant, low temperature. For weakly exothermic reactions, the electron transfer increases rapidly with increasing ΔE . For strongly exothermic reactions, which do not involve too much nuclear rearrangement, the rate, as

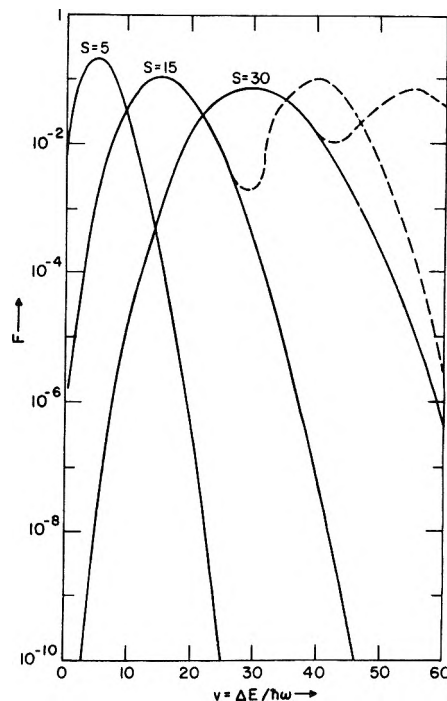


Figure 10. Franck-Condon factors, F , as a function of the exothermicity, ΔE , of an electron transfer reaction. The curves apply to a displaced (vibrational mode(s) have different internuclear distances in the products than in the reactants) harmonic oscillators of frequency $\hbar\omega$. A larger S indicates larger displacement(s). The decrease in F , and hence reaction rate, will not greatly slow the reaction at large values of ΔE if a low-lying electronic excited state of the products is available to dissipate energy, as exemplified by the dashed lines, which include the effect of a low-lying excited state at $25 \hbar\omega$ (2.5 eV for example if $\hbar\omega$ is 0.1 eV).

a function of ΔE , reaches a maximum and decreases at high ΔE .²⁰⁻²⁶ F decreases at high ΔE because vibrational wavefunctions for the vibrationally excited products oscillate rapidly, causing cancellation of overlap with the more slowly changing $v = 0$ states of the reactants. Illustrative examples are sketched in Figure 10.

The examples of F vs. ΔE of Figure 10 are just the well known calculation of nuclear overlap for a displaced harmonic oscillator³⁰ using Jortner's²¹ extension of the form to more than one oscillator. If n vibrational modes are displaced by the electron transfer, each mode having a dimensionless, reduced displacement $\Delta_i = (\mu_i\omega_i/\hbar)^{1/2}\Delta q_i$, then the total "electron-phonon coupling strength" for the reaction is $S = \sum_i (\Delta_i^2/2)$. The Franck-Condon factor $F = \exp(-S)S^p/p!$, where μ_i , ω_i , and Δq_i are the reduced mass, angular frequency, and the change in equilibrium internuclear distance of the i th vibrational mode. When vibrational modes with different frequencies are coupled to the electron transfer, the F vs. ΔE curve is more skewed so that F rises relatively faster at low ΔE and falls off more slowly at high ΔE .²⁰ Figure 10 does not include the effects of "low frequency phonon modes" ($\hbar\omega < kT$) which were included by Ulstrup and Jortner.²⁰ The rigidity of the glassy matrices used in this work probably minimizes the participation of low frequency modes, which would not relax around the electron before it reacts with scavengers.

The rate and distance dependence of a tunneling reaction are determined by two parameters, B and F , the binding energy which holds the electron on the donor, and the Franck-Condon factor. If B and F are known then the tunneling rates as a function of distance can be calculated. The decay curve for electron donors in the presence of randomly distributed acceptors is given by^{1d,2,3,6}

$$P = \exp(-2.51 \times 10^{-3} a^3 M) \quad (3)$$

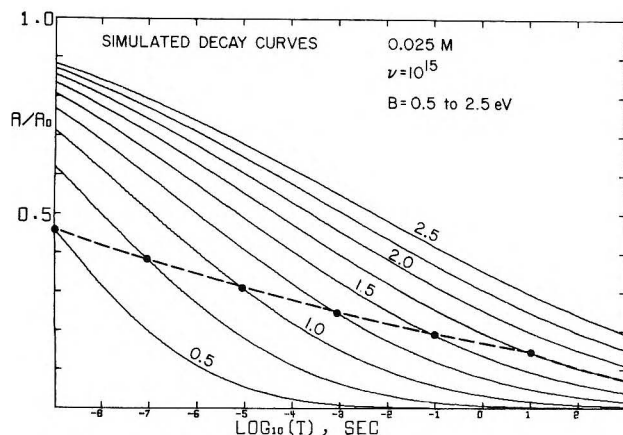


Figure 11. Simulated decay curves from eq 2 and 3 for reaction of electron donors, such as trapped electrons, having various constant binding energies, B . A constant Franck-Condon factor, $F = 1$, is assumed. The dashed line shows a hypothetical decay (for the unlikely case of constant $F = 1$) of solvated electrons in EtOH at 77 K assuming that $B = 0.5$ eV at 10^{-9} s and increases by 0.125 eV per decade until 10 s where it remains constant at 1.75 eV.

where P is the fraction of the electron donors which remain unreacted at a time when the tunneling distance is a in angstrom. M is the concentration in moles liter $^{-1}$. Figure 11 shows simulated decay curves from eq 2-3 for several different values of the binding energy, B , assuming a constant Franck-Condon factor, $F = 1$, and a hypothetical curve (for EtOH) where B increases with time but F remains constant.

D. Interpretation of the Data Using Radiationless Transition Theory. 1. Reactions in MeOH Glass. The Case of Nearly Constant, Nearly Equal Trap Depths. In MeOH glass (+5% ethylene glycol) the electrons are well solvated in deep traps by 10^{-8} s 11 , probably because the small size of the MeOH molecule facilitates fast reorientation of the first solvation layer. Therefore, as in aqueous glasses, all reactions of solvated electrons in MeOH glass will be accompanied by relatively large changes (distortions and displacements) of the molecular vibrations of the solvent molecules surrounding the trapping site. The dependence of the electron tunneling rate on the exothermicity of the reaction, ΔE , is expected to be like the $S = 30$ curve in Figure 10. The rate (for a given distance) will be nearly independent of ΔE , within an order of magnitude, over a large range for strongly exothermic ($\Delta E = 20\text{--}40\hbar\omega$, e.g., 2-4 eV for $\hbar\omega = 0.1$ eV) reactions. The rates of weakly exothermic reactions will decrease by many orders of magnitude as ΔE approaches zero. At low temperatures the rate practically vanishes for endothermic reactions. Table I presents electron affinities, when available, for acceptors used in this work. An assumption which seems to reasonably correlate the results is that $\Delta E \approx 0$ for reaction of e_s^- in MeOH (or in EtOH glass at long times) with a molecule which has a gas-phase electron affinity of about zero (e.g., biphenyl). This would mean that a vacant, but fully formed trap, assumed to be 1.75 eV deep, could be compared with the EA's of molecules added to MeOH or EtOH glass by assuming that the trap had an electron affinity of about zero on the gas phase scale. The molecular electron affinities in these alcohol glasses would then be about 1.75 eV larger than in the gas phase. The difference between a molecular electron affinity in a condensed medium (EA_m) and in the gas phase is $EA_m - EA_g = V_0 + P_-$, where V_0 is the energy required to inject an electron from vacuum into the medium, and P_- is the polarization energy of the molecular anion in the medium.³⁷ The estimates given here

TABLE I: Electron Affinities (EA) of Electron Acceptors^a

Compound	EA (gas)	Ref
Benzene	-1.0 ± 0.5	<i>a</i>
Phenol		
Cadmium (acetate)		
Acetone (Act)	0 ± 0.5	<i>b</i>
Styrene (Sty)	-0.55	39
Biphenyl (Ph ₂)	0.05	30
Naphthalene (Nap)	0.152	30
Phenanthrene (Phen)	0.308	30
CS ₂		
CCl ₄		
Acetophenone	0.334	33
<i>trans</i> -Stilbene (Stilb)	0.4	30
Benzaldehyde (Bzal)	0.42	33
Triphenylethylene	0.45	<i>c</i>
Pyrene	0.579	33
Copper(II) (acetate)		
Benzophenone (Bp)		
9-Fluorenone (Fluo)		
I ₂	(1.6 ± 0.2)	<i>d</i>
Nitrobenzene (NB ₂)	1.26	32
Tetranitromethane (TNM)	1.63	32
Picric acid	(1.9)	<i>e</i>
OsO ₄		
(TCNE)	2.8	32, <i>f</i>

^a From EA(benzene) relative to a number of aromatics in ref 34. ^b Estimated using aqueous redox measurements from ref 36. ^c Estimated to be the average of EA's for di- and tetraphenylethylene, taken from ref 33. ^d A calculated value, ref 35. ^e Estimated by comparison of values in ref 32. ^f TCNE seems to be either strongly complexed or decomposed in EtOH, and is unable to accept electrons from aromatics of lower EA. This behavior does not seem to occur in higher alcohols, 2-propanol and 1-pentanol, or in MTHF. The absorption spectrum of TCNE is altered in EtOH. ^g The acceptors are ordered according to their relative reactivities with solvated electrons in alcohol glasses.

practically coincide with estimates of V_0 (0.1 eV) and P_+ (2.0 eV) given for positive ions in EtOH glass by Grand and Bernas.³⁸

In accordance with these predictions, the decay curves for the strongest acceptors (nitrobenzene, C(NO₂)₄, I₂, and picric acid) in MeOH practically coincide. The differences are within experimental uncertainty. For these acceptors, the decay curves are well represented by eq 2 and 3 with $F \approx 1$ and $B \approx 1.75$ eV. See examples of calculated curves in Figure 11.

Also as expected, the decay curves for weaker acceptors are shifted to longer times, often by many order of magnitude, due to small Franck-Condon factors, F , at small values of ΔE . For a reaction with $F = 10^{-6}$, the decay curve would be simply translated along the log (t) axis by a factor of 10^6 . This behavior is only approximately found in the experiments, for the decay curves for weak acceptors are flatter on the log (t) plots than those of strong acceptors. The same problem was encountered in aqueous glasses.^{2,3} At least two reasons for the "flattening" of decay curves for weak acceptors may be given. One is that the trapped electrons have similar, but not identical trap depths. If the spread of the trap depths is, for example, 20%, or 0.35 eV for an average trap depth of 1.75 eV, then ΔE 's for reaction with identical acceptors may differ by 0.35 eV for different trapped electrons. This would have little effect on the Franck-Condon factors for strongly exothermic reactions where $F \approx 1$ and is nearly independent of ΔE . However weakly exothermic reactions with ΔE 's differing by 0.35 eV may have Franck-Condon factors differing by many orders of magnitude. Similarly, the small increases in trap depth with time in MeOH may lead

to large changes in rates for weakly exothermic reactions. Both of these effects will flatten the decay curves for weakly exothermic reactions relative to decay curves for strongly exothermic reactions. Furthermore, the Franck-Condon factor or "Franck-Condon weighted density functions"³¹ may show considerable vibrational structure at small ΔE 's which is washed out at large ΔE 's. This effect also would lead to large differences in rates for trapped electrons with small differences in their trapping energies, causing "flattening" of the decay curves for weakly exothermic reactions.

2. *Reactions in EtOH Glass. Increasing Trap Depths Cause Either Decreasing or Increasing Franck-Condon Factors.* For weak acceptors, the trapped electron yields observed at $\approx 10^{-6.5}$ s are reduced, probably due to vigorous reaction of shallowly trapped electrons in the picosecond and early nanosecond regions. These reactions continue into the microsecond region but become very slow at longer times as the traps deepen, making ΔE very small or even endothermic. For these weak acceptors, the deepening of traps with time causes decreasing reaction rates at longer times (relative to the case of constant trap depths) for two reasons: the decreasing tunneling barrier permeability due to increasing barrier height, B , and the decreasing Franck-Condon factors, F , due to decreasing ΔE . The decay curves for reactions of trapped electrons with weak acceptors are strikingly different in EtOH than MeOH, where the trap depths are nearly constant with time.

For strong electron acceptors, the decay curves in EtOH are expected, and found, to be much more similar to those in MeOH. At short times when the traps in EtOH glass are shallow, the tunneling barrier height is smaller, speeding up the reaction. However the higher value of ΔE while the traps are shallow is likely to decrease the Franck-Condon factor for very exothermic reactions. These effects will partly cancel each other. Furthermore, shallow traps probably have nuclear configurations similar to unrelaxed solvent, so that less distortion and displacement of vibrational modes (small S) occurs upon electron transfer to an acceptor when the traps are shallow. This leads to a stronger decrease of the Franck-Condon factor for strongly exothermic reactions. (See Figure 10 and ref 20-21 for more detail.)

If F remained constant, independent of changes of the trap depths with time, then the decay curve might look similar to the dashed curve in Figure 11. A decrease in F for shallowly trapped electrons at short times would raise the dashed curve closer to the curve with constant $B = 1.75$ eV. A large decrease in F might even cause the shallowly trapped electrons to react slower at short times than deeply trapped electrons (e.g., in MeOH) would. This would raise the dashed curve above the 1.75 eV solid curve at short times. This appears to have occurred in EtOH glass with three strong acceptors, nitrobenzene, I_2 , and tetranitromethane. Apparently these acceptors captured few of shallowly trapped electrons in EtOH during the picosecond and early nanosecond time regions. During the late nanosecond and microsecond regions, the decay curves "caught up" as the traps deepened, increasing F . This effect will not occur if the acceptor undergoes large vibrational displacements or distortions when it captures an electron, or if the anion of the acceptor has low lying electronic excited states. Picric acid appears to be such a case.

Conclusions

The reactions of solvated and trapped electrons with added electron acceptors shows a rich variety of behavior, which might seem puzzling at first glance. Closer in-

spection shows that the data are fully rationalized in terms of electron tunneling directly to the acceptors, with no intermediate "trap to trap" transfers. The rates of the electron tunneling reactions are controlled by the Franck-Condon principle as has been elaborated in several recently developed theories of electron transfer.

References and Notes

- (1) (a) B. G. Ershov and E. L. Tseitlin, *Khim. Vys. Energ.*, **4**, 186 (1970); (b) F. Kieffer, C. Meyer, and J. Rigaut, *Chem. Phys. Lett.*, **11**, 359 (1971); (c) K. I. Zamaraev, R. F. Khairutdinov, A. I. Mikhailov, and V. I. Goldanskii, *Dokl. Akad. Nauk. SSSR*, **199**, 640 (1971); (d) J. R. Miller, *J. Chem. Phys.*, **56**, 5173 (1972); (e) J. Kroh and Cz. Stradowski, *Int. J. Radiat. Phys. Chem.*, **5**, 243 (1973); (f) K. I. Zamaraev and R. F. Khairutdinov, *Chem. Phys.*, **4**, 181 (1974); (g) R. B. Zhutkovskii, R. O. Khairutdinov, and K. I. Zamaraev, *Khim. Vys. Energ.*, **7**, 558 (1973); (h) J. Kroh and Cz. Stradowski, *Int. J. Radiat. Phys. Chem.*, **7**, 23 (1975); (i) A. Namiki, M. Noda, and T. Higashimura, *Bull. Chem. Soc. Jpn.*, **48**, 3073 (1975); (j) E. J. Marshall, M. J. Philling, and S. A. Rice, *J. Chem. Soc., Faraday Trans. 2*, **71**, 1555 (1975).
- (2) J. R. Miller, *J. Phys. Chem.*, **79**, 1070 (1975).
- (3) J. R. Miller, *Chem. Phys. Lett.*, **22**, 180 (1973).
- (4) J. R. Miller and J. E. Willard, *J. Phys. Chem.*, **76**, 2641 (1972).
- (5) P. Cordier, J.-F. Delouis, F. Kieffer, C. Lapersonne, and J. Rigaut, *C. R. Acad. Sci. Paris, Ser. C*, **279**, 589 (1974).
- (6) J. R. Miller, *Science*, **189**, 221 (1975).
- (7) D. DeVault and B. Chance, *Biophys. J.*, **6**, 825 (1966); D. DeVault, J. Parkes, and B. Chance, *Nature (London)*, **215**, 642 (1967); J. D. McElroy, D. C. Mauzerall, and G. Feher, *Biochim. Biophys. Acta*, **333**, 261 (1974).
- (8) J. T. Richards and J. K. Thomas, *J. Chem. Phys.*, **53**, 218 (1970).
- (9) L. Kevan, *Chem. Phys. Lett.*, **11**, 140 (1971); *J. Chem. Phys.*, **56**, 838 (1972).
- (10) N. V. Klassen, H. A. Gillis, G. G. Teather, and L. Kevan, *J. Chem. Phys.*, **62**, 2474 (1975).
- (11) J. R. Miller, B. E. Clift, J. J. Hines, R. F. Runowski, and K. W. Johnson, *J. Phys. Chem.*, **80**, 457 (1976).
- (12) J. H. Baxendale and P. H. G. Sharpe, *Chem. Phys. Lett.*, **39**, 401 (1976).
- (13) D. C. Walker, "Proceedings of the International Conference on Electrons in Fluids", Banff, Sept., 1976, to be published in *Can. J. Chem.*
- (14) (a) G. V. Buxton and K. G. Kemsley, *J. Chem. Soc., Faraday Trans. 1*, **72**, 466 (1976); (b) G. V. Buxton and K. G. Kemsley, *ibid.*, **72**, 1333 (1976).
- (15) (a) H. Hase, M. Noda, and T. Higashimura, *J. Chem. Phys.*, **54**, 2975 (1971); (b) H. Hase, T. Warashina, M. Noda, A. Namiki, and T. Higashimura, *ibid.*, **57**, 1039 (1972).
- (16) T. Shida, S. Iwata, and T. Watanabe, *J. Phys. Chem.*, **76**, 3683 (1972).
- (17) J. Kroh, E. Romanowska, and Cz. Stradowski, *Chem. Phys. Lett.*, **47**, 597 (1977).
- (18) T. Higashimura, A. Namiki, M. Noda, and H. Hase, *J. Phys. Chem.*, **76**, 3744 (1972); A. Namiki, M. Noda, and T. Higashimura, *Chem. Phys. Lett.*, **23**, 402 (1973).
- (19) D. C. Walker and R. May, *Int. J. Radiat. Phys. Chem.*, **6**, 345 (1974).
- (20) J. Ulstrup and J. Jortner, *J. Chem. Phys.*, **63**, 4358 (1975).
- (21) J. Jortner, *J. Chem. Phys.*, **64**, 4860 (1976).
- (22) N. R. Kestner, J. Logan, and J. Jortner, *J. Phys. Chem.*, **78**, 2148 (1974).
- (23) R. P. VanDaynae and S. F. Fischer, *Chem. Phys.*, **5**, 183 (1974).
- (24) J. J. Hopfield, *Proc. Natl. Acad. Sci. U.S.A.*, **71**, 3640 (1974).
- (25) (a) S. Efrima and M. Bixon, *Chem. Phys. Lett.*, **25**, 34 (1974); (b) S. Efrima and M. Bixon, *J. Chem. Phys.*, **64**, 3639 (1976); (c) S. Efrima and M. Bixon, *Chem. Phys.*, **13**, 447 (1976).
- (26) W. Schmickler, *J. Chem. Soc., Faraday Trans. 2*, **72**, 307 (1976).
- (27) (a) P. P. Schmidt, *J. Chem. Phys.*, **56**, 2775 (1972); (b) *ibid.*, **58**, 4384 (1973).
- (28) C. B. Duke in "Tunneling in Solids", E. Burstein, Ed., Academic Press, New York, N.Y., 1969; B. Brockelhurst, *Chem. Phys.*, **2**, 6 (1973).
- (29) G. W. Robinson and R. P. Frosch, *J. Chem. Phys.*, **37**, 1962 (1962).
- (30) E. Hutchisson, *Phys. Rev.*, **36**, 410 (1930); C. Manneback, *Physica*, **17**, 1001 (1951); S. Kiode, *Z. Naturforsch. A*, **15**, 123 (1960).
- (31) F. Metz, *Chem. Phys.*, **18**, 385 (1976).
- (32) E. M. Chen and W. E. Wentworth, *J. Chem. Phys.*, **63**, 3183 (1975).
- (33) M. Szwarc and J. Jagur-Grodzinski in "Ions and Ion Pairs in Organic Reactions", M. Szwarc, Ed., Wiley, 1974, pp 26 and 38.
- (34) F. Gutmann and L. E. Lyons, "Organic Semiconductors", Wiley, New York, N.Y., 1967, see pp 698-705.
- (35) J. Jortner and U. Sokolov, *Nature (London)*, **190**, 1 (1961).
- (36) M. Breitenkamp, A. Henglein, and J. Lilie, *Ber. Bunsenges. Phys. Chem.*, **80**, 973 (1976).
- (37) B. Raz and J. Jortner, *Chem. Phys. Lett.*, **4**, 155 (1969).
- (38) D. Grand and A. Bernas, *J. Phys. Chem.*, **81**, 1209 (1977).
- (39) L. G. Christophorou, "Atomic and Molecular Radiation Physics", Wiley, New York, N.Y., 1971, p 567.

An Ultrasonic Absorption Investigation of Lanthanide Chloride Complexation in Aqueous Methanol

Herbert B. Silber,* David Boulter, and Timothy White

Division of Earth and Physical Sciences, The University of Texas at San Antonio, San Antonio, Texas 78285 (Received September 1, 1977)

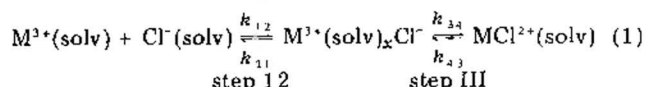
Publication costs assisted by the Robert A. Welch Foundation and the Petroleum Research Fund

Ultrasonic absorption measurements on 0.200 M solutions of NdCl_3 and GdCl_3 as a function of water mole fraction in aqueous methanol solutions indicate that the complexation reactions are coupled to a solvation number change as the solvent composition varies, which results in a complex of different coordination number. This change does not occur in ErCl_3 solutions, indicating that lanthanide solvation changes are predominantly steric in nature. The complex formation rate constants, k_{34} , are determined to be $4.5 \times 10^8 \text{ s}^{-1}$ for NdCl_3^{2+} and $2.4 \times 10^7 \text{ s}^{-1}$ for GdCl_3^{2+} .

Introduction

The existence of two forms of solvated lanthanide ions, differing only in the numbers of coordinated water molecules, has been postulated for many years within the lanthanide series.¹ Coupled to this has been a region within the lanthanide series where both forms of the solvated cation are in equilibrium. Recently, Geier has suggested that all trivalent lanthanide ions in dilute solution have the same number of bound solvent molecules and any solvation number changes occur during the metal ion-ligand complexation process.² This latter hypothesis has been supported by Bear in his study of lanthanide tartrate formation in aqueous solution.³ In principle, the determination of whether the solvation number is a function of the solvated cation alone, or whether it is a consequence of the cation complexation process, should be solved through x-ray studies on lanthanide solutions. Early x-ray studies by Brady⁴ on concentrated solutions of ErCl_3 and ErBr_3 indicate that information can be obtained about the solvated cations by this technique. Recently, Wertz and co-workers⁵ have returned to the problem of solvent structuring by the lanthanide ions. Although this technique can give the solvation number in the case of a predominantly outer-sphere complex such as LaCl_3 , these measurements cannot distinguish between the explanations for the postulated solvation number change in lanthanide systems, especially in the case of inner-sphere complexes where the solvation shell is perturbed by the presence of an anion. An alternative approach to this question is based upon the spectroscopic observations on the different environments surrounding lanthanide chloride and nitrate salts in aqueous and anhydrous solutions,⁶ coupled to ultrasonic absorption measurements on lanthanide systems in mixed solvents.

The complexation reaction between a lanthanide ion, $\text{M}^{3+}(\text{solv})$, and chloride ion is given by



where $\text{M}^{3+}(\text{solv})\text{Cl}^-$ is an outer-sphere ion pair and $\text{MCl}_2^{+}(\text{solv})$ is an inner-sphere ion pair. Solv represents bound solvent molecules composed of water, methanol, or mixtures of the two. Both reaction steps involve loss of bound solvent, step 12, from the inner solvation shell of the chloride ion and step III from the lanthanide ion solvation shell. Ultrasonic absorption measurements on constant concentration lanthanide salt solutions as a

function of water mole fraction in aqueous methanol indicate that for several cation-ligand complexes, the complexation step is coupled to a solvation number change equilibrium reaction in addition to the desolvation steps shown in reaction 1.⁷⁻¹² Erbium was selected as the test lanthanide ion because in aqueous solutions it lies outside of the region of the postulated solvation number change. However, in aqueous methanol, the $\text{Er}(\text{III})$ complexation process is coupled to an additional solvation number change when the ligand is nitrate,⁷ perchlorate,⁹ bromide,¹³ or iodide,¹² but no solvation number change occurs with chloride.⁸ These results indicate that steric crowding in the inner solvation shell is responsible for the solvation number change reaction, since it occurs only with the larger ligands. Similar studies on the neodymium and gadolinium salts of the ligands which undergo this solvation change reaction also process this solvation change, although some differences are observed between the light and heavy lanthanides.^{10,11} This study of gadolinium and neodymium complexation with chloride was initiated to determine if the ligand size is the predominant factor in the desolvation reaction, or if by changing the cation size a similar process occurs.

Experimental Section

Stock solutions of the lanthanide chloride salts were prepared by heating the oxide (Alpha Inorganics) with HCl in water. Whenever possible aqueous stock solutions were used. When methanol solutions were required, the aqueous solution was heated to near dryness; methanol was added; the solution was reheated to near dryness; and the process was repeated. Karl-Fisher titrations were carried out to determine the residual water in the stock solutions. The concentration of salt in all solutions except those in the kinetic analysis was 0.200 M. The kinetic analyses were carried out in solutions containing 10% water by volume, corresponding to a water mole fraction, $X_{\text{H}_2\text{O}}$, of 0.2.

The ultrasonic relaxation apparatus and technique have been described earlier.¹⁴ The only modification was the use of the Matec No. 755 RF plug-in, which provides greater power output and accuracy at frequencies below 20 MHz than the older equipment. All ultrasonic absorption measurements were carried out at 25 °C. For a system undergoing chemical relaxation, the sound absorption, α/f^2 , is given by

$$\alpha/f^2 = B + \sum [A_i/(1 + (f/f_i)^2)] \quad (2)$$

where f is the sound frequency, f_i is the characteristic

TABLE I: Relaxation Data at 25 °C

X_{H_2O}	$10^{17}A_{12},$ Np cm ⁻¹ s ²	$f_{12},$ MHz	$10^{17}A_{III},$ Np cm ⁻¹ s ²	$f_{III},$ MHz	$10^{17}B_{17},$ Np cm ⁻¹ s ²
A. 0.200 M NdCl ₃ Solutions					
~0	20.4 ± 1.5	433 ± 163	151.2 ± 2.5	18.3 ± 0.61	30.7
0.022	26.7 ± 1.9	272 ± 48	171.2 ± 2.5	19.0 ± 0.6	30.6
0.043	37.7 ± 2.5	196 ± 20	168.3 ± 2.5	19.5 ± 0.7	30.5
0.12	51.6 ± 5.2	199 ± 25	129.2 ± 4.5	30.1 ± 1.8	30.6
0.20	77.7 ± 6.2	149 ± 11	78.4 ± 5.2	32.7 ± 3.0	29.6
0.26	61.9 ± 10.5	180 ± 25	55.5 ± 9.8	48.0 ± 7.3	31.4
0.35	66.8 ± 10.7	179 ± 27	31.3 ± 9.9	43.0 ± 12.9	32.4
0.48	60.2 ± 4.5	154 ± 12	9.8 ± 3.7	26.8 ± 18.4	34.7
0.68	19.6 ± 6.0	226 ± 69	13.7 ± 5.6	55.8 ± 19.5	34.6
0.83 ^a	7.9 ± 0.3	212 ± 25			26.4
0.95 ^b					24.8
1.0 ^b					22.0
B. 0.200 M GdCl ₃ Solutions					
0.027	24.5 ± 3.3	273 ± 94	391.6 ± 31.1	10.7 ± 0.9	30.6
0.048	23.0 ± 1.5	510 ± 216	437.1 ± 12.4	11.5 ± 0.4	30.6
0.068	28.4 ± 3.1	260 ± 64	484.5 ± 17.5	12.4 ± 0.6	30.6
0.085	49.3 ± 5.8	198 ± 39	465.5 ± 8.8	17.0 ± 0.7	30.5
0.15	46.4 ± 5.7	152 ± 22	424.4 ± 6.9	17.4 ± 0.7	30.2
0.20	69.2 ± 6.0	107 ± 8	357.7 ± 5.5	17.7 ± 0.7	30.0
0.35	85.6 ± 21.0	105 ± 18	82.4 ± 17.4	26.6 ± 7.4	32.4
0.38	77.4 ± 10.8	115 ± 13	89.8 ± 7.9	23.1 ± 4.2	32.4
0.41	67.3 ± 19.2	139 ± 33	78.3 ± 16.8	34.4 ± 8.2	33.4
0.43	80.0 ± 7.8	123 ± 10	44.4 ± 6.1	26.2 ± 6.1	33.7
0.58 ^c	58.5 ± 3.2	79 ± 10			37.2 ± 3.4
0.69	32.6 ± 4.0	259 ± 73	23.2 ± 4.9	19.4 ± 9.7	34.2
0.83 ^a	11.1 ± 0.4	129 ± 33			26.3
1.00 ^b					22.6

^a Only the high frequency relaxation is present. ^b No relaxations are present. ^c Could not be resolved in terms of two relaxations.

relaxation frequency for each step, A_i is the characteristic relaxation amplitude for each step, and B is the solvent absorption in the absence of any chemical effects. The excess absorption, μ , is the difference between the system absorption and the solvent.

A Beckman Acta UV-visible spectrophotometer was utilized to determine the chloride association constants at 23.6 °C using an approximate technique.¹⁵ Hypersensitive peaks at 577.8, 521.7, and 346.4 nm were utilized for Nd(III) and 278.6, 275.5, and 273.8 nm for Gd(III). The measured association constants of 3.3 for NdCl²⁺ and 3.7 for GdCl²⁺ were assumed to be valid at 25 °C because of the low ΔH value.

Results

No excess absorption occurs in either lanthanide salt solution in water, indicating the absence of inner-sphere complexation, a feature observed in previous studies by x-ray⁵ and NMR.^{16,17} Below water mole fraction of 0.95, the GdCl₃ and NdCl₃ solutions have a sound absorption greater than aqueous methanol in the presence or absence of NaCl¹⁸ (Figure 1), attributed to chemical relaxation phenomena. Assuming the presence of only one relaxation results in a calculated B significantly greater than that present in the solvent containing NaCl, a nonassociating salt. An unusually large B value indicates the presence of a second relaxation and the data are therefore calculated by our double relaxation program. These calculated relaxation results are summarized in Table I.

By analogy to similar systems in water¹⁴ and in aqueous methanol,⁷⁻¹² the two relaxations are identified with the two steps of reaction 1. The high frequency relaxation corresponds to step 12 and the low frequency relaxation to step III. The excess absorption maximum, μ_{max} , is proportional to the concentrations of reacting species times the square of the reaction volume change, defined as

$$\mu_{max} = f_i A_i (C/2) \quad (3)$$

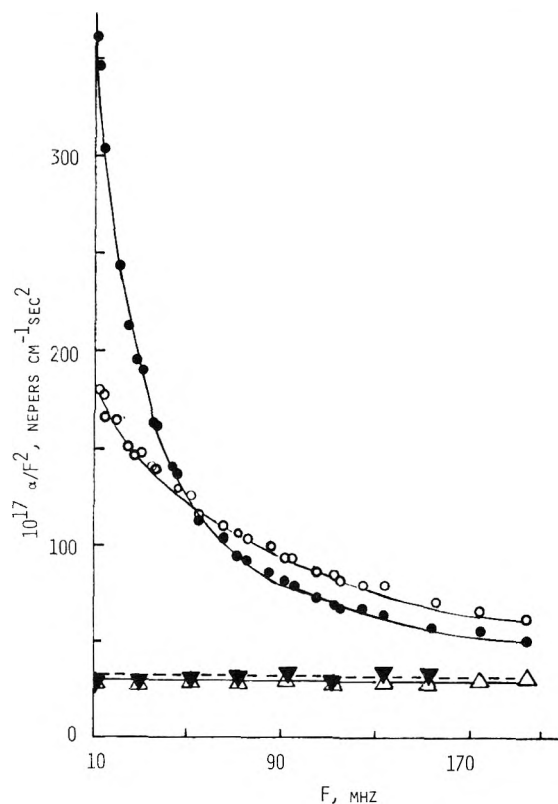


Figure 1. Ultrasonic absorption data in aqueous methanol at $X_{H_2O} = 0.2$ and 25 °C: (Δ) solvent; (∇) 0.200 M NaCl; (\circ) 0.200 M NdCl₃; (\bullet) 0.200 M GdCl₃.

Here C is the sound velocity in the solutions, assumed to be the same as that in the solvent.^{7,19} The variations in μ_{max} with water mole fraction are shown in Figure 2 for the high and low frequency relaxations. These data will be discussed later in terms of lanthanide solvation equilibria.

TABLE II: Relaxation Data for Kinetic Analysis at $X_{H_2O} = 0.2$

c, M	$\theta(c), M$	$10^{17}A_{12},$ $Np\text{ cm}^{-1}\text{ s}^2$	f_{12}, MHz	$10^{17}f_{III},$ $Np\text{ cm}^{-1}\text{ s}^2$	f_{III}, MHz
NdCl₃, $X_{H_2O} = 0.195, B = 29.6 \times 10^{-17} Np\text{ cm}^{-1}\text{ s}^2$					
1.000	2.248	226.1 ± 15.5	228 ± 19	245.5 ± 14.1	48.1 ± 3.0
0.500	1.214	130.8 ± 8.6	193 ± 13	169.0 ± 7.7	42.8 ± 2.2
0.300	0.782	96.6 ± 7.6	174 ± 15	115.5 ± 6.5	35.9 ± 2.6
0.200	0.555	77.7 ± 6.2	149 ± 11	78.4 ± 5.2	32.7 ± 3.0
0.072	0.232	39.1 ± 2.3	135 ± 9	48.3 ± 4.2	16.1 ± 2.7
GdCl₃, $X_{H_2O} = 0.198, B = 30.0 \times 10^{-17} Np\text{ cm}^{-1}\text{ s}^2$					
1.000	2.225	155.0 ± 7.3	218 ± 20	1164.7 ± 11.7	19.2 ± 0.4
0.500	1.196	115.7 ± 11.3	132 ± 14	802.5 ± 13.0	18.0 ± 0.7
0.200	0.545	69.2 ± 6.0	107 ± 8	357.7 ± 5.5	17.7 ± 0.7
0.080	0.251	40.8 ± 4.0	88 ± 7	136.6 ± 3.2	16.7 ± 1.1

TABLE III: Rate Constants and Equilibrium Constants for $NdCl^{2+}$ and $GdCl^{2+}$ Formation

	$NdCl^{2+}$		$GdCl^{2+}$	
	Eq 7-8	Eq 10-12	Eq 7-8	Eq 10-12
$k_{12}, M^{-1}\text{ s}^{-1}$	3.8×10^8	2.9×10^8	4.1×10^8	4.1×10^8
k_{21}, s^{-1}	5.1×10^8	8.1×10^8	4.1×10^8	4.3×10^8
$K_{12} = k_{12}/k_{21}$	0.73	0.52	1.0	2.9
k_{34}, s^{-1}	2.5×10^8	4.5×10^8	0.24×10^8	0.32×10^8
k_{43}, s^{-1}	1.8×10^8	0.83×10^8	1.0×10^8	0.91×10^8
$K_{III} = k_{34}/k_{43}$	1.4	5.4	0.24	0.34
K_T (spectroscopic)	3.3	3.3	3.7	3.7
K_T (kinetic)	1.8		1.3	

The four rate constants for reaction 1 can be obtained by measuring the relaxation frequencies as a function of salt concentrations and these results are summarized in Table II. The increased accuracy at low frequency has improved the relaxation data, thereby allowing the calculation of the rate constants by the exact rather than the approximate methods. For reaction 1, Tamm²⁰ has shown that

$$\tau^{-1} = 2\pi f_{12,III} = \frac{1}{2} [\Sigma k \pm ((\Sigma k)^2 - 4\pi k)^{1/2}] \quad (4)$$

where

$$\Sigma k = k_{12}\theta(c) + k_{21} + k_{34} + k_{43} \quad (5)$$

$$\pi k = k_{12}\theta(c)[k_{34} + k_{43}] + k_{21}k_{43} \quad (6)$$

and $\theta(c)$ is a function of concentration. Adding the two roots of eq 4 together yields

$$2\pi[f_{12} + f_{III}] = \Sigma k \quad (7)$$

and multiplying them together yields

$$4\pi^2 f_{12} f_{III} = \pi k \quad (8)$$

Graphs of $2\pi(f_{12} + f_{III})$ and $4\pi^2 f_{12} f_{III}$ as a function of $\theta(c)$ allow a simultaneous solution for the rate constants from the two slopes and two intercepts. Normally the complex association constants are developed in terms of activities and $\theta(c)$ is also in terms of activities.¹⁴ The spectrophotometric constant obtained in this study is in terms of concentrations, resulting in the following simplification:

$$\theta(c) = [M^{3+}(\text{solv})] + [Cl^-(\text{solv})] \quad (9)$$

The results of these calculations are included in Table III. Previous calculations in lanthanide systems have been based on the assumption that $k_{12}k_{21} \gg k_{34}, k_{43}$, a result which yields comparisons among lanthanide systems, but is not accurate. In order to evaluate the effect of using the approximate equations, the rate constants are recalculated based upon the above assumption. In this case

$$\tau_{12}^{-1} = 2\pi f_{12} = k_{12}\theta(c) + k_{21} \quad (10)$$

$$\tau_{III}^{-1} = 2\pi f_{III} = k_{34}\phi(c) + k_{43} \quad (11)$$

$$\phi(c) = \theta(c)/[\theta(c) + k_{12}^{-1}] \quad (12)$$

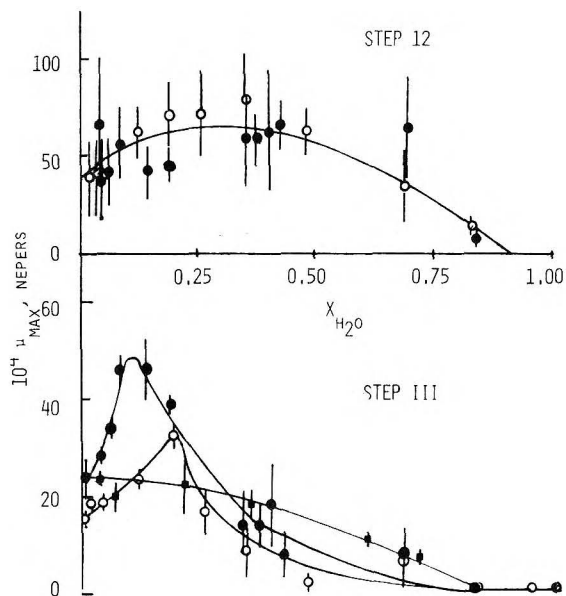


Figure 2. Excess absorption maxima for inner- and outer-sphere complexation as a function of solvent composition: (O) 0.200 M $NdCl_3$; (●) 0.200 M $GdCl_3$; (■) 0.092 M $ErCl_3$.

where $K_{12} = k_{12}/k_{21}$ and the overall complex formation constant, K_f , is

$$K_f = K_{12}(1 + K_{III}) \quad (13)$$

For the kinetic analysis K_{12} is a fitted parameter obtained from the more accurate low frequency data by a method described earlier.²¹ These results are also summarized in Table III.

Discussion

We believe the variation in excess absorption maximum, μ_{max} , with solvent composition for constant concentration salt solutions measures specific interactions between the salt and the solvent. Early ultrasonic absorption studies on aqueous alcohol solutions^{22,23} demonstrated a strong water-alcohol interaction for all alcohols except methanol. For the higher alcohol-water solutions, the existence of a large variation in sound absorption with water content can be attributed to either the formation of specific complexes

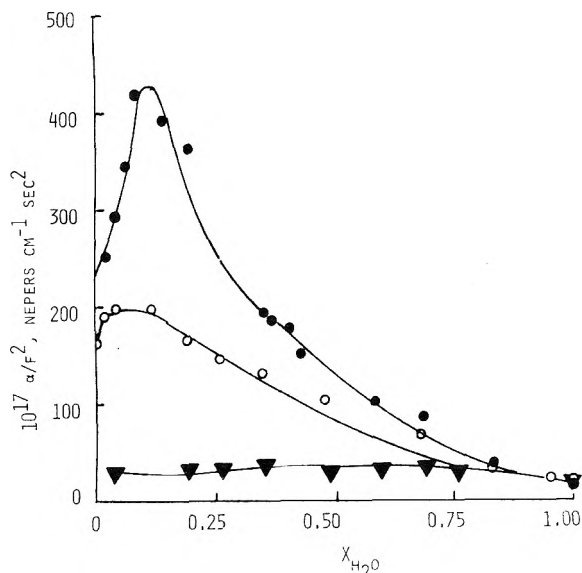


Figure 3. Ultrasonic absorption for 0.200 M salts at 25 °C and 10.4 \pm 0.1 MHz: (\blacktriangledown) NaCl; (O) NdCl₃; (\bullet) GdCl₃.

between water and alcohol molecules or to concentration-fluctuation effects. Recent measurements on aqueous methanol have established the existence of a small maximum in sound absorption with water mole fraction.^{18,24} However, the addition of a nonassociating salt such as NaCl does not significantly alter the shape of the solvent absorption with water mole fraction curve.¹⁸ The only significant difference between the aqueous methanol solutions with and without NaCl is a small increase in α/f^2 below $X_{H_2O} = 0.65$, explained in terms of the formation of small concentrations of outer-sphere complex. No strong salt-solvent interactions could be detected at any solvent composition for 0.200 M NaCl solutions. The NaCl solution with the lowest water mole fraction of 0.043 contained 0.010 mol of NaCl, 1.242 mol of methanol, and 0.055 mol of water. Assuming reasonable solvation numbers for Na⁺ and Cl⁻ leads to the conclusion that insufficient water is present to completely solvate the ions, requiring that the inner solvation shells be composed of methanol and water molecules. Increasing the water content should result in the replacement of methanol by water molecules in the inner-solvation shell resulting in a volume change from 40 to 18 cm³ per mole of solvent. Even though this volume change should exist, it is not detected by our ultrasonic measurements.

Figures 1 and 3 show the sound absorption as a function of frequency and demonstrate that the absorption is significantly different for a rare earth chloride than for the solvent or solvent plus a nonassociating salt. At least two relaxations are present for GdCl₃ and NdCl₃ solutions, whereas no variation in α/f^2 exists with frequency for either aqueous methanol or aqueous methanol with 0.200 M NaCl. This unusual variation in sound absorption with water mole fraction at constant frequency is confirmed when the excess absorption maximum is plotted as a function of solvent composition in Figure 2.

If the only change that occurs as water is added to a methanolic solution of an associating salts is the shift from inner- to outer-sphere ion pairs or solvated ions, then a graph of μ_{max} as a function of water mole fraction should result in a decreasing excess absorption maximum with increasing water content for step III, as has been observed for ErCl₃.²⁵ This is not the case for GdCl₃ and NdCl₃. One explanation for the increase in μ_{maxIII} with increasing water mole fraction is that it reflects the large volume change

associated with the replacement of water for methanol in the inner-solvation shell. This explanation was suggested to describe the small increase in μ_{maxIII} observed for Nd(C₂O₄)₃ and Gd(C₂O₄)₃ with increasing X_{H_2O} in aqueous methanol.¹¹ However, the absence of the maximum for ErCl₃ solutions at 0.096 and 0.200 M²⁶ in the region where water replaces methanol appears to rule out this explanation for the lanthanide chlorides. Both Figures 2 and 3 lead to the conclusion that the observed sound absorption variations with solvent composition are a consequence of specific salt-solvent interactions, rather than reflecting general salt effects. Significant differences in both curves are observed for the lanthanide salts, reflecting differences in the solvated cations or complexes.

The major difference is the increasing μ_{max} with X_{H_2O} observed for GdCl₃ and NdCl₃, which is absent for ErCl₃. We attribute this maximum in Figure 2 to the coupling of an additional reaction step to the inner-sphere complexation process for GdCl₃ and NdCl₃. As in other lanthanide systems,⁷⁻¹² we speculate this step is a change in coordination number of the lanthanide cation resulting in the loss of additional solvent molecules during the complexation process. The observation that this desolvation equilibrium does not occur for all of the lanthanide chlorides indicates that it is not strictly a function of the anion, but rather of the size of both the cation plus anion. Furthermore, these data indicate that the solvation number change occurs during complexation, consistent with the hypothesis of Geier.²

Other differences are also observed between the Er(III), Nd(III), and Gd(III) chlorides. At low water mole fractions, the addition of small quantities of water to the ErCl₃ solutions results in a large decrease in f_{III} , attributed to the destruction of the bis complex. Further additions of water then lead to an increasing f_{III} , which is typical for lanthanide complexation reactions when only the one to one complex is formed.¹² This effect is absent for both Nd(III) and Gd(III) chloride solutions indicating that only the one to one complex forms in aqueous methanol. Also, the amplitude of μ_{max} at any water composition is greater for the Gd(III) than for Nd(III) salt, as was observed in the case of the perchlorates.¹¹ Since the overall complexation constants for the two complexes are approximately the same, this amplitude effect is independent of K_f . The kinetic data in Table II indicate that the association constant for inner-sphere complex is approximately an order of magnitude greater for Nd ($K_f = 1.4$) than for Gd ($K_f = 0.24$) and if the amplitude variation is a function of the concentration of inner-sphere complex, then the amplitude should be greater for NdCl₃ than for GdCl₃, contrary to experiment. Therefore, the sound amplitude variation must reflect a larger reaction volume change for GdCl₃ formation than for NdCl₃ formation. Within experimental error, for the high frequency process, μ_{max12} is essentially the same for both salts. Since the high frequency process represents solvent-separated outer-sphere complexes, it is not expected that significant differences should be served for different lanthanide cations. The small increase in μ_{max} with X_{H_2O} is similar to that observed in the nitrate system and may reflect either a loosening of solvent molecules in the cation solvent shell, a change in bound solvent molecules from methanol to water, or the large errors associated with the high frequency data. This study cannot distinguish between the possibilities.

There exists discrepancies between our ultrasonic results and published solution x-ray studies.^{5,27,28} Wertz's investigations on LaCl₃, NdCl₃, and GdCl₃ indicate outer-

sphere complexes with eight coordination in water in the inner-sphere, with some differences observed for La(III) in the presence of excess chloride.^{5,27} However, alternate preliminary measurements on lanthanide chlorides in water by Habenschuss and Spedding indicate a coordination number in water of nine for PrCl_3 and approximately eight for the heavy chlorides.²⁸ These differences if confirmed, may represent chemical differences caused by sample preparation or they may indicate the experimental errors associated with solution x-ray. Wertz has reported that the coordination number of NdCl_3 in methanol is also eight,²⁷ requiring the absence of a coordination number change in aqueous methanol, in disagreement with the present study. Wertz added anhydrous NdCl_3 to methanol, whereas we prepare our samples by adding HCl to the oxide and removing most of the water by heating. In a previous study of ErI_3 complexation in aqueous methanol, the addition of the anhydrous lanthanide halide to methanol resulted in the evolution of gaseous iodine and the formation of unidentified erbium compounds which were not ErI_3 .¹² Although we have not added anhydrous rare earth chlorides to methanol, sample decomposition can be present and would be expected to yield different results. Alternately, the order of magnitude greater salt concentrations and the correspondingly higher ionic strengths used in the x-ray study may result in a different structure for the lanthanide complex than that occurring in our ultrasonic studies.

The errors associated with the determination of the rate constants are relatively large. The average calculated error in each term involving the sums of relaxation times is $\pm 8\%$ and the product terms is $\pm 14\%$. Coupled to the uncertainties in the $\theta(c)$ expression, we estimate that the rate constants given by the exact treatment are valid to within $\pm 25\text{--}30\%$. Thus, the agreement between the kinetic and spectroscopic equilibrium constants are within experimental error.

An examination of the rate constants in Table III demonstrates that the assumptions utilized in the approximate equations (10–12) are not valid. However, the results for GdCl_3 indicate that the approximate calculation yields surprisingly good agreement with the exact solution, attributed to the relatively large separation between the two relaxation frequencies. Since this large separation often occurs,^{7–12} the approximate technique can yield reasonable estimates of the rate constants. The complex formation rate constant, k_{34} , for NdCl_3^{2+} in aqueous methanol is $2.5 \times 10^8 \text{ s}^{-1}$, similar to that observed for NdSO_4^+ ($1.9 \times 10^8 \text{ s}^{-1}$)²⁵ and NdNO_3^{2+} ($1.5 \times 10^8 \text{ s}^{-1}$)¹⁰ in water, consistent with the observation that the lanthanide complex formation constant is independent of solvent.^{7–12,29} The GdCl_3^{2+} k_{34} rate constant of $2.4 \times 10^7 \text{ s}^{-1}$ is abnormally low by an order of magnitude for a Gd(III) system.¹¹ Although a small k_{34} is often indicative of steric effects in chelate formation, chloride is a monodentate ligand. Since

the GdCl_3^{2+} complex formation yields a large reaction volume change, and since the solvation number change is steric in nature, the relatively slow complexation rate may represent steric crowding in the solvation shell between the solvent molecules and the chloride ion.

In summary, this study has demonstrated that lanthanide solvation number changes are a function of the size of both the cation and the ligand. Also, evidence is presented in favor of the mechanism of this solvation number change occurring during the complexation process, rather than being a function of the solvated cations alone.

Acknowledgment. Acknowledgment is made to The Robert A. Welch Foundation of Houston, Texas and to the donors of the Petroleum Research Fund, administered by the American Chemical Society, for the support of this research. This work was in partial fulfillment of the undergraduate requirements for Mr. Boulter and Mr. White.

Supplementary Material Available: A listing of the ultrasonic absorption (13 pages). Ordering information is available on any current masthead page.

References and Notes

- (1) F. H. Spedding, M. J. Pikal, and B. O. Ayres, *J. Phys. Chem.*, **70**, 2440 (1966).
- (2) G. Geier and U. Karlen, *Helv. Chim. Acta*, **54**, 135 (1971).
- (3) S. S. Yun and J. L. Bear, *J. Inorg. Nucl. Chem.*, **37**, 1757 (1975).
- (4) G. W. Brady, *J. Chem. Phys.*, **33**, 1079 (1961).
- (5) L. S. Smith, Jr., and D. L. Wertz, *J. Am. Chem. Soc.*, **97**, 2365 (1975); M. L. Steele and D. L. Wertz, *ibid.*, **98**, 4424 (1976).
- (6) S. Freed and H. F. Jacobson, *J. Chem. Phys.*, **6**, 654 (1938).
- (7) J. Reidler and H. B. Silber, *J. Inorg. Nucl. Chem.*, **36**, 175 (1974).
- (8) J. Reidler and H. B. Silber, *J. Phys. Chem.*, **78**, 424 (1974).
- (9) H. B. Silber, *J. Phys. Chem.*, **78**, 1940 (1974).
- (10) H. B. Silber and J. Fowler, *J. Phys. Chem.*, **80**, 1451 (1976).
- (11) H. B. Silber and A. Pezzica, *J. Inorg. Nucl. Chem.*, **38**, 2053 (1976).
- (12) H. B. Silber, *Proc. 12th Rare Earth Res. Conf.*, **1**, 9 (1976).
- (13) H. B. Silber and G. Bordonaro in "Progress in the Science and Technology of the Rare Earths", in press.
- (14) H. B. Silber, N. Scheinin, G. Atkinson, and J. J. Grecsek, *J. Chem. Soc., Faraday Trans. 1*, **68**, 1200 (1972).
- (15) F. J. C. Rossotti and H. Rossotti, "The Determination of Stability Constants", McGraw-Hill, New York, N.Y., 1961, p. 276.
- (16) A. Fratiello, V. Kubo, S. Peak, B. Sanchez, and R. E. Schuster, *Inorg. Chem.*, **10**, 2552 (1971).
- (17) J. Reuben, *J. Phys. Chem.*, **79**, 2154 (1975).
- (18) H. B. Silber, *J. Inorg. Nucl. Chem.*, **39**, 2284 (1977).
- (19) O. Nomoto, *J. Phys. Soc. (Jpn.)*, **8**, 553 (1953).
- (20) K. Tamn in "Dispersion and Absorption of Sound by Molecular Processes", D. Sette, Ed., Academic Press, New York, N.Y., 1963.
- (21) J. Reidler and H. B. Silber, *J. Phys. Chem.*, **77**, 1275 (1973).
- (22) C. J. Burton, *J. Acoust. Soc. Am.*, **20**, 186 (1948).
- (23) L. R. O. Storey, *Proc. Phys. Soc. (London)*, **365**, 943 (1952).
- (24) W. D. T. Dale, P. A. Flavell, and P. Kruus, *Can. J. Chem.*, **54**, 355 (1976).
- (25) The ErCl_3 data from ref 8 were recalculated using improved solvent backgrounds from ref 18. No significant change occurs in the step III parameters in this recalculation.
- (26) H. B. Silber, work in progress.
- (27) M. L. Steele and D. L. Wertz, *Inorg. Chem.*, **16**, 1225 (1977).
- (28) A. Habenschuss and F. H. Spedding, *Proc. 11th Rare Earth Res. Conf.*, **11**, 909 (1974).
- (29) J. L. Bear and C. T. Lin, *J. Inorg. Nucl. Chem.*, **34**, 3268 (1972).

Behavior of Ruthenium in Fluoride-Volatility Processes. 3. Thermal Decomposition of RuOF₄

Tsutomu Sakurai* and Akira Takahashi

Fluorine Chemistry Laboratory, Japan Atomic Energy Research Institute, Tokai-mura, Naka-gun, Ibaraki-ken (319-11), Japan (Received April 25, 1977; Revised Manuscript Received November 28, 1977)

Publication costs assisted by the Japan Atomic Energy Research Institute

Solid RuOF₄ releases its oxygen even at room temperature. The rate of this thermal decomposition, expressed in mol of O₂/°C, reaches a maximum at about 70 °C and then decreases markedly with temperature; RuOF₄ is an unstable material contrary to the description of earlier literature. The vapor pressure of RuOF₄ was checked by transpiration method; it is expressed approximately by the following equation in a temperature range 0–70 °C: $\ln P_{\text{mm}} = 8.48 - 2.74 \times 10^3(1/T)$. Since the bulk of solid RuOF₄ decomposes at about 70 °C, the vapor pressure measurement is meaningless over 70 °C. Infrared analysis of the solid indicates that the Ru=O bonds change into single bonds upon condensation; this may be related to the instability of solid RuOF₄.

Introduction

Although the product of RuO₂–F₂ reaction had been suggested to be RuF₅ by many other workers,^{1,2} we reported in the previous work that it was RuOF₄.³ The heaviest species in the mass spectrum of the product was RuOF₄⁺; chemical analysis gave a value 4.0 ± 0.1 for the F/Ru mole ratio in the product, and mass spectrometry confirmed the release of oxygen from the product. The papers so far published on RuOF₄ are very few; the only paper may be by Holloway and Peacock. They reported in 1963⁴ that they had obtained RuOF₄ by the reaction of ruthenium metal with a mixture of bromine trifluoride and bromine at 25 °C. Its magnetic moment and vapor pressure data were presented; they used a static method in measuring the vapor pressure.

According to our experiments, however, RuOF₄ is a rather unstable material; it releases oxygen even at room temperature.³ Therefore, it appears that the static method is not suitable for measuring RuOF₄ vapor pressure, therefore the earlier data are obscure. On the other hand, the property of releasing oxygen seems to be peculiar to RuOF₄, because no such data have been reported for other oxide tetrafluorides such as MoOF₄, WOF₄, and ReOF₄.⁵ The question was raised, why RuOF₄ was so unstable.

These uncertainties on the properties of RuOF₄ urged us to study its properties in further detail. In the present work, the temperature dependence of the thermal decomposition is studied with attention to the oxygen quantity released from the solid, the vapor pressure is measured by a transpiration method, and the instability is discussed on the basis of the infrared spectra obtained.

Experimental Section

Materials. Commercial grade RuO₂·nH₂O of purity higher than 99.9% was heated in air at 700 °C; the x-ray diffraction pattern of the resulting substance agreed with that of RuO₂.⁶ Infrared analysis showed no presence of water in the substance. Its specific surface area, determined by the BET method using krypton, was 6.3 m²/g. Fluorine from Matheson Co. was passed through a chemical trap charged with sodium fluoride for removal of hydrogen fluoride. Helium of purity higher than 99.999% served as the carrier of fluorine and RuOF₄, after passage through a cold trap at –196 °C.

Apparatus and Procedure. The apparatuses used were made of corrosion-resistant materials such as Monel, nickel,

copper, and Teflon. Monel valves of Autoclave Engineers and Hoke Inc. were used for the connecting lines through which fluorine and RuOF₄ were passed. Leakage of the apparatuses was checked with a helium leak detector, which was kept below 10^{–9} atm cm³/s.

RuOF₄ was prepared by the reaction of RuO₂ with fluorine.³ RuO₂ (1–2 g) was placed in a “boat” reactor, heated under high vacuum to remove moisture, and then fluorinated with 20% F₂ in a He stream at 300–400 °C. The volatile products from the reactor were collected in a Monel container cooled to –196 °C. At the end of the fluorination, the container was evacuated at 0 °C by pumping to remove HF and trace amount of RuO₄ (by-product). The container was then separated from the fluorinating apparatus and positioned in another apparatus shown in Figure 1 for the measurements of the vapor pressure and thermal decomposition of RuOF₄.

The transpiration method was employed for vapor pressure measurement in order to avoid the influence of the oxygen released from RuOF₄. The RuOF₄ container was thermostated at an operating temperature between 0 and 100 °C and then helium was allowed to pass through it at a constant flow rate between 2 and 25 cm³/min for a specific period. The effluent gas from the container was passed through a connecting line kept at a temperature slightly higher than that of the container and then introduced into a trap cooled to –196 °C, where the RuOF₄ vapor in the gas stream condensed. The temperature of the container was kept constant to within ±0.2 °C and the flow rate of helium was regulated with bellows valves from Nuclear Products Co. with an error smaller than ±0.2 cm³/min. A mass flow meter of Hasting Raydist a Tel-edyne Co. Model LF-20 measured the flow rate of He. After completion of each run, the trap was evacuated, warmed to room temperature, and then allowed to introduce about 60 mL of 2 N NaOH (containing 1.5% K₂S₂O₈) through a Teflon stopcock with the aid of vacuum. Immediately after separation of the trap from the apparatus, a small quantity of 2 N NaOH was admitted to the sidearm of the trap for collecting the RuOF₄ deposited therein. Chemical analysis of ruthenium and fluorine followed this hydrolysis of the RuOF₄ collected. The ALC photometric method was used for the determination of fluorine⁷ and spectrophotometry with 8-quinolinol was used for the determination of ruthenium.⁸ It was experienced in the previous³ and present works that on hy-

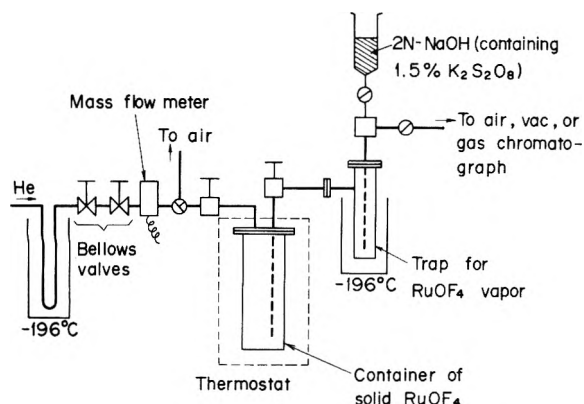


Figure 1. The apparatus used for measuring the vapor pressure and thermal decomposition of RuOF_4 . The RuOF_4 container was thermostated at the desired temperature and He was allowed to pass through it at a constant flow rate. RuOF_4 vapor in the He stream was collected in the cold trap and, at the end of the run, it was hydrolyzed with a NaOH solution for calculation of its partial pressure in the gas stream. The effluent gas from the trap was introduced into a gas chromatograph for the determination of the oxygen liberated from RuOF_4 solid.

drolisis about 6% of the ruthenium unavoidably precipitated as hydroxide; so a step of dissolving it was necessary before the determination of ruthenium. This operation increased greatly the complexity of the analysis of ruthenium. In the present work, ruthenium analysis was made with some typical samples only to confirm that the fluorine-to-ruthenium mole ratio in solution was close to the theoretical value (= 4). The RuOF_4 partial pressure in the helium stream was calculated from the analytical values of fluorine.

The apparatus in Figure 1 was also used in measuring the quantity of the oxygen produced by the thermal decomposition of RuOF_4 . In this case, the effluent gas from the trap was fed to Hitachi Model 063 gas chromatograph. The flow rate of helium was kept constant at $20 \text{ cm}^3/\text{min}$ according to specifications of the instrument. At a temperature of the container between room temperature and 400°C , helium was allowed to pass through the system until oxygen was no longer detectable in the effluent gas from the trap. The helium flow was then turned off, and temperature of the container was raised for the next higher temperature measurement. Measurements were thus made stepwise: the temperature was raised by 5 or 10°C in each step up to 100°C , and then 100°C in each step beyond 100°C . Finally, chemical analysis of the residue in the container was carried out in the same manner as in the previous work.³

The infrared absorption spectrum of solid RuOF_4 was obtained in a manner similar to that in the previous work.³ An absorption cell flanged at one end was connected directly to the "boat" reactor so as to enable gaseous RuOF_4 to diffuse smoothly into the cell from the reactor. RuO_2 (200–300 mg) was placed in the reactor and heated to 300 – 350°C , then fluorine was admitted to the system to a pressure of 200 mmHg. Gaseous RuOF_4 diffusing from the reactor was allowed to condense on the silver chloride windows kept at room temperature. Infrared spectra were scanned with Japan Spectroscopic Co. Model IRA-2 recording spectrophotometer (400 – 4000 cm^{-1}). The windows were not corroded by the solid; therefore they were used repeatedly after wiping with gauze.

Results and Discussion

Thermal Decomposition. Mass spectrometry confirmed in the previous work³ that the gas produced by the thermal decomposition was only oxygen; no free fluorine and oxygen fluorides were detected. In the present work, the

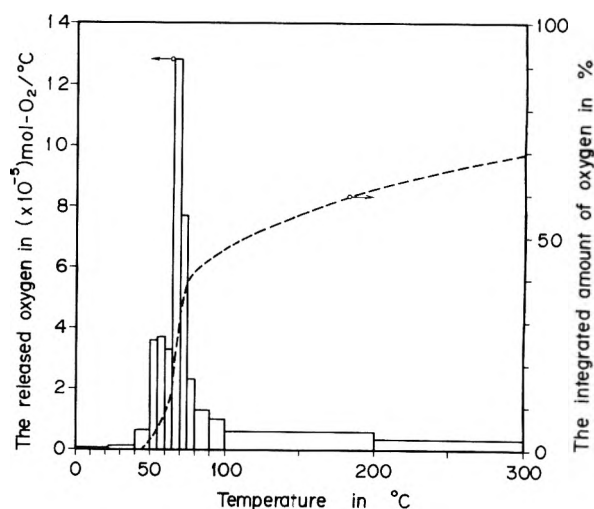
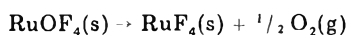


Figure 2. The amount of the oxygen produced by the thermal decomposition of solid RuOF_4 . The histogram shows the average per degree of temperature rise, and the broken line shows the integrated amount of oxygen in its ratio to the theoretical value calculated from the initial RuOF_4 quantity 1.786 g ($9.25 \times 10^{-3} \text{ mol}$).

temperature dependence of the thermal decomposition was studied. The amount of released oxygen depended on both the quantity and temperature of the solid. Moreover, it was found that the solid liberated oxygen only when the temperature was being raised. After the temperature became constant, the liberation of oxygen slowed gradually and ceased within 1–2 h. Further increase in temperature resulted in an additional release of oxygen. This finding means that thermal decomposition takes place partially depending upon temperature.

The measurement of oxygen was carried out in each 5 , 10 , or 100°C rise in temperature up to 400°C , and the average per degree of the rise was taken, i.e., $\text{mol of O}_2/^\circ\text{C}$. The results up to 300°C are shown in Figure 2 as a histogram. The release of oxygen reaches a maximum at about 70°C and then decreases sharply with temperature; however, a small amount of oxygen is liberated even at 400°C . The broken line in the figure shows the integrated amount of the oxygen in its ratio to the theoretical value calculated from the initial amount of solid RuOF_4 . The oxygen quantity amounted to about 80% of the theoretical value in heating to 400°C . The remaining oxygen ($\sim 20\%$) is partly present in the form of RuOF_4 in the cold trap and is partly confined still in the residual solid in the container. The value of 80% obtained for the oxygen quantity substantiates the previous conclusion³ that the product of the RuO_2 – F_2 reaction is RuOF_4 . Also, it is evident from the present experiments that solid RuOF_4 is so unstable as to decompose below 100°C . Since chemical analysis gave values of 3.8–4.0 for the F/Ru mole ratio in the residual solid, it is considered that the thermal decomposition proceeds to produce RuF_4 and O_2 :



The residual solid was black and sensitive to moisture. We have not succeeded in x-ray analysis of RuF_4 . The only paper so far published on RuF_4 may be by Holloway and Peacock.⁹ They prepared RuF_4 by the reduction of RuF_5 with I_2 and attempted x-ray analysis; however, the crystal structure data were not presented.

In other experiments, the interaction of gaseous RuOF_4 with the surface of a Monel tube was checked by the use of radioactive $^{103}\text{RuO}_2$.¹⁰ The $^{103}\text{RuO}_2$ was obtained by irradiating RuO_2 in JRR-2 for 180 h in a neutron flux of $4.3 \times 10^{12} \text{ n/cm}^2 \text{ s}$.¹¹ About 30 mg of it was fluorinated in the same manner as described already, and the resulting

TABLE I: Dependence of RuOF₄ Partial Pressure on Helium Flow Rate at 50 °C

He flow rate, cm ³ (NTP)/min	Duration of gas flow, h	Fluorine quantity in solution, mg	RuOF ₄ partial pressure, ^a mmHg
9.7	4.0	5.1	0.48
9.7	4.0	4.4	0.42
5.0	4.0	3.0	0.55
19.1	1.3	2.6	0.34
14.4	2.0	2.8	0.35
2.5	8.0	4.0	0.75
19.6	2.0	3.0	0.28
2.1	8.0	4.1	0.81
2.1	8.0	4.3	0.82

^a Calculated from the fluorine quantity, He flow rate, and duration of gas flow.

gaseous mixture was passed through the tube heated to 100–200 °C. Then, a scintillation detector was scanned along the length of the tube. The decomposition of gaseous RuOF₄ in small quantity was observed through the increase of radioactivity. However, once coated with ruthenium, the surface no longer decomposed gaseous RuOF₄.

In order to observe RuOF₄, the gas in the RuOF₄ container was expanded into an evacuated Pyrex container cooled to –196 °C. A small amount of yellowish green RuOF₄ condensed in the Pyrex container. However, it turned black gradually when warmed to 30 °C; the thermal decomposition of solid RuOF₄ takes place even in a Pyrex container. Thus, RuOF₄ turned out to be a rather unstable material.

Vapor Pressure. Since the earlier vapor pressure study used a static method,⁴ it may include an error arising from the oxygen released. We tried to check the vapor pressure by means of a transpiration method. The instability of RuOF₄ forced us to use the product container of the fluorinating apparatus as the transpiration chamber. This greatly restricted the favorable structure of the transpiration chamber, e.g., the heat shield^{12,13} was not available because a small opening became plugged during the fluorination. The present experiments were carried out under such a disadvantageous condition.

Bell, Merten, and Tagami have obtained saturation at flow rates between 1 and 5 cm³/min.¹³ So, in the present experiments, the helium flow rate was varied over 2 cm³(NTP)/min and the dependence of RuOF₄ partial pressure on the helium flow rate was studied at 0, 30, 50, 70, and 90 °C. Calculations¹² made with the diffusion coefficients of various binary systems of helium¹⁴ suggest that the diffusion effect¹² is negligible in the present case even at 2 cm³/min. In measurements at 70 and 90 °C, the solid RuOF₄ sample was replaced with a fresh one after each run, for fear that the effect of the thermal decomposition at about 70 °C was superimposed on the flow rate dependence in the subsequent run. Table I shows the results of the experiments at 50 °C. At each temperature, an increase in the flow rate resulted in a decrease of the partial pressure. These results indicate that saturation is attained at flow rates less than 2 cm³/min. In the present work, however, it was difficult to find the point of saturation in such a small flow rate range as 0–2 cm³/min.

Approximate values of RuOF₄ vapor pressure were obtained in the following way. Kubaschewski and Evans describe¹⁵ that, theoretically, the saturation of carrier gas should be attained at a zero flow rate; many workers once obtained vapor pressures by extrapolation to zero flow rate.¹⁶ In practice, however, the saturation is usually reached at low yet finite flow rates; the extrapolation may result in an overestimation of vapor pressures. These facts suggest however that the RuOF₄ vapor pressure will be in

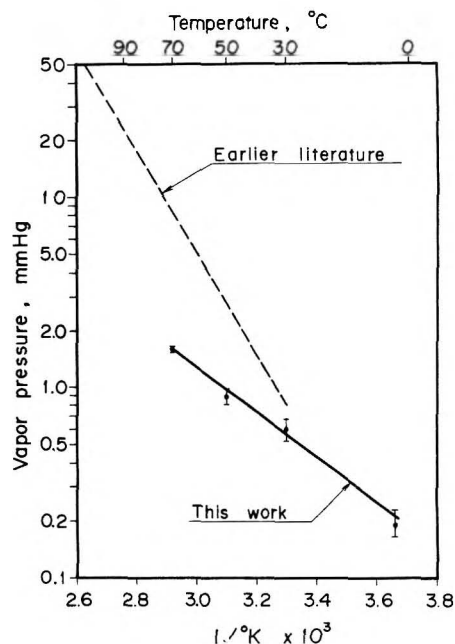


Figure 3. Vapor pressure of RuOF₄. The full line shows the vapor pressure obtained in the present work by the use of the transpiration method. The thermal decomposition shown in Figure 2 made the measurement difficult over 70 °C. The broken line approximates the vapor pressure reported by the earlier workers;⁴ they used static method.

the range between the partial pressure at the least flow rate (2 cm³/min) and the value obtained by extrapolation of the plots of the partial pressure back to zero flow rate. By regarding this range as an uncertainty inherent in the present experiments, we estimated the vapor pressure at 0, 30, 50, and 70 °C; the results are shown in Figure 3. (Table I gave a value of 0.89 ± 0.08 mmHg as the vapor pressure at 50 °C.) The full line approximating the plots is expressed by the following equation:

$$\ln P_{\text{mm}} = 8.48 - 2.74 \times 10^3(1/T)$$

where T is temperature in K and P_{mm} the vapor pressure is mmHg. The measurements were meaningless above 70 °C, because the bulk of solid RuOF₄ decomposed at about 70 °C and the layer of the resulting RuF₄ prevented the subsequent vaporization of the remaining RuOF₄. The partial pressure was only 0.68 mmHg at 90 °C and 2.1 cm³/min. Therefore, the apparent vapor pressure of RuOF₄ cannot increase beyond 70 °C. In this respect, the earlier data,⁴ which are approximated by a broken line in the figure, are erroneous. Although approximate, the present study has revealed the characteristic of RuOF₄ vapor pressure.

In the present study, it was assumed that there was no interaction between solid RuOF₄ and RuF₄. This assumption is supported by the reproducibility of the partial pressure shown in Table I. The experimental runs in the table were carried out in that order. The obtained partial pressure depends on He flow rate but it is almost independent of the order of the run. This means that RuF₄ does not affect RuOF₄ vapor pressure below 70 °C.

Instability of RuOF₄. The following two facts indicate that RuOF₄ is more stable in the gaseous state than in the solid state.

(i) Gaseous RuOF₄ can be transferred from the fluorinating reactor to the product container through the connecting line heated to 150 °C.

(ii) In the mass spectrum of RuOF₄,³ the highest peak is for the fragment RuOF₃⁺ and in all of the fragments expected for RuOF₄, only the peak due to RuF₄⁺ does not appear. This means that the rupture of a Ru–F bond of

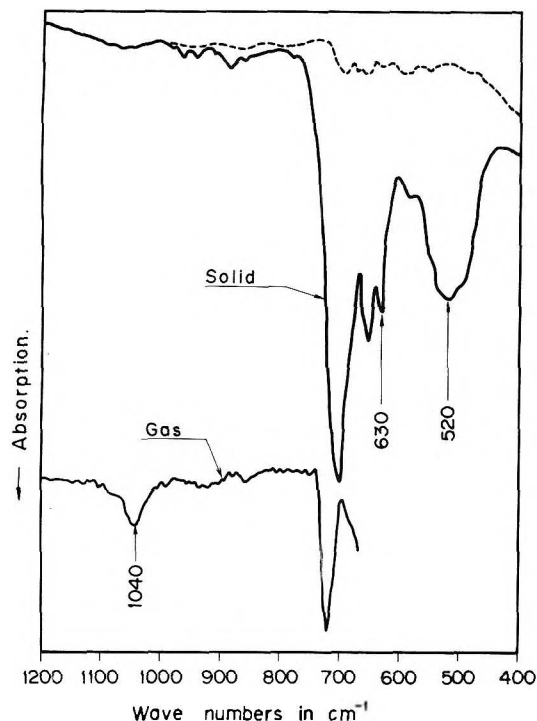


Figure 4. Infrared spectra of solid and gaseous RuOF_4 ; the latter is from the previous work for comparison.³ The band at 1040 cm^{-1} can be assigned to $\text{Ru}=\text{O}$ bonds,²² which disappears upon condensation. The disappearance of this band may be related to the instability of solid RuOF_4 .

the molecule is brought about by electron impact in preference to that of the $\text{Ru}=\text{O}$ bond. (RuF_4^+ gives the highest peak in the mass spectrum of RuF_5 .¹⁷) Besides the relative instability of RuOF_4 to MoOF_4 and WOF_4 , we must therefore discuss the lower stability of its solid.

Instability of RuOF_4 in comparison with MoOF_4 and WOF_4 may be explained as follows. In these oxide tetrafluorides each metal is in the hexavalent state. Mo(VI) is stable because its electron configuration is the same as that of the ground state ($4d^5 5s^1$).¹⁸ W(VI) is obtained by promoting one $6s$ electron to the $5d$ orbital ($6s^2 5d^4 \rightarrow 6s^1 5d^5$); this promotion can take place easily because there is not much difference in energy between the $6s$ and $5d$ orbitals. The presence of one electron in each of the five d orbitals also contributes to the stability of both Mo(VI) and W(VI) .¹⁸ On the contrary, Ru(VI) is in an excited state and therefore unstable, because promotion of one $4d$ electron to the $5p$ orbital is necessary to produce the hexavalent state ($5s^1 4d^7 \rightarrow 5s^1 4d^6 5p^1$). The fact that Ru(VI) rarely forms its binary compounds supports the instability of Ru(VI) ; RuF_6 which may be the only binary compound of Ru(VI) is known to be unstable.¹⁹ The instability of RuOF_4 partly arises from Ru(VI) being in an excited state.

The structure of solid RuOF_4 is not known, because its x-ray diffraction pattern has not been obtained yet. However, infrared analysis provided a clue to the structure of solid RuOF_4 . Figure 4 shows the infrared absorption spectra of solid and gaseous RuOF_4 ; the latter is from the previous work for comparison.³ The spectrum of the gas is similar to those of gaseous MoOF_4 ²⁰ and WOF_4 .²¹ presented by other workers, both in position of the two bands and their relative intensities; the bands at 1040 and 720 cm^{-1} are assigned to the stretching vibrations of the $\text{Ru}=\text{O}$ ²² and Ru-F bonds, respectively.

However, a difference is noted between the spectrum of solid RuOF_4 and those of MoOF_4 and WOF_4 solids. In the case of MoOF_4 , the similarity of spectra of its solid and

vapor indicates that the metal-oxygen multiple bonds are still held by the solid. Edwards and Steventon concluded that the solid had a Mo-F-Mo bridge system.²⁰ Also, the spectra of solid and gaseous WOF_4 are similar to each other.²¹ Edwards and Jones however suggests from the crystal structure that in the case of solid WOF_4 the band at 1050 cm^{-1} is due to a W-F stretching frequency and a part of the band system centered at 650 cm^{-1} relates to W-O-W bridge bonds. Their conclusion was that solid WOF_4 consisted of tetramer molecular units with an oxygen bridge system.

Contrary to these two studies, the spectrum of solid RuOF_4 involves no band around 1040 cm^{-1} ; instead, it has such a characteristic band at 630 cm^{-1} as is not seen in the spectra of either MoOF_4 or WOF_4 solid (see Figure 4). This reveals that $\text{Ru}=\text{O}$ bonds disappear on condensation. The instability of solid RuOF_4 is related to the disappearance of $\text{Ru}=\text{O}$ bonds.

Comparison of the spectra of solid RuOF_4 and WOF_4 does not permit assignment of the bands between 600 and 700 cm^{-1} in the former to Ru-O-Ru bridge bonds, because there is no band around 1050 cm^{-1} which would be expected from analogy to WOF_4 for the frequency of the Ru-F bonds trans to the oxygen bridge bonds. Moreover, the earlier study on $[\text{Cl}_5\text{Ru-O-RuCl}_5]^{4-}$ ions makes the presence of the oxygen bridge bonds in solid RuOF_4 improbable, because it indicates that Ru-O-Ru bridge bonds are not so unstable as to decompose at temperatures below 100°C .²³ From the comparison with the absorptions of solid MoOF_4 , we assign the two sharp bands at 700 and 650 cm^{-1} to Ru-F stretching frequencies, the broad band centered at 520 cm^{-1} to the stretching vibration of Ru-F-Ru bridge bonds, and the characteristic band at 630 cm^{-1} to the stretching frequency of the Ru-O single bonds containing an unpaired electron.

The change of $\text{Ru}=\text{O}$ bonds into single bonds may be explained as follows. On condensation, a fluorine atom of a neighboring RuOF_4 molecule approaches the particular RuOF_4 molecule considered from a direction trans to its $\text{Ru}=\text{O}$ bond, forming a fluorine bridge bond. This raises²⁴ the potential energy of the $\text{Ru}=\text{O}$ bond through d -level splitting of the Ru atom and leads to breaking of the π bond, which causes the change of double bonds into single bonds.

Thus, we concluded that the instability of solid RuOF_4 was brought about by the change of $\text{Ru}=\text{O}$ bonds into unstable single bonds in condensation. Solid RuOF_4 was found to decompose in large quantity at about 70°C . This thermal decomposition may be responsible for the complicated behavior of ruthenium encountered in the fluoride-volatility processes.²⁵

Acknowledgment. We thank Mr. S. Tsujimura, Dr. M. Iwasaki, and Mr. T. Tsujino for their valuable discussion. We are also indebted to Dr. H. Hashitani, Mr. T. Adachi, and Mr. H. Yoshida for their aid in chemical analysis, to Mr. A. Hoshino in gas chromatography, and to Dr. K. Ohwada and Mr. H. Shinohara in infrared analysis.

References and Notes

- (1) D. V. Steidl and R. L. Jarry, *USAEC Rep.*, **ANL-7575**, 55 (1969); R. C. Vogel et al., *ibid.*, **ANL-7550**, 28 (1968).
- (2) M. A. Hepworth and P. L. Robinson, *J. Inorg. Nucl. Chem.*, **4**, 24 (1957).
- (3) T. Sakurai and A. Takahashi, *J. Inorg. Nucl. Chem.*, **39**, 427 (1977).
- (4) J. H. Holloway and R. D. Peacock, *J. Chem. Soc.*, 527 (1963).
- (5) G. H. Cady and G. B. Hargreaves, *J. Chem. Soc.*, 1568 (1961).
- (6) U.K.A.E.A. (Reactor group), A.S.T.M. card No. 18-1139.
- (7) H. Hashitani and H. Muto, *Jpn. Anal.*, **14**, 1114 (1965).
- (8) H. Hashitani, K. Katsuyama, and K. Motojima, *Talanta*, **16**, 1553 (1969).
- (9) J. H. Holloway and R. D. Peacock, *J. Chem. Soc.*, 3892 (1963).

- (10) T. Sakurai and A. Takahashi, unpublished results.
- (11) T. Sakurai, A. Takahashi, and Y. Komaki, *J. Nucl. Sci. Technol.*, **11**, 74 (1974).
- (12) U. Merten, *J. Phys. Chem.*, **63**, 443 (1959).
- (13) (a) W. E. Bell, U. Merten, and M. Tagami, *J. Phys. Chem.*, **65**, 510 (1961); (b) W. E. Bell and M. Tagami, *ibid.*, **67**, 2432 (1963).
- (14) R. C. Reid and T. K. Sherwood, "The Properties of Liquids and Gases", McGraw-Hill, New York, N.Y., 1966, p 520.
- (15) O. Kubaschewski and E. L. Evans, "Metallurgical Thermochemistry", Pergamon Press, New York, N.Y., 1958, p 151.
- (16) (a) N. G. Schmahl and P. Sieben, "National Physical Laboratory Symposium No. 9, The Physical Chemistry of Metallic Solutions and Intermetallic Compounds", Vol. 1, Her Majesty's Stationary Office, London, 1959, p 2k; (b) T. Kikuchi, T. Kurosawa, and T. Yanahashi, *J. Jpn. Inst. Met.*, **28**, 497 (1964).
- (17) T. Sakurai and A. Takahashi, unpublished results.
- (18) E. Cartmell and G. W. A. Fowles, "Valence and Molecular Structures", Butterworths, London, 1961, p 49.
- (19) H. H. Claassen, H. Selig, J. G. Malm, C. L. Chernick, and B. Weinstock, *J. Amer. Chem. Soc.*, **83**, 2390 (1961).
- (20) A. J. Edwards and B. R. Steventon, *J. Chem. Soc. A*, 2503 (1968).
- (21) A. J. Edwards and G. R. Jones, *J. Chem. Soc. A*, 2074 (1968).
- (22) C. G. Barraclough, J. Lewis, and R. S. Nyholm, *J. Chem. Soc. A*, 3552 (1959).
- (23) A. M. Mathieson, D. P. Mellor, and N. C. Stephenson, *Acta Crystallogr.*, **5**, 185 (1952).
- (24) Reference 18, p 192.
- (25) G. Manevy et al., French Report CEA-N-1479, 243 (1971).

The Apparent Molal Volumes and Adiabatic Compressibilities of Aqueous Amino Acids at 25 °C

Frank J. Millero,*† Antonio Lo Surdo,† and Charles Shin†

Rosenstiel School of Marine and Atmospheric Science, University of Miami, Miami, Florida 33149 (Received October 21, 1977)

Publication costs assisted by the National Science Foundation

The apparent molal volumes and adiabatic compressibilities of 15 amino acids in water have been determined at 25 °C from precise density and sound measurements. The electrostriction partial molal volume and compressibility of the amino acids were determined from $\bar{V}^0(\text{meas}) - \bar{V}^0(\text{int})$ and $K^0(\text{meas}) - K^0(\text{int})$. The values of $\bar{V}^0(\text{int})$ have been estimated from \bar{V}^0 of the uncharged amide isomers and \bar{V}^0_{cryst} , the crystal molal volume. Both $\bar{V}^0(\text{elect})$ and $K^0(\text{elect})$ yield values of 4.1 ± 0.4 for the number of water molecules hydrated to the amino acids. Group contributions for the partial molal volume and adiabatic compressibilities have been determined from the amino acids. The volume results are in good agreement with the values calculated by other workers on soluble organic solutes.

Introduction

Recently there has been an increased interest in the state of water in the living cell. Since most biological macromolecules are physiologically active in aqueous solutions, a knowledge of water-protein interaction is necessary to understand the role of water solvated to soluble organics in the living cells. A better understanding of this type of interaction may be obtained from dipolar ions. Since amino acids are zwitterions in aqueous solutions,¹⁻³ their volume and compressibility properties should reflect structural interactions with water molecules as in the case of electrolytes.

Many experiments⁴ on the properties of protein solutions indicate that ca. 0.3 g of water per gram of dry protein are bound or hydrated in aqueous solutions. Work on the volume properties of proteins and some amino acids have shown that they undergo a decrease in volume upon dissolving in water.⁵⁻¹⁴ This decrease in volume upon dissolution is similar to what occurs for electrolytes¹⁵ and can be attributed to electrostriction due to water-protein, and water-amino acid interactions. The number of water molecules determined from the electrostriction of proteins¹⁶ and amino acids^{17,18} (using methods that have been applied to electrolytes)¹⁹ agree very well with the values determined by other methods.^{4,14,17,18} Although these results might indicate that proteins behave as electrolytes, the effect of pressure on the specific volumes¹² indicate that the so-called "bound water" behaves more like water solvated to soluble organic solutes.¹⁶ To better

understand the hydration of proteins and amino acids, basic physico-chemical properties are needed. In this communication, we report on the volume and compressibility measurements made on amino acids in water at 25 °C.

Experimental Section

The amino acids used in these studies were obtained from ICN Pharmaceuticals, Inc., and were used without further purification. All solutions were made by weight with ion-exchanged (Millipore Super Q) water. All weights were vacuum corrected.

The densities were measured at 25 °C to $\pm 3 \times 10^{-6}$ g cm⁻³ with a vibrating flow densimeter (Sodev, Inc.). The values of $\Delta d = d - d_0$, where d and d_0 are the densities of the solution and water are listed in Table I.²⁰ The system was calibrated with N₂ gas and ion-exchanged water using the densities of Kell.²¹ The accuracy (± 3 ppm) of the system has been determined by measuring the densities of standard seawater solutions.²²

The sound velocities were measured at 2 MHz to a precision of ± 0.02 m s⁻¹ using a "sing around" sound velocimeter (Nusonic, Inc.). The system was calibrated with pure water using the sound velocities of Del Grosso and Mader.²³ The accuracy (± 0.1 m s⁻¹) has been determined by measuring the speed of sound in seawater solutions.²⁴

The relative sound velocities (Δu) of the aqueous solutions at 25 °C are listed in Table I²⁰ and were determined from the frequency measurements using

$$\Delta u = u - u_0 = \frac{(f - f^0)u^0}{f^0(1 - f\tau)} \quad (1)$$

* Rosenstiel School of Marine and Atmospheric Science, Miami Fla. 33149.

† Chemistry Department, University of Miami, Coral Gables, Fla. 33100.

TABLE II: Limiting Values of Apparent Molal Volumes, ϕ_V^0 , Adiabatic Compressibilities, $\phi_{K(S)}^0$, S_V , and $S_{K(S)}$ for Aqueous Amino Acids at 25 °C^a

Compound	ϕ_V^0 , cm ³ mol ⁻¹	S_V	σ^b	$10^4\phi_{K(S)}^0$, cm ³ mol ⁻¹ bar ⁻¹	$10^4S_{K(S)}$	$\sigma(10^4)^c$
<i>D</i> -Alanine	60.43	0.778	0.09	-25.53	5.01	0.28
<i>L</i> -Alanine	60.47	0.661	0.02	-25.56	4.75	0.60
<i>D,L</i> -Alanine	60.50	0.618	0.07	-25.03	4.08	0.13
<i>L</i> -Arginine	127.34	1.623	0.12	-26.62	12.06	0.20
<i>D,L</i> -Aspartic acid	73.83	9.588	0.08	-33.12	47.78	0.07
<i>L</i> -Cysteine	73.44	1.376	0.03	-32.82	7.92	0.26
Glutamic acid	85.88	6.652	0.01	-36.17	16.06	0.38
Glycine	43.19	0.864	0.02	-27.00	4.56	0.44
Histidine	98.79	3.295	0.04	31.84	-13.91	0.29
<i>L</i> -Leucine	107.74	-0.059	0.05	-31.78	13.61	0.56
<i>D,L</i> -Methionine	105.35	1.072	0.02	-31.18	14.28	0.25
Phenylalanine	121.48	11.731	0.08	-34.54	36.26	1.48
<i>L</i> -Proline	82.83	0.466	0.08	-23.25	5.79	0.11
<i>D</i> -Tryptophan	143.91	0.233	0.14	-30.24	-41.10	0.23
<i>L</i> -Valine	90.78	0.250	0.01	-30.62	8.43	0.23

^a The least-squares program used to obtain these coefficients had a weighting factor related to the errors in ϕ_V and $\phi_{K(S)}$.
^b Standard error in ϕ_V , cm³ mol⁻¹. ^c Standard error in $\phi_{K(S)}$, cm³ mol⁻¹ bar⁻¹.

where u and u_0 are the speed of sound in the solution and in water, f and f^0 are the pulse repetition frequencies in solution and water, and τ is the electronic delay time. The value of τ was determined by calibration with (Millipore Super Q) ion-exchanged water at various temperatures.

The temperature of the various thermostated bath systems regulating the densimeter and sound velocimeter was set to ± 0.002 °C using a platinum resistance thermometer (calibrated by the National Bureau of Standards), and a G-2 Mueller Bridge.

Results

The apparent molal volumes, ϕ_V , and the adiabatic apparent molal compressibilities, $\phi_{K(S)}$, of the amino acids solutions were determined, respectively, from the density, d , and adiabatic compressibility, β_S , of the solution using the equations

$$\phi_V = \frac{M}{d} + \frac{(d_0 - d)10^3}{mdd_0} \quad (2)$$

and

$$\phi_{K(S)} = \frac{1000(\beta_S d^0 - \beta_S^0 d)}{mdd_0} + \frac{\beta_S M}{d} \quad (3)$$

where d_0 is the density of water, m is the molality, M is the molecular weight of the solute, and $\beta_S^0 = 44.773_5 \times 10^{-6}$ bar⁻¹ is the adiabatic compressibility for water. The adiabatic compressibilities (β_S) of the aqueous solutions at 25 °C were calculated from the sound speeds (u) using $\beta_S = 1/\rho u^2 d$ (4)

The densities and sound velocities were determined from the relative densities and sound speeds given in Table I by using $d_0 = 0.997045$ g cm⁻³ and $u_0 = 1496.69$ m s⁻¹.²³ The values of ϕ_V and $\phi_{K(S)}$ are listed in Table I,²⁰ and are plotted, respectively, vs. m in Figures 1 and 2. The curves represent the least-squares best fit.

The values of ϕ_V and $\phi_{K(S)}$ were least-squares fitted to the equations

$$\phi_V = \phi_V^0 + S_V m \quad (5)$$

and

$$\phi_{K(S)} = \phi_{K(S)}^0 + S_{K(S)} m \quad (6)$$

where $\phi_V^0 = \bar{V}^0$ and $\phi_{K(S)}^0 = \bar{K}^0$ are, respectively, the infinite dilution partial molal volumes and adiabatic partial

TABLE III: A Comparison of the Infinite Dilution Partial Molal Volumes for Amino Acids Obtained in This Study with Literature Values

Compound	ϕ_V^0 , cm ³ mol ⁻¹	
	This work	Literature values
Alanine	60.47	60.61, ^a 60.6, ^a 60.6, ^b 61, ^c 60.47 ^d
Glycine	43.19	43.3, ^a 43.22, ^a 43.29, ^f 43.20, ^g 43.5, ^b 44 ^c
Histidine	98.79	99.3 ^h
Leucine	107.74	107.5, ^a 108, ^c 107.75 ^d
Phenylalanine	121.48	121.2, ^a 121.3 ^c
Proline	82.83	81.0, ^a 81.0, ^b 81 ^c
Tryptophan	143.91	144.1 ^b
Valine	90.78	91.3, ^a 90.78, ^a 91, ^c 91.05 ^b

^a Reference 14. ^b Reference 1. ^c Reference 2. ^d Reference 29. ^e Reference 25. ^f Reference 28. ^g Reference 27. ^h Reference 26.

molal compressibilities, and S_V and $S_{K(S)}$ are the experimental slopes. The values of ϕ_V^0 , $\phi_{K(S)}^0$, S_V , and $S_{K(S)}$ for the amino acids studied at 25 °C are listed in Table II along with the standard deviations (σ). The infinite dilution partial molal volumes of the amino acids reported in the literature^{1,2,5,8,14,18,25-29} are compared with our results in Table III. Our results are in good agreement with the literature values. There is little compressibility data for the amino acids in the literature. The infinite dilution apparent molal compressibilities of Gucker and Haag¹⁷ for alanine and glycine (respectively, $10^4\phi_K = -24.56$ and -26.84) are in good agreement with our $\phi_{K(S)}^0$ values (Table II).

Shown in Figure 1 are plots of ϕ_V vs. m for the amino acids at 25 °C. The ϕ_V of the amino acids is a linear function of the molal concentration. With the exception of leucine, all amino acids have positive slopes. Large positive slopes are found for amino acids having aromatic rings and terminal $-(O=)C-OH$ and $H_2N-(HN=)C-NH_2$ groups (Table II). Amino acids with aliphatic and sulfur groups, and cyclic groups have smaller slopes. Leucine has a small negative slope. Histidine with two nitrogens on a ring has a large positive slope, while tryptophan with one nitrogen on an aromatic ring has a smaller positive slope (Table II).

Shown in Figure 2 are plots of $\phi_{K(S)}$ vs. m for the amino acids at 25 °C. The $\phi_{K(S)}$ of the amino acids are linear functions of the molal concentration. The slopes for the compressibility data behave similarly to the slopes of the volume data, i.e., positive $S_{K(S)}$ slopes are observed for all

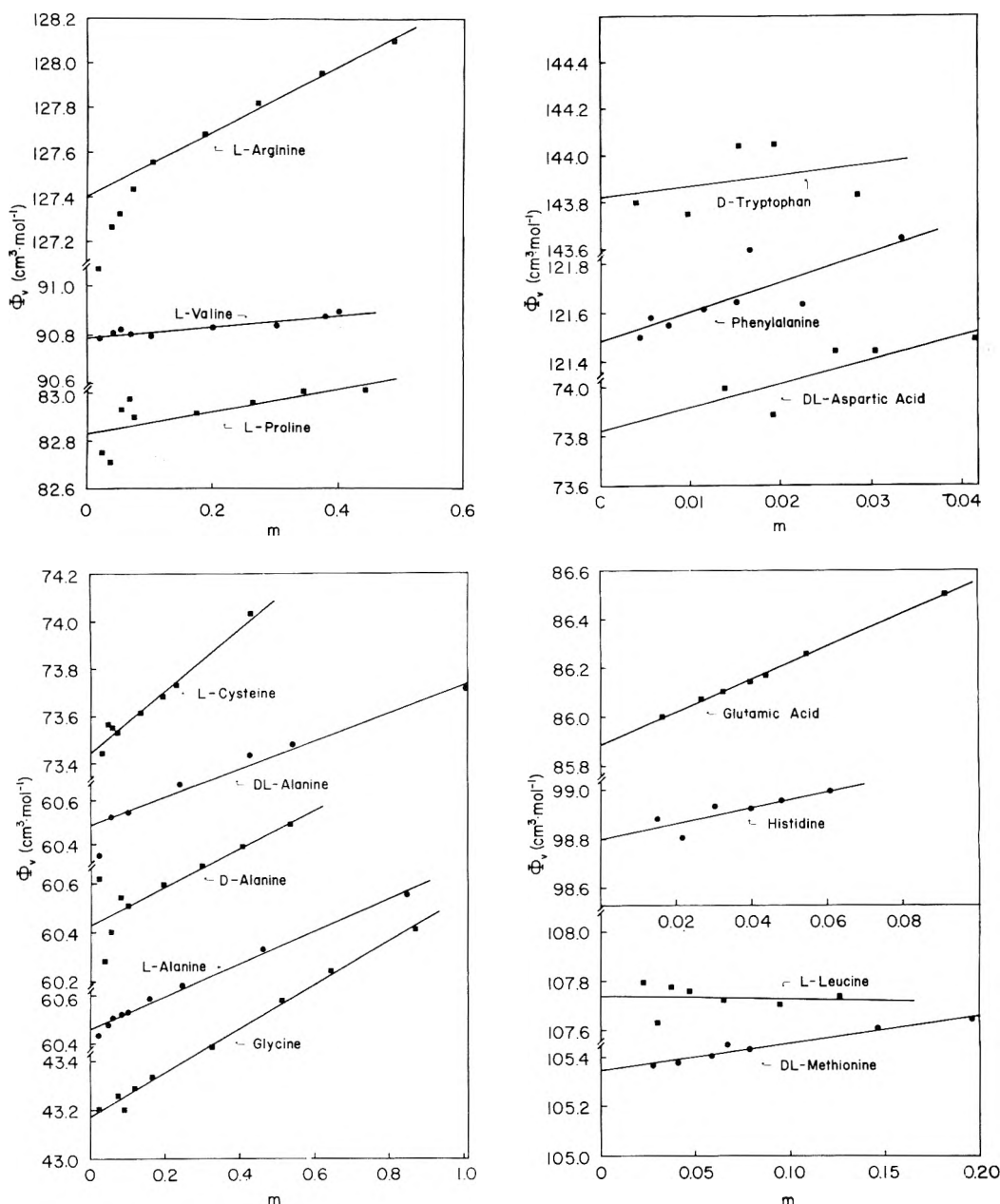


Figure 1. Plot of ϕ_v vs. m for amino acids in water at 25 °C.

amino acids studied with the exception of histidine and tryptophan which have large negative slopes. Amino acids with complex functional groups have greater positive slopes when compared with the slopes of the amino acids having aliphatic and sulfur groups.

Discussion

The partial molal volumes of the amino acids at infinite dilution, as shown in Figure 3, are a linear function of the molecular weight. These results indicate that the volume contribution of the hydrocarbon portion of the amino acids is proportional to the molecular weight (similar to other organic solutes) and the volume contribution due to $\text{NH}_3^+\text{CHC}(=\text{O})\text{O}^-$ is not strongly affected by the hydrocarbon groups. A similar correlation of the partial molal compressibilities does not exist. This is expected since the compressibilities (which vary from -23 to -36×10^{-4}) are more closely related to solute-water interactions. These results led us to examine the additivity properties for the hydrocarbon portion of the amino acids.

The first investigation of the additivity properties of group partial molal volumes in homologous series of or-

ganic solutes in water was made by Traube.³⁰ Recent studies of partial molal volumes of tetraalkylammonium halides,³¹ azoniaspiroalkane bromides,³² alcohols,^{33,34} alkylamines hydrobromides,^{35,36} cyclic amines hydrobromides,³⁷ aliphatic acids,³⁸ dicarboxylic acids,^{38,39} and sodium salts of aliphatic and dicarboxylic acids^{38,39} have been utilized to calculate the group partial molal volumes, $\bar{V}^0(\text{group})$. Values for \bar{V}^0 of $-\text{CH}_3$, $-\text{CH}_2-$, and $-\text{CH}$ groups are given in Table IV. For methylene groups on carbon atoms, $\bar{V}^0(-\text{CH}_2-) = 15.9 \text{ cm}^3 \text{ mol}^{-1}$ which is in excellent agreement with $\bar{V}^0(-\text{CH}_2-) = 16.1 \text{ cm}^3 \text{ mol}^{-1}$ found by Traube.³⁰ The values of $-\text{CH}_2-$ on nitrogen are smaller than those on carbon. For methyl groups $\bar{V}^0(-\text{CH}_3) = 18.1 \text{ cm}^3 \text{ mol}^{-1}$.^{31,32}

Also listed in Table IV are the various groups contributing to the \bar{V}^0 of aqueous amino acids solutions at 25 °C obtained from the literature data. The values of \bar{V}^0 for H_2N^+ , H_3N^+ , $\text{HO}-\text{C}(=\text{O})-$, and $-\text{C}(=\text{O})-\text{O}^-$ were estimated by two independent methods: (1) by least-squares fitting \bar{V}^0 of the compounds containing the group vs. the molecular weight of the hydrocarbon portion of the compound and (2) by additivity. The two methods give

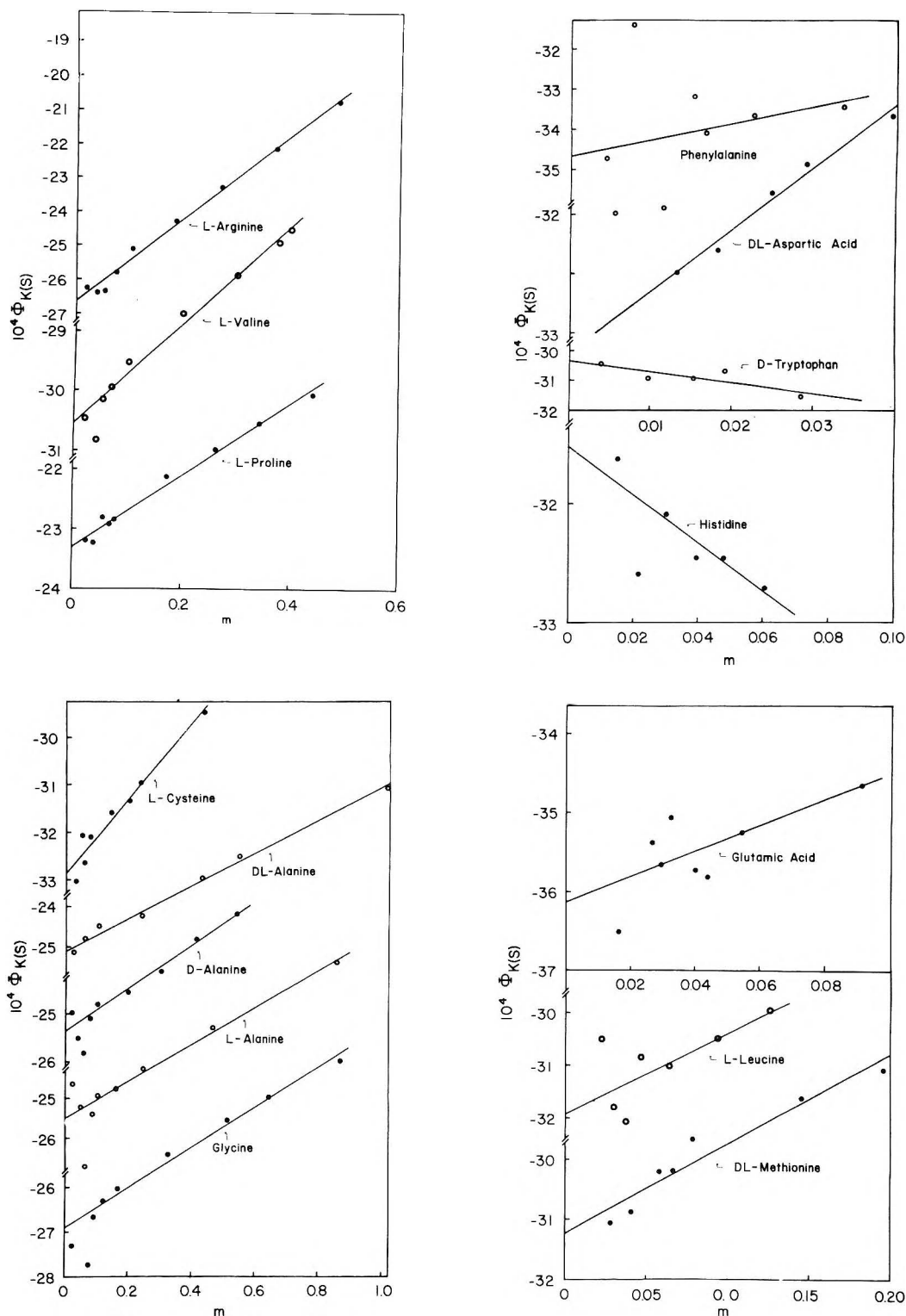


Figure 2. Plot of $\phi_{K(S)}$ vs. m for amino acids in water at 25 °C.

the same results within experimental uncertainties. The values of $\bar{V}^0(-\text{COOH}) = 25.8 \pm 0.5$ and $34.3 \pm 0.4 \text{ cm}^3 \text{ mol}^{-1}$ were estimated, respectively, from the homologous series of $[\text{CH}_2]_n(\text{COOH})_2$ and $\text{CH}_3(\text{CH}_2)_n\text{COOH}$;^{38,39} the values of $\bar{V}^0(-\text{COO}^-) = 17.8 \pm 0.4$ and $26.3 \pm 0.8 \text{ cm}^3 \text{ mol}^{-1}$ were estimated from the homologous series $[\text{CH}_2]_n(\text{COONa})_2$ and $\text{CH}_3(\text{CH}_2)_n\text{COONa}$, respectively;^{38,39} and $\bar{V}^0(-\text{NH}_3^+) = 14.0 \pm 0.6 \text{ cm}^3 \text{ mol}^{-1}$ was estimated from the homologous series $\text{CH}_3(\text{CH}_2)_n\text{NH}_3^+$.^{35,36} For these estimated values we assume $\bar{V}^0(\text{H}^+) = -5.4$, $\bar{V}^0(\text{Na}^+) = -6.6$, $\bar{V}^0(\text{Br}^-) = 30.21$, $\bar{V}^0(-\text{CH}_2-) = 15.9$, and $\bar{V}^0(-\text{CH}_3) = 18.1 \text{ cm}^3 \text{ mol}^{-1}$.³⁶ The value of $\bar{V}^0(-\text{COOH})$ we find from the monocarboxylic acids is $8.5 \text{ cm}^3 \text{ mol}^{-1}$ larger than determined from the

dicarboxylic acids. Høiland³⁸ has obtained similar values ($25.6 \text{ cm}^3 \text{ mol}^{-1}$) for $-\text{COOH}$ from mono- and dicarboxylic acids by using $\bar{V}^0(\text{CH}_3) = 26.1 \text{ cm}^3 \text{ mol}^{-1}$. We feel that this value for $-\text{CH}_3$ is too large and that the differences between the values of $\bar{V}^0(-\text{COOH})$ are real. The decrease in volume is related to an increase in hydration (or hydrogen bonding) when the carboxylic groups are on the same $-\text{CH}_2-$ group. Similar differences are found for the $\bar{V}^0(-\text{COO}^-)$ calculated from the Na salts of the di- and monocarboxylic acids.

We have examined the recent \bar{V}^0 data of Zana⁴⁰ on butylcarboxylic acids, butylcarboxylate ions, and butylammonium ions, and we found that the \bar{V}^0 of the groups

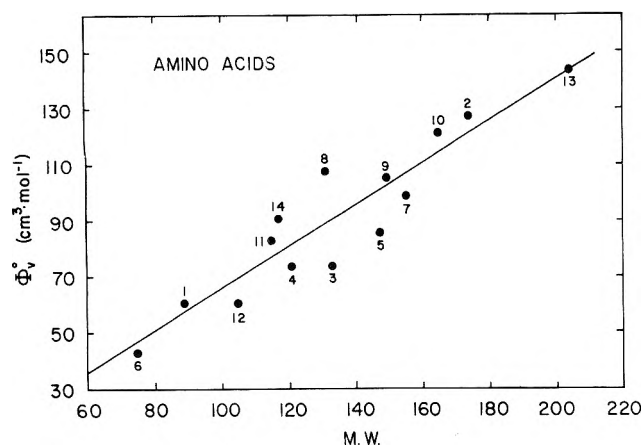


Figure 3. Plot of ϕ_v^0 vs. mol wt for amino acids in water at 25 °C: (1) alanine, (2) arginine, (3) aspartic acid, (4) cysteine, (5) glutamic acid, (6) glycine, (7) histidine, (8) leucine, (9) methionine, (10) phenylalanine, (11) proline, (12) serine, (13) tryptophan, and (14) valine.

TABLE IV: Partial Molal Volumes for Various Functional Groups at Infinite Dilution in Water at 25 °C

Group	\bar{V}^0 , cm ³ mol ⁻¹	Method
O		
-C-OH	34.3	From $\text{CH}_3(\text{CH}_2)_n\text{COOH}^a$
	25.8	From $[\text{CH}_2]_n(\text{COOH})_2^{a,b}$
O		
-C-O ⁻	26.3	From $\text{CH}_3(\text{CH}_2)_n\text{COONa}^a$
	17.8	From $[\text{CH}_2]_n(\text{COONa})^{a,b}$
-NH ₃ ⁺	14.0	From $\text{CH}_3(\text{CH}_2)_n\text{NH}_3^{+c}$
>NH ₂ ⁺	18.4	From cyclic amines ^d
-N ⁺ -	11.7	From R_4NX and azoniaspiroalkane halides ^e
-CH ₃	18.1	On carbon atoms from $\text{R}_4\text{NX}^{e,f}$
-CH ₂ -	16.1	From Traube ^g
	15.9	On carbon atoms from $\text{R}_4\text{NX}^{e,f}$ and RNH_3X^h
	14.8	On $\text{H}_3\text{N}^+-\text{CH}-\text{C}(=\text{O})-\text{O}^-$, from α,ω -aminocarboxylic acids ⁱ
	14.1	On cyclic amines ^d
	13.8	From azoniaspiroalkane halides ^e
-CH	12.0	From alcohols ^j
	12.4	Estimated by additivity from -CH ₃ and -CH ₂ - groups on R_4NX
-C-	9.1	Estimated by additivity from -CH ₃ , -CH ₂ , >CH and -H
	9.9	Estimated by Traube at 16 °C ^g
-H	3.0	Estimated from -CH ₃ , -CH ₂ - from R_4NX , and -CH from alcohols
	3.1	Estimated by Traube ^g
-S-	15.5	Estimated by Traube at 16 °C ^g
-OH	12.0	From mono and dialkylamino alcohols ^h
	11	From alcohols ^j

^a Reference 38. ^b References 38 and 39. ^c References 35 and 36. ^d Reference 37. ^e Reference 32. ^f Reference 31. ^g References 1, 2, and 30. ^h Reference 34. ⁱ Reference 14. ^j Reference 33.

obtained from these data are in good agreement with our group values. It should be noted that these group values contain contributions due to the intrinsic size of the group, $\bar{V}^0(\text{int})$, as well as hydration and hydrophobic effects which are especially important with aliphatic side chains and side chains that can hydrogen bond with water.

The group \bar{V}^0 s can be used to estimate the \bar{V}^0 of glycine. From the groups $\bar{V}^0(-\text{NH}_3^+) = 14.0$, $\bar{V}^0(-\text{C}(=\text{O})-\text{O}^-) =$

17.8, and $\bar{V}^0(-\text{CH}_2-) = 15.9 \text{ cm}^3 \text{ mol}^{-1}$, we obtain

$$\bar{V}^0(\text{glycine})_{\text{calcd}} = \bar{V}^0(-\text{NH}_3^+) + \bar{V}^0(-\text{CH}_2-) + \bar{V}^0(-\text{C}(=\text{O})-\text{O}^-) = 47.7 \text{ cm}^3 \text{ mol}^{-1} \quad (7)$$

For $\bar{V}^0(-\text{C}(=\text{O})-\text{O}^-) = 26.3 \text{ cm}^3 \text{ mol}^{-1}$, $\bar{V}^0(\text{glycine})_{\text{calcd}} = 56.2 \text{ cm}^3 \text{ mol}^{-1}$. These estimates are in poor agreement with the measured value of $43.2 \text{ cm}^3 \text{ mol}^{-1}$. The measured value is 4.5–13.0 $\text{cm}^3 \text{ mol}^{-1}$ lower than predicted. These results indicate that the decrease in volume due to $-\text{NH}_3^+$ and $-\text{C}(=\text{O})-\text{O}^-$ on glycine are greater than on aliphatic compounds. This is presumably due to the inductive effect of the two charged groups increasing the hydration. Similar effects are found for dicarboxylic acids and their Na salts.

In Table V we list the various groups contributing to the \bar{V}^0 of the amino acids. These values are determined from the experimental data and are compared with the group values calculated from first principles using the literature values given in Table IV. While most of these calculated results are in excellent agreement, the last two entries are in poor agreement (Table V), even when using the lower value for $-\text{COOH}$ (Table IV).

At 25 °C, the isoelectric points of aspartic and glutamic acids are about pH 2.8 and 3.2, respectively.⁴¹ At this pH, the amino group carries a positive charge and the two carboxyl groups carry one equivalent of negative charge between them, most of it on the α -carboxyl group, which has the lower pK value.⁴² Thus, the $-\text{COOH}$ group on the side chains of these acids is expected to be ionized and, therefore, it could account for the poor agreement in the last two entries in Table V. If we assume that the $-\text{COOH}$ group is ionized and use the $\bar{V}^0(-\text{COO}^-)$ values (Table IV), a better agreement between observed and calculated values is obtained for the last two entries listed in Table V. Similarly, the isoelectric point of arginine is close to pH 11.⁴² At this pH, ionization of the $\text{H}_2\text{NC}(\text{NH}_2)_2^-$ group can occur and the value of \bar{V}^0 for $\text{H}_2\text{NC}(\text{NH}_2)_2(\text{CH}_2)_2^-$ is for some ionized form of this group (Table V).

Although the values of ϕ_K^0 for the amino acids are not linear functions of the molecular weight, it is possible to estimate group contributions for \bar{K}_S^0 from the data. Literature data are available for the \bar{K}_S^0 for alcohols,⁴³ amines, and the tetraalkylammonium salts.⁴⁴ From these results, it is possible to estimate \bar{K}_S^0 values for $-\text{CH}_2-$ and $-\text{CH}_3$. These values are given in Table VI along with the values estimated from the amino acids. Further studies on a large number of organic solutes in water are needed before the reliability of these group contributions can be assessed.

The partial molal volumes of the amino acids can be examined by a simple model

$$\bar{V}^0(\text{amino acid}) = \bar{V}^0(\text{int}) + \bar{V}^0(\text{elect}) \quad (8)$$

where $\bar{V}^0(\text{int})$ is the intrinsic partial molal volume of the amino acid and $\bar{V}^0(\text{elect})$ is the electrostriction partial molal volume due to the hydration of the amino acid. The $\bar{V}^0(\text{int})$ is made up of two terms, the van der Waals volume (\bar{V}_W^0) and the volume due to packing effects (\bar{V}_P^0)

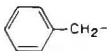
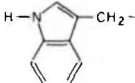
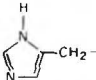
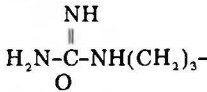
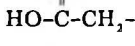
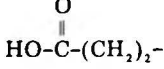
$$\bar{V}^0(\text{int}) = \bar{V}_W^0 + \bar{V}_P^0 \quad (9)$$

The $\bar{V}^0(\text{elect})$ can be estimated from the experimentally measured \bar{V}^0 s providing a reasonable estimate can be made for $\bar{V}^0(\text{int})$

$$\bar{V}^0(\text{elect}) = \bar{V}^0(\text{amino acid}) - \bar{V}^0(\text{int}) \quad (10)$$

Earlier workers^{17,18,27,45–50} have estimated values of $\bar{V}^0(\text{int})$ for amino acids by assuming they are equal to the partial molal volume of the equivalent amide. Since experimental

TABLE V: Partial Molal Volume of Various Functional Groups Calculated from Amino Acids at Infinite Dilution in Water at 25 °C

Group	$\bar{V}^0, \text{cm}^3 \text{mol}^{-1}$		Δ	Method
	From amino acids	Calcd ^a		
$-\text{CH}_2-$	16.9	15.4	1.5	From leucine-valine
$-\text{CH}_3$	17.3	18.4	-1.1	From alanine-glycine
$-\text{CH}(\text{CH}_3)_2$	47.6	49.2	-1.6	From valine-glycine
$-\text{CH}_2\text{CH}(\text{CH}_3)_2$	64.5	64.6	-0.1	From leucine-glycine
$-\text{CH}_2\text{SH}$	30.3	29.9	0.4	From cysteine-glycine
$-(\text{CH}_2)_2\text{SCH}_3$	62.2	60.7	1.5	From methionine-glycine
$-\text{SH}$	14.4			Estimated by additivity from $-\text{CH}_2\text{SH}$ and $-\text{CH}_2-$ from R_4NX
	78.3			From phenylalanine-glycine
	100.6			From tryptophan-glycine
	55.7			From histidine-glycine
	84.2			From arginine-glycine
	30.6	41.2 ^b 49.7 ^c	-10.6 -19.1	From aspartic acid-glycine
	42.7	56.6 ^b 65.1 ^c	-13.9 -22.4	From glutamic acid-glycine

^a Calculated using $\bar{V}^0(-\text{C}^-) = 9.4$ (average value), $\bar{V}^0(-\text{H}) = 3.0$, $\bar{V}^0(-\text{S}-) = 11.4$, and $\bar{V}^0(-\text{COOH}) = 25.8$ and $34.3 \text{ cm}^3 \text{mol}^{-1}$ (Table IV). ^b $\bar{V}^0(-\text{COOH}) = 25.8 \text{ cm}^3 \text{mol}^{-1}$. ^c $\bar{V}^0(-\text{COOH}) = 34.3 \text{ cm}^3 \text{mol}^{-1}$.

data are not available for all the necessary amides, we have estimated the various amides by using the group contributions discussed earlier and the \bar{V}^0 of glycolamide.^{18,27} The values of $\bar{V}^0(\text{elect})$ calculated in this manner are given in Table VII. The values of $\bar{V}^0(\text{elect})$ vary from -10.8 to -15.1 $\text{cm}^3 \text{mol}^{-1}$ (av -13.1 $\text{cm}^3 \text{mol}^{-1}$) and are in good agreement with earlier estimates.^{18,27} Since amides are hydrated, one might expect the magnitude of the values of $\bar{V}^0(\text{elect})$ calculated in this manner to be too low. Another approach that can be used to estimate $\bar{V}^0(\text{int})$ is from crystal molar volumes, $\bar{V}^0_{\text{cryst}} = (\text{mol wt})/d_{\text{cryst}}$, making the appropriate corrections for packing densities. The packing density (ρ) is defined by

$$\rho = \bar{V}_W^0 / \bar{V}^0_{\text{cryst}} = \bar{V}_W^0 / (\bar{V}_W^0 + \bar{V}_P^0) \quad (11)$$

where \bar{V}_W^0 is the van der Waals volume and \bar{V}_P^0 is the packing volume in the crystal. The packing density for molecules in organic crystals is about 0.7.⁵¹ This gives $\bar{V}_W^0 = 0.7\bar{V}^0_{\text{cryst}}$. The packing densities of organic solutes in water have values of 0.57–0.59 for hydrocarbons, alcohols, and carboxylic acids⁵² and 0.61 for amines.⁵³ The packing density for random packing spheres is 0.634.⁵⁴ If we use the values of 0.60 and 0.634, the $\bar{V}^0(\text{int})$ for the amino acids in solution is given by

$$\bar{V}^0(\text{int}) = (0.7/0.6)\bar{V}^0_{\text{cryst}} \quad (12)$$

and

$$\bar{V}^0(\text{int}) = (0.7/0.634)\bar{V}^0_{\text{cryst}} \quad (13)$$

The values of $\bar{V}^0(\text{int})$ for the amino acids have been estimated from eq 12 and 13 using \bar{V}^0_{cryst} determined from the work of Berlin and Pallansch.⁷ The values of $\bar{V}^0(\text{elect})$ calculated from the values of $\bar{V}^0(\text{int})$ using eq 10 are given in Table VII and are compared with those calculated from

$\bar{V}^0(\text{elect}) = \bar{V}^0 - \bar{V}^0(\text{isomer})$. The values of $\bar{V}^0(\text{elect})$ range from -11.6 to -39.0 (av -22.3) $\text{cm}^3 \text{mol}^{-1}$ for $\rho = 0.6$, and -8.7 to -29.2 (av -16.3) $\text{cm}^3 \text{mol}^{-1}$ for $\rho = 0.634$. In contrast, the values of $\bar{V}^0(\text{elect})$ estimated from the isomer method range from -10.8 to -15.1 (av -13.1) $\text{cm}^3 \text{mol}^{-1}$.

The values of $\bar{V}^0(\text{elect})$ estimated by these methods are in reasonable agreement. For amino acids with only hydrocarbon side chains $\bar{V}^0(\text{elect})$ is ~ -12 to $-24 \text{ cm}^3 \text{mol}^{-1}$ for $\rho = 0.6$ and ~ -9 to $-16 \text{ cm}^3 \text{mol}^{-1}$ for $\rho = 0.634$ (Table VII). Since the packing densities of the amino acids could vary as much as 14%, the values of $\bar{V}^0(\text{elect})$ estimated from $\bar{V}^0(\text{cryst})$ have larger errors (5 $\text{cm}^3 \text{mol}^{-1}$) than those estimated from the isomer amides. The values of $\bar{V}^0(\text{elect})$ estimated from the isomer amides is $\sim -13 \text{ cm}^3 \text{mol}^{-1}$. For the amino acids, $\bar{V}^0(\text{elect})$ is much larger in magnitude than predicted from theoretical models of Fuoss⁵⁵ and Kirkwood⁵⁶

$$\bar{V}^0(\text{elect}) = - \frac{3\mu^2 N}{4b^3 D^2} \left(\frac{\partial D}{\partial P} \right)_T \quad (14)$$

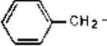
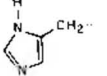
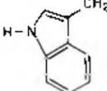
where μ is the dipole moment, N is Avogadro's number, b is the radius of a sphere containing the dipole, D is the dielectric constant, and P the pressure. For glycine $\bar{V}^0(\text{elect}) = -4 \text{ cm}^3 \text{mol}^{-1}$ (Yayanos¹³) compared with the calculated value of $-13 \text{ cm}^3 \text{mol}^{-1}$.

The decrease in volume due to electrostriction can be related to the number of water molecules (n_H) hydrated to the amino acid by¹⁹

$$\bar{V}^0(\text{elect}) = n_H (\bar{V}_E^0 - \bar{V}_B^0) \quad (15)$$

where \bar{V}_E^0 is the molar volume of electrostricted water and \bar{V}_B^0 is the molar volume of bulk water (18.069 $\text{cm}^3 \text{mol}^{-1}$ at 25 °C). This model assumes that for every water

TABLE VI: Apparent Molal Adiabatic Compressibilities of Various Functional Groups Calculated from Amino Acids at Infinite Dilution in Water at 25 °C

Group	$10^4 \phi_K(S)^a$ $\text{cm}^3 \text{mol}^{-1} \text{bar}^{-1}$ (from amino acids)	Method
$\text{H}_3\text{N}^+-\text{CH}(\text{O})-\text{C}-\text{O}^-$	-27.00	Assumed value from glycine
$-\text{CH}_2-$	-1.16	CH_2 next to $\text{H}_3\text{N}^+\text{CHC}(=\text{O})\text{O}^-$ from leucine-valine
	-3.05	CH_2 next to terminal $-\text{COOH}$ from glutamic acid-aspartic acid
	-1.6 ± 0.6	From alcohols ^a
	-1.2 ± 0.8	Average value from R_4NX^b
$-\text{CH}_3$	1.63	From alanine-glycine
	2.0 ± 0.2	From methylamines ^b
	0.8	From alcohols ^a
$-\text{CH}(\text{CH}_3)_2$	-3.62	From valine-glycine
$-\text{CH}_2\text{CH}(\text{CH}_3)_2$	-4.78	From leucine-glycine
$-\text{CH}_2\text{SH}$	-5.82	From cysteine-glycine
$-(\text{CH}_2)_2\text{SCH}_3$	-4.18	From methionine-glycine
$\text{HO}-\text{C}(\text{O})-\text{CH}_2-$	-6.12	From aspartic acid-glycine
$\text{HO}-\text{C}(\text{O})-(\text{CH}_2)_2-$	-9.17	From glutamic acid-glycine
 - CH_2-	-7.54	From phenylalanine-glycine
 - CH_2-	-4.84	From histidine-glycine
 - CH_2-	-3.24	From tryptophan-glycine
$\text{H}_3\text{N}^+-\text{C}(\text{NH})-(\text{CH}_2)_3-$	-0.38	From arginine-glycine

^a Reference 39. ^b Reference 43.

molecule taken from the bulk phase to the region near the amino acid, the volume is decreased by $(\bar{V}_E^0 - \bar{V}_B^0)$. For electrolyte solutions $(\bar{V}_E^0 - \bar{V}_B^0) \approx -3.0 \text{ cm}^3 \text{mol}^{-1}$.¹⁹ Using this value of $(\bar{V}_E^0 - \bar{V}_B^0)$ and the values of $\bar{V}^0(\text{elect})$, calculated by various methods (Table VII), the n_H values were estimated from eq 15. Individual values of n_H range, respectively (columns a to c, Table VII), from 3.9 to 13.0 (av 7.4 ± 2.4), from 2.9 to 9.8 (av 5.4 ± 1.8), and from 3.6 to 5.0 (av 4.4 ± 0.3). Although these values are in reasonable agreement, the values of n_H calculated from $\bar{V}^0(\text{elect})$ in column a, Table VII, are probably too large. For all the methods used, the higher values of n_H occur for amino acids with side chains which can hydrogen bond with water.

By differentiating eq 15 with respect to pressure, one obtains (assuming $\partial \bar{V}_E^0 / \partial P$ and $\partial n_H / \partial P = 0$)

$$\bar{K}^0(\text{elect}) = -[\partial \bar{V}^0(\text{elect}) / \partial P] = n_H (\partial \bar{V}_B^0 / \partial P) \quad (16)$$

where $(\partial \bar{V}_B^0 / \partial P) = -\beta_B^0 \bar{V}_B^0$ is related to the compressibility (β_B^0) of bulk water. Upon rearranging and substituting for $\partial \bar{V}_B^0 / \partial P$, we have

$$n_H = -\bar{K}^0(\text{elect}) / \beta_B^0 \bar{V}_B^0 \quad (17)$$

TABLE VII: Values of $\bar{V}^0(\text{elect})$ for Amino Acids Estimated by Various Methods

Amino acid	$-\bar{V}^0(\text{elect}), \text{cm}^3 \text{mol}^{-1}$		
	a	b	c
Alanine	15.34	11.26	13.0 ^d
Arginine	26.05	17.83	13.0
Aspartic acid	21.09	16.00	13.0
Cysteine	21.10	16.33	13.0
Glutamic acid	23.74	17.86	13.0
Glycine	11.62	8.68	13.1 ^d
Histidine	29.40	22.53	10.8 ^d
Leucine	23.39	16.36	13.0
Methionine	27.44	20.32	13.0
Phenylalanine	25.09	17.23	13.7 ^d
Proline	14.77	9.54	13.8 ^d
Serine	17.20	13.05	12.9 ^d
Tryptophan	38.95	29.15	15.1 ^d
Valine	17.10	11.32	13.0
Average	22.31	16.25	13.10

^a $\bar{V}^0(\text{elect}) = \bar{V}^0 - \bar{V}^0(\text{int})$, where $\bar{V}^0(\text{int}) = (0.7/0.6) \bar{V}^0_{\text{cryst}}$. ^b $\bar{V}^0(\text{elect}) = \bar{V}^0 - \bar{V}^0(\text{int})_{\text{sol}}$, where $\bar{V}^0(\text{int})_{\text{sol}} = (0.7/0.634) \bar{V}^0_{\text{cryst}}$. ^c $\bar{V}^0(\text{elect}) = \bar{V}^0 - \bar{V}^0(\text{int})$, where $\bar{V}^0(\text{int}) = \bar{V}^0(\text{isomer})$ and $\bar{V}^0(\text{isomer}) = \bar{V}^0(\text{glycolamide}) + \bar{V}^0(\text{amino acid}) - \bar{V}^0(\text{glycine})$. ^d Reference 18; ref 1, p 159.

The $\bar{K}^0(\text{elect})$ can be calculated from the experimental values of $\bar{K}^0(\text{amino acid})$ from

$$\bar{K}^0(\text{elect}) = \bar{K}^0(\text{amino acid}) - \bar{K}^0(\text{int}) \quad (18)$$

Since one would expect $\bar{K}^0(\text{int})$ to be small (it is less than $5 \times 10^{-4} \text{ cm}^3 \text{mol}^{-1} \text{bar}^{-1}$ for ionic crystals and many dissolved organic solutes in water), as a first approximation, one can assume $\bar{K}^0(\text{int}) \approx 0$. The \bar{K}^0 for a few amides have been measured and are all $\sim 3 \times 10^{-4} \text{ cm}^3 \text{mol}^{-1} \text{bar}^{-1}$.¹⁷ Thus, one might expect $\bar{K}^0(\text{int})$ for the amino acids to be equal to $\sim 3 \times 10^{-4} \text{ cm}^3 \text{mol}^{-1} \text{bar}^{-1}$. The values of $\bar{K}^0(\text{elect})$ calculated from eq 18 assuming $\bar{K}^0(\text{int}) \approx 3.0 \times 10^{-4} \text{ cm}^3 \text{mol}^{-1} \text{bar}^{-1}$ are given in Table VIII. For glycine and alanine, we have used $\bar{K}^0(\text{isomer}) = 2.70 \times 10^{-4}$ and $3.35 \times 10^{-4} \text{ cm}^3 \text{mol}^{-1} \text{bar}^{-1}$ for glycolamide and lactamide, respectively.¹⁷ For $\bar{K}^0(\text{int}) \approx 0$, the values of $\bar{K}^0(\text{elect})$ are those given in Table II. The values of n_H calculated from eq 17 using the $\bar{K}^0(\text{elect})$ values determined by these two methods are also given in Table VIII. Individual values of n_H range from 2.9 to 4.5 (av 3.6 ± 0.5) for $\bar{K}^0(\text{int}) \approx 0$, and from 3.2 to 4.8 (av 4.0 ± 0.5) for $\bar{K}^0(\text{int}) \approx 3 \times 10^{-4} \text{ cm}^3 \text{mol}^{-1} \text{bar}^{-1}$. These values are in good agreement with the values calculated from $\bar{V}^0(\text{elect})$.

The hydration model as well as the continuum model¹⁹ indicate that $\bar{V}^0(\text{elect})$ is directly proportional to $\bar{K}^0(\text{elect})$:

$$\bar{V}^0(\text{elect}) = k \bar{K}^0(\text{elect}) \quad (19)$$

where, for the hydration model

$$k = -(\bar{V}_E^0 - \bar{V}_B^0) / \beta_B^0 \bar{V}_B^0 \quad (20)$$

and for the continuum model for ionic solutes

$$k = \frac{(\partial \ln D / \partial P)}{(\partial^2 \ln D / \partial P^2) - 2(\partial \ln D / \partial P)^2} \quad (21)$$

At 25 °C, using $(\partial \ln D / \partial P) = 47.10 \times 10^{-6}$ and $(\partial^2 \ln D / \partial P^2) = -71.53 \times 10^{-10}$ given by Owen et al.⁵⁷ the continuum model yields $k = 4.1 \times 10^3 \text{ bar}$. [In previous studies¹⁹ eq 21 was given without the factor of 2 in front of the term $(\partial \ln D / \partial P)^2$ which gives a slightly higher value of k , i.e., $k = 5.0 \times 10^3 \text{ bar}$.]

Differentiation of eq 14 with respect to pressure and substituting into eq 19 yields eq 21 for a zwitterion in a

TABLE VIII: Values of $\bar{K}_S^0(\text{elect})$ and n_H for Amino Acids Estimated by Various Methods

Amino acid	$-10^4 \bar{K}_S^0(\text{elect}),^a$ $\text{cm}^3 \text{mol}^{-1} \text{bar}^{-1}$	n_H			
		From compressibility		From volume	
		b	c	d	e
d-Alanine	28.88	3.16	3.57	3.41	3.94
l-Alanine	28.91	3.16	3.57	3.41	3.94
dl-Alanine	28.37	3.09	3.51	3.41	3.94
l-Arginine	29.62	3.29	3.66	5.40	3.94
dl-Aspartic acid	36.12	4.09	4.46	4.85	3.94
l-Cysteine	35.82	4.06	4.43	4.95	3.94
Glutamic acid	39.17	4.48	4.84	5.41	3.94
Glycine	29.70	3.34	3.67	2.63	3.97
Histidine	34.84	3.94	4.29	6.83	3.27
l-Leucine	34.78	3.93	4.30	4.96	3.94
dl-Methionine	34.18	3.85	4.22	6.16	3.94
Phenylalanine	37.54	4.28	4.64	5.22	4.15
l-Proline	26.25	2.87	3.24	2.89	4.18
d-Tryptophan	33.24	3.72	4.11	8.83	4.58
l-Valine	33.62	3.78	4.16	3.43	3.94
Average	32.74 ± 3.84	3.67 ± 0.49	4.04 ± 0.47	4.79 ± 1.67	3.97 ± 0.26

^a $\bar{K}_S^0(\text{elect}) = \bar{K}^0(\text{amino acid}) - \bar{K}^0(\text{int})$ where $\bar{K}^0(\text{int}) = \bar{K}^0(\text{isomer})$ for glycine (2.7×10^{-4}) and alanine (3.35×10^{-4}), ref 17, and $\bar{K}^0(\text{int}) = 3 \times 10^{-4}$ for the other amino acids. ^b $n_H = -\bar{K}_S^0(\text{elect})/\bar{V}_B^0\beta_B^0$ where $\bar{K}_S^0(\text{elect}) = \bar{K}^0(\text{amino acid})$.

^c $n_H = -\bar{K}_S^0(\text{elect})/\bar{V}_B^0\beta_B^0$ where $\bar{K}_S^0(\text{elect})$ given in column 1. ^d $n_H = \bar{V}^0(\text{elect})/-3.3$ where $\bar{V}^0(\text{elect}) = \bar{V}^0(\text{amino acid}) - (0.7/0.634)\bar{V}^0(\text{cryst})$, column b of Table VII. ^e $n_H = \bar{V}^0(\text{elect})/-3.3$ where $\bar{V}^0(\text{elect}) = \bar{V}^0(\text{amino acid}) - \bar{V}^0(\text{isomer})$, column c of Table VII.

continuum. Thus, at 25 °C, $k = 4.1 \times 10^3$ bar for both dipolar ions and ionic solutes in a continuum model. The results are too scattered for a plot of $\bar{V}^0(\text{elect})$ vs $\bar{K}^0(\text{elect})$ to be meaningful. However, the slope, $k = \bar{V}^0(\text{elect})/\bar{K}^0(\text{elect})$, calculated for our best average estimate of $\bar{V}^0(\text{elect})$ and $\bar{K}^0(\text{elect})$, is found to be $4.5 (\pm 0.5) \times 10^3$ bar which is in reasonable agreement with the continuum model k value. For various electrolytes the hydration model yields $k = 3.6 \times 10^3$ bar, whereas for ion pair formation, and for ionization of weak acids and bases, k is 3.7×10^3 and 4.7×10^3 bar, respectively.¹⁹ The experimental values of these slopes, k , are in reasonable agreement with the continuum model.

The calculated value from $k = 4.1 \times 10^3$ bar yields a value of $(\bar{V}_E^0 - \bar{V}_B^0) = -k\bar{V}_B^0\beta_B^0 = -3.3 \text{ cm}^3 \text{mol}^{-1}$ which is smaller than the value $(-2.7 \text{ cm}^3 \text{mol}^{-1})$ for ions. By using this lower value, $(\bar{V}_E^0 - \bar{V}_B^0) = -3.3 \text{ cm}^3 \text{mol}^{-1}$, and the $\bar{V}^0(\text{elect})$ listed in columns b and c, Table VII, the n_H values were recalculated from eq 15. The results are given in Table VIII, along with the n_H values determined from the compressibility data. The values of n_H calculated, by several methods, from the volume and compressibility data are in good agreement. For the volume data individual values of n_H range from 2.6 to 8.9 (av 4.8 ± 1.7) and from 3.3 to 4.6 (av 4.0 ± 0.3), columns c and d, Table VIII, respectively. Combining the values of n_H from the compressibility and volume data, we obtain an average of 4.1 water molecules hydrated to the $\text{NH}_3^+\text{CHC}(=\text{O})\text{O}^-$ group.

In summary, volume and compressibility data have been determined for aqueous amino acids solutions and the results have been used to estimate the number of hydrated water molecules. The electrostriction partial molal volume and compressibility were determined from the measured \bar{V}^0 and \bar{K}^0 , and $\bar{V}^0(\text{int})$ and $\bar{K}^0(\text{int})$. The $\bar{V}^0(\text{int})$ were estimated from the crystal volume (\bar{V}^0_{cryst}) and \bar{V}^0 of uncharged isomers. Group contributions for \bar{V}^0 and \bar{K}^0 have been determined by several methods. The volume results are in good agreement with the values calculated by other workers. This simplistic approach of relating the volume and compressibility behavior with purely Coulombic interactions seems successful in obtaining credible values for such properties as apparent hydration numbers

when applied to electrolytes and amino acids in aqueous solutions. However, this approach tends to mask contributions from other types of interactions (i.e., hydrophobic hydration) particularly in the case of proteins, amino acids, and soluble organic solutes which have side chains that can hydrogen bond with water.

Acknowledgment. The authors gratefully acknowledge the valuable comments provided by Professor John T. Edsall. They also acknowledge the support of the Office of Naval Research (N00014-75-C-0173) and the Oceanographic Section of the National Science Foundation (OCE73-00351-A01) for this study.

Supplementary Material Available: Table I consists of experimental data for 15 amino acids in water at 25 °C. The data are relative density and sound speed, and apparent molal volume and adiabatic compressibility (6 pages). Ordering information is available on any current masthead page.

References and Notes

- (1) E. J. Cohn and J. T. Edsall, "Proteins, Amino Acids and Peptides as Ions", Reinhold, New York, N.Y., 1943.
- (2) J. P. Greenstein and M. Winitz, "Chemistry of the Amino Acids", Vol. I, Wiley-Interscience, New York, N.Y., 1961.
- (3) J. W. Larson and L. G. Hepler, "Solute-Solvent Interactions", J. F. Coetzee and C. D. Ritchie, Ed., Marcel Dekker, New York, N.Y., 1969.
- (4) G. Ling in "Water and Aqueous Solutions", R. A. Horne, Ed., Wiley-Interscience, New York, N.Y., Chapter 16, 1972.
- (5) H. Chick and C. J. Martin, *Biochem. J.*, **7**, 92 (1913).
- (6) T. L. McMeekin, M. Groves, and N. J. Hipp, *J. Polym. Sci.*, **12**, 309 (1954).
- (7) E. Berlin and M. J. Pallansch, *J. Phys. Chem.*, **72**, 1887 (1968).
- (8) J. Bernhardt and H. Pauly, *J. Phys. Chem.*, **79**, 584 (1975).
- (9) M. O. Dayhoff, G. E. Perlmann, and D. A. MacInnes, *J. Am. Chem. Soc.*, **74**, 2515 (1952).
- (10) M. J. Hunter, *J. Phys. Chem.*, **70**, 3285 (1966).
- (11) H. B. Bull and K. Breeze, *J. Phys. Chem.*, **72**, 1817 (1968).
- (12) F. J. Millero, G. K. Ward, and P. V. Chetirkin, *J. Biol. Chem.*, **251**, 4001 (1976); *ibid.*, in press.
- (13) A. A. Yayanos, *J. Phys. Chem.*, **75**, 1783 (1971).
- (14) J. Kirchnerova, P. G. Farrell, and J. T. Edward, *J. Phys. Chem.*, **80**, 1974 (1976).
- (15) F. J. Millero, *Chem. Rev.*, **71**, 147 (1971).
- (16) F. J. Millero, G. K. Ward, and P. V. Chetirkin, *J. Sol. Chem.*, to be submitted.
- (17) F. T. Gucker, Jr., and R. M. Haag, *J. Acoust. Soc. Am.*, **25**, 470 (1953).
- (18) E. J. Cohn, T. L. McMeekin, J. T. Edsall, and M. H. Blanchard, *J. Am. Chem. Soc.*, **56**, 784 (1934).

- (19) F. J. Millero, G. K. Ward, F. K. Lepple, and E. V. Hoff, *J. Phys. Chem.*, **78**, 1636 (1974).
- (20) Available as supplementary material. See paragraph at the end of the paper.
- (21) G. S. Kell, *J. Chem. Eng. Data*, **15**, 119 (1970).
- (22) F. J. Millero, D. Lawson, and A. Gonzalez, *J. Geophys. Res.*, **81**, 1177 (1976).
- (23) V. A. Del Grosso and C. W. Mader, *J. Acoust. Soc. Am.*, **52**, 961 (1972).
- (24) F. J. Millero and T. Kubinski, *J. Acoust. Soc. Am.*, **57**, 312 (1975).
- (25) H. D. Ellerton, G. Reinfelds, D. E. Mukahy, and P. J. Dunlop, *J. Phys. Chem.*, **68**, 398 (1964).
- (26) F. T. Gucker, Jr., and T. W. Allen, *J. Am. Chem. Soc.*, **64**, 191 (1942).
- (27) F. T. Gucker, Jr., W. L. Ford, and C. E. Moser, *J. Phys. Chem.*, **43**, 153 (1939).
- (28) H. F. V. Tyrrell and M. Hennerby, *J. Chem. Soc. A*, 2724 (1968).
- (29) J.-D. C. Ahluwalia, C. Ostiguy, G. Perron, and J. E. Desnoyers, *Can. J. Chem.*, **55**, 3364 (1977).
- (30) J. Traube, *Samm. Chem. Vortr.*, **4**, 255 (1899).
- (31) J. E. Desnoyers and M. Arel, *Can. J. Chem.*, **47**, 547 (1969).
- (32) W.-Y. Wen, A. Lo Surdo, C. Jolicœur, and J. Boileau, *J. Phys. Chem.*, **80**, 466 (1976).
- (33) C. Jolicœur and G. Lacroix, *Can. J. Chem.*, **54**, 624 (1976).
- (34) S. Cabani, V. Mollica, L. Lepori, and S. T. Lobo, *J. Phys. Chem.*, **81**, 987 (1977).
- (35) J. E. Desnoyers and M. Arel, *Can. J. Chem.*, **45**, 359 (1967).
- (36) F. J. Millero in "Water and Aqueous Solutions", R. A. Horne, Ed., Wiley-Interscience, New York, N.Y., 1972. [$V^{\circ}(\text{H}^+) = -5.4 \text{ cm}^3 \text{ mol}^{-1}$ reported by R. Zana and E. Yeager, *J. Phys. Chem.*, **70**, 954 (1966); **71**, 4241 (1967)].
- (37) C. Jolicœur, J. Boileau, S. Banzinet, and P. Picker, *Can. J. Chem.*, **53**, 716 (1975).
- (38) H. Høiland, *Acta Chem. Scand., Ser. A*, **28**, 699 (1974).
- (39) H. Høiland, *J. Chem. Soc., Faraday Trans. 1*, **71**, 797 (1975).
- (40) R. Zana, *J. Phys. Chem.*, **81**, 1817 (1977).
- (41) Reference 1, Chapter 4, p 85.
- (42) Professor J. T. Edsall, personal communication.
- (43) H. Høiland and E. Vikingstad, *Acta Chem. Scand., Ser. A*, **30**, 692 (1976).
- (44) L. H. Laliberte and B. E. Conway, *J. Phys. Chem.*, **74**, 4116 (1970).
- (45) T. L. McMeekin, E. J. Cohn, and J. H. Weare, *J. Am. Chem. Soc.*, **57**, 626 (1935).
- (46) J. P. Greenstein and J. Wyman, Jr., *J. Am. Chem. Soc.*, **58**, 463 (1936).
- (47) J. P. Greenstein, J. Wyman, Jr., and E. J. Cohn, *J. Am. Chem. Soc.*, **57**, 637 (1935).
- (48) J. Daniel and E. J. Cohn, *J. Am. Chem. Soc.*, **58**, 415 (1936).
- (49) J. T. Edsall and J. Wyman, Jr., *J. Am. Chem. Soc.*, **57**, 1964 (1935).
- (50) J. Z. Dalton and C. L. A. Schilde, *J. Biol. Chem.*, **103**, 549 (1933); **109**, 241 (1935).
- (51) E. J. King, *J. Phys. Chem.*, **73**, 1220 (1969).
- (52) (a) W. L. Masterton, *J. Chem. Phys.*, **22**, 1830 (1954); (b) R. Kobayashi and D. L. Katz, *Ind. Eng. Chem.*, **45**, 440 (1953).
- (53) (a) R. E. Verrall and B. E. Conway, *J. Phys. Chem.*, **70**, 3961 (1966); (b) B. E. Conway, R. E. Verrall, and J. E. Desnoyers, *Trans. Faraday Soc.*, **62**, 2738 (1966); (c) S. D. Hamann and S. C. Lim, *Aust. J. Chem.*, **7**, 329 (1954).
- (54) (a) G. D. Scott, *Nature (London)*, **185**, 68 (1960); (b) J. D. Bernal and J. L. Finney, *Discuss. Faraday Soc.*, **43**, 62 (1967); (c) W. C. Duer, J. R. Greenstein, G. B. Oglesby, and F. J. Millero, *J. Chem. Ed.*, **54**, 139 (1977).
- (55) R. M. Fuoss, *J. Am. Chem. Soc.*, **58**, 982 (1936).
- (56) J. K. Kirkwood, *Chem. Rev.*, **19**, 275 (1936).
- (57) B. B. Owen, R. C. Miller, C. E. Milner, and H. L. Cogan, *J. Phys. Chem.*, **65**, 2065 (1961).

Standard Thermodynamics of Transfer. Uses and Misuses

A. Ben-Naim

Department of Physical Chemistry, The Hebrew University of Jerusalem, Jerusalem, Israel (Received July 29, 1977; Revised Manuscript Received December 16, 1977)

The standard free energy of transfer of a solute A between two solvents a and b is discussed at both a thermodynamic and a statistical mechanical level. It is shown that whereas thermodynamics alone cannot be used to choose the "best" standard quantity, statistical mechanics can help to make such a choice. It is shown that $\Delta\mu_A^{\circ}$, the standard free energy of transferring A, computed by the use of the *number density* (or *molarity*) scale, has the following advantages: (1) it is the simplest and least ambiguous quantity; (2) it is the quantity that directly probes the difference in the solvation properties of the two solvents with respect to the solute A; (3) it can be used, without any change of notation, in any solution, not necessarily a dilute one, and including even pure A; (4) by straightforward thermodynamic manipulations one obtains the entropy, enthalpy, volume changes, etc. for the same process. All of these quantities have advantages similar to the ones indicated for the free energy change. Because of the advantages of this particular choice of standard quantities, we propose to "standardize" the use of the standard thermodynamic quantities of transfer and refer to them as the *local-standard* quantities. Some common misconceptions and misinterpretations of other standard quantities are indicated.

1. Introduction

The purpose of this paper is to examine critically some thermodynamic quantities which are ubiquitous in the field of aqueous solutions. Part of the material presented here has already been published before,^{1,2} but here we shall present the issue in more detail. Also some new and more fundamental arguments are given which have not been presented previously.

Today, there are a growing number of articles ranging from solution chemistry to biochemistry and biology in which standard thermodynamic quantities of transfer are used. In many of these papers the authors make certain statements concerning the interpretation of these concepts without taking the trouble of checking their validity.

The central issue of this paper is to show that standard thermodynamic quantities of transferring a solute between two phases, based on the *molar concentration* scale, have unique advantages over all other standard quantities. The main reason for that is that these standard quantities are completely devoid of any contribution from the translational degree of freedom of the solute. Therefore they are referred to as the *local-standard* quantities of transfer.

The *local* character of these quantities are quite easy to see in the standard free energy of transfer. Here a mere choice of the correct concentration scale leads directly to the required standard quantity. The identification of the *local-standard* entropy, enthalpy, or volume of transfer is more intricate and involves some subtle arguments. To

the best of the author's knowledge these quantities, though of fundamental nature, have never been applied before in the field of solvation thermodynamics.

In order to establish the above contention, one needs to appeal to some statistical mechanical arguments. These are presented in section 3. It will be shown that really only very basic knowledge of statistical mechanics^{3,4} is required in order to follow all the arguments presented in this paper.

2. Specific Objectives

The specific points which will be addressed in this paper are the following:

(a) Thermodynamics alone does not provide a molecular interpretation for some of the standard chemical potentials, entropies, enthalpies, etc. One needs some appeal to statistical mechanical concepts to gain a clear insight into the content of these quantities. Therefore, the general expression of the chemical potential is derived in the T, P, N ensemble, which is the most useful for practical applications. It is shown that the number density (or molar concentration) scale is the most useful and meaningful one to use in constructing various standard quantities for transfer.

(b) Analysis of the use of the "unitary standard states" reveals some misconceptions. It is unfortunate that the term "unitary" has been attached to one quantity, whereas in fact, it should have been reserved for a different one altogether.

(c) We advocate the use of certain quantities, commonly referred to as "standard", and usually defined only for very dilute solutions, for any solution without restricting the solute concentration. These will be referred to as generalized standard quantities.

(d) The entropies and the enthalpies of transfer, when properly evaluated and interpreted, do not involve the temperature dependence of the molar-concentration scale. This temperature dependence of the molar concentration has been a traditional argument against the uses of the molar concentration scale. Similar considerations apply to the pressure dependence of the molar concentration.

(e) The local-standard free energy of solution of a solute, based on the molar concentration scale, has the property that it directly measures the free energy of interaction of the solute with the solvent. If the solvent becomes rarefied this quantity tends to zero as one should expect from such a quantity. Other standard quantities diverge when the solvent becomes rarefied and therefore cannot serve as bona-fide measures of the solvation free energy of the solute.

3. Fundamental Equation for the Chemical Potential

To keep the mathematical complexity of our presentation to the bare minimum necessary, we consider a system of two components A and B of simple spherical and structureless molecules at a given temperature T and pressure P .⁵ These are the most important variables for the practical applications that will be discussed.

We start with the classical canonical partition function for a fluid mixture of N_A molecules of A and N_B molecules of B⁴

$$Q(T, V, N_A, N_B) = \frac{q_A^{N_A} q_B^{N_B}}{N_A! N_B! \Lambda_A^{3N_A} \Lambda_B^{3N_B}} \times \int \cdots \int d\mathbf{R}^{N_A} d\mathbf{R}^{N_B} \exp[-\beta U(N_A, N_B)] \\ = \frac{q_A^{N_A} q_B^{N_B} Z(N_A, N_B)}{N_A! N_B! \Lambda_A^{3N_A} \Lambda_B^{3N_B}} \quad (3.1)$$

Here $\beta = (kT)^{-1}$, with k the Boltzmann constant. q_A and q_B are the internal partition functions of a single A or B molecule, respectively. We shall not require the explicit form of these functions, and for demonstrating our result we put $q_A = q_B = 1$ without affecting any of our conclusions. Λ_A^3 is the momentum partition function, which results from the integration over all possible momenta of a single molecule. $U(N_A, N_B)$ represents the total potential energy of interaction among all the $N_A + N_B$ molecules which are at some particular configuration $\mathbf{R}_1, \dots, \mathbf{R}_{N_A}, \mathbf{R}_{N_A+1}, \dots, \mathbf{R}_{N_A+N_B}$, where \mathbf{R}_i is the position vector of the i th molecule. The integration is over all possible configurations of the $N_A + N_B$ molecules. The integral on the right-hand side of (3.1) is referred to as the configurational partition function and is denoted by $Z(N_A, N_B)$.

The isothermal-isobaric partition function is defined by

$$\Delta(T, P, N_A, N_B) = C \int_0^\infty dV Q(T, V, N_A, N_B) \exp[-\beta PV]$$

where C has the dimensions of a reciprocal volume. Its exact specification will be of no concern to us since we shall be interested only in ratios of partition functions, in which case this constant cancels out.

The fundamental connection with thermodynamics is given by

$$G(T, P, N_A, N_B) = -kT \ln \Delta(T, P, N_A, N_B) \quad (3.2)$$

where G is the Gibbs free energy of the system.

The chemical potential (CP) of component A, e.g., is defined by

$$\mu_A = (\partial G / \partial N_A)_{T, P, N_B} = -kT (\partial \ln \Delta / \partial N_A)_{T, P, N_B} \quad (3.3)$$

and because of the extensive character of the free energy we can replace the derivative in (3.3) by the difference

$$\mu_A = G(T, P, N_A + 1, N_B) - G(T, P, N_A, N_B) \quad (3.4)$$

provided we take the proper thermodynamic limit.

For purposes of interpretation of certain quantities it is useful to introduce an auxiliary quantity which we shall refer to as the pseudo-chemical potential (PCD).² As in (3.4) the pseudo-chemical potential is the free energy change required to introduce a single A molecule into the system, but with the additional restriction that the newly added molecule be placed at some fixed point \mathbf{R}_0 .

Thus instead of (3.4) we define the PCP as

$$\tilde{\mu}_A = G(T, P, N_A + 1, N_B; \mathbf{R}_0) - G(T, P, N_A, N_B) \quad (3.5)$$

Clearly since all points in a homogeneous fluid are equivalent, $\tilde{\mu}_A$ is not a function of the point \mathbf{R}_0 . The tilde on $\tilde{\mu}_A$ serves to remind us that the added particle is placed at some fixed point. Note also that the process of adding a particle to a fixed position cannot be performed experimentally. Hence $\tilde{\mu}_A$ is not a measurable quantity, but neither is μ_A ! Only differences in chemical potentials are measurable quantities, and we shall find that differences in $\tilde{\mu}_A$ are measurable and furthermore they are useful quantities for interpretation of standard free energies of transfer.

We now write the statistical mechanical expressions for $G(T, P, N_A + 1, N_B)$ and for $G(T, P, N_A + 1, N_B; \mathbf{R}_0)$. For simplicity we omit T, P from our notations. Thus

$$\exp[-\beta G(N_A + 1, N_B)] = \frac{\int dV \int \cdots \int d\mathbf{R}_0 d\mathbf{R}^{N_A} d\mathbf{R}^{N_B} \exp[-\beta U(N_A + 1, N_B) - \beta PV]}{(N_A + 1)! N_B! \Lambda_A^{3(N_A + 1)} \Lambda_B^{3N_B}} \quad (3.6)$$

$$\exp[-\beta G(N_A + 1, N_B; \mathbf{R}_0)] = \frac{\int dV \int \cdots \int d\mathbf{R}^{N_A} d\mathbf{R}^{N_B} \exp[-\beta U(N_A + 1, N_B) - \beta PV]}{N_A! N_B! \Lambda_A^{3N_A} \Lambda_B^{3N_B}} \quad (3.7)$$

It is instructive to examine the difference between the two expressions in (3.6) and (3.7). The factor $(N_A + 1)!$ in (3.6) is replaced by $N_A!$ in (3.7). The reason is that in the first case we have $N_A + 1$ indistinguishable A molecules, whereas in the second case we have only N_A indistinguishable molecules; the newly added molecule is distinguishable by the very fact that it is placed at a fixed position \mathbf{R}_0 . Since in the second case the added particle is devoid of translational degrees of freedom it does not contribute a factor Λ_A^3 to the partition function. Hence we have $\Lambda_A^{3(N_A + 1)}$ in the first case and only $\Lambda_A^{3N_A}$ in the second. For the same reason the integration in (3.6) is over all the locations of the $N_A + 1 + N_B$ molecules. In (3.7) the location of the added molecule is *fixed* at \mathbf{R}_0 and integration extends only over all locations of the $N_A + N_B$ molecules.

Having the statistical mechanical expressions for $G(N_A, N_B)$ in (3.2), for $G(N_A + 1, N_B)$ in (3.6) and for $G(N_A + 1, N_B; \mathbf{R}_0)$ in (3.7) we can form the differences in (3.4) and (3.5) to obtain the CP and the PCP of the component A. It is convenient to define $B_A(\mathbf{R}_0)$ by

$$U(N_A + 1, N_B) = U(N_A, N_B) + B_A(\mathbf{R}_0) \quad (3.8)$$

where $B_A(\mathbf{R}_0)$ is the interaction energy of an A molecule at \mathbf{R}_0 , with the rest of the system, at some specific configuration symbolically denoted by (N_A, N_B) . We shall refer to $B_A(\mathbf{R}_0)$ as the "binding energy" of A.

There is a standard procedure to compute the CP from the partition functions (3.6) and (3.2). A very detailed derivation may be found in Appendix F of ref 2. Briefly, the process is

$$\begin{aligned} \exp[-\beta \mu_A] &= \frac{\exp[-\beta G(N_A + 1, N_B) + \beta G(N_A, N_B)]}{\Lambda_A^3 \rho_A} \\ &= \frac{\Delta(T, P, N_A + 1, N_B)}{\Delta(T, P, N_A, N_B)} \\ &= \frac{\langle \exp[-\beta B_A(\mathbf{R}_0)] \rangle_0}{\Lambda_A^3 \rho_A} \end{aligned} \quad (3.9)$$

where we have defined the number density $\rho_A = (N_A + 1)/V \approx N_A/V$, and V is the average volume of the system at T, P, N_A, N_B . The symbol $\langle \rangle_0$ represents an average over all configurations of the molecules in the system except the newly added molecule. We use the conditional probability density of finding a specific configuration of $N_A + N_B$ molecules given that the system has volume V , i.e.

$$P(N_A, N_B/V) = \frac{\exp[-\beta U(N_A, N_B)]}{\int \cdots \int d\mathbf{R}^{N_A} d\mathbf{R}^{N_B} \exp[-\beta U(N_A, N_B)]} \quad (3.10)$$

An expression similar to (3.9) but without the factor $\Lambda_A^3 \rho_A$

can be obtained for $\tilde{\mu}_A$.² These two are written in a more familiar form as

$$\mu_A = kT \ln \rho_A \Lambda_A^3 - kT \ln \langle \exp[-\beta B_A(\mathbf{R}_0)] \rangle_0 \quad (3.11)$$

$$\tilde{\mu}_A = -kT \ln \langle \exp[-\beta B_A(\mathbf{R}_0)] \rangle_0 \quad (3.12)$$

Combining (3.11) with (3.12) we obtain the final result

$$\mu_A = \tilde{\mu}_A + kT \ln \rho_A \Lambda_A^3 \quad (3.13)$$

which is valid for any composition of the mixture. So far, we have invoked no assumption of *ideality* of the mixture in any sense. The meaning of (3.13) is very simple and should be noted carefully. The work required to add a new A molecule to the system (at T, P, N_B constant) is split into two parts corresponding to two consecutive steps; first we add the particle at a fixed position, e.g., \mathbf{R}_0 , the corresponding work being $\tilde{\mu}_A$, then we relax the constraint imposed on the particle, i.e., we let the particle wander over the entire volume. The second contribution, $kT \ln (N_A \Lambda_A^3 / V)$, involves three important factors: N_A , Λ_A^3 , and V . The acquisition of translational momentum brings in the factor Λ_A^3 . The accessibility of the entire volume to the released molecule brings in the factor V , and the indistinguishability of this molecule from all other A molecules brings in the factor N_A . It is appropriate to call this term the *liberation* free energy, i.e., the free energy change due to the release of the new particle from a fixed position. The decomposition of μ_A as given by (3.13) is valid only within the realm of classical statistical mechanics.

Formally the same expression for the chemical potential may be obtained in the T, V, N or in the T, V, μ ensembles, with the understanding that N or V may be either constants or fluctuating quantities. For the purpose of comparison with experimental results, especially when dealing with the entropy, enthalpy, and volume of transfer, the T, P, N ensemble is the most useful one. This is the main reason for choosing this particular ensemble in the derivation of (3.13) in this paper.

It should be noted, however, that the decomposition of μ_A into two terms does not necessarily require two steps. Another way of viewing (3.13) is to assume that we have chosen the center of the coordinate system at the center of the added A molecule. Thus $\tilde{\mu}_A$ depends on the nature of the environment of A as seen from this position, and $kT \ln \rho_A \Lambda_A^3$ is the contribution to μ_A due to the translational freedom of this molecule.

In a similar fashion one can split any other partial molar quantity of A into two parts. For instance, taking the derivative of (3.13) with respect to the temperature we obtain

$$\bar{S}_A = -\frac{\partial \tilde{\mu}_A}{\partial T} - \frac{\partial}{\partial T} (kT \ln \rho_A \Lambda_A^3)$$

where the first term on the right-hand side of the equation is the entropy change due to the addition of A to a fixed position; the second term may be referred to as the *liberation entropy* of A.⁶

In the following, it will be convenient to use a somewhat more detailed notation for $\tilde{\mu}_A$, namely

$$\tilde{\mu}_A = W(A|A + B; x_A) \quad (3.14)$$

Here, we read $W(A|A + B; x_A)$ as the coupling work of an A molecule to the rest of the system composed of A and B with composition x_A .

It should be noted that the form of μ_A in (3.13) has been obtained by a statistical mechanical argument. It can by no means be obtained from purely thermodynamic ar-

guments. We also note that if internal degrees of freedom exist the chemical potential will have the form

$$\mu_A = W(A|A + B; x_A) + kT \ln (\rho_A \Lambda_A^3 q_A^{-1}) \quad (3.15)$$

However for simplicity we have assumed that $q_A = 1$.

4. Some Practical Examples

In this section, we give some illustrations of the general relation (3.13) which are useful in applications. First, we rewrite the general expression for the chemical potential in any mixture of A and B. In this paper we always write CP per particle not per mole as is more common in thermodynamics.

$$\mu_A = \bar{\mu}_A + kT \ln \rho_A \Lambda_A^3 = W(A|A + B; x_A) + kT \ln \rho_A \Lambda_A^3 \quad (4.1)$$

Three cases of special interest are given.

(a) *Pure A*. Let ρ_A^P be the density of pure A (at a specified T and P). The chemical potential of pure A is

$$\mu_A^P = W(A|A) + kT \ln \rho_A^P \Lambda_A^3 \quad (4.2)$$

where $W(A|A)$ is the coupling work of one A molecule to its environment which is pure A. We note that μ_A^P is a proper chemical potential of A in a *real state*,⁷ i.e., in the pure state, and that it contains the characteristic term $kT \ln \rho_A$, which must appear in any proper expression of the chemical potential. Since in this case we have a one component system, ρ_A^P is not an arbitrary density, but is determined by T and P .

(b) *Symmetrical Ideal (SI) Solution*. Suppose that A and B are very similar to each other, e.g., two isotopes of the same molecule, such that for each composition, the total interaction potential energy among the $N_A + N_B$ molecules does not change upon replacing some (or all) the B's by A's. Thus we have for any x_A the equality

$$W(A|A + B; x_A) = W(A|A) \quad (4.3)$$

where the number density of the pure A, ρ_A^P , is equal to the total number density in the mixture, i.e., $\rho_A^P = \rho_A + \rho_B$.

In words, the equality 4.3 means that the coupling work of one A molecule against a mixture of A and B is not affected by replacing all the B's by A's.

The equality 4.3, if assumed to be valid for all compositions, is a *sufficient* condition for symmetrical ideal behavior. A more detailed discussion on the necessary and sufficient conditions may be found in ref 2, Chapter 4.

From (4.1), (4.2), and (4.3) we obtain in this case

$$\begin{aligned} \mu_A^{SI} &= W(A|A + B; x_A) + kT \ln \rho_A \Lambda_A^3 \\ &= W(A|A) + kT \ln \rho_A \Lambda_A^3 \\ &= \mu_A^P - kT \ln \rho_A^P \Lambda_A^3 + kT \ln \rho_A \Lambda_A^3 \\ &= \mu_A^P + kT \ln x_A \end{aligned} \quad (4.4)$$

The last relation is very well known for SI solutions. It is presumed to hold for any composition x_A . In particular for $x_A = 1$ we obtain the chemical potential of pure A (at the same P and T). We see that in a SI solution the "natural" composition variable is the mole fraction. Indeed this has been used for solutions of two very similar components such as two isotopes, or even for solutions containing two slightly different components. An example is the theory of regular solutions. Another case where the mole fraction is appropriate is for the chemical potential of the *solvent* A, when the concentrations of all the *solutes* are very small, i.e., $x_A \approx 1$. In fact the mole fraction is

useful in most cases where the two components play a symmetric role, e.g., in drawing a phase diagram of a two-component system. Here clearly the range of variation of x between $0 \leq x \leq 1$ makes its use very convenient. These cases will not concern us in this paper. We shall be interested in the *solvation* properties of a solute in a solvent (the latter may be either a pure liquid or mixture of any number of components).

(c) *Extremely Dilute Solutions of A in B*. In the limit of very dilute solutions of A in B, an A molecule is practically surrounded by B molecules (from the molecular point of view it is sufficient to consider in this case a solution containing a *single* A in pure B). In this limit we obtain from (4.1)

$$\begin{aligned} \mu_A &= W(A|B) + kT \ln \rho_A \Lambda_A^3 \\ &= [W(A|B) + kT \ln \Lambda_A^3] + kT \ln \rho_A \\ &= \mu_A^{\circ\rho} + kT \ln \rho_A \end{aligned} \quad (4.5)$$

where we have introduced the (conventional) standard chemical potential of A. The superscript ρ indicates that we have used the number density ρ_A as our concentration unit. It is very important to note that $\mu_A^{\circ\rho}$ is *not* a *proper chemical potential* of A in any real state, since it lacks the characteristic term $kT \ln \rho_A$.⁸ This quantity is simply defined in (4.5), and it is only in the limit of very dilute solution that we could have written a relation such as (4.5) with $\mu_A^{\circ\rho}$ independent of ρ_A . At this point we can write the analogue of (4.5) for the general case (4.1) so that for any composition, (4.1) may be rewritten as

$$\begin{aligned} \mu_A &= [W(A|A + B; x_A) + kT \ln \Lambda_A^3] + kT \ln \rho_A \\ &= \mu_A^{*\rho}(\rho_A) + kT \ln \rho_A = [\mu_A^{\circ\rho} + kT \ln \gamma_A^D] + kT \ln \rho_A \end{aligned} \quad (4.6)$$

where we have introduced a *generalized standard chemical potential* of A in any mixture of A and B. This relation is valid independent of any assumption of ideality. We have stressed the dependence of this quantity on the density of A. The relation between $\mu_A^{\circ\rho}$ and $\mu_A^{*\rho}(\rho_A)$ is simply

$$\mu_A^{\circ\rho} = \lim_{\rho_A \rightarrow 0} [\mu_A^{*\rho}(\rho_A)] \quad (4.7)$$

or equivalently

$$W(A|B) = \lim_{\rho_A \rightarrow 0} [W(A|A + B; x_A)] \quad (4.8)$$

(the limits are taken at constant T and P). The use of the generalized standard chemical potential is, of course, equivalent to the use of activity coefficient that account for the deviations from the ideal dilute limit. This is shown in the last expression on the right-hand side of (4.6). The point which is stressed here is that $\mu_A^{*\rho}$ may be used in constructing the free energy of transfer of A from one phase to the other, in such a way that it has the same significance as the (conventional) standard free energy of transfer. For examples see sections 5.2 and 5.3.

In the realm of dilute solutions one often uses other concentration scales and we cite here some of the most common ones. The mole fraction, x_A , in very dilute solution is given by

$$x_A = \frac{\rho_A}{\rho_A + \rho_B} \approx \rho_A / \rho_B^P \quad (4.9)$$

substituting in (4.5) we obtain

$$\begin{aligned}\mu_A &= [W(A|B) + kT \ln \Lambda_A^3 \rho_B^p] + kT \ln x_A \\ &= \mu_A^{\circ x} + kT \ln x_A\end{aligned}\quad (4.10)$$

where we have introduced the standard chemical potential of A in the mole fraction scale. Again, it is very important to observe that $\mu_A^{\circ x}$ is *not* a proper chemical potential of A in any real state.^{7,8} It does contain the term $kT \ln \rho_B^p$ but not the characteristic term $kT \ln \rho_A$ that should be present in a proper chemical potential. Failure to recognize this point is a major source of many misinterpretations. This is especially so when one uses the same notation for $\mu_A^{\circ x}$ in (4.10) and for μ_A^p in (4.4), a very common and unfortunate practice.

At this point it is instructive to note a common interpretation of $\mu_A^{\circ x}$ as a CP of A in a "hypothetical standard state" of pure A, i.e., one substitutes $x_A = 1$ in (4.10) and thus confers a meaning on $\mu_A^{\circ x}$ as a CP of pure A. The substitution of $x_A = 1$ in (4.10) is inappropriate since we have derived this equation only in the limit of extremely dilute solution and therefore (4.10) is not expected to hold at $x_A = 1$. More important, such a hypothetical state requires one to envisage a *pure* liquid A in which each A is supposed to be surrounded exclusively by B molecules [since $\mu_A^{\circ x}$ contains the term $W(A|B)$], and naturally one would expect that in a *pure* A each A molecule should be surrounded by A molecules only! The most important argument however against the use of such hypothetical states is simply that in *all* applications of standard thermodynamic quantities, they are never required. As will be demonstrated below all the significant quantities can be properly interpreted without ever resorting to such hypothetical states. Therefore we recommend here to abandon the practice of using such hypothetical states.

At this point a citation of Friedman's review on this topic which advocates a different view is appropriate:⁹ "The hypothetical, $x_A = 1$ standard state for the solution is the most frequently chosen, and it has been used in some key papers on the thermodynamics of solvation.¹⁰⁻¹² This seems to be sufficient reason to continue its use, but it must be noted that, from the theoretical point of view, it does not have an advantage over other standard states for solutions except in special cases: Isotope mixtures and substitutional solid solutions are examples".

As we have seen above, in the case of isotopic mixtures and in the case of lattice models for solutions¹³ it is *advantageous* to use the *real pure* state as a standard state. The present author is not aware of any example of isotopic mixtures or substitutional solid solutions where it is *advantageous* to use such a *hypothetical state*. Furthermore, we believe that the mere fact that a quantity is frequently used is *not* a sufficient reason to continue its use.

The second concentration scale is the molality scale which, for very dilute solution, is related to the density ρ_A by

$$m_A = 1000\rho_A/M_B\rho_B^p \quad (4.11)$$

substituting in (4.5) we obtain

$$\begin{aligned}\mu_A &= \left[W(A|B) + kT \ln \frac{M_B \rho_B^p \Lambda_A^3}{1000} \right] + kT \ln m_A \\ &= \mu_A^{\circ m} + kT \ln m_A\end{aligned}\quad (4.12)$$

where M_B is the molecular weight of B, and $\mu_A^{\circ m}$ is the standard chemical potential of A in the molality scale. Again we stress that $\mu_A^{\circ m}$ is not a proper chemical potential of A for the same reasons given above for $\mu_A^{\circ x}$.

Another concentration unit that has been suggested, and sometimes claimed to be advantageous in aqueous solu-

tions, is the aquamolality. This is the number of moles of a solute dissolved in 55.51 moles of water.¹⁴ Very similar units have been employed¹⁵ for reporting the solubility of gases in aqueous solutions of tetraalkylammonium salts, i.e., the number of milliliters of gas dissolved in 1000 g of water.

Clearly one can construct many other concentration scales. If these are well-defined quantities there is nothing wrong in their application for reporting *solubilities*. The central issue of the following sections is not to discuss the relative merit of different units for reporting *solubilities* but to examine the standard thermodynamic quantities which are based on the choice of these different scales. For this purpose the molarity scale has a unique advantage over all other scales.

5. Standard Free Energy of Transfer, Measurement, and Interpretation

5.1. *Very Dilute Solutions.* In section 4 we have developed some expressions for the chemical potential of A in various two component solutions. The experimentally measurable quantities are, however, not the chemical potentials but *differences* in chemical potentials.

The first step in constructing a free energy change for transferring A between the two phases, e.g., a and b is to form the difference in the *chemical potential* of A in the two phases, and not the difference in SCP. Thus we write

$$\Delta G(a \rightarrow b) = (\mu_A^b - \mu_A^a) dN_A \quad (5.1)$$

This is the work required to transfer dN_A molecules (or moles) from one phase, a, to another phase, b, where the phases have been fully specified in terms of their temperature, pressure, and composition. In the following we shall always transfer a single A molecule, i.e., dN_A will be taken to be unity (T , P , and N_B are kept constant).

For convenience, we shall denote by c_A any one of the concentration units that were mentioned in section 4. We start by treating *very dilute* solutions of A in B, for which we can write

$$\mu_A = \mu_A^{\circ c} + kT \ln c_A \quad (5.2)$$

where $\mu_A^{\circ c}$ is formally defined by the limit

$$\mu_A^{\circ c} = \lim_{c_A \rightarrow 0} [\mu_A - kT \ln c_A]$$

Consider now two phases a and b in which the concentrations are c_A^a and c_A^b , respectively. The free energy change for the transfer of one A molecule from a to b is

$$\Delta G \left[\begin{matrix} a \rightarrow b \\ c_A^a, c_A^b \end{matrix} \right] = \mu_A^b - \mu_A^a = \mu_A^{\circ cb} - \mu_A^{\circ ca} + kT \ln (c_A^b/c_A^a) \quad (5.3)$$

Now consider a special case where the concentration of A is the same in the two phases, in which case we obtain

$$\Delta G \left[\begin{matrix} a \rightarrow b \\ c_A^a = c_A^b \end{matrix} \right] = \mu_A^{\circ cb} - \mu_A^{\circ ca} \quad (5.4)$$

This is a simple but an important result, it says that *differences* in the SCP of A between two phases is equal to the free energy of transferring A from a to b, *provided the concentrations c_A^a and c_A^b are the same in the two phases*. This conclusion is valid for *any* concentration scale. The important point to be noted is that while each of the *standard* chemical potentials is not a chemical potential of A in any real system, the difference in SCP

is here equal to a difference in chemical potentials. In section 5.4 we shall see that this result is not always true, however.

Clearly the process which has been indicated symbolically by $[a \rightarrow b; c_A^a = c_A^b]$ can be carried out experimentally. However, the actual measurement of $\mu_A^{\circ cb} - \mu_A^{\circ ca}$ is carried out under different experimental conditions, as follows.

Consider two phases a and b separated by a partition which is permeable to A only. If equilibrium with respect to diffusion of A between the two phases is established we have the condition of chemical equilibrium, i.e.

$$0 = \mu_A^b - \mu_A^a = \mu^{\circ cb} - \mu_A^{\circ ca} + kT \ln (c_A^b/c_A^a)_{eq} \quad (5.5)$$

where $(c_A^b/c_A^a)_{eq}$ is the partition coefficient of A between the two phases in equilibrium.

Now we make an important observation. If the concentrations of A appearing in all the above equations are all small enough so that the limit of a dilute ideal solution is attained, then $\mu_A^{\circ cb}$ and $\mu_A^{\circ ca}$ are independent of c_A^b and c_A^a , respectively. Thus one can determine the partition coefficient $(c_A^b/c_A^a)_{eq}$ in (5.5) (experimentally), from which we evaluate $\mu_A^{\circ cb} - \mu_A^{\circ ca}$. This difference, being independent of the concentrations of A, will be the same as the one in (5.3) and (5.4). Hence we can say that the *standard free energy change* obtained experimentally through (5.5) gives us a measure of the *free energy change* for transferring one A molecule from a to b *provided* that $c_A^a = c_A^b$ and that these, as well as c_A^a and c_A^b in (5.5), are small enough to ensure the validity of the dilute ideal behavior.

5.2. Concentrated Solutions. All the arguments given above hold for any concentration scale. It will break down if the solutions are not very dilute. In this case, one can still formally write (5.5) with no restrictions on c_A^a and c_A^b , but now measurement of the partition coefficient $(c_A^b/c_A^a)_{eq}$ will give us a quantity which we denote by

$$\mu_A^{*cb}(c_A^b) - \mu_A^{*ca}(c_A^a) = -kT \ln (c_A^b/c_A^a)_{eq} \quad (5.6)$$

where we have explicitly denoted the dependence of the generalized SCP¹⁶ on the concentration. Each of the μ_A^{*c} is defined as in (4.6), for the appropriate concentration scale.

Here the quantity determined experimentally by (5.6) *cannot* be interpreted as we have done in (5.3) and (5.4). For if we write the analogue of (5.4) for the general case we obtain

$$\Delta G \left[\begin{array}{c} a \rightarrow b \\ c_A^a = c_A^b \end{array} \right] = \mu_A^{*cb}(c_A^b) - \mu_A^{*ca}(c_A^a) \quad (5.7)$$

However now the value of $c_A^a = c_A^b$ in (5.7) is in general different from the equilibrium values of c_A^a and c_A^b in (5.6). Thus determination of $\mu_A^{\circ cb} - \mu_A^{\circ ca}$ through (5.5) and interpretation through (5.3) and (5.4) is valid only for *very dilute solutions* of A in the two phases, this being the case for any particular concentration scale that is used for c_A . This is quite a serious limitation in application to real solutions.

At this stage there is no obvious reason to single out one unit over the other, i.e., one can construct SFE of transferring A from a to b at equal "mole fraction", equal "molarity", "molality", or "aquamolality" or any other concentration units. All these are different quantities. It is not surprising to find that Arnett and McKelvey¹⁴ have announced a "shocking" finding that the SFE of transferring of propane between H₂O to D₂O even changes sign upon changing the concentration units.¹⁷

In fact this example should serve as a warning signal that the choice of a standard state is not merely a matter of choosing the "units", as, for instance, in the case of choosing between centimeters and inches. We shall see in the following that the choice of the correct standard state is of fundamental significance.

Thus, one can construct SCP and SFE of transfer using any one of the concentration scales. Thermodynamics alone cannot be used to determine the most useful or meaningful choice. We shall see that by using a statistical mechanical argument such a decision can indeed be made.

5.3. Interpretation of the SFE of Transfer for the General Case. Consider the very general expression for the chemical potential of A in any solvent (which may be a mixture of two or more components, in any composition). In analogy with (4.1) we write

$$\mu_A = \tilde{\mu}_A + kT \ln \rho_A \Lambda_A^3 = W(A|\mathbf{x}) + kT \ln \rho_A \Lambda_A^3 \quad (5.8)$$

where the vector \mathbf{x} describes the composition of the system. We can determine experimentally the partition coefficient of A in the two phases. As in (5.5) we now have

$$0 = \mu_A^b - \mu_A^a = W(A|\mathbf{x}^b) - W(A|\mathbf{x}^a) + kT \ln (\rho_A^b/\rho_A^a)_{eq} \quad (5.9)$$

where $(\rho_A^b/\rho_A^a)_{eq}$ is the partition coefficient of A in the two phases, measured in number densities (or molar densities). Now in contrast to the process described after eq 5.5 where after determining $\mu_A^{\circ cb} - \mu_A^{\circ ca}$ *experimentally*, we had to resort to eq 5.3 to obtain a proper interpretation. Here we have a direct interpretation of the simple quantity $W(A|\mathbf{x}^b) - W(A|\mathbf{x}^a)$, which conveys information on the solvation of A in the two phases. This difference is by *definition* the difference in the coupling work of one A molecule to the surroundings in the two phases. Equivalently, this is the free energy change for transferring an A molecule from a fixed position in a to a fixed position in b.

$$\tilde{\mu}_A^b - \tilde{\mu}_A^a = \mu_A^{*\rho b} - \mu_A^{*\rho a} = W(A|\mathbf{x}^b) - W(A|\mathbf{x}^a) \quad (5.10)$$

Thus the important advantage of the generalized SFE of transfer is its applicability to any concentration of A, including the case of pure A (see below).

If A is very dilute in the two phases, $\mu_A^{*\rho b} - \mu_A^{*\rho a}$ becomes independent of the concentration of A, and coincides with the quantity $\mu_A^{\circ \rho b} - \mu_A^{\circ \rho a}$.

5.4. Particular Example, One Phase is Pure A. As a particular example of the application of (5.9) and (5.10) consider a solute A, e.g., CCl₄, distributed between two phases, a being pure A and b being an aqueous solution of A. (In this particular situation if we remove the partition separating the two phases, some water will dissolve in CCl₄ and thereby slightly modify the partition coefficient of CCl₄ in the two phases. The distinction between the two cases is, however, of no importance for our purposes.) In this case, the generalized standard free energy of transfer of A between the two phases is (see (5.9) and (5.10))

$$\mu_A^{*\rho w} - \mu_A^{*\rho A} = W(A|W) - W(A|A) = -kT \ln (\rho_A^w/\rho_A^A)_{eq} \quad (5.11)$$

where ρ_A^A is the number density of pure CCl₄, and ρ_A^w is the equilibrium density of CCl₄ in water. Note that there is no restriction on the aqueous solution to be DI. The first equality in (5.11) provides the *interpretation* of this

quantity as the free energy change for transferring A from a fixed position in pure A, to a fixed position in the aqueous solution (which in the particular example given above is almost pure W). The second equality in (5.11) provides the means of measuring this quantity, simply from the number densities of A in the two phases at equilibrium.

At this point we present one common misuse of standard free energy of transfer. Consider a very dilute solution of CCl_4 in water. For the two phases we can write

$$\mu_A^w = W(A|W) + kT \ln \Lambda_A^3 \rho_A^w \quad (5.12)$$

$$\mu_A^A = W(A|A) + kT \ln \Lambda_A^3 \rho_A^A \quad (5.13)$$

One can think of several processes of transfer:

(1) Transfer of A between the two phases at equilibrium

$$\mu_A^w - \mu_A^A = 0 \quad (5.14)$$

(2) Transfer of A from pure A to some arbitrary concentration of A in W, in which case we have

$$\mu_A^w - \mu_A^A = W(A|W) - W(A|A) + kT \ln (\rho_A^w / \rho_A^A) \quad (5.15)$$

where ρ_A^A is the density of A in pure A and ρ_A^w is any arbitrary density of A in W (of course within the limits of the solubility of A in W but otherwise arbitrary).

(3) The transfer of one A from a fixed position in pure A to a fixed position in W, in which case we have the quantity defined in (5.11).

The first two are *real* processes which can actually be carried out in the laboratory. The third is a theoretical and well-defined process, the free energy change of which is indirectly a *measurable quantity* through (5.11).¹⁸ This is the quantity that measures the difference in the solvation properties in the two phases.

However suppose we form the difference

$$\mu_A^A - \mu_A^{\circ w} = W(A|A) - W(A|W) + kT \ln \rho_A^A \quad (5.16)$$

This quantity, though measurable through the relation

$$0 = \mu_A^A - \mu_A^w = \mu_A^A - \mu_A^{\circ w} - kT \ln (\rho_A^w)_{\text{eq}}$$

(where ρ_A^w is the equilibrium density of A in W), is *not* a free energy of transfer of A between any two real states.¹⁹ The reason is simple; whereas μ_A^A is a *proper* CP of A in a real system, $\mu_A^{\circ w}$ is not! Therefore the quantity $\mu_A^A - \mu_A^{\circ w}$ may not be assigned the meaning of a free energy of transfer of A between two phases.

The difficulty is not removed by changing to mole-fraction units. For dilute solution, we write $\rho_A \approx \rho_w^w x_A$ where ρ_w^w is the number density of W in pure W and we obtain the analogue of (5.16) (see also (4.10)):

$$\mu_A^A - \mu_A^{\circ w} = W(A|A) - W(A|W) + kT \ln (\rho_A^A / \rho_w^w) \quad (5.17)$$

Again, this quantity bears no direct relation to the free energy for transferring A between two real phases.¹⁹

The literature unfortunately contains many quantities of somewhat indefinite meaning such as (5.17). We shall present one example only, which is very instructive for reasons that will become clear in the following.

In a recent paper, Reynolds et al.²⁰ writes: "Hydrophobic free energy may be defined in terms of the unitary free energy of transfer of a non-polar solute from a non-polar reference solvent such as a liquid hydrocarbon

to an aqueous medium...For pure hydrocarbon one may use the solubility of the hydrocarbon in water (X_s in mole fraction units)".

For reasons of clarity we write their eq 2 in their own notation, and in the corresponding notation of this paper.

$$\begin{aligned} \mu_w^{\circ} - \mu_{\text{HC}}^{\circ} &= -kT \ln x_s \\ \mu_A^{\circ w} - \mu_A^A &= -kT \ln (x_A^w)_{\text{eq}} \end{aligned} \quad (5.18)$$

Thus μ_{HC}° is the CP of the *pure hydrocarbon*, which we denote by A, and from the context and from their ref 21 it is clear that μ_w° is the SCP of A in W defined in the limit of dilute solution. x_s is what we denote by $(x_A^w)_{\text{eq}}$.

The authors of ref 20 do not explain why the quantity defined in (5.18) has the meaning they claim for it (see citation preceding 5.18). Instead they write: "The necessity of using unitary units in these equations has been spelled out in several places".²¹⁻²³

Since Reynolds et al. employ the quantity in (5.18), but do not explain its meaning, we examine the references cited by them.²⁴

Gurney²² does speak of "unitary" and "cratic units" (see next section) on pages 90-92 of his book, but in no place does he discuss or interpret quantities of the form (5.18).

Kauzmann²³ also cites Gurney's *units*. He not only *does not* support the meaning assigned to (5.18), but correctly notes that if one transfer A from pure A to a solution of A in water the correct *entropy change* is (in our notation)

$$\Delta S = S_A^{\circ w} - S_A^A - k \ln x_A^w \quad (5.19)$$

We shall discuss entropies of transfer in section 7. However what Kauzmann says about the entropy change is equally true for the free energy change. Namely, the free energy change for transferring A from pure A to a dilute aqueous solution of A in W, at any arbitrary concentration x_A^w , is simply

$$\Delta G = \mu_A^{\circ w} - \mu_A^A + kT \ln x_A^w \quad (5.20)$$

This is a meaningful quantity, which clearly differs from (5.18). In particular, if we put $x_A^w = (x_A^w)_{\text{eq}}$ in (5.20) we obtain $\Delta G = 0$.

Thus neither ref 20 nor the references cited therein provide the explanation to the meaning assigned to (5.18). What remains from (5.18) is simply another way of re-writing the solubility of A in W. No further meaning can be assigned to the quantity $\mu_A^{\circ w} - \mu_A^A$ as a free energy of transfer of A between two phases. This is in contrast to the significant meaning that can be assigned to the quantity defined in (5.10), or its low-concentration limit.

6. "Unitary" and "Cratic" Terms. Which Quantity Do We Want?

6.1. *Mixing Free Energy*. We devote a special section to the analysis of the terms "unitary" and "cratic" since these have recently been used (and more often misused) quite extensively. We start by stating our conclusion in this section, which is: The use of these terms, as introduced originally by Gurney²² is appropriate and meaningful only within the context of SI solutions, or solutions which are viewed as deviating from SI behavior, such as the case of regular solutions. However, these terms are inappropriate and somewhat misleading when applied to the problem of solvation of one molecule in a solvent.

The free energy of mixing of two components (at T, P constants)²⁵⁻²⁷ is

$$\Delta G^M = (N_A \mu_A + N_B \mu_B) - (N_A \mu_A^P + N_B \mu_B^P) \quad (6.1)$$

If the solution is SI, i.e., if one can write

$$\mu_A = \mu_A^p + kT \ln x_A \quad (6.2)$$

and a similar relation for B, then one obtains the well-known result

$$\Delta G^M(\text{SI}) = N_A kT \ln x_A + N_B kT \ln x_B \quad (6.3)$$

At the time Gurney published his book (1953)²² the theory of mixtures was worked out either for gaseous mixtures or for solid solutions,¹⁵ but there had been very little discussion of *liquid* mixtures.²³ It is therefore no wonder that Gurney derived his equations mainly for these cases. On page 89 of his book²² Gurney coined the adjective "cratic" meaning "mixing" by saying: "We may speak of the *cratic* part when we wish to refer to the part that arises from *mixing* a certain number of solute particles with a certain number of solvent particles, *regardless* of the *species of particles* that have been mixed". This is a clear-cut reference to the term on the right-hand side of (6.3). If the solution is nonideal [in the sense of (6.3)] we obtain

$$\Delta G^M = [N_A kT \ln x_A + N_B kT \ln x_B] + [N_A kT \ln \gamma_A + N_B kT \ln \gamma_B] \quad (6.4)$$

where now one should make a distinction between the free energy of "mixing", which is the entire right-hand side of (6.4), and the "cratic" term in Gurney's sense as cited above. Another example which is relevant to the subject matter of this paper is the case when A is very dilute in B, in which case the CP of A and B are written as

$$\mu_A = \mu_A^{\circ x} + kT \ln x_A \quad (6.5)$$

$$\mu_B = \mu_B^p + kT \ln x_B \quad (6.6)$$

and the free energy of mixing (6.1) in this case is

$$\Delta G^M(\text{DI}) = [N_A kT \ln x_A + N_B kT \ln x_B] + N_A (\mu_A^{\circ x} - \mu_A^p) \quad (6.7)$$

Again we note that one should make the distinction between the "mixing free energy" which is the entire quantity in (6.7), and the "cratic" term in Gurney's sense, which we have included in the square brackets in (6.7). Although it is clear from (6.6) and (6.7) that the term $kT \ln x_B$ is the contribution of B to the mixing free energy, compound A makes two contributions to (6.7) and its contribution to the free energy of mixing is *not* $kT \ln x_A$ alone.

Thus, although it is clear that the term $kT \ln x_A$ in (6.5) is dependent only on the *number of particles* involved, this term is *not* the contribution of A to the mixing free energy. Therefore, care must be exercised in using the adjective "cratic", in the sense of "mixing", for this term alone.²⁹ One obvious reason for the existing confusion is that it is very common to use the same notation for μ_A^p and for $\mu_A^{\circ x}$, although the two quantities have completely different meanings.

The term that remains after extracting the cratic term is referred to as the "unitary term", and in Gurney's words²² this "is independent of the composition of the solution...which is characteristic of the particles taking part in the process".

Gurney was discussing extremely dilute solutions (ref 22, p 91) and having identified a term which he called "cratic", he defined what *remains* as the "unitary term" and writes: "Now at all temperatures the unitary term...is independent of the composition of the solution". This is

correct *only* for the examples examined by Gurney. Clearly, in the case of dilute solutions (as in (6.5) and (6.6)) or in SI solutions what remains after extracting the "cratic" term is a quantity which is "independent of the composition of the solution". This is, however, not valid in general.

One can easily find examples (from nonideal solutions) where the term that remains after extracting the "cratic" term still depends on the composition of the system.

One common misuse of Gurney's ideas is that the "cratic" term should be removed before one gets a meaningful quantity. As an example, Arnett and McKelvey write the following.¹⁴

"The second is a formal contribution reflecting the concentration units and is a mixing term or 'cratic factor', which *must* be expunged before free energy or entropy changes are open to discussion". However is this true? We have seen in (5.19) and (5.20) two well-defined processes in which the entropy and the free energy change *does* contain the "cratic" term.

Perhaps the most important aspect of Gurney's terminology that has been misused is the *meaning* of the "unitary" term. In the special case of SI solution or in (6.6) the "unitary" term has a clear-cut meaning: it is simply the CP of the pure component. However in general, the very act of extracting a cratic term, does not confer any *meaning* on what is left. One must examine the meaning of the unitary term in each particular example.

Therefore, the identification of the term $kT \ln x_A$ as the sole contribution to the mixing free energy is, in general, incorrect. What remains after extracting this term is a quantity which may depend on the composition, and its significance remains obscure.

6.2. Which Quantity to Choose? For convenient reference we collect together some of the quantities discussed in this paper

$$\mu_A^{\circ b} - \mu_A^{\circ a} = W(A|b) - W(A|a) \quad (6.8)$$

$$\mu_A^{\circ b} - \mu_A^{\circ a} = W(A|x^b) - W(A|x^a) \quad (6.9)$$

$$\mu_A^{\circ x b} - \mu_A^{\circ x a} = W(A|b) - W(A|a) + kT \ln (\rho_b^p / \rho_a^p) \quad (6.10)$$

$$\mu_A^{\circ m B} - \mu_A^{\circ m D} = W(A|B) - W(A|D) + kT \ln (\rho_B^p M_B / \rho_D^p M_D) \quad (6.11)$$

$$\mu_A^A - \mu_A^{\circ x w} = W(A|A) - W(A|W) + kT \ln (\rho_A^A / \rho_W^w) \quad (6.12)$$

For many years people working in the field of solution chemistry have been endeavoring to find a thermodynamic quantity that will probe the difference in the *solvation properties* of a solute in different solvents. In Tanford's words:²¹ The quantity sought should reflect "the difference between the free energy of interactions with the solvent".

A glance at eq 6.8-6.12 shows that the quantity that comes closest, in spirit, to what we are seeking is (6.8). This is also the *simplest* and the *most meaningful* quantity in the list. Furthermore, it can be extended to any solute concentration (6.9), including the case of pure A.

Some authors claim⁹ that the choice between the various standard quantities in the above list is of no fundamental importance. Perhaps the most dramatic rebuttal of this contention can be demonstrated now. A quantity that is presumed to describe the "free energy of interaction with the solvent" is expected to decrease to zero when the *solvent* density tends to zero. *Only* the two quantities defined in (6.8) and (6.9) have this property. On the other hand, all other quantities *diverge* to either $-\infty$ or $+\infty$ when

one of the solvent densities tends to zero. Therefore, these quantities cannot serve as bona fide measures of the free energy of interaction with solvent!

In spite of the obvious simplicity of (6.8), other authors have advocated the use of other quantities included in the above list. The reason for that stems from the fact that thermodynamics alone cannot discriminate between the relative significance of the various standard quantities. This fact, together with the common practice of using the same notation for e.g., μ_A^p and μ_A^{ox} , has led to a wrong interpretation of the term $kT \ln x_A$. As a result there has been a strong tendency to prefer the mole-fraction scale.^{21,31} On the other hand, if we start from the statistical mechanical expression for the chemical potential, we observe that the very definition of μ_A^{op} in (4.5) [or μ_A^{*p} in (4.6)] has removed the term $kT \ln \rho_A$. The next step was to form differences in μ_A^{op} in two phases, thereby also cancelling out the term $kT \ln \Lambda_A^3$. What remains is a quantity (6.8) which is devoid of the liberation free energy and hence is a measure of the difference in the solvation properties of A in the two solvents.

In the early development of the theory of solutions, various lattice models¹³ were commonplace in the literature. In these models the momentum partition function and the volume of the system were not features. These two factors are essential parts of the liberation free energy in liquid mixtures as explained in section 3.

Thus using Gurney's procedure of extracting the "cratic" term, $kT \ln x_A$ in the definition of μ_A^{ox} does remove the factor $kT \ln N_A$. Formation of differences of μ_A^{ox} in two phases further eliminates $kT \ln \Lambda_A^3$. However this, unfortunately, leaves the factor $kT \ln (V^a/V^b)$ in each of the quantities in (6.10) to (6.12). In other words, the Gurney procedure does not eliminate the entire liberation free energy from $\mu_A^{oxb} - \mu_A^{oxa}$.

7. Temperature and Pressure Dependence

7.1. The Standard Entropy of Transfer. The temperature (and pressure) dependence of the molar concentration has been a major argument against its use. In a recent review¹⁴ we find the following argument: "The mole fraction scale enjoys freedom both from temperature and density effects and is therefore preferred here".

The view that the temperature dependence of the molarity scale is a disadvantage, in constructing SFE's of transfer, is extremely widespread. It is ironic to note that this very property of the molarity scale is in fact its advantage.

However even without reference to standard states we think that the objection to molar concentrations has been misdirected.

Of course if we have a 1 M solution of KCl, prepared at 25 °C, the molarity will be different at 35 °C. However, whether it is convenient or not, this is the scale that should be used for certain purposes (e.g., for spectroscopic measurements or for volumetric titration). One cannot avoid the temperature dependence of the ρ concentration merely by transformation to other concentration scales. Fortunately this apparent inconvenience of the molarity scale is irrelevant when using the interpretation of the SFE of transfer, advocated in sections 5 and 6. In fact, the temperature dependence of the volume enters into all the SFE's except that based on molar concentration. This will now be shown.

Let us first see where the temperature dependence enters in the common use of the standard entropy of transfer. For simplicity we shall discuss the DI solution (the same is true for concentrated solutions). As in (5.3) the free energy change is written as

$$\Delta G \left[\begin{array}{c} a \rightarrow b \\ C_A^a, C_A^b \end{array} \right] = \mu_A^{ocb} - \mu_A^{oca} + kT \ln (C_A^b/C_A^a) \quad (7.1)$$

where C_A^a is the concentration of A in any scale. The corresponding entropy change is

$$-\Delta S \left[\begin{array}{c} a \rightarrow b \\ C_A^a, C_A^b \end{array} \right] = \frac{\partial}{\partial T} (\mu_A^{ocb} - \mu_A^{oca}) + k \ln (C_A^b/C_A^a) + kT \frac{\partial}{\partial T} [\ln (C_A^b/C_A^a)] \quad (7.2)$$

and for the particular process where $C_A^a = C_A^b$, as in (5.4) we obtain the result

$$-\Delta S \left[\begin{array}{c} a \rightarrow b \\ C_A^a = C_A^b \end{array} \right] = \frac{\partial}{\partial T} (\mu_A^{ocb} - \mu_A^{oca}) + kT \frac{\partial}{\partial T} [\ln (C_A^b/C_A^a)] \quad (7.3)$$

where all the derivatives are at constant P , N_A , and N_B .

It is important to note that the substitution $C_A^b = C_A^a$ in (7.2) is made *after* the differentiation with respect to temperature *not before*.

The usual argument against using the molarity scale is the following: if we put $C_A = x_A$, or $C_A = m_A$ the last term on the right-hand side of (7.3) drops. However, if we put $C_A = \rho_A$ it does not. The three possible results are

$$-\Delta S \left[\begin{array}{c} a \rightarrow b \\ x_A^a = x_A^b \end{array} \right] = \frac{\partial}{\partial T} (\mu_A^{oxb} - \mu_A^{oxa}) \quad (7.4)$$

$$-\Delta S \left[\begin{array}{c} a \rightarrow b \\ m_A^a = m_A^b \end{array} \right] = \frac{\partial}{\partial T} (\mu_A^{omb} - \mu_A^{oma}) \quad (7.5)$$

$$-\Delta S \left[\begin{array}{c} a \rightarrow b \\ \rho_A^a = \rho_A^b \end{array} \right] = \frac{\partial}{\partial T} (\mu_A^{opb} - \mu_A^{opa}) + kT \frac{\partial}{\partial T} (\ln (V^a/V^b)) \quad (7.6)$$

where the last term on the right-hand side of (7.6) contains the temperature dependence of the volume of the phases a and b. It is apparent that the two quantities in (7.4) and (7.5) are simpler to evaluate, since there the temperature dependence of the volume does not enter; this is the basic objection to the use of the ρ concentration scale.

Our first objection to this argument is that the choice between the various quantities in (7.4) to (7.6) should be made on their scientific merits, not on their relative ease of evaluation. However fortunately, at the thermodynamic level there is no way of determining which of the processes indicated is preferable.

The interest in solvation entropies of solutes^{32,33} perhaps even preceded that of the free energy changes. In this case the interest was focused more on the "structure" around the solute than on the "interaction" with the solvent. It was natural to seek a "standard" quantity that will not carry in it the translational entropy of the solute, but will "sense" the local environment of the solute. As in the case of the free energy, thermodynamics alone could not offer any means by which one could make a choice of the "best", or most informative quantity. As a result, various standard states for the entropy have been suggested.

In contrast to our discussion of the free energy, where thermodynamics alone could not be used to make a choice, in the case of the entropy it looks, at first sight, as if the process $[a \rightarrow b; \rho_A^a = \rho_A^b]$ indicated in (7.6) gives a more

complicated expression for the entropy change. However this impression is more apparent than real. If we look more carefully into the content of the quantities on the right-hand side of (7.4) and (7.5) we see that the temperature dependence of the volume is hidden within the quantities $\mu_A^{\circ xb}$ or $\mu_A^{\circ mb}$ [see (4.10) and (4.12)]. So really one has the same term as the one on the right-hand side of (7.6) also in (7.4) and (7.5). This is not the important point however. If we are interested in the difference in the solvation entropies in the two phases, then we should start with the free energy change

$$\Delta G \left[\begin{array}{c} a \rightarrow b \\ R_A^a, R_A^b \end{array} \right] = W(A|b) - W(A|a) \quad (7.7)$$

the corresponding entropy change is

$$-\Delta S \left[\begin{array}{c} a \rightarrow b \\ R_A^a, R_A^b \end{array} \right] = \frac{\partial}{\partial T} [W(A|b) - W(A|a)] \\ = \frac{\partial}{\partial T} [\mu_A^{\circ \rho b} - \mu_A^{\circ \rho a}] \quad (7.8)$$

which is the entropy change for transferring one A molecule from a fixed position in a to a fixed position in b (at constant T, P). Comparing with (7.6) we see that here the temperature dependence of the volume *does not appear*. As a particular example, consider the transfer of A from a rarefied gas phase to a liquid, in which case we assume that $W(A|gas) = 0$ and hence

$$-\Delta S \left[\begin{array}{c} g \rightarrow l \\ R_A^g, R_A^l \end{array} \right] = \frac{\partial}{\partial T} (W(A|liquid)) \quad (7.9)$$

a quantity that can be used to study the solvation properties in any solvent. All the other entropy changes in (7.4) to (7.6) contain additional terms that are irrelevant for such a study.

The described process in (7.9) can be easily generalized to any solution, not necessarily the DI one. Thus, using the generalized SFE of transfer, as defined in (5.10) or (5.11), we can obtain the generalized standard entropy of transfer by

$$-\Delta S \left[\begin{array}{c} a \rightarrow b \\ R_A^a, R_A^b \end{array} \right] = \frac{\partial}{\partial T} [\mu_A^{\circ \rho b} - \mu_A^{\circ \rho a}] \quad (7.10)$$

where there is no restriction on the concentration of the solute A.

There is an important point which should be noted here. The two processes $[a \rightarrow b; \rho_A^a = \rho_A^b]$ and $[a \rightarrow b; R_A^a, R_A^b]$ have the *same* free energy change but have *different* entropy and volume changes. The reason lies in the different character of the two equalities.

$$\Delta G \left[\begin{array}{c} a \rightarrow b \\ \rho_A^a = \rho_A^b \end{array} \right] \stackrel{(I)}{=} \mu_A^{\circ \rho b} - \mu_A^{\circ \rho a} \stackrel{(II)}{=} \\ \Delta G \left[\begin{array}{c} a \rightarrow b \\ R_A^a, R_A^b \end{array} \right] \quad (7.11)$$

Equality I is valid *only* at the point $\rho_A^a = \rho_A^b$ (see (5.4) and (5.7)), but equality II is an *identity*. Therefore when differentiating with respect to temperature (at P, N_A, N_B constants) equality II gives the entropy change for that process (eq 7.8 or 7.10) whereas equality I does not give the entropy change for that process (see eq 7.6), i.e., differentiating (7.11) term by term with respect to temperature gives

$$-\Delta S \left[\begin{array}{c} a \rightarrow b \\ \rho_A^a = \rho_A^b \end{array} \right] \neq \frac{\partial}{\partial T} [\mu_A^{\circ \rho b} - \mu_A^{\circ \rho a}] = \\ -\Delta S \left[\begin{array}{c} a \rightarrow b \\ R_A^a, R_A^b \end{array} \right]$$

Note the inequality on the left-hand side. Up to this point we have compared several processes of transfer. Since we have now established the *local* character of the thermodynamics of transfer $[a \rightarrow b; R_A^a, R_A^b]$ we now suggest a shorter symbol for this process, namely $(a \rightarrow b; L)$, where L represents local.

Now the three derivatives of the standard free energies of transfer listed in (7.4) to (7.6) when rewritten from the molecular point of view look quite different, namely [see (6.8), (6.10), and (6.11)]

$$\frac{\partial}{\partial T} (\mu_A^{\circ \rho b} - \mu_A^{\circ \rho a}) = \frac{\partial}{\partial T} [W(A|b) - W(A|a)] = -\Delta S(a \rightarrow b; L) \quad (7.12)$$

$$\frac{\partial}{\partial T} (\mu_A^{\circ xb} - \mu_A^{\circ xa}) = \frac{\partial}{\partial T} [W(A|b) - W(A|a) + kT \ln (\rho_b^P / \rho_a^P)] \quad (7.13)$$

$$\frac{\partial}{\partial T} (\mu_A^{\circ mb} - \mu_A^{\circ ma}) = \frac{\partial}{\partial T} [W(A|b) - W(A|a) + kT \ln (\rho_b^P M_b / \rho_a^P M_a)] \quad (7.14)$$

We see that, in contrast to the impression obtained from (7.4) to (7.6) as to the relative simplicity of the various entropies, the derivative of $\mu_A^{\circ \rho b} - \mu_A^{\circ \rho a}$ in (7.12) gives *exactly* the entropy change for the process that *does not* contain any contribution from the liberation entropy. The other two derivatives do contain residual contributions from the liberation entropy. Thus $\Delta S(a \rightarrow b; L)$ may justifiably be referred to as the *local* standard entropy of transfer.

In conclusion the temperature dependence of the volume, a major objection¹⁴ to the use of ρ concentration in these quantities, actually *does not* appear in a proper interpretation of the derivatives of $\mu_A^{\circ \rho b} - \mu_A^{\circ \rho a}$, but *does appear* in the other derivatives of SFE of transfer such as (7.13) and (7.14).

7.2. *Other Standard Quantities of Transfer.* The *local* enthalpy of transfer is defined by

$$\Delta H(a \rightarrow b; L) = \Delta G(a \rightarrow b; L) + T\Delta S(a \rightarrow b; L) \\ = -T^2 \frac{\partial}{\partial T} \left[\frac{W(A|b) - W(A|a)}{T} \right] \quad (7.15)$$

This quantity does not contain any contribution from the liberation enthalpy. On the other hand *all* the enthalpy changes that correspond to the processes indicated on the left-hand side of (7.4) to (7.6) *do* contain the temperature dependence of the volume. This can be easily checked by forming the combination $\Delta H = \Delta G + T\Delta S$ for each of these three processes. Similarly the *local* volume of transfer is

$$\Delta V(a \rightarrow b; L) = (\partial/\partial P)(\mu_A^{\circ \rho b} - \mu_A^{\circ \rho a}) = \\ (\partial/\partial P)[W(A|b) - W(A|a)] \quad (7.16)$$

Note that the same comment made above for the enthalpy change applies for the volume change. Thus for *all* of the processes indicated on the left-hand side of (7.4) to (7.6) the volume of transfer will have a term including the isothermal compressibilities of the two phases. For ex-

ample, for the process corresponding to (7.4) we have

$$(\partial/\partial P)(\mu_A^{\text{oxb}} - \mu_A^{\text{oxa}}) = (\partial/\partial P)[W(A|b) - W(A|a) + kT \ln \rho_b^b/\rho_a^a] = \Delta V(a \rightarrow b; L) + (\partial/\partial P)[kT \ln (V^a/V^b)] \quad (7.17)$$

Again we note that whereas $\Delta V(a \rightarrow b; L)$ has a truly local character, the volume change corresponding to the process in (7.17) *diverges* if one phase is a rarefied gas, for which case we obtain

$$\frac{\partial}{\partial P}(kT \ln V^g) = \frac{kT}{V^g} \frac{\partial V^g}{\partial P} \sim \frac{kT}{P} \rightarrow \infty$$

for $P \rightarrow 0$.

The common way of bypassing the difficulty of divergence is to consider the partial molar volume of A in the liquid only i.e., at infinite dilution we have

$$\bar{V}_A^\circ = \frac{\partial \mu_A}{\partial P} = \frac{\partial W(A|b)}{\partial P} - \frac{kT}{V^b} \frac{\partial V^b}{\partial P} = \Delta V(g \rightarrow b; L) - \frac{kT}{V^b} \frac{\partial V^b}{\partial P} \quad (7.18)$$

Again we see that \bar{V}_A° includes the compressibility of the liquid b, which is not necessarily a negligible quantity. (Here, we have assumed that the *local* volume change from the gas to the liquid is equal to the volume change for introducing A to a fixed point in the liquid). It must be noted, however, that $\Delta V(a \rightarrow b; L)$ in (7.16) does not correspond to the process indicated in (7.6). This is the volume change for transferring A from a fixed position in a to a fixed position in b, and it is obtained by a direct differentiation of $\Delta \mu_A^{\text{op}}$ with respect to pressure. To the best of the author's knowledge, this quantity, though the most significant one, has never been used as a "standard" volume of transfer.

Finally the *local* standard energy of transfer is

$$\Delta E(a \rightarrow b; L) = \Delta H(a \rightarrow b; L) - P \Delta V(a \rightarrow b; L) \quad (7.19)$$

This quantity when applied to the process of transfer from a gas to a liquid is the simplest quantity that reflects the energetic changes in the liquid caused by the introduction of a solute.

The above list of quantities pertinent to the process ($a \rightarrow b; L$) are all free of contributions from the "liberation" step in introducing a particle into the solution. All of these can be applied to *any* concentration of the solute A. They are the simplest to obtain experimentally and they can be used as probes of the thermodynamics of solvation of a specific solute.

We suggest that the quantities listed in this section be used for tabulation of the thermodynamics of transfer of solute between two phases. In such tables one needs to specify the temperature, the pressure, and the composition of the two phases. The most common application will be the limiting values of these quantities at $\rho_A \rightarrow 0$, and the phases a and b will be the pure solvents. However without any change of notation one can use pure A as one phase, or any mixture of solvents, e.g., of water and ethanol, as another. Thus they can be used in a uniform manner in all cases of interest. This is not possible with the conventional SFE of transfer from pure A to dilute A in W, or for the conventional *volume* of transfer from the gas to the liquid.

8. Summary and Conclusion

The essential issue addressed in this paper is the following: The statistical mechanical construction of the

(conventional or generalized) standard free energy of transfer involves three steps

$$\mu_A = W(A|\text{solvent}) + kT \ln \rho_A \Lambda_A^3 \quad (8.1)$$

$$\mu_A^{*\rho} \equiv \mu_A - kT \ln \rho_A = W(A|\text{solvent}) + kT \ln \Lambda_A^3 \quad (8.2)$$

$$\Delta \mu_A^{*\rho} \equiv \mu_A^{*\rho b} - \mu_A^{*\rho a} = W(A|b) - W(A|a) \quad (8.3)$$

Alternatively, we start from the general expression for the chemical potential of A in any solvent.³⁴ We first define the generalized standard chemical potential (which in the limit of $\rho_A \rightarrow 0$ coincides with the conventional standard chemical potential of A, μ_A^{op}). In this step we have removed *part* of the liberation free energy of A. In the second step we form the difference in the generalized SCP of A in two phases, and thereby remove the remaining part of the liberation free energy. What remains is a simple and measurable quantity that is a proper free energy change for the process of transferring A from a fixed position in a to a fixed position in b.

The thermodynamic construction of the SFE of transfer is different. We first form the difference of the chemical potentials of A in two phases (assuming ideal dilute solutions)

$$\mu_A^b - \mu_A^a = \mu_A^{\text{ocb}} - \mu_A^{\text{oca}} + kT \ln (C_A^b/C_A^a) \quad (8.4)$$

thereby removing the term $kT \ln \Lambda_A^3$. We then make a particular choice of concentrations $C_A^a = C_A^b$ to obtain

$$\Delta G \left[\begin{array}{c} a \rightarrow b \\ C_A^b = C_A^a \end{array} \right] = \mu_A^{\text{ocb}} - \mu_A^{\text{oca}} \quad (8.5)$$

In this step we remove the term $kT \ln N_A$ also, which is part of the liberation free energy. It is *only* with the choice of $C_A = \rho_A$ that the term $kT \ln V$ is also removed. For *all* other concentration scales we can write the transformation of variables as $\rho_A = T_A C_A$, and hence

$$\Delta G \left[\begin{array}{c} a \rightarrow b \\ C_A^b = C_A^a \end{array} \right] = W(A|b) - W(A|a) + kT \ln (T_A^b/T_A^a) \quad (8.6)$$

The transformation functions, T_A , contain the volume (as well as other factors) of the phases. From the above presentation it is crystal-clear that the simplest quantity is obtained in (8.6) by the choice of $C_A = \rho_A$, i.e., $T_A^a = T_A^b = 1$. In which case (8.6) coincides with the limit ($\rho_A \rightarrow 0$) of (8.3).

The quantity defined in (8.3) is the most appropriate measure for the difference in the solvation free energy of A in the two phases. Similar considerations apply to all other thermodynamic quantities derived from the free energy. Furthermore, this quantity may be used for any concentration of the solute without changing its significance, an extension which is not always possible with other concentration scales. In addition, for complex solvents, e.g., a mixture of water, ethanol, and KCl, this quantity is computed using the least ambiguous concentration scale.

The thermodynamic quantities derived from $\Delta \mu_A^{*\rho}$ can be used as well-defined probes of the local environment of the solute A in various solvents. Hence we have referred to these as the *local*-thermodynamic quantities of transfer. All of these are completely devoid of any contribution from the liberation free energy, or its derivatives.

Acknowledgment. I am very grateful to Professors S. Baer and M. Cohen for many helpful discussions on the

contents of this paper. Comments on the manuscript by J. Gordon, R. Battino, J. Edsall, J. P. O'Connell, J. S. Rowlinson, W. Yang-Wen, Z. Elkoski, B. Gerber, and Y. Marcus are gratefully acknowledged. In particular I am grateful to Dr. J. Gordon for his critical and thoughtful comments.

Appendix I. Notations and Abbreviations

CP	chemical potential
PCP	pseudo-chemical potential
SCP	standard chemical potential
SFE	standard free energy
SI	symmetrical ideal
DI	dilute ideal
ρ_i^j	the number density of species i in phase j
μ_i^j	the chemical potential of species i in phase j
μ_i^p	the chemical potential of pure i (also denoted by μ_i^j)
μ_A^{ocb}	the standard chemical potential of A in phase b , based on the concentration scale c
μ_A^{*cb}	the generalized standard chemical potential of A in phase b , based on the concentration scale c

References and Notes

- (1) A. Ben-Naim in "Solutions and Solubilities", Vol. VIII of "Techniques of Chemistry", M. R. J. Dack, Ed., Wiley, New York, N.Y., 1975.
- (2) A. Ben-Naim, "Water and Aqueous Solutions, Introduction to a Molecular Theory", Plenum Press, New York, N.Y., 1974.
- (3) The minimum is indeed very little. All that is needed is the basic relation between the free energy and the partition function, and a general familiarity with the form of the classical partition function. About one quarter of Hill's book⁴ is sufficient.
- (4) T. L. Hill, "Introduction to Statistical Thermodynamics", Addison-Wesley, Reading, Mass., 1960, Chapters 1-4.
- (5) All the results of this paper are valid also for nonspherical molecules. The presentation of this case is, however, more complicated.
- (6) The term "translational entropy" could also be used for this term. However, for consistency of nomenclature we prefer to refer to this term as the liberation entropy, in analogy with the liberation free energy in (3.13).
- (7) The term "proper chemical potential" is used here in the ordinary sense of "chemical potential". This is done to emphasize the distinction between this quantity and a quantity such as μ_A^{ox} that is not proper chemical potential of A . A proper chemical potential of A has the characteristic property that it diverges to $-\infty$ when $\rho_A \rightarrow 0$.
- (8) Both μ_A^{op} and μ_A^{ox} in (4.10) do not diverge as $\rho_A \rightarrow 0$, and therefore are not considered to be proper chemical potential of A .⁷
- (9) H. L. Friedman in "Water, A Comprehensive Treatise", F. Franks, Ed., Vol. 3, Plenum Press, New York, N.Y., 1973.
- (10) H. S. Frank, *J. Chem. Phys.*, **13**, 493 (1945).
- (11) H. S. Frank and M. W. Evans, *J. Chem. Phys.*, **13**, 509 (1945).
- (12) H. L. Friedman, "Ionic Solution Theory", Interscience, New York, N.Y., 1962.
- (13) E. A. Guggenheim, "Mixtures", Oxford University Press, London, 1952.
- (14) E. Arnett and D. R. McKelvey in "Solute-Solvent Interactions", J. F. Coetzee and C. D. Ritchie, Ed., Marcel Dekker, New York, N.Y., 1969, Chapter 6.
- (15) W. Y. Wen and J. H. Hung, *J. Phys. Chem.*, **74**, 170 (1970).
- (16) In previous publications^{1,2} this quantity has been referred to as the "nonconventional" standard chemical potential. We now feel that the term "generalized standard chemical potential" is more appropriate.
- (17) In the author's opinion, there is nothing "shocking" or even surprising in this finding. This observation is simply a result of comparing the ratios of two different quantities, not the same quantity in different units. Alternatively, one compares ΔG for two different processes and there is no reason that these will have the same magnitude or sign.
- (18) This is not an uncommon situation in physical chemistry. As an example, consider pure argon, and consider the "theoretical" process of bringing two specific molecules from fixed positions at infinite separation to some close separation R . Clearly, the free energy of this process cannot be measured directly, but theory shows that this free energy is related to the pair correlation function of the liquid, a quantity which can be evaluated from x-ray diffraction measurements. For details, see ref 2, Chapter 3.
- (19) The author was unable to find any process for which this quantity represents its free energy change. Suggestions by the readers will be appreciated.
- (20) J. A. Reynolds, D. B. Gilbert, and C. Tanford, *Proc. Natl. Acad. Sci., U.S.A.*, **71**, 2925 (1974).
- (21) C. Tanford, "The Hydrophobic Effect", Wiley, New York, N.Y., 1973, pp 4-21.
- (22) R. W. Gurney, "Ionic Processes in Solutions", McGraw-Hill, New York, N.Y., 1953, pp 90-91. (Reprinted by Dover publication, New York, N.Y.).
- (23) W. Kauzmann, *Adv. Protein Chem.*, **14**, 1 (1959).
- (24) Tanford's notation is quite confusing since μ_{HC}^0 is used once as a chemical potential of pure hydrocarbon and once as the SCP of one hydrocarbon in another hydrocarbon (e.g., n -hexane in n -decane). Therefore it is really difficult to criticize the arguments presented in ref 21.
- (25) E. A. Guggenheim, "Thermodynamics", North-Holland Publishing Co., Amsterdam, 1959, Chapter 5.
- (26) G. N. Lewis and M. Randall, "Thermodynamics", Revised by K. S. Pitzer and L. Brewer, McGraw-Hill, New York, N.Y., 1961, Chapter 21.
- (27) K. Denbigh, "The Principles of Chemical Thermodynamics", Cambridge University Press, London, 1966.
- (28) J. S. Rowlinson, "Liquids and Liquid Mixtures", Butterworths, London, 1969.
- (29) It is interesting to note that the term $kT \ln \rho_A \Lambda_A^3$ is also referred to as the mixing free energy.³⁰ We believe that the term "liberation free energy" is more appropriate. This term is present also when there are only A molecules, and even when there is a single A molecule, in which case $\rho_A = 1/V$, and this term does not have the meaning of "mixing".
- (30) H. Reiss, H. L. Frisch, and J. L. Lebowitz, *J. Chem. Phys.*, **31**, 369 (1959).
- (31) Similar claim has been made by C. Tanford, *Adv. Protein Chem.*, **24**, 1 (1970).
- (32) R. A. Robinson and R. H. Stokes, "Electrolyte Solutions", Butterworths, London, 1959.
- (33) B. E. Conway and J. O'MBockris in "Modern Aspects of Electrochemistry", Vol. I, Butterworths, London, 1954.
- (34) Note that we have restricted our discussion to classical systems only. In a quantum mechanical treatment, it is not clear whether the very separation of the chemical potential into an "interaction" and "liberation" parts is possible. Fortunately for all practical purposes in solution chemistry we can safely apply classical statistical mechanics. Also we have treated structureless molecules only. If internal properties of the molecules are taken into consideration one must interpret the standard quantities in a slightly different way, e.g., require that the molecule be placed at a fixed position and orientation.

Statistical Mechanical Theory of Nonionic Micelles

A. Wulf[†]

Department of Applied Mathematics, Research School of Physical Sciences, The Australian National University, Canberra, A.C.T. 2600, Australia (Received September 12, 1977)

Publication costs assisted by the Instituto Venezolano de Investigaciones Cientificas

A statistical mechanical theory of nonionic (single-component) micelles, well suited for applications, is developed by a simple extension of Hill's theory of solutions. An expression for the Gibbs potential of a dilute micellar solution is derived which involves the micelle size distribution and certain effective micelle partition functions. Using this Gibbs potential, both micelle thermodynamics and micelle structure and size distribution can be simply and directly treated. The thermodynamics obtained agrees with Hall and Pethica's small system thermodynamics treatment within the approximations (ideality, monodispersity, neglect of solvent composition changes) made by these authors. The micelle size distribution is found to obey Tanford's law of mass action type relation with a size dependent free energy. An approximate but detailed consideration of the effective micelle partition function leads to the local packing condition for micelles recently introduced by Israelachvili, Mitchell, and Ninham. Interactions between micelles can be included in the present statistical theory by an expansion in powers of micelle molalities; a rough, excluded volume type estimate indicates that these interactions only become important for the micelle properties when the total amphiphile molality (moles of amphiphile per mole of solvent) is greater than about 10^{-2} .

I. Introduction

A statistical mechanical theory of nonionic micelles¹ is developed in this paper. The treatment amounts to a straightforward generalization of Hill's theory of solutions² which is based on a statistical ensemble first extensively used by Stockmayer.³ An expression for the Gibbs potential of a micellar solution is derived; it involves the distribution of micelle aggregation numbers and also certain effective micelle partition functions. From this Gibbs potential the small system thermodynamics of Hall and Pethica⁴ for (single-component) nonionic micelles can be derived very simply. We note, however, that except in the monodisperse limit the micellar enthalpy and volume differences defined by Hall and Pethica are not identical with the quantities measured in a dilution experiment.

Tanford⁵ has introduced a theory, based on the law of mass action, which relates micelle sizes and the critical micelle concentration to a size dependent free energy of micellization. Israelachvili, Mitchell, and Ninham^{6,7} modified Tanford's theory by introducing a local packing criterion which imposes certain geometrical constraints on the allowed micelle structures. We indicate how contact between these theories and the present statistical theory is made by means of suitable approximations to evaluate the effective micelle partition functions. In particular, an approximate derivation of the local packing condition of ref 6 mentioned above is given. This packing condition appears to be of considerable importance. It links together micelles, vesicles, and bilayers in one theory,⁷ and may be important in the organization of biological membranes, as suggested by Israelachvili.⁸

Interactions between micelles can be included in the theory by an expansion in powers of micelle molalities which is formally similar to the virial expansion of a multicomponent imperfect gas. For simplicity, the expansion is carried out here only to second order; the expansion coefficients obtained are similar to second virial coefficients, except that potentials of mean force, rather than the direct interaction potentials between particles,

must be used. If it is assumed that these expansion coefficients are determined mainly by the spatial dimensions of the micelles, one estimates $c_{\text{tot}} \sim 10^{-2}$ for the total amphiphile molality c_{tot} (in moles of amphiphile per mole of water solvent) at which interactions between micelles become important for the micelle structures. (For very long cylindrical micelles, c_{tot} might be smaller, see end of section VI.) This is much larger than typical cmc's in aqueous solutions which have molalities of order 10^{-5} .

Statistical theories of micelles have been previously published by Hoeve and Benson⁹ and by Aranow.¹⁰ The work of Hoeve and Benson is based on the canonical ensemble; they did not consider interactions between micelles or derive any thermodynamics. Aranow starts with the same ensemble used here, but then assumes that the solution is incompressible and bases his subsequent development on Hill's physical cluster theory.¹¹ As a consequence, Aranow's theory centers around the micelle size distribution, and thermodynamic quantities or the micelle structures are hardly considered. (On the other hand, Aranow presents an approximate treatment of ionic micelles which we do not consider.)

In sections II–IV we develop the general theory, and in sections V and VI we consider briefly applications to micelle thermodynamics and micelle structure, respectively.

II. Micelles in Water as a Multicomponent Solution

In this section we derive an expression for the Gibbs thermodynamic potential $G(M_i, N_n, p, T)$ of a dilute solution of N_n micelles of aggregation numbers n , $n = 1, 2, 3, \dots$, in M_0 molecules of solvent (water) and M_i , $i = 1, 2, \dots, r$ ions of various salts. We assume here that the salts in solution are fully dissociated. [If the salts are not perfect electrolytes, one should consider partial dissociation. The degree of dissociation depends on p , T , the total salt concentrations, and the molar ratios $c_n = N_n/M_0$. For small c_n , the shift of the dissociation equilibrium away from the unperturbed value represented by $M_i = M_i^0$ (neutral salt molecules and ions now), that obtains for the solution of water and salts only, is small. It is not difficult to see that in first order this shift is accounted for by including

[†] Visiting Fellow. Permanent Address: Centro de Fisica, Instituto Venezolano de Investigaciones Cientificas (IVIC), Apartado 1827, Caracas 101, Venezuela.

an additional term quadratic in the c_n in $G(M_i, N_n, p, T)$, eq 18, and putting $M_i = M_i^0$. For strong electrolyte salts the correction term should be unimportant.] We also assume that $M_i \ll M_0$ ($i = 1, 2, \dots, r$), although this is not necessary for the formal theory (in the general case $\sum_{i=0}^r M_i$ replaces M_0). To keep equations simple and compact, we write M_i, N_n, \dots for the sets of numbers $\{M_i\}, \{N_n\}, \dots$ occurring in the arguments of various functions; e.g., $G(M_i, N_n, p, T)$ means $G(\{M_i\}, \{N_n\}, p, T)$.

It is convenient to formally treat micelles of different aggregation numbers n as different solutes, with chemical potentials μ_n . The fact that $\mu_n = n\mu_1 = n\mu$, where μ is the chemical potential of a single amphiphile in solution, can be recovered at any time by requiring that the system be in equilibrium with respect to the transformation n micelles $1 \rightleftharpoons 1$ micelle n (micelle $m \equiv$ micelle of aggregation number m). The identity of all the amphiphile molecules is automatically taken into account in section III where G is minimized with respect to the molar ratios $c_n = N_n/M_0$, subject to the single constraint $M_0 \sum n c_n = N =$ fixed total number of amphiphiles.

We use the constant pressure, semigrand ensemble $\Gamma(M_i, p, T, \mu_n)$ with fixed M_i but varying N_n . This ensemble is convenient for several reasons. It singles out the components of interest, the micelles in the present case, for special consideration; it leads naturally to the physically appropriate Gibbs potential $G(M_i, N_n, p, T)$; and it allows the effect of interactions between micelles to be accounted for by an expansion in powers of the c_n . We have^{2,3}

$$\Gamma(M_i, p, T, \mu_n) = e^{-\sum_{i=0}^r M_i \mu_i' / kT} \sum_{N_n \geq 0} \left[\prod_1^L \lambda_n^{N_n} \right] \Delta_{\{N_n\}}(M_i, p, T) \quad (1)$$

where

$$\Delta_{\{N_n\}} = \sum_V e^{-pV/kT} Q(M_i, N_n, V, T) \quad (2)$$

$$\lambda_n = e^{\mu_n/kT} \quad (3)$$

and L is some arbitrary, large number (much greater than the average micelle aggregation number). The usual notation of statistical mechanics is used. The quantities μ_i' are the chemical potentials of the solvent (water) molecules ($i = 0$) and salt ions. Q is the canonical partition function and Δ is the isothermal-isobaric partition function,¹² so that

$$G(M_i, N_n, p, T) = -kT \ln \Delta_{\{N_n\}}(M_i, p, T) \quad (4)$$

For convenience we shall use the abbreviations

$$\left. \begin{matrix} Y_0 \\ Y_n \\ Y_{nm} \end{matrix} \right\} = Y_{\{N_j\}} \left\{ \begin{matrix} \text{all } N_j = 0 \\ \text{all } N_j = 0 \text{ except } N_n = 1 \\ \text{all } N_j = 0 \text{ except } N_n = 1, \\ \quad N_m = 1 \text{ (or } N_n = 2, \text{ if } n = m) \end{matrix} \right.$$

For the micelle problem, we factor $\Delta_{\{N_n\}}$ into a part depending on the properties of single micelles and a part, $\tilde{\Delta}_{\{N_n\}}$, which accounts for the interactions between micelles and their movement in the system volume:

$$\Delta_{\{N_n\}} = \left[\prod_1^L q_n^{N_n} \right] \tilde{\Delta}_{\{N_n\}} \quad (5)$$

Explicit expressions for the effective micelle partition functions q_n and the first few $\tilde{\Delta}_{\{N_n\}}$ are given in section IV. (The q_n will be chosen to be intensive quantities, each

corresponding to a single micelle n fixed at a point in the solution.) We now rewrite eq 1 as

$$\Gamma/\Delta_0 = 1 + \sum' X_{\{N_n\}} \prod_1^L z_n^{N_n} \quad (6)$$

where the prime on the summation indicates that at least one of the N_n is nonvanishing and the quantities z_n, X are given by

$$z_n = v_0' q_n \lambda_n \quad v_0' = \tilde{\Delta}_n / M_0 \Delta_0$$

$$X_{\{N_n\}} = (\tilde{\Delta}_{\{N_n\}} / \Delta_0) v_0'^{\sum N_n} \quad (7)$$

It is shown in section IV that v_0' is independent of n . Note that, for any n

$$X_n = M_0 \quad (8)$$

As pointed out by Hill,¹³ there is a formal analogy between expression 6 for Γ/Δ_0 and the grand canonical partition function for an imperfect gas (gas mixture, in our case). Thus the gas theory expansions can be carried over to the problem of solutions with only some trivial changes in notation ($X_N \leftrightarrow Z_N/N!$, $N_0 \leftrightarrow V$, $-\mu_e' \leftrightarrow p$, where μ_e' is defined below). Here we restrict ourselves to the "second virial" approximation, which can easily be obtained directly by elementary manipulations. With the definitions

$$M_0 \mu_e = \sum_{i=0}^r M_i \mu_i'$$

$$\mu_e' = \mu_e(p, T, M_i/M_0, c_n) - \mu_e(p, T, M_i/M_0, 0) \quad (9)$$

one obtains

$$\mu_e' = -(kT/M_0) \ln \Gamma/\Delta_0 =$$

$$-kT \sum' \theta_{\{N_n\}} \prod_1^L z_n^{N_n} \quad (10)$$

where, up to the terms second order in the z_n

$$\theta_n = 1$$

$$M_0 \theta_{nm} = X_{nm} - X_n X_m \quad (n \neq m) \quad (11)$$

$$M_0 \theta_{nn} = X_{nn} - 1/2 X_n^2$$

From eq 6 and 10

$$c_n = \frac{z_n}{M_0} \frac{\partial \ln \Gamma/\Delta_0}{\partial z_n} = \sum' N_n \theta_{\{N_m\}} \prod_1^L z_m^{N_m} \quad (12)$$

Equation 12 can be inverted to give

$$z_n = c_n - \sum_{m \neq n} \theta_{mn} c_m c_n - 2\theta_{nn} c_n^2 - \dots \quad (13)$$

This shows that $z_n \rightarrow c_n$ as $c_n \rightarrow 0$. From eq 10 and 13 we obtain

$$-\mu_e' / kT = \sum_n z_n + \sum_{m < n} \sum \theta_{mn} z_m z_n + \sum_n \theta_{nn} z_n^2 + \dots$$

$$= \sum_n c_n - 1/2 \sum_{m \neq n} \sum \theta_{mn} c_m c_n - \sum_n \theta_{nn} c_n^2 - \dots \quad (14)$$

To calculate $G(M_i, N_n, p, T)$ we may write

$$e^{-\sum M_i \mu_i' / kT} = \Delta_{\{N_n\}} \prod_1^L \lambda_n^{\tilde{N}_n} \quad (15)$$

where the \tilde{N}_n maximize the summand in eq 1 and are the observed values of N_n in the thermodynamic limit. Combining eq 4 and 15 we obtain the expected result

$$G(M_i, N_n, p, T) = \sum_0^r M_i \mu_i' + kT \sum_1^L N_n \ln \lambda_n \quad (16)$$

From eq 7 and 13 we find, in the "second virial" approximation

$$\begin{aligned} \ln \lambda_n &= \ln \left[\frac{z_n}{v_0' q_n} \right] = \ln \left[\frac{c_n}{v_0' q_n} \right] + \\ &\quad \ln \left[1 - \frac{\sum_{m \neq n} \theta_{mn} c_m - 2\theta_{nn} c_n}{v_0' q_n} \right] \\ &= \ln \left[\frac{c_n}{v_0' q_n} \right] - \sum_{m \neq n} \theta_{mn} c_m - 2\theta_{nn} c_n \end{aligned} \quad (17)$$

With eq 17 and 14, G can be written completely in terms of its natural variables $M_i, N_n = M_0 c_n$:

$$\begin{aligned} G(M_i, N_n, p, T) &= \frac{\mu_e(p, T, M_i/M_0, 0)}{M_0 kT} + \frac{kT}{\mu_e'(p, T, M_i/M_0, c_n)} + \sum_1^L c_n \ln \lambda_n \\ &= \frac{\mu_e(p, T, M_i/M_0, 0)}{kT} + \sum_n c_n \ln \frac{c_n}{v_0' q_n} - \sum_{m \leq n} \sum \theta_{mn} c_m c_n \end{aligned} \quad (18)$$

III. Equilibrium Conditions for Micelles

The equilibrium state of a micellar solution at given p, T, M_i , and total number of amphiphiles N is determined by minimizing G . The minimization is with respect to the micelle variables on which the q_n depend and the c_n , subject to the constraint $M_0 \sum n c_n = N$. Introducing the Lagrange multiplier α , we minimize the function

$$\Psi = \frac{G}{M_0 kT} - \left[\frac{\alpha}{kT} \right] \sum n c_n \quad (19)$$

where α may in principle be determined at the end by requiring

$$M_0 \sum_1^L n c_n = N$$

We have, from $\partial \Psi / \partial c_n = 0$

$$c_n \approx q_n v_0' e^{n\alpha/kT} \left(1 + \sum_{m \neq n} \theta_{mn} c_m + 2\theta_{nn} c_n \right) \quad (20)$$

Substituting (20) into (18) and (19) gives

$$\begin{aligned} \Psi - \mu_e/kT &\approx - \sum_n c_n + \sum_{m \leq n} \sum \theta_{mn} c_m c_n \\ &\approx - \sum_n q_n v_0' e^{n\alpha/kT} - \\ &\quad \sum_{m \leq n} \sum \theta_{mn} q_m q_n v_0'^2 e^{(m+n)\alpha/kT} \end{aligned} \quad (21)$$

According to the estimate given at the end of section VI, the interaction term in eq 21 is negligible except at total amphiphile concentrations several orders of magnitude larger than typical cmc's. When the interaction term in (21) can be neglected, the minimization of Ψ with respect to variables (such as volume and shape) characterizing the micelle structures gives the simple condition, for each n

$$q_n = \text{maximum} \quad (22)$$

It is easy to verify that α is the amphiphile chemical potential μ :

$$\begin{aligned} \mu &= \frac{\partial G}{\partial N} = \sum_n \left[\frac{\partial G}{\partial c_n} \right] \frac{\partial c_n}{\partial N} = \alpha \sum_n M_0 n \frac{\partial c_n}{\partial N} = \\ &\quad \alpha \frac{\partial}{\partial N} \sum_n M_0 n c_n = \alpha \frac{\partial N}{\partial N} = \alpha \end{aligned}$$

since $\partial \Psi / \partial c_n = 0$.

Equations 20 and 21 give a formal solution, in the "second virial" approximation, to the problem of determining the micelle structure and the micelle distribution c_n (eq 21 is to be minimized with respect to the micelle variables in each q_n).

IV. The Quantities q_n and $\bar{\Delta}_{[N_n]}$

Having set up the formal theory, we now require statistical mechanical expressions for $q_n, \bar{\Delta}_{[N_n]}$, etc. We shall make the usual assumption of solution theory that vibrational degrees of freedom of the molecules are separable and that the translational and rotational (external and internal) degrees of freedom may be treated classically.^{9,14} Then the canonical partition function Q is given by

$$\begin{aligned} Q(M_i, N_n, V, T) &= \left[\frac{1}{\Lambda^{3N} \prod_{n=1}^L (n!)^{N_n} N_n!} \right] \times \\ &\quad \int d\{N\} e^{-\beta U(\{N\})} \left[\frac{1}{\prod_{i=0}^r \Lambda_i^{3M_i} M_i!} \right] \times \\ &\quad \int d\{M\} e^{-\beta [U(\{M\}) + V(\{M\}, \{N\})]} \end{aligned} \quad (23)$$

where Λ, Λ_i are functions of temperature only, arising from the vibrational partition functions and the integrations over translational and rotational momenta of the amphiphiles and particles i . The symbols $\{N\}$ and $\{M\}$ represent the translational and rotational (external and internal) coordinates of the N amphiphiles and M_i particles $i, i = 0, 1, \dots, r$, and $d\{N\}, d\{M\}$ represent the appropriate corresponding volume elements;¹⁴ $U(\{x\})$ denotes the sum of all interactions and conformational energies of molecules within the set $\{x\}$, while $V(\{x\}, \{y\})$ denotes the sum of all interactions between x and y ; $\beta = 1/kT$; and the prime on the integral over $\{N\}$ indicates that the amphiphiles are grouped into N_n micelles $n, n = 1, 2, \dots, L$. It is understood that each micelle n has a certain volume and shape, denoted by Ω_n .

The following observation is useful in carrying out sums of the type of eq 2. Let s be a finite integer and $F(\rho_i)$ be a continuous function of the densities $\rho_i = M_i/V$. Then we have

$$\begin{aligned} \Delta[F, s] &\equiv \sum_V e^{-pV/kT} Q_0(M_i, V, T) V^s F(\rho_i) \\ &= \Delta_0 \sum_V P_0(V; p, T, M_i) V^s F(\rho_i) \\ &\equiv \Delta_0 \langle V^s F(\rho_i) \rangle \end{aligned} \quad (24)$$

where

$$P_0(V; p, T, M_i) = e^{-pV/kT} Q_0(M_i, V, T) / \Delta_0$$

is a normalized probability distribution for V for the system M_i of solvent (water) plus salt ions (Q_0 is the canonical partition function for this system). In the thermodynamic limit, $M_i \rightarrow \infty$, this distribution becomes infinitely sharp around $V = V_0(M_i, p, T)$, the volume of the system M_i (i.e., $\langle (\delta V)^2 \rangle^{1/2} / V_0 \rightarrow 0$). Therefore, with $\rho_{i0} = M_i / V_0$, we obtain

$$\Delta[F, s] = \Delta_0 V_0^s F(\rho_{i0}) [1 + O(\langle (\delta V)^2 \rangle^{1/2} / V_0)] \quad (25)$$

When quantities $\Delta[F, s]$ are combined to give intensive properties, the correction term in the square brackets in (25) gives a vanishing contribution in the thermodynamic limit.

We define q_n by

$$Q(M_i, N_n = 1, V, T) = Q_0(M_i, V, T) 4\pi V q_n(\rho_i, T, \Omega_n) \quad (26)$$

where the argument of Q on the left-hand side indicates that a single micelle Ω_n is present and no other micelles ($N_m = 0$ for $m \neq n$). It is also assumed, for definiteness, that the micelles have an axis of symmetry (this is satisfied by all plausible models for micelles), giving an orientational integral 4π which has been factored out explicitly on the right-hand side of eq 26. Equation 26 implies that $-kT \ln(4\pi V q_n)$ is the increase in Helmholtz free energy due to the addition, at constant V, T , of a micelle Ω_n to the system M_i of solvent and salt ions.¹⁵

Using eq 23 and definition 26, an alternative expression for q_n can easily be written which is useful because it is amenable to approximate model calculations. The expression is¹⁶

$$q_n(\rho_i, T, \Omega_n) = (1/n! \Lambda^{3n}) f'' d\{N\}_n e^{-\beta U(\{N\}_n)} e^{-\beta \phi_n(\rho_i, T, \{N\}_n)} \quad (27)$$

where the double prime indicates that the micelle is fixed in space and

$$-\beta f_n = \ln \left\{ (1/Q_0) \left(\prod_i \Lambda_i^{3M_i} M_i! \right) \times \int d\{M\} e^{-\beta [U(\{M\}) + V(\{M\}, \{N\}_n)]} \right\} \quad (28)$$

The symbol $\{N\}_n$ represents the coordinates of N amphiphiles with $N = n$. Equation 28 shows that f_n is the difference in Helmholtz free energy between system M_i containing a fixed, inert micelle $\{N\}_n$ and system M_i alone; i.e., f_n is the reversible work required to insert an inert micelle $\{N\}_n$ into system M_i at fixed V, T .

Using eq 2, 26, 24, and 25 we obtain

$$\Delta_n = \Delta_0 4\pi V_0 q_n(\rho_{i0}, T, \Omega_n) = \tilde{\Delta}_n q_n \quad (29)$$

From this we see that $v_0' = \tilde{\Delta}_n / M_0 \Delta_0 = 4\pi V_0 / M_0$ is independent of n , as stated in section II.

For large n we expect $f_n(\rho_i, T, \{N\}_n)$ depends, to a good approximation, on Ω_n and not on the detailed amphiphile coordinates $\{N\}_n$. In this case $e^{-\beta \phi_n(\rho_i, T, \{N\}_n)}$ can be taken out of the integrand in eq 27.

Next, we can write

$$Q(M_i, N_n = 1, N_m = 1, V, T) = Q_0(M_i, V, T) q_n q_m \int d\mathbf{R}_n d\hat{\Omega}_n \int d\mathbf{R}_m d\hat{\Omega}_m e^{-\beta W_{nm}} \quad (30)$$

where the partition function on the left-hand side is for system M_i containing two micelles Ω_n, Ω_m ($n \neq m$) and no other micelles (or amphiphiles), and $\mathbf{R}_k, \hat{\Omega}_k$ denote the position and orientation of micelle Ω_k . It is clear from (26) that $-kT \ln(d\mathbf{R}_k d\hat{\Omega}_k q_k)$ is the free energy increase due to the addition, at fixed V, T, M_i , of a micelle Ω_k in $d\mathbf{R}_k d\hat{\Omega}_k$. Therefore, it follows from eq 30 that

$$W_{nm} = W_{nm}(\mathbf{R}_{nm}, \hat{\Omega}_n, \hat{\Omega}_m; \rho_i, T)$$

is an interaction free energy, or potential of mean force, between two micelles Ω_n, Ω_m at $\mathbf{R}_n, \hat{\Omega}_n$ and $\mathbf{R}_m, \hat{\Omega}_m$. It is easy to see that $W_{nm} \rightarrow 0$ as $\mathbf{R}_{nm} \rightarrow \infty$.¹⁷ The detailed calculation of potentials of mean force in ionic solutions

is a difficult problem on which much work remains to be done.¹⁸

Using eq 30 and 25 we obtain

$$\Delta_{nm} = \Delta_0 q_n(\rho_{i0}, T, \Omega_n) q_m(\rho_{i0}, T, \Omega_m) \times \int_{V_0} d\mathbf{R}_n d\hat{\Omega}_n \int_{V_0} d\mathbf{R}_m d\hat{\Omega}_m e^{-\beta W_{nm}}$$

so that

$$\tilde{\Delta}_{nm} = \Delta_0 \int_{V_0} d\mathbf{R}_n d\hat{\Omega}_n \int_{V_0} d\mathbf{R}_m d\hat{\Omega}_m e^{-\beta W_{nm}} \quad (31)$$

where it is understood that W_{nm} is evaluated at $\rho_i = \rho_{i0}$.

Similarly, we see from eq 23 that

$$Q(M_i, N_n = 2, V, T) = Q_0 q_n^2 \frac{1}{2!} \int d\mathbf{R}_n d\hat{\Omega}_n \int d\mathbf{R}_n' d\hat{\Omega}_n' e^{-\beta W_{nn}}$$

where W_{nn} is the potential of mean force between two micelles Ω_n (with $W_{nn} \rightarrow 0$ as $|\mathbf{R}_n - \mathbf{R}_n'| \rightarrow \infty$). Therefore

$$\tilde{\Delta}_{nn} = (\Delta_0/2) \int d\mathbf{R}_n d\hat{\Omega}_n \int d\mathbf{R}_n' d\hat{\Omega}_n' e^{-\beta W_{nn}} \quad (32)$$

With the above expressions, we can obtain the coefficients θ_{nm} . Thus, from eq 7, 31, and 11 one finds

$$\theta_{nm} = [\rho_0 / (4\pi)^2 V_0] \int d\mathbf{R}_n d\hat{\Omega}_n \times \int d\mathbf{R}_m d\hat{\Omega}_m (e^{-\beta W_{nm}} - 1) \quad (33)$$

where $\rho_0 = \rho_{00} = M_0 / V_0$. Similarly

$$\theta_{nn} = (1/2) [\rho_0 / (4\pi)^2 V_0] \times \int d\mathbf{R}_n' d\hat{\Omega}_n' (e^{-\beta W_{nn}} - 1) \quad (34)$$

These quantities are analogous to second virial coefficients of a gas mixture.

This completes our development of the statistical theory. In the next two sections we consider some applications.

V. Thermodynamics of Micelles

Hall and Pethica⁴ applied the small system thermodynamics of Hill¹⁹ to micellar solutions, obtaining a variety of interesting thermodynamic relations between micellar properties.

The first topic in this section is a demonstration of how the Gibbs potential $G(M_i, N_n, p, T)$, which contains all the thermodynamics of a dilute solution of single-component micelles, leads to the basic eq 16.62 and 16.63 of Hall and Pethica.⁴ These equations form the starting point for these authors' thermodynamic treatment of single-component micelles. There are three assumptions involved in these equations: (i) interactions between micelles are negligible; (ii) changes in the solvent composition are negligible; (iii) the micellar solution may be treated as monodisperse (this is implied by eq 16.49 of Hall and Pethica).

Neglecting the interaction terms in eq 18 of section II and comparing the resulting Gibbs potential with eq 16.46 of ref 4 we obtain, for the micelle chemical potential μ^*

$$\mu^* / kT = -\ln q_n v_0' e + \ln c_n \quad (35)$$

where the (effective) micelle aggregation number \bar{n} maximizes the micelle distribution

$$c_n = q_n v_0' e^{n\mu/kT} \quad (36)$$

(This is eq 20 of section III without the interaction terms.) Thus \bar{n} satisfies the equation

$$\partial(\ln q_n v_0') / \partial \bar{n} = -\mu / kT \quad (37)$$

Since the solution is assumed monodisperse, $c_n = c_{mic} =$

total micelle concentration. Comparing eq 35 and Hall and Pethica's eq 16.49, we have the identification

$$\bar{G}(\bar{n}, T, p) = -kT \ln q_{\bar{n}} v_0' e = \bar{n} \mu - kT \ln (c_{\text{mic}} e) \quad (38)$$

for the standard chemical potential of a micelle (we use the notation G instead of F for Gibbs potentials). The second part of eq 38 follows by use of eq 36 for $n = \bar{n}$.

It is easy to verify from eq 18 and 38 that $\partial \bar{G}/\partial p = \bar{V}$ and $-\partial \bar{G}/\partial T = \bar{S}$ are the partial micellar volume and entropy, respectively. Thus the total volume of the solution is given by²⁰

$$V_T = (\partial G/\partial p)_{M_i, N, T} = V_0' - kT \sum_n N_n \partial (\ln q_n v_0' e) / \partial p \approx V_0' + N_{\bar{n}} (\partial/\partial p) [-kT \ln q_{\bar{n}} v_0' e] = V_0' + N_{\bar{n}} \partial \bar{G} / \partial p \quad (39)$$

where V_0' is the partial volume of system M_i plus N_1 single amphiphiles. Similarly, $S_T = S_0' + N_{\bar{n}} (-\partial \bar{G}/\partial T)$. With these observations and eq 37 we have

$$d\bar{G} = -\bar{S} dT + \bar{V} dp + \mu d\bar{n} \quad (40)$$

where changes in the concentrations M_i/M_0 are disregarded, following assumption (ii) above. From the second part of eq 38 and eq 40 we obtain

$$0 = -\bar{S} dT + \bar{V} dp - \bar{n} d\mu + d(kT \ln c_{\text{mic}}) \quad (41)$$

where we have dropped an unimportant term $k dT$ (ref 21). (This term arises from the chemical potential shift of the solvent, eq 14, and such effects are not to be considered within approximation (ii) above.) Equations 40 and 41 are the required eq 16.42 and 16.63 of ref 4, specialized to single-component micelles. All the thermodynamic derivations of Hall and Pethica for single-component micelles are based on eq 40 and 41, together with $\mu = \mu_0 + kT \ln \gamma_1 c_1$, which follows from eq 20 (with $\mu_0 = -kT \ln q_1 v_0'$ and $\gamma_1 = [1 + 2\theta_{11}c_1 + \dots]^{-1}$).

Next, as an example to show that thermodynamic relations can also be easily obtained directly from eq 18 and 20, we consider the volume difference ΔV between the average partial volumes of an amphiphile in a micelle and in free solution.

From eq 39 it is clear that

$$-\Delta V/kT = \left\{ \sum_{n=2}^L N_n [\partial (\ln q_n v_0') / \partial p] / \sum_{n=2}^L n N_n \right\} - \partial (\ln q_1 v_0') / \partial p \quad (42)$$

From eq 36 we obtain

$$c_n \partial (\ln q_n v_0') / \partial p = \partial c_n / \partial p - c_n n \partial (\mu/kT) / \partial p \quad (43)$$

and

$$\partial (\ln q_n v_0') / \partial p = \partial \ln c_n / \partial p - n \partial (\mu/kT) / \partial p \quad (44)$$

Using eq 43 and 44, eq 42 becomes

$$-\frac{\Delta V}{kT} = \frac{1}{\bar{n}} \frac{\sum_2^L [\partial c_n / \partial p - n c_n \partial (\mu/kT) / \partial p]}{\sum_2^L c_n} - \frac{\partial \ln c_1}{\partial p} + \frac{\partial (\mu/kT)}{\partial p} = \frac{1}{\bar{n}} \frac{\partial \ln c_{\text{mic}}}{\partial p} - \frac{\partial \ln c_1}{\partial p} \quad (45)$$

where

$$\bar{n} = \frac{\sum_2^L n c_n}{\sum_2^L c_n} \quad c_{\text{mic}} = \sum_2^L c_n \quad (46)$$

Equation 45 is identical with eq 16.83 of ref 4, except that we have put the activity coefficient $\gamma_1 = 1$.²² Note that eq 45 is valid for general micelle distribution c_n . A parallel argument to the above for ΔH , the difference between the partial enthalpies of an amphiphile in a micelle and in free solution, leads to eq 16.82 of Hall and Pethica.

If we take the independent variables in (45) to be p , T , c_{mic} , we find

$$\frac{\partial}{\partial \ln c_{\text{mic}}} \frac{\Delta V}{kT} = \frac{\partial}{\partial \ln c_{\text{mic}}} \frac{\partial \ln c_1}{\partial p} = \frac{\partial}{\partial p} \frac{\partial \ln c_1}{\partial \ln c_{\text{mic}}} = -\frac{1}{\bar{n}^2} \left[\frac{\partial \bar{n}}{\partial p} \right]_{T, c_{\text{mic}}} \quad (47)$$

since

$$\frac{\partial \ln c_{\text{mic}}}{\partial \ln c_1} = \bar{n} \quad (48)$$

as can easily be verified from eq 36 and 46. Equation 47 is another of the thermodynamic relations derived in ref 4.²³

As the last topic of this section, we show that, strictly, it is only in the monodisperse limit that the actual micellar enthalpy and volume changes in a dilution experiment are given by the quantities ΔH , ΔV defined above.

Suppose that the amounts of solvent (water) and salts are increased by a small fraction ϵ , $M_i \rightarrow (1 + \epsilon)M_i$, while the amount of amphiphile $N = \sum_1^L n N_n$ is fixed. From eq 36 we have, for the change ΔN_n in the number of micelles n

$$\Delta N_n = \Delta (M_0 q_n v_0' e^{n\mu/kT}) = \epsilon M_0 c_n + M_0 c_n n \Delta \mu / kT \quad (49)$$

to first order in ϵ . The change in chemical potential μ is determined by the condition that

$$0 = \Delta N = \sum_1^L n \Delta N_n = \epsilon M_0 \sum_1^L n c_n + M_0 (\Delta \mu / kT) \sum_1^L n^2 c_n$$

or

$$\Delta \mu / kT = -\epsilon \frac{\sum_1^L n c_n}{\sum_1^L n^2 c_n} \equiv -\epsilon / n_t \quad (50)$$

The enthalpy H_T of the solution is given by

$$-H_T/kT^2 = \partial (G/kT) / \partial T = -H_0/kT^2 - \sum_n N_n \partial (\ln q_n v_0') / \partial T$$

(neglecting interactions between micelles) and the change in enthalpy on dilution by

$$-\Delta H_T/kT^2 = -\Delta H_0/kT^2 - \sum_n \Delta N_n \partial (\ln q_n v_0') / \partial T$$

The second term on the right-hand side is the contribution ΔH_T^{mic} due to the micelles; with eq 49 and 50 it can be written

$$\frac{\Delta H_T^{\text{mic}}}{\epsilon M_0 kT^2} = \sum_1^L c_n (1 - n/n_t) \partial (\ln q_n v_0') / \partial T = (\partial c_1 / \partial T) (1 - 1/n_t) + \sum_2^L (\partial c_n / \partial T) (1 - n/n_t)$$

In the second step above we used a relation analogous to

eq 43 but with temperature instead of pressure derivatives; the term

$$-\left[\partial(\mu/kT)/\partial T\right] \sum_1^L (1 - n/n_i) n c_n$$

vanishes by the definition of n_i , eq 50. From eq 49 and 50, the increment ΔN_1 in the number of free amphiphiles in solution is

$$\Delta N_1 = \epsilon M_0 (1 - 1/n_i) c_1 = -\epsilon M_0 \sum_2^L n (1 - n/n_i) c_n$$

Therefore the enthalpy change $\Delta H'$ per new free amphiphile in solution is given by

$$\frac{\Delta H'}{kT^2} = \frac{\Delta H_T^{\text{mic}}}{\Delta N_1 kT^2} = \frac{\partial \ln c_1}{\partial T} - \frac{\sum_2^L \frac{\partial c_n}{\partial T} (1 - n/n_i)}{\sum_2^L n (1 - n/n_i) c_n} \quad (51)$$

On the other hand, the partial enthalpy difference ΔH of Hall and Pethica is given by

$$\frac{\Delta H}{kT^2} = -\frac{\partial \ln c_1}{\partial T} + \frac{1}{n} \frac{\partial \ln c_{\text{mic}}}{\partial T} \quad (52)$$

We only have $\Delta H' = -\Delta H$ in situations (most likely the monodisperse limit) where the factors $1 - n/n_i$ can be taken out of the sums in eq 51. Then the second term in (51) becomes

$$\left(\sum_2^L c_n \frac{\partial T}{\partial T}\right) / \left(\sum_2^L c_n\right) = (1/\bar{n}) \partial(\ln c_{\text{mic}}) / \partial T$$

The physical reason why, in general, $\Delta H' \neq -\Delta H$ is that not all the amphiphiles from large, broken down micelles go into solution as single molecules but, instead, some form smaller micelles.

VI. Micelle Structure

Two applications of the statistical theory, of a microscopic rather than thermodynamic nature, are considered in this section. This requires the use of models for the effective micelle partition functions q_n and the expansion coefficients θ_{mn} .

First we give an approximate derivation of the local packing condition of Israelachvili, Mitchell, and Ninham.⁶ This derivation indicates that the local packing condition, which requires that each amphiphile take up the same optimum surface area and volume (rather than just requiring the micelle as a whole to have the optimum area per amphiphile), should be satisfied within about 10%. Thus the ellipsoidal type micelles considered by Tanford,⁵ especially those of large eccentricity, are not allowed.⁶ Secondly, on the assumption that the quantities θ_{nm} are determined mainly by the excluded volume effect, a crude estimate of c_{tot} is made, where c_{tot} is the total amphiphile molar ratio N/M_0 at which interactions between micelles become important to determine c_n and the micelle structures; we find $c_{\text{tot}} \sim 10^{-2}$.

In passing, we note that eq 36 implies

$$\mu_n^0 + (kT/n) \ln c_n = \mu_1^0 + kT \ln c_1 \quad (53)$$

where

$$\mu_m^0(p, T, M_i) = -(kT/m) \ln q_m v_0' \quad (54)$$

This establishes the connection between the statistical theory and the theories of ref 5 and 6.

We begin by rewriting eq 27 in the form

$$v_0' q_n = (v_0' / \Lambda^{3n} n!) [f'' d\{N\}_n e^{-\beta(U_0 + \sum_1^n H_{\alpha})} e^{-\beta(U_e + f_n)}] \quad (55)$$

where

$$U = U_e + U_0 + \sum_1^n H_{\alpha} \quad (56)$$

U_e is the direct electrostatic repulsion energy between the polar head groups, U_0 is the van der Waals energy and short range repulsions between the n amphiphiles, and H_{α} is the conformational energy of amphiphile α , $\alpha = 1, 2, \dots, n$. It is clear from eq 28, and the comments following it, that $W_n \equiv U_e + f_n$ represents surface terms in the free energy required to set up a micelle Ω_n in system M_i (we disregard a small term $p \times \text{volume of } \Omega_n$). It has been argued that a reasonable approximation for W_n is^{5,6}

$$W_n(A) = \gamma [(A - A') + A_0^2/A] \quad (57)$$

where A and A' are the micelle surface area and the area occupied by the head groups, respectively, γ is the hydrocarbon-water surface tension, and A_0 is an optimum surface area proportional to n and dependent on M_i/M_0 . Typically, $\beta W_n/n \sim 10\text{--}20kT$ ($T \sim 300$ K). The term proportional to $1/A$ accounts for the electrostatic head-group repulsion.^{5,6} With the approximation (57), eq 55 becomes

$$v_0' q_n \approx (v_0' / \Lambda^{3n} n!) [f'' d\{N\}_n e^{-\beta(U_0 + \sum_1^n H_{\alpha})} e^{-\beta W_n(A)}] \quad (58)$$

Tanford's model results when it is assumed that the effect of the square bracket in (58) is to fix the density of the micelle interior and to determine, independently, the length of an alkyl chain in a micelle as the length b of a free chain at temperature T . (Thus, Tanford does not allow spheres of radius $\neq b$.)

The Local Packing Condition. We now show that a more detailed consideration of the square bracket in (58) leads to a different type of constraint on micelle structures, namely, the local packing condition introduced in ref 6.

The calculation will be based on a kind of cell model approximation for the micelle. We imagine a micelle Ω_n to be divided into n cells which have volumes v_{α} and surface areas a_{α} at the interface with water ($\alpha = 1, 2, \dots, n$). Each molecule is restricted to its cell.²⁴ The configuration integral h_{α} of molecule α is done by integrating the position of the head group over a_{α} and summing over the allowed chain conformations (those which keep the molecule within its cell); we make the approximation of factoring h_{α} into a head group contribution $h_{1\alpha}$ and a chain contribution $h_{2\alpha}$. Then eq 58 can be written

$$v_0' q_n \approx (v_0' / \Lambda^{3n}) e^{-\beta W_n(A)} e^{-\beta U_b(\sum_1^n v_{\alpha}/n)} h_{2n}(v_n, T) \times \prod_{\alpha=1}^{n-1} h_{1\alpha}(a_{\alpha}) h_{2\alpha}(v_{\alpha}, T) \quad (59)$$

where U_b is the mean attractive van der Waals energy of the micelle, which we assume depends only on the density of the micelle interior. (The head group $\alpha = n$ is kept fixed to determine the position of the micelle.)

Maximizing $\ln v_0' q_n$ with respect to a_{α} and v_{α} we obtain

$$-\beta W_n'(A) + \frac{1}{h_{1\alpha}} \frac{\partial h_{1\alpha}}{\partial a_{\alpha}} = 0 \quad (60)$$

$$-\beta U_b'(\sum_1^n v_{\alpha}/n) \frac{1}{v_n} + \frac{1}{h_{2\alpha}} \frac{\partial h_{2\alpha}}{\partial v_{\alpha}} = 0 \quad (61)$$

where $f'(x) \equiv df/dx$. Since electrostatic and double layer effects are supposed to be already included in $W_n(A)$, there is no compelling reason why the functions $h_{1\alpha}$ should be different at different cells.²⁵ Therefore we assume

$$h_{1\alpha}(a_\alpha) = h_1(a_\alpha) \quad (62)$$

On the other hand, because of the factor

$$e^{-\beta \sum_1^n H_\alpha}$$

in the integral in eq 58, it is not strictly true that $h_{2\alpha}$ is independent of the particular shape of cell α . However, we can write

$$h_{2\alpha} = e^{-\beta \Delta E_\alpha} h_2 \quad (63)$$

where ΔE_α is the excess conformational energy of chain α over the average per chain in the micelle; then we have

$$\frac{1}{h_{2\alpha}} \frac{\partial h_{2\alpha}}{\partial v_\alpha} = \frac{1}{h_2} \frac{\partial h_2}{\partial v_\alpha} - \beta \frac{\partial \Delta E_\alpha}{\partial v_\alpha} \quad (64)$$

There is strong experimental evidence supporting the hypothesis of a liquid-like micelle interior;¹ clearly, we obtain liquid-like behavior in the present model if

$$\left| \frac{\partial \Delta E_\alpha}{\partial v_\alpha} \right| \ll \left| \frac{U_b'}{n} \right| = \left| \frac{\partial U_b}{\partial v_\alpha} \right| \quad (65)$$

This condition should be satisfied quite well, since²⁶

$$\left| \frac{\partial \Delta E_\alpha}{\partial v_\alpha} \right| \sim \frac{kT}{v_\alpha}$$

while

$$\left| \frac{\partial U_b}{\partial v_\alpha} \right| \sim \frac{20kT}{v_\alpha}$$

It now follows from (60) and (62) that, in equilibrium $a_\alpha = \bar{a}$ (independent of α)

Similarly, from (61), (64), and (65) it follows that

$$v_\alpha \approx \bar{v} \quad (67)$$

Equations 66 and 67 express the local packing condition of ref 6: each amphiphile in a micelle takes up the same surface area \bar{a} (at the boundary with water) and the same volume \bar{v} . The above argument suggests that it is obeyed within about 10%.

The solution of (61) must give $\bar{v} \approx$ volume per hydrocarbon chain in bulk hydrocarbon fluid, since the same equation applies for a cell model of bulk hydrocarbon.

When \bar{a} is several times the area a_c occupied by the head group hard core, then $(1/h_1)\partial h_1/\partial \bar{a} \lesssim 1/\bar{a}$, and we find $\bar{a} \approx a_0 \equiv A_0/n$. This follows because $\beta W_n'(A) = \beta \gamma(1 - A_0^2/A^2)$, so that (60) gives, in this case

$$1 - a_0^2/\bar{a}^2 = \frac{1}{h_1} \frac{\partial h_1}{\partial \bar{a}} / \beta \gamma \lesssim \frac{1}{\beta \gamma \bar{a}} \quad (68)$$

Since $\beta \gamma \bar{a} \geq 10$, the solution of (68) within about 5% is $\bar{a} = a_0$. When $\bar{a} \lesssim 2a_c$, the second term of eq 60 (steric repulsion) must be considered.

Interactions between Micelles. The interactions between micelles become important when the second term of eq 21 is comparable to the first. For a solution of micelles of aggregation number $n \approx M$, with negligible spread about M , this happens when

$$|\theta_{MM} c_M| \sim 1 \quad (69)$$

If the coefficients θ are determined mainly by the short-range repulsions preventing overlap of micelles, then by eq 34

$$-\theta_{MM} = \frac{1 \text{ pair excluded volume of micelles } M}{2 \cdot 4\pi v_0}$$

$v_0 = M_0/V_0 =$ volume per solvent (water) molecule

For spherical micelles, $-\theta_{MM} = 16\pi R^3/3v_0$ and $M\bar{v} = 4\pi R^3/3$, so that $-\theta_{MM} = 4M\bar{v}/v_0$, where $\bar{v} =$ volume per amphiphile in a micelle. For long, rodlike micelles of length and diameter l, d , we have $-\theta_{MM} \sim (\pi/4)(l^2 d/v_0)$ (ref 27) and $M\bar{v} = \pi d^2 l/4$, so $-\theta_{MM} \sim l M\bar{v}/v_0 d$. From this and eq 69, it follows that, for $\bar{v}/v_0 \sim 10$

$$c_{\text{tot}} \approx M c_M \sim \begin{cases} (4\bar{v}/v_0)^{-1} \sim 3 \times 10^{-2} & (\text{spheres}) \\ (\bar{l} \bar{v}/dv_0)^{-1} \sim d/10l & (\text{long rods}) \end{cases} \quad (70)$$

When the θ 's are dominated by the short-range repulsions, the interaction term of eq 21 favors those shapes that give smallest excluded volume. In particular, it is clear from (70) that for a fixed total amphiphile concentration N/M_0 , the interaction term does not allow rods to have larger l/d ratio than about $M_0 v_0/N\bar{v}$. (This assumes orientationally disordered rods.)²⁸

Acknowledgment. I thank Professor B. W. Ninham for critically reading and suggesting improvements in preliminary versions of this work. Useful discussions with Dr. J. N. Israelachvili, Dr. D. J. Mitchell, and Professor B. W. Ninham are also gratefully acknowledged. Note: Hill and Chen have given a general theory of aggregation in solutions (T. L. Hill and Y. Chen, *Biopolymers*, 12, 1285 (1973)). This theory uses the grand canonical ensemble for a solution under osmotic conditions, so that the connection with thermodynamics is made through the osmotic pressure; it does not seem to be particularly convenient for a treatment of micelles. (I am indebted to one of the anonymous referees for pointing out this paper.)

References and Notes

- (1) For background on amphiphile molecules and micelles, the book by Tanford may be consulted: C. Tanford, "The Hydrophobic Effect", Wiley, New York, N.Y., 1973. A recent review on micelles in aqueous solutions has been given by L. R. Fisher and D. G. Oakenfull, *Chem. Soc. Rev.*, 6, 25 (1977).
- (2) T. L. Hill, *J. Am. Chem. Soc.*, **79**, 4885 (1957); *J. Chem. Phys.*, **30**, 93 (1959).
- (3) W. H. Stockmayer, *J. Chem. Phys.*, **18**, 58 (1950).
- (4) D. G. Hall and B. A. Pethica in "Nonionic Surfactants", M. J. Schick, Ed., Marcel-Dekker, New York, N.Y., 1967.
- (5) C. Tanford, *J. Phys. Chem.*, **78**, 2469 (1974).
- (6) J. N. Israelachvili, D. J. Mitchell, and B. W. Ninham, *J. Chem. Soc., Faraday Trans. 2*, **72**, 1525 (1976).
- (7) J. N. Israelachvili, D. J. Mitchell, and B. W. Ninham, *Biochim. Biophys. Acta*, in press.
- (8) J. N. Israelachvili, *Biochim. Biophys. Acta*, in press.
- (9) C. A. T. Hoeve and G. C. Benson, *J. Phys. Chem.*, **61**, 1149 (1957).
- (10) R. H. Aronow, *J. Phys. Chem.*, **67**, 556 (1963).
- (11) T. L. Hill, "Statistical Mechanics", McGraw-Hill, New York, N.Y., 1956, Section 27.
- (12) Reference 11, Section 14.
- (13) T. L. Hill, *J. Chem. Phys.*, **26**, 955 (1957).
- (14) Reference 11, Section 40.
- (15) Thus, $-kT \ln(4\pi V q_n)$ is the chemical potential of a single micelle Ω_n in system M ; ($c_n = 1/M_0$, all other $c_m = 0$), in agreement with eq 7, 13 and $v_0' = 4\pi V_0/M_0$ (which is shown following eq 29).
- (16) If a dimensionless q_n is desired, one can integrate in (27) the position of the micelle over a small volume $\omega \ll$ volume of micelle Ω_n , and replace V_0 in (29) by V_0/ω . For convenience, one can simply imagine that such a small ω is chosen as the unit of volume.
- (17) Divide the system into two halves of volume $V/2$, each containing one of the micelles n, m fixed in $dR_n d\Omega_n$ and $dR_m d\Omega_m$. Then we have, for the free energies, $F(V, T; n, m) = F(V/2, T; n) + F(V/2, T; m) - 2A\sigma$, where A is the area of the surface of separation and σ an appropriate surface tension. In the limit $R_{nm} \rightarrow \infty$ ($V \rightarrow \infty$), σ is independent of the presence of the micelles, so we have also $F_0(V, T) = 2F_0(V/2, T) - 2A\sigma$, with the same σ . Subtracting these

- two equations, we obtain the required result.
- (18) F. E. Harris and S. A. Rice, *J. Chem. Phys.*, **25**, 955 (1956); H. L. Friedman, "Ionic Solution Theory", Wiley-Interscience, New York, N.Y., 1962.
- (19) T. L. Hill, "Thermodynamics of Small Systems", Vols. 1 and 2, W. A. Benjamin, New York, N.Y., 1963-1964.
- (20) Note that since in equilibrium $\partial G/\partial c_n = (\mu/kT)M_0 n$ (section III), we have $\sum (\partial G/\partial c_n)(\partial c_n/\partial p)_N = (\mu/kT)(\partial N/\partial p)_N = 0$.
- (21) This term can be absorbed into redefined quantities $\bar{S}' = \bar{S} - k$ and $\bar{G}' = \bar{G} + kT$, which clearly does not change any of the micelle thermodynamic relations of ref 4, section 16.3c.
- (22) If the interaction terms for free amphiphiles in solution are kept in eq 20, so that $c_1 = q_1 v_0' e^{u_1/kT} \gamma_1^{-1}$, then the first term of eq 44 becomes $\partial(\ln \gamma_1 c_1)/\partial p$ for $n = 1$.
- (23) Equation 16.91 of ref 4 is in error by a factor of T as is easily seen by dimensional considerations.
- (24) The communal free energy, which arises from the diffusion of molecules throughout the whole system volume, is less than kT per

- molecule for a fluid and can safely be neglected here. (For communal entropy, see ref 11, Chapter 8.)
- (25) The function $h_{1\alpha}(a_\alpha)$ measures the "free surface" available to the head group hard core of amphiphile α .
- (26) (i) It takes energy $\sim kT$ (~ 300 K) for an additional gauche rotation in an alkyl chain (P. J. Flory, "Statistical Mechanics of Chain Molecules", Interscience, New York, N.Y., 1969). (ii) The cohesive energy of organic fluids is roughly $U_0 \sim -N(V_0/V)E_0$, N = number of molecules, V = volume, $E_0 \sim 20$ kT (see, e.g., A. Wulf, *J. Chem. Phys.*, **64**, 104 (1976)). Thus, $U_0'/N \sim -(V_0/V)E_0 N/V \sim -E_0/v$, $v = V/N$.
- (27) The pair excluded volume for long rods (of length and diameter l , d) which make an angle γ with one another is $2l^2 d \sin \gamma$. The general problem for arbitrary rods was solved by Onsager (L. Onsager, *Ann. N.Y. Acad. Sci.*, **51**, 627 (1949)).
- (28) Condition 70 for rods can be written $M_0 \bar{v}/v_0 \sim N\bar{v}/V_0 \sim d/l$, and may be satisfied before the Onsager orientational transition takes place at $N\bar{v}/V_0 \sim 4d/l$ (ref 27).

Effect of Organic Additives on Micellar Systems Studied by Positron Annihilation Techniques¹

Yan-ching Jean and Hans J. Ache*

Department of Chemistry, Virginia Polytechnic Institute and State University, Blacksburg, Virginia 24061 (Received October 26, 1977)

Publication costs assisted by the Petroleum Research Fund

The rate constants for the reactions of positronium with nitrobenzene and cupric chloride in various aqueous micellar systems, such as sodium dodecylsulfate, hexadecyltrimethylammonium bromide, sodium octylsulfonate, hexadecylpyridinium chloride, and Tergitol-NPX, were measured in the presence of organic additives, such as benzene, benzyl alcohol, *n*-hexane, and 1-hexanol. The results show that the positronium reactivity toward nitrobenzene or cupric chloride substantially increases, when benzene or benzyl alcohol are added to sodium dodecylsulfate, hexadecyltrimethylammonium bromide, and hexadecylpyridinium chloride solutions, whereas only a slight increase was observed in Tergitol-NPX and no increase in sodium octylsulfonate solutions. In the former systems the rate constants are generally higher in the presence of benzene or benzyl alcohol than in aqueous solutions of nitrobenzene or cupric chloride and approach in the case of nitrobenzene values obtained for positronium reactions with nitrobenzene in benzene solution, whereas *n*-hexane or 1-hexanol generally exhibit only a small effect. A possible explanation for the observed behavior may be that the aromatic additives become incorporated into the micelle, possibly close to the micelle-water interface where they form clusters or aggregates in which the nitrobenzene probe molecule resides. In this benzene-like microenvironment the nitrobenzene molecule exhibits the same reactivity toward positronium as in benzene solutions. By the same token in the case of *n*-hexane or 1-hexanol additives, the corresponding rates slightly decrease with additive concentration and approach rate constants observed in a *n*-hexane-like environment. It appears that the positron annihilation technique can provide a sensitive method of studying the microenvironment of probe molecules in micellar systems.

Introduction

An important aspect in the evaluation of the physical and structural properties of micelles is the study of the location, disposition, and orientation of solubilized species in the micelle.²⁻⁶

Several techniques such as ESR, NMR, fluorescence probes, and other spectroscopic techniques have been employed to define the location of the solubilize in the micelle. An important result of these investigations was that the solubilize is relatively mobile, rather than being held at a given position in a tight configuration. It appears that numerous parameters influence the solubilization process and the micellar interior can neither be considered completely hydrocarbon-like nor do the properties of the region near the micellar surface parallel those of bulk water. This situation seems to be even more complex in reacting systems, where the environment of initial, transition, and final states of the reactants in the micelle may differ.

In a previous paper⁷ we have reported on the results of a study in which the reactions of positronium with probe molecules such as nitrobenzene in micellar systems were investigated as a new tool for the determination of the location of the probe in the micelle.

This new method is based on the fact that the rate constants for the reaction of the positronium⁸ (Ps), which is the bound state of an electron and a positron, with a probe molecule is a function of the environment in which it occurs.^{9,10} Thus the nature of the microenvironment in which the probe molecule is located when it reacts with the Ps atom can be determined by comparing the observed rate constants in the micellar solutions with the rate constants obtained in standard solutions. As a result of these experiments we suggested that the nitrobenzene probe is in most of these micellar system located close to the surface or in the Stern layer.⁷

In the present study we have extended the application of the positron annihilation technique to the investigation

of the physical and structural changes which micelles undergo upon addition of solutes, in as much as they might affect the physical and chemical properties of solubilized species, such as the location of the probe molecules in the micelle, and the permeability of the micelle.^{2-6,11}

For this purpose a series of experiments were carried out in which the rate constants for the reactions between Ps and nitrobenzene or Cu²⁺ ions in various micellar systems, such as sodium dodecylsulfate, hexadecylpyridinium chloride, hexadecyltrimethylammonium bromide, sodium octylsulfonate, and Tergitol-NPX were determined in the presence of several organic additives, such as benzyl alcohol, benzene, *n*-hexane, and 1-hexanol.

Experimental Section

(A) *Purity of Compounds.* Sodium dodecylsulfate (NaLS), obtained from Aldrich Co., was recrystallized in 95% ethanol and dehydrated in a desiccator (with P₂O₅) under vacuum. The purification process was repeated until subsequent melting point measurements agreed with literature values within ± 1.0 °C. Hexadecyltrimethylammonium bromide (CTAB) and hexadecylpyridinium chloride (CPyCl) were obtained from Pfaltz-Bauer, Inc. and purified in a similar way by carrying out the recrystallization in methanol. Sodium octylsulfonate (NaOSO) was obtained from Pfaltz-Bauer Inc. and was purified in the same way as NaLS. The source of Tergitol-NPX was Union Carbide Co. All these latter compounds were of highest purity available (>99%) and were dehydrated by the addition of molecular sieves to the liquid compound. The water used in this investigation was demineralized and triple distilled with a purity better than 99.9%.

(B) *Positron Lifetime Measurements and Preparation of the Sample.* Positron lifetime measurements were carried out by the usual delayed coincidence method as previously described.¹² The resolution of the system, as measured by the fwhm of the prompt coincidence spectrum of a ⁶⁰Co source without changing the 1.27- and 0.511-MeV bias, was found to be less than 0.36 ns fwhm. Specially designed cylindrical sample vials (Pyrex glass 100 mm long and 10 mm i.d.) were filled with about 2 mL of the appropriate solution. The positron sources consisted of 3~5 mCi ²²Na diffused into a thin foil of soda lime glass.

The relative amount of positron annihilation occurring in the glass was found to be less than 2%, for which corrections were made. The radioactive glass sources were suspended in the center of the ampoule and all solutions were carefully degassed by freeze-thaw techniques to remove oxygen. The vials were subsequently sealed off and the measurements carried out at 22 °C.

Results and Discussion

(1) *General Method of Data Analysis.* The general method of the data analysis in micellar systems containing a probe molecule which is highly reactive toward Ps has been discussed in great detail in the previous paper⁷ to which reference is made. In analogy to the data analysis described in this reference it can be shown that λ_2 , which is the slope of the long-lived component in the positron lifetime spectra, can be correlated to the pertinent rate constants for the reaction of the Ps with the various components of such a micellar system and their respective concentration by the following equation:

$$\lambda_2 = K_{\text{mic}(\text{H}_2\text{O})} \{M_{(\text{H}_2\text{O})}\} + K_{\text{mic}}^A \{A_m\} + K_{\text{H}_2\text{O}}^A \{A_{(\text{H}_2\text{O})}\} + K_{\text{mic}} \{S_m\} + K_{\text{obsd}}^0 \{S_0\} \quad (1)$$

where $K_{\text{mic}(\text{H}_2\text{O})}$ is the observed rate constants for the

reaction of Ps with the micelle in water, which was found (in separate experiments) to be less than $10^7 \text{ M}^{-1} \text{ s}^{-1}$. K_{mic}^A and $K_{\text{H}_2\text{O}}^A$ are the observed rate constants for the reaction between Ps and the additive (A) in the micelle and in the aqueous phase, respectively, and are for the systems chosen in this study of the order of 10^7 to $10^8 \text{ M}^{-1} \text{ s}^{-1}$. K_{mic} and K_{obsd}^0 are the observed rate constants for the reaction of Ps with the probe molecules (nitrobenzene or Cu²⁺) in the micellar or aqueous phase, respectively, they were found to be $>10^9 \text{ M}^{-1} \text{ s}^{-1}$. $\{M\}$, $\{A\}$, and $\{S\}$ are the corresponding concentrations of the micelle, additive, and probe. Note that $\{S_m\} + \{S_0\}$ is the total concentration of probe molecules $\{S_T\}$. The subscript m refers to the micellar phase of the micellar solution, while the subscript zero refers to the aqueous phase. In the absence of additives eq 1 can be simplified to

$$\lambda'_2 = K'_{\text{mic}(\text{H}_2\text{O})} \{M'_{(\text{H}_2\text{O})}\} + K'_{\text{mic}} \{S'_m\} + K'_{\text{obsd}}^0 \{S'_0\} \quad (2)$$

The first term in eq 1 and 2 can be obtained from the measurement of λ_2 without probe molecules present, i.e., $\{S_m\} + \{S_0\} = 0$ or $\{S'_m\} + \{S'_0\} = 0$:

$$\lambda_2^0 = K_{\text{mic}(\text{H}_2\text{O})} \{M_{(\text{H}_2\text{O})}\} + K_{\text{mic}}^A \{A_m\} + K_{\text{H}_2\text{O}}^A \{A_{(\text{H}_2\text{O})}\} \quad (3)$$

$$\lambda'_2{}^0 = K'_{\text{mic}(\text{H}_2\text{O})} \{M'_{(\text{H}_2\text{O})}\} \quad (4)$$

By substituting eq 3 and 4 into eq 1 and 2, respectively one obtains

$$\lambda_2 - \lambda_2^0 = K_{\text{mic}} \{S_m\} + K_{\text{obsd}} \{S_0\} \quad (5)$$

$$\lambda'_2 - \lambda'_2{}^0 = K'_{\text{mic}} \{S'_m\} + K'_{\text{obsd}} \{S'_0\} \quad (6)$$

At high surfactant concentration one can safely assume that a probe molecule such as nitrobenzene is completely located in the micelle, therefore $\{S_0\}$ and $\{S'_0\}$ will be zero.

Thus from the experimentally observed positronium reaction rates λ_2 , λ_2^0 , λ'_2 , and $\lambda'_2{}^0$, the ratio $K_{\text{mic}}/K'_{\text{mic}}$ can be directly determined:

$$K_{\text{mic}}/K'_{\text{mic}} = (\lambda_2 - \lambda_2^0)/(\lambda'_2 - \lambda'_2{}^0) \quad (7)$$

It represents the relative changes of the rate constant for the reaction between Ps and probe molecule due to the presence of the additive.

In the case of Cu²⁺ ions which are insoluble in the hydrophobic core of the micelle but may be partially adsorbed on the surface of some of the micelles studied no such simplification can be made; thus

$$\frac{\lambda_2 - \lambda_2^0}{\lambda'_2 - \lambda'_2{}^0} = \frac{K_{\text{mic}} \{S_m\} + K_{\text{obsd}} \{S_0\}}{K'_{\text{mic}} \{S'_m\} + K'_{\text{obsd}}^0 \{S'_0\}} \quad (8)$$

Or if one defines

$$K_{\text{obsd}} = (\lambda_2 - \lambda_2^0)/\{S_T\}$$

and

$$K'_{\text{obsd}} = (\lambda'_2 - \lambda'_2{}^0)/\{S_T\}$$

then

$$\frac{K_{\text{obsd}}}{K'_{\text{obsd}}} = \frac{K_{\text{mic}} + (K_{\text{obsd}} - K_{\text{mic}})(\{S_0\}/\{S_T\})}{K'_{\text{mic}} + (K'_{\text{obsd}} - K'_{\text{mic}})(\{S'_0\}/\{S_T\})} \quad (9)$$

(2) *The Effect of Additives on the Positron Annihilation Process in Micellar Systems.* In the first series of experiments the effect of additives, such as benzyl alcohol, benzene, 1-hexanol, and *n*-hexane on the positron lifetime spectra in aqueous micellar systems, such as NaLS, CTAB, CPyCl, NaOSO, and Tergitol-NPX was studied.

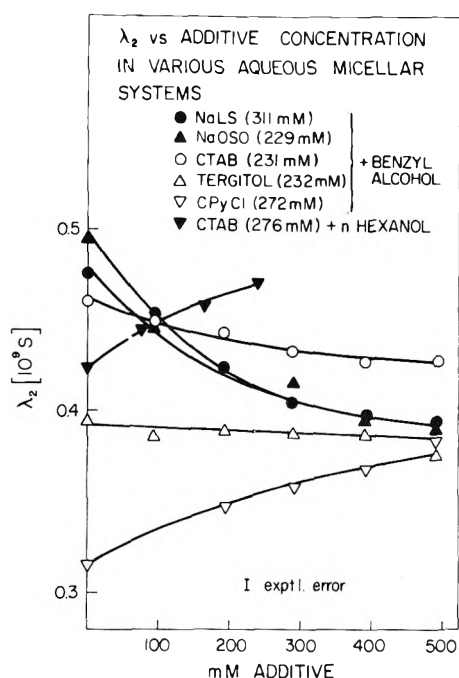


Figure 1. λ_2 vs. additive concentration in various aqueous micellar systems at room temperature.

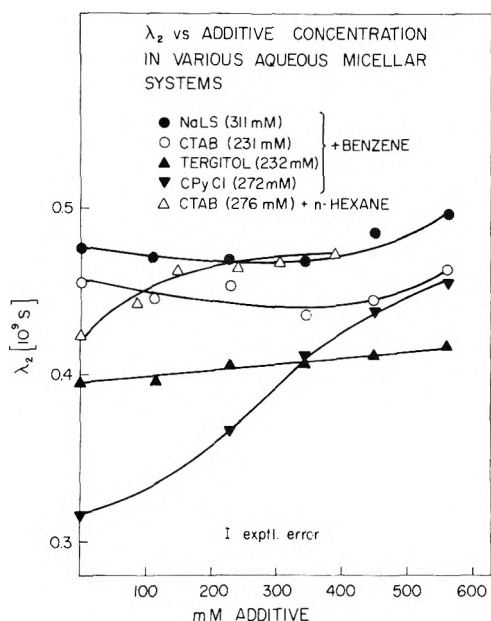


Figure 2. λ_2 vs. additive concentration in various aqueous micellar systems at room temperature.

While the effect of additives on these micellar systems on the Ps formation probability as expressed by the intensity, I_2 , of the long-lived component in the positron lifetime is generally very small ($\pm 2\%$ absolute), over the whole range, i.e., up to 600 mM of additives, the corresponding positron decay rates, λ_2 , show more drastic changes as seen in Figures 1 and 2, where λ_2 for the various systems is plotted as a function of additive concentration.

However, no general trends emerge from these data; while in some systems benzyl alcohol additives reduce λ_2 , others enhance λ_2 . With benzene a more consistent trend, i.e., a slight enhancement of λ_2 with increasing additive concentration is observed.

The cause for this behavior is probably due to changes in micellar shape or size upon addition of these compounds¹¹ and will be discussed in context with the results obtained in the presence of probe molecules, see section 3 and 4.

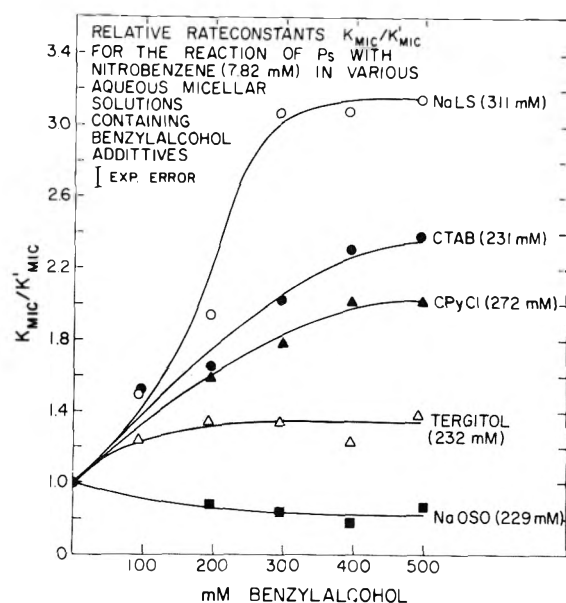


Figure 3. K_{mic}/K'_{mic} (relative rate constants for reaction of Ps with nitrobenzene in micellar solutions with and without additives present) vs. concentration (mM) of benzyl alcohol additives.

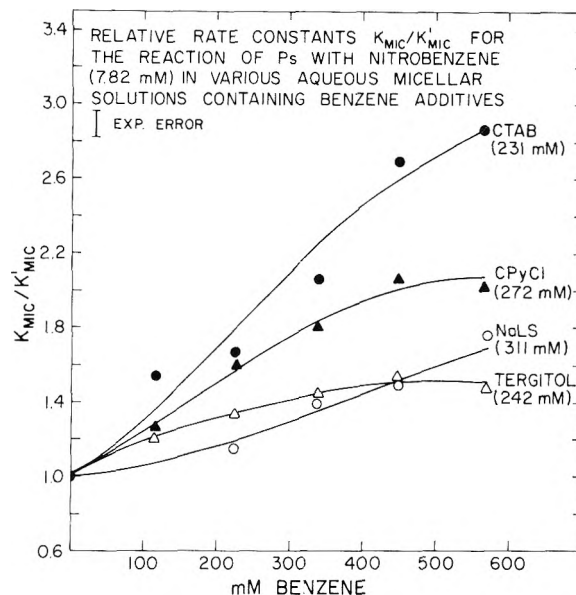


Figure 4. K_{mic}/K'_{mic} (relative rate constants for reaction of Ps with nitrobenzene in micellar solutions with and without additives present) vs. concentration (mM) of benzene additives.

(3) *The Effect of Additives on the Positron Annihilation Process in Micellar Systems in the Presence of Nitrobenzene as a Probe Molecule.* As discussed in a previous paper⁷ at high surfactant concentration one can assume that the relatively small amount of nitrobenzene molecules, less than 10 mM, is completely located in the micellar phase. Thus $[S_0]$ and $[S'_0]$ will be equal to zero, and the ratio of K_{mic}/K'_{mic} can be obtained from eq 7. It represents the relative changes of the Ps reaction rate constant caused by the presence of the additives. These K_{mic}/K'_{mic} ratios are plotted as a function of additive concentration in Figures 3–5 for the various micellar systems.

The maximal concentrations of additives used in these studies and the absolute rate constants observed under these conditions are listed in Table I.

Information about the environment of the probe molecules in the micellar systems can be obtained by comparing the observed rate constants for positron annihilation in the micellar systems with those obtained in the aqueous

TABLE I: Rate Constants for Ps-Nitrobenzene Interactions in Various Aqueous Micellar Solutions with Different Additives

Nitrobenzene, mM	Surfactants	Additive	K_{obsd} at 22 °C ^a ($10^{10} \text{ M}^{-1} \text{ s}^{-1}$)
7.82	0	0	1.02
7.82	115 mM NaLS	0	0.83
7.82	115 mM NaLS	483 mM benzyl alcohol	1.52
7.82	311 mM NaLS	0	0.45
7.82	311 mM NaLS	483 mM benzyl alcohol	1.42
7.82	311 mM NaLS	563 mM benzene	0.86
7.82	243 mM CTAB	0	0.57
7.82	243 mM CTAB	483 mM benzyl alcohol	1.37
7.82	243 mM CTAB	563 mM benzene	1.76
9.33	276 mM CTAB	0	0.53
9.33	276 mM CTAB	239 mM 1-hexanol	0.51
9.33	276 mM CTAB	383 mM <i>n</i> -hexane	0.39
7.82	272 mM CPyCl	0	0.35
7.82	272 mM CPyCl	483 mM benzyl alcohol	1.20
7.82	272 mM CPyCl	563 mM benzene	0.76
7.82	229 mM NaOSO	0	0.59
7.82	229 mM NaOSO	483 mM benzyl alcohol	0.51
7.82	232 mM Tergitol	0	0.50
7.82	232 mM Tergitol	483 mM benzyl alcohol	0.70
7.82	232 mM Tergitol	563 mM benzene	0.88

^a Experimental error is $\pm 0.04 \times 10^{10} \text{ M}^{-1} \text{ s}^{-1}$.TABLE II: Rate Constants for the Ps-Cu²⁺ Interaction in Various Aqueous Micellar Solutions with Different Additives Present

CuCl ₂ , mM	Surfactant	Additive	K_{obsd} at 22 °C ^a ($10^{10} \text{ M}^{-1} \text{ s}^{-1}$)
25.07	0	0	0.23
25.07	295 mM CTAB	0	0.08
25.07	295 mM CTAB	483 mM benzyl alcohol	0.22
25.07	295 mM CTAB	563 mM benzene	0.18
25.07	272 mM CPyCl	0	0.05
25.07	272 mM CPyCl	483 mM benzyl alcohol	0.15
25.07	272 mM CPyCl	563 mM benzene	0.13
25.07	229 mM NaOSO	0	0.15
25.07	229 mM NaOSO	483 mM benzyl alcohol	0.15
20.05	232 mM Tergitol	0	0.22
20.05	232 mM Tergitol	483 mM benzyl alcohol	0.19
20.05	232 mM Tergitol	563 mM benzene	0.20

^a Experimental error is $\pm 0.02 \times 10^{10} \text{ M}^{-1} \text{ s}^{-1}$.

phase or in a hydrocarbon system having a hydrocarbon chain length similar to those of the surfactants forming the micelles.

On the basis of this comparison we previously reached the conclusion⁷ that the nitrobenzene probe molecule is located in most of the micellar systems under investigation in the Stern layer, with the exception of the NaOSO solutions, where the nitrobenzene may be located in a hydrocarbon-like environment.

From Figure 3, where the relative changes of the rate constants, $K_{\text{mic}}/K'_{\text{mic}}$, are plotted as a function of benzyl alcohol concentration, it is obvious that the addition of benzyl alcohol causes an enhancement of the Ps reactivity with nitrobenzene in NaLS, CTAB, CPyCl, and to a lesser degree in Tergitol while no effect or a slight decrease is seen in the case of NaOSO. Similar trends, although definitely less pronounced in the case of NaLS, can be recognized if benzene is the additive as shown in Figure 4.

A completely different behavior is observed for 1-hexanol and *n*-hexane additives, as demonstrated for the CTAB system in Figure 5, where the changes of $K_{\text{mic}}/K'_{\text{mic}}$ are displayed as a function of the nature and concentration of the various additives.

Since, as discussed above,⁹⁻¹⁰ the rate constants for Ps reactions with probe molecules such as nitrobenzene are sensitive to the nature of the environment in which they occur it seems logical to relate these trends to changes of

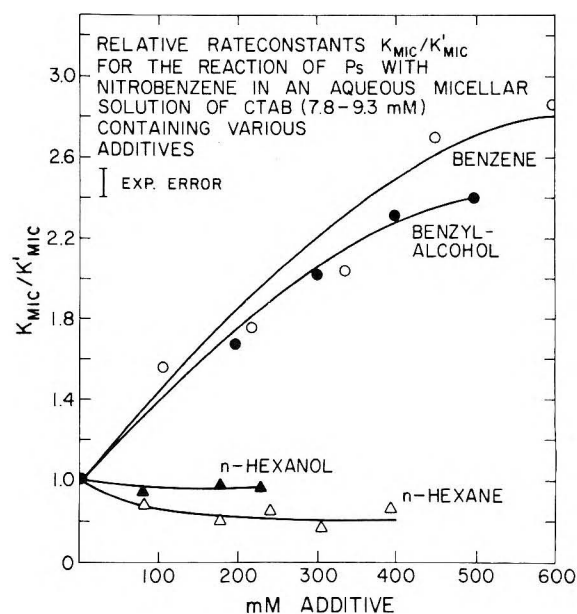


Figure 5. Relative rate constants for the reaction of Ps with nitrobenzene in CTAB solutions (243–276 mM) as a function of additive concentration.

the environment of the nitrobenzene probe in the micelle.

By comparing the absolute rate constants K_{obsd} at high additive concentrations as listed in Table I with those

obtained for the nitrobenzene probe molecule in pure water, benzyl alcohol, benzene, and other hydrocarbon solutions or mixtures of hydrocarbons, alcohols, and water, as listed in Table II, it becomes rather obvious that, e.g., the addition of benzene to CTAB results in absolute rate constants, K_{obsd} , which are definitely greater than those observed in the aqueous phase, or in homogeneous mixtures of the corresponding hydrocarbons with the same amount of benzene, and approach those observed in benzene solutions.

In other micellar systems such as NaLS, CPyCl, and Tergitol, the effect of benzene additives is less pronounced.

The implication of these results seems to be that the addition of benzene to the micellar systems, most obvious in the case of CTAB, provides an environment for the nitrobenzene probe molecules which is benzene-like. One can visualize that this is accomplished by benzene cluster formation and benzene gel formation within the micelle.¹¹ Evidence for such a benzene microenvironment in which solubilized species may reside has recently been obtained from optical spectra and the measurement of dielectric constants in aqueous NaLS systems to which benzene was added.¹³ The authors postulate that the solubilized benzene is concentrated primarily at the micelle water interface rather than in the hydrocarbon core.

A very similar behavior is observed for the Ps rate constants in micellar systems containing benzyl alcohol additives. In this case NaLS and CTAB show the most pronounced increase, with K_{obsd} values exceeding even those obtained for Ps nitrobenzene interaction in pure benzyl alcohol solutions, whereas on the other hand a slight decrease is observed in NaOSO solutions.

If the above assumption, namely, that additives such as benzene or benzyl alcohol are forming clusters at the micelle-water interface in which the probe molecule can be located is correct, then one would expect that the greatest effect on the Ps-nitrobenzene rate constants is seen in those cases where the nitrobenzene is initially, i.e., without additives present, near the micelle-water interface or in the Stern layer.

In our previous paper⁷ we have postulated this to be the case in the NaLS, CTAB, CPyCl, and Tergitol systems, whereas the indication was that nitrobenzene is located in the hydrocarbon-like layer of the NaOSO micelles. The results shown in Figures 3-5 and Tables I and II are consistent with the expected trend.

The fact that the rate constants, K_{obsd} , in the presence of benzyl alcohol exceed those observed in pure benzyl alcohol solution requires some additional discussion. The fact that K_{obsd} approaches values typically found in aromatic solvents might suggest that the benzyl alcohol molecules form aggregates in the micelles which show a particular arrangement, e.g., with the aromatic ring directed to the center of the cluster and the -OH group pointing outward. In such a case one could rationalize the similarity of the rate constants observed in micellar systems with benzyl alcohol additives and in (pure) benzene solutions.

Further substance to the postulate that these additives form clusters in or at the micelle surface is added by the fact that 1-hexanol and *n*-hexane additive in the CTAB system slightly decrease the Ps rate constants, again consistent with the hypothesis that in this case nitrobenzene is located in a 1-hexanol or *n*-hexane microenvironment, where the rate constants for Ps-nitrobenzene interactions, as shown in Table II, are considerably lower.

The above explanation postulates that the effect of the additive is a change of the environment of the probe

molecule, which subsequently affects the rate of the reaction between Ps and the nitrobenzene probe. This is in contrast to the previous interpretation of the effects of additives preferred by several authors where the increase of the reactivity of a probe molecule in a micelle in the presence of additives such as benzyl alcohol was interpreted in terms of an enhanced permeability of the micelle^{11b,i} allowing, e.g., a quencher molecule to approach the probe more freely. An unambiguous answer to this question is difficult to obtain. Studies of the microviscosity, e.g., of pyrene probes in NaLS with or without additives seemed to indicate very little change in the environment.^{11b} However, pyrene is supposedly located deeper in the core and its environment may therefore not be subjected to changes in the presence of such additives. It could very well be that the positron annihilation technique does not pick up differences in the permeability of micelles because of the intrinsic properties of the Ps atom, and recognizes only variations in the local environment of the probe molecule, while fluorescence techniques are affected by both factors.

(4) *The Effect of Additives on the Positron Annihilation Process in Micellar Systems in the Presence of Cu²⁺ Ions.* As discussed in the previous paper,⁷ Cu²⁺ ions are adsorbed on the surface of ionic micelles due to an electrostatic attraction between surface charge and Cu²⁺ ions or counterion charge and Cu²⁺ ions. As a result of this adsorption process the rate constants between Cu²⁺ ions and Ps dropped considerably below the values observed in aqueous solutions of Cu²⁺. The reason for the reduced reactivity of Ps toward adsorbed Cu²⁺ may be seen in the fact that the Cu²⁺ when adsorbed on the surface loses the character of the hydrated Cu²⁺ by partial bond formation, complexation, etc. with the surface molecules, and thus reacts at a different rate with Ps.

An indication how the surface of the micelles is changed in the presence of additives, such as benzyl alcohol or benzene, may therefore be obtained by comparing the rate constants for Ps interactions in micellar solution containing Cu²⁺ ions with or without the presence of these additives.

Since Cu²⁺ ions can be considered insoluble in the hydrophobic micellar phase, one can assume $[S_m]$ and $[S'_m]$ in eq 8 equal to zero, and one obtains for the ratio of the Ps reaction rate constants with or without additives present the following equation:

$$\frac{K_{\text{obsd}}^0}{K'_{\text{obsd}}^0} = \frac{\lambda_2 - \lambda_p}{\lambda'_2 - \lambda_p} \quad (10)$$

(K_{obsd}^0 and K'_{obsd}^0 are the Ps reaction rate constants for Cu²⁺ in the presence or absence of additives, respectively).

The ratio $K_{\text{obsd}}^0/K'_{\text{obsd}}^0$ which represents the change caused by the additives is plotted for various aqueous CuCl₂ micellar solutions in Figures 6 and 7, with the absolute values of K_{obsd} under the conditions listed in Table III.

The results show that both benzene and benzyl alcohol significantly increase the Ps reaction rates in micellar systems, such as CPyCl and CTAB, where previous results have shown a drastic drop in the Cu²⁺-Ps reaction rates when micelles are formed, while no such effect is observed in the case of Tergitol, which as a neutral micelle has shown no attraction for Cu²⁺ ions.

It seems that these results suggest that the addition of benzene or benzyl alcohol to the CPyCl or CTAB leads to drastic changes of the micelle structure in or close to the micellar-water interface, caused by the formation of benzene clusters etc. (see above) resulting in a release of Cu²⁺ otherwise adsorbed on the micellar surface.

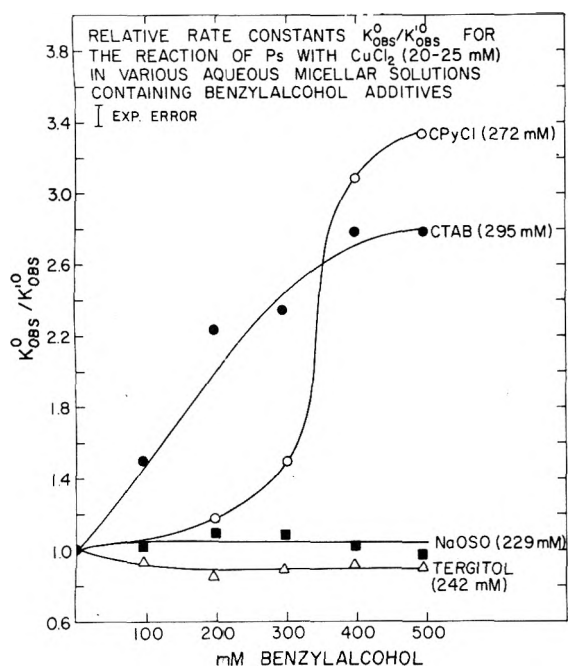


Figure 6. $K_{\text{obs}}^0/K_{\text{obs}}$ (relative rate constants for reaction of Ps with CuCl_2 in micellar solutions) vs. concentration (mM) of benzyl alcohol additives.

TABLE III: Rate Constants for Ps-Nitrobenzene Interactions in Various Solutions

Solutions	K_{obs}^0 ($10^{10} \text{ M}^{-1} \text{ s}^{-1}$)
Water	1.00
1-Pentanol	0.86
Benzyl alcohol	1.16
n-Hexane	0.30
n-Octane	0.69
n-Dodecane	1.28
n-Hexadecane	1.15
Benzene	2.55
Water + 386 mM benzyl alcohol	0.82
n-Dodecane + 242 mM benzyl alcohol	1.02
n-Dodecane + 563 mM benzene	1.06
n-Hexadecane + 563 mM benzene	1.00
n-Hexadecane + 239 mM hexanol	0.96
n-Hexadecane + 383 mM n-hexane	0.97

An interesting case is the NaOSO system. Prior experiments⁷ with this system containing Cu^{2+} ions have shown a clear drop of the rate constants for the reaction between Ps and Cu^{2+} upon micelle formation, which indicated extensive Cu^{2+} adsorption on the surface of this micelle. The present results as shown in Figure 6 provide no evidence for a release of Cu^{2+} from the surface in the presence of benzyl alcohol additives. We would like to interpret these results by assuming that if this micelle solubilizes benzyl alcohol at all, that it becomes incorporated not in form of clusters near the surface but more likely in a homogeneous form in the hydrocarbon-like core of the micelle consistent with the fact that the rate constant for the Ps-nitrobenzene interaction is not affected by the presence of additives either, as discussed in section 3.

Summary

The results of this study have shown that the positron annihilation technique is a sensitive tool for the investi-

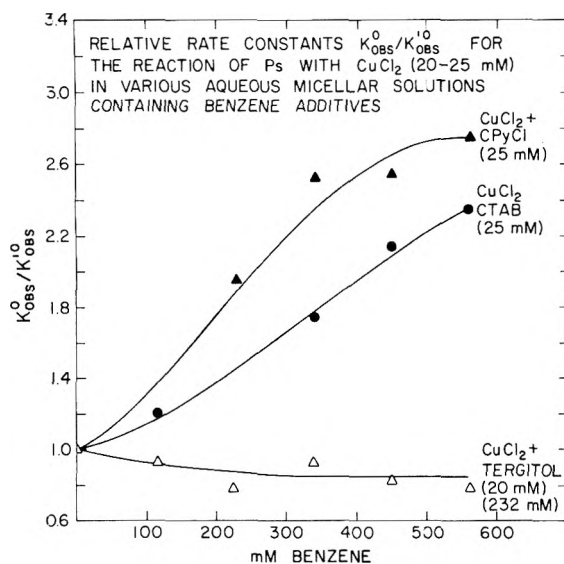


Figure 7. $K_{\text{obs}}^0/K_{\text{obs}}$ (relative rate constants for reaction of Ps with CuCl_2 in micellar solutions vs. concentration (mM) of benzene additives.

gations of changes introduced by the presence of additives in micellar systems.

It appears that additives such as benzyl alcohol, benzene, 1-hexanol, and n-hexane form clusters in most of the micellar systems studied in this research at or near the micellar-water interface also leading to changes in the micellar surface charge.

References and Notes

- (1) Work supported by the U.S. Energy Research and Development Administration. Acknowledgment is made to the Donors of the Petroleum Research Fund, administered by the American Chemical Society, for the partial support of this research.
- (2) J. K. Thomas, *Acc. Chem. Res.*, **10**, 133 (1977).
- (3) J. H. Fendler and E. J. Fendler, "Catalysis in Micellar and Macromolecular Systems", Academic Press, New York, N.Y., 1975.
- (4) E. J. Fendler and J. H. Fendler, *Adv. Phys. Org. Chem.*, **6**, 1472 (1970).
- (5) P. H. Elworthy, A. T. Florence, and C. B. MacFarlane, "Solubilization by Surface Active Agents", Chapman and Hall, London, 1968.
- (6) C. Tanford, "The Hydrophobic Effect", Wiley-Interscience, New York, N.Y., 1973.
- (7) Y. C. Jean and H. J. Ache, *J. Am. Chem. Soc.*, **99**, 7504 (1977).
- (8) For general references on positron annihilation, see (a) J. Green and J. Lee, "Positronium Chemistry", Academic Press, New York, N.Y., 1964; (b) V. I. Goldanskii, *At. Energy Rev.*, **6**, 3 (1968); (c) J. D. McGervey in "Positron Annihilation", A. T. Stewart and L. O. Roellig, Ed., Academic Press, New York, N.Y., 1967, p 143; (d) J. A. Merrigan, S. J. Tao, and J. H. Green, "Physical Methods of Chemistry", Vol. I, Part III, D. A. Weissberger and B. W. Rossiter, Ed., Wiley, New York, N.Y., 1972; (e) H. J. Ache, *Angew. Chem., Int. Ed. Engl.*, **11**, 179 (1972); (f) J. H. Green, *MTP Int. Rev. Sci.*, **8**, 251 (1972); (g) V. I. Goldanskii and V. G. Firsov, *Annu. Rev. Phys. Chem.*, **22**, 209 (1971).
- (9) W. J. Madia, A. L. Nichols, and H. J. Ache, *J. Am. Chem. Soc.*, **97**, 5041 (1975).
- (10) E. S. Hall and H. J. Ache, *Radiochem. Radioanal. Lett.*, **23**, 283 (1975).
- (11) For examples, see (a) M. F. Merson and A. Holtzen, *J. Phys. Chem.*, **71**, 3320 (1967); (b) R. L. Venable and R. V. Nauman, *ibid.*, **68**, 3498 (1964); (c) J. E. Gordon, J. C. Robertson, and R. L. Thorne, *ibid.*, **74**, 957 (1970); (d) J. W. Larsen and L. J. Magid, *Tetrahedron Lett.*, **29**, 2663 (1973); (e) J. J. Minch, M. Giaccio, and R. Wolff, *J. Am. Chem. Soc.*, **97**, 3766 (1975); (f) S. J. Rechfeld, *J. Phys. Chem.*, **74**, 117 (1970); (g) H. Griffith and A. S. Waggoner, *Acc. Chem. Res.*, **2**, 17 (1969); (h) M. Grätzel and J. K. Thomas, *J. Am. Chem. Soc.*, **95**, 6885 (1973); (i) P. P. Infelta, M. Grätzel, and J. K. Thomas, *J. Phys. Chem.*, **78**, 190 (1974); (j) P. Mukerjee, J. R. Cardinal, and N. R. Desai in "Micellization, Solubilization and Microemulsions", Vol. 1, K. L. Mittal, Ed., Plenum Press, New York, N.Y., 1977, pp 241-261; (k) M. Wong, M. Grätzel, and J. K. Thomas, *J. Am. Chem. Soc.*, **98**, 2391 (1976).
- (12) T. L. Williams and H. J. Ache, *J. Chem. Phys.*, **50**, 4493 (1969).
- (13) For further references see, e.g., ref 11j.

The Interaction of Rare Gas Atoms with Graphitized Carbon Black

William A. Steele[†]

School of Chemistry, The University, Bristol, England (Received August 9, 1977)

Publication costs assisted by the Petroleum Research Fund

Gas-solid virial coefficients are calculated for a summed (4-10) power law. This potential, which is derivable from a model that represents the total as a pairwise sum of gas atom-solid atom energies, is known to be a particularly apt representation of the rare gas-graphite basal plane interactions. After comparing the theoretical virial coefficients with those for other model gas-solid potentials, they are fitted to previously reported data for rare gases on graphitized carbon blacks. Over the available temperature range, the fit is excellent; in addition, values for the parameters of the pairwise potential are obtained which are in moderate agreement with estimates based on the Lorentz-Berthelot combining rules; deviations from the rules are similar to those observed for other mixed atom pairs.

Introduction

It has been known for some time that graphitized carbon black (gcb) is almost uniquely useful as an adsorbent in fundamental studies of physisorption.¹ Its utility derives primarily from the ease of preparing and maintaining this material with a high area surface composed almost entirely of basal planes. In addition, theoretical calculations of gas-solid interaction energies for these systems are facilitated by the fact that the solid is composed of one kind of atom, present in a crystal lattice of known spacing any symmetry. Undoubtedly the most straightforward test of a given model of the gas-solid interaction energy is based on a comparison between experimental Henry's constants (gas-solid virial coefficients) and theory.^{2,3} Specifically, the virial coefficient B_{AS} is related to the moles adsorbed N_a by

$$\lim_{P \rightarrow 0} (P/N_a) = (kT/B_{AS}) \quad (1.1)$$

In addition, B_{AS} is related to the gas-solid potential function $u_s(\mathbf{r})$ by

$$B_{AS} = \int \{\exp[u_s(\mathbf{r})/kT] - 1\} d\mathbf{r} \quad (1.2)$$

where \mathbf{r} denotes the position of a gas atom relative to the solid.

This approach to the characterization of gas solid interactions was developed and exploited primarily by Halsey and co-workers.⁴⁻⁷ As part of this endeavor,⁷ they reported careful measurements of B_{AS} for a number of rare gases over a graphitized carbon black generally described as P33 (2700⁰) (or P33, for convenience). Their data were then fitted to theoretical B_{AS} curves calculated using various inverse power law representations of $u_s(\mathbf{r})$; that is, the dependence of $u_s(\mathbf{r})$ upon τ , the two-dimensional position vector that specifies the position of a gas atom in the plane parallel to the surface, was neglected and the resulting potential, which depends only upon z , the perpendicular gas-solid separation, was written as

$$u_s(z) = \epsilon_{1s} c_{mn} \{ (s_0/z)^m - (s_0/z)^n \} \quad (1.3)$$

where

$$c_{mn} = \left(\frac{n}{m-n} \right) \left(\frac{n}{m} \right)^{m/(n-m)} \quad (1.4)$$

Thus, ϵ_{1s} is the well depth of the potential, s_0 is the gas-

surface distance at which the energy passes through zero, and the indices m, n characterize the steepness of the potential.

In order to make reasonable choices for the indices in the power law potential of eq 1.3, one requires some kind of model. One of the most popular for nonconducting solids is to represent the total energy as a sum of pairwise interactions between the gas and the solid atoms:

$$u_s(\mathbf{r}) = \sum_i e_{gs}(\mathbf{r}_i) \quad (1.5)$$

As a first approximation, the Lennard-Jones (6-12) interaction law may be used for the pairwise energy $e_{gs}(\mathbf{r}_i)$:

$$e_{gs}(\mathbf{r}_i) = 4\epsilon_{gs} \{ (\sigma_{gs}/r_i)^{12} - (\sigma_{gs}/r_i)^6 \} \quad (1.6)$$

Although $u_s(\mathbf{r})$ is in general a rather complicated function of \mathbf{r} , there are several ways to generate simple approximations for this energy. If one replaced the sums in eq 1.5 by integrals over the volume of the solid, a (3-9) power law in z results; if one replaces the sums by an integral over the surface plane and neglects the interactions with more distant planes of atoms in the solid, a (4-10) potential is obtained. Sams et al.⁷ compared their data with virial coefficients calculated for both of these functions as well as the (3-12) and the rather unrealistic (3- ∞) law, which will not be mentioned further here.

Following the original investigation, Morrison and Ross⁸ have reanalyzed the data using a harmonic approximation to $u_s(z)$ and, most recently, Putnam and Fort⁹ have reported additional low temperature measurements of B_{AS} for Kr on gcb and have carried out a careful reanalysis of the data for this system using a number of (4- m) and (3- m) power law potentials. Putnam and Fort also noted that estimates of the τ dependent part of $u_s(\mathbf{r})$ based on a Fourier representation of the pairwise sum were quite small for reasonable estimates of σ_{gs} and ϵ_{gs} ,¹⁰ and thus, that a calculation of B_{AS} made using the τ averaged potential $w_0(z)$ should be quite accurate. Of the various power laws considered for $w_0(z)$, they concluded that a (3- m) potential gave the best fit to the Kr data, with $m = 12$ being marginally better than $m = 9$. Oddly, they did not consider the τ averaged potential obtained from the model of additive energies and a (6-12) pairwise interaction. This function can be written

$$w_0(z) = \epsilon_{1s} \sum_{j=0}^{\infty} \left[\frac{2}{3} \left(\frac{\sigma_{gs}}{z + jd} \right)^{10} - \frac{5}{3} \left(\frac{\sigma_{gs}}{z + jd} \right)^4 \right] \quad (1.7)$$

where d is the distance between basal planes in gcb and

[†]Unilever Visiting Professor. Permanent Address: Department of Chemistry, The Pennsylvania State University, University Park, Pa. 16802.

the well-depth ϵ_{1s} is related to the pairwise well depth by

$$\epsilon_{gs} = \frac{5a_c}{6\pi\sigma_{gs}^2} \epsilon_{1s} \quad (1.8)$$

where a_c is the area per carbon atom in the basal plane (2.62 \AA^2). Values of the interplanar distance d in graphite are appreciably dependent upon temperature and upon the state of crystalline perfection of the sample; we will take $d = 3.37 \text{ \AA}$, but the uncertainty in this number is at least 1%.

The work reported here should be considered as an extension of the study of Putnam and Fort wherein the model leading to eq 1.7 is tested against the available virial coefficient data for rare gases on gcb. The data are most extensive for Ar and Kr, but some information at least is available for all rare gases from He to Xe. We will see that the summed (4-10) law (denoted by $\Sigma(4-10)$) fits the data as precisely as the (3-12) law across the experimental temperature ranges (accurate data at higher temperatures are needed if one is to distinguish between the two representations) and that the fit of experiment to theory leads to values of ϵ_{gs} and σ_{gs} for the rare gas-carbon atom pairs which are in reasonable agreement with other estimates of these parameters. These results thus give strong support to the pairwise summation model (as well as defining best values of the parameters to use in it). In addition to being of interest in connection with the general theory of gas-solid interactions,¹¹ the results should be helpful in developing interpretations of the interesting and complex phase behavior found in high-density monolayers of these gases on gcb.¹²

Theory and Experiment

For an (m, n) power law potential, the reduced virial coefficient $B_{AS}^* = B_{AS}/A\sigma_0$, where A is the area of the solid, can be expressed as a power series in $T^* = kT/\epsilon_{1s}$;⁶ alternatively, a simple Simpson's rule integration yields these quantities for any z -dependent function. For potentials such as the $\Sigma(4-10)$ defined in eq 1.7, it is convenient to define $B_{AS}^* = B_{AS}/A\sigma_{gs}$ and also, $d^* = d/\sigma_{gs}$. Values of B_{AS}^* were calculated for three choices of d^* using Simpson's rule integration; the results are tabulated in the Appendix (Supplementary material; see paragraph at end of text regarding supplementary material) together with a retabulation of the virial coefficients for the (4-10) potential (which were found to be incorrectly given in an earlier listing by Yaris and Sams⁶).

It should be noted that the awkward infinite sums in the $\Sigma(4-10)$ equation can be approximated to good accuracy by closed form expressions. Specifically, the Euler-MacLaurin theorem gives

$$\sum_{j=1}^{\infty} \frac{1}{(z^* + jd^*)^4} = \frac{1}{2(z^* + d^*)^4} + \frac{1}{3d^*(z^* + d^*)^3} + \frac{d^*}{3(z^* + d^*)^5} - \frac{d^{*3}}{6(z^* + d^*)^7} + \dots \quad (2.1)$$

If this series is truncated omitting the last term in eq 2.1, one has

$$\sum_{j=0}^{\infty} \frac{1}{(z^* + jd^*)^4} = \frac{1}{z^{*4}} + \frac{2z^{*2} + 7zd^* + 7d^{*2}}{6d^*(z^* + d^*)^5} \quad (2.2)$$

This expression is accurate to better than 0.3% over the important range of z^* and d^* ; inclusion of the last term in eq 2.1 improves accuracy by nearly another factor of 10. The Euler-MacLaurin theorem can also be used to give the contribution of higher terms to the sum of inverse tenth powers. However, these terms are so small compared

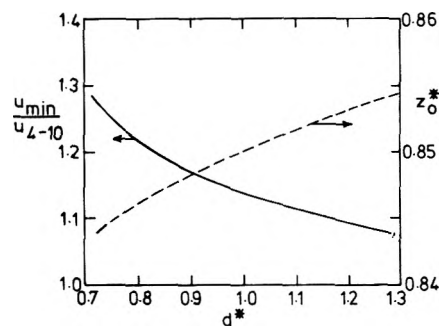


Figure 1. Well depths and distances of zero energy for the $\Sigma(4-10)$ potential are shown as a function of the reduced interplanar distance $d^* = d/\sigma_{gs}$. u_{4-10} is the well depth for the unsummed 4-10 potential; the distance z_0^* is in reduced units obtained by dividing z_0 by σ_{gs} .

TABLE I: Constants in Eq 2.4

Potential	a	b
(3-9)	0.92207	0.8194
(3-12)	0.92058	0.9699
(4-10)	0.92544	1.0919
$\Sigma(4-10)$		
$d^* = 0.8$	1.14718	1.3511
$d^* = 1.0$	1.06366	1.3065
$d^* = 1.2$	1.01657	1.2819
Summed (6-12)		
$d^* = 0.8$	1.14726	1.3513
$d^* = 1.0$	1.06550	1.3121
$d^* = 1.2$	1.03208	1.3380

to the leading term that a simpler approximation can be used:

$$\sum_{j=0}^{\infty} \frac{1}{(z^* + jd^*)^{10}} = \frac{1}{z^{*10}} + \frac{1}{9d^*(z^* + 0.72d^*)^9} \quad (2.3)$$

Of course, the inclusion of the interaction with non-surface planes gives rise to a well depth u_{\min}/ϵ_{1s} and a distance z_0 of zero energy which depend upon the parameter d^* . Figure 1 shows the variation in well depth with d^* relative to the (4-10) value (i.e., relative to the value for $d^* = \infty$). Also shown is the variation in $z_0^* = z_0/\sigma_{gs}$ (limiting value at large $d^* = 0.8584$). These changes obviously affect the calculated B_{AS}^* at a given reduced temperature T^* . In addition, the shapes of the energy vs. distance curves for the $\Sigma(4-10)$ potentials differ from the (m, n) functions, which leads to subtle differences in the shapes of the curves of B_{AS}^* vs. T^* . In order to exhibit these differences most clearly, we take advantage of the fact that plots of $\ln B_{AS}^*$ vs. $1/T^*$ are almost linear at low T^* .⁵ Thus, we define a difference function Δ which reflects deviations from this linearity:

$$\Delta = (a/T^*) - b - \ln B_{AS}^* \quad (2.4)$$

The constants a and b for the various potentials are obtained by defining Δ to be zero at $1/T^* = 7$ and 10. Values calculated in this way are given in Table I and plots of these parameters as functions of d^* are shown in Figure 2 for the $\Sigma(4-10)$ potentials. The values of Δ calculated from eq 2.4 for these and several other potential functions are plotted in Figure 3.

A glance at Figure 3 shows immediately that high temperature data are a necessity if one is to use the quality of fit between theory and experiment to distinguish between models. For example, earlier analyses of the Kr-gcb data show that the experimental temperature range corresponds to $1/T^* > 4.5$. In this region a fit of data to theory enables one to distinguish between the (4-10) and the other functions, if the data are good enough. Indeed, Putnam and Fort conclude that the $(3-m)$ functions give

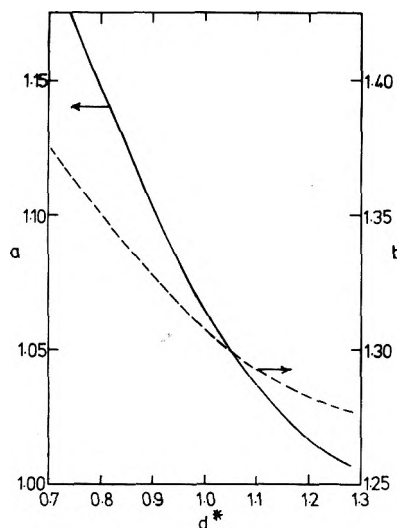


Figure 2. Plots of the slopes a and intercepts b defined by fitting $\ln B_{AS}^*$ to a linear function of $1/T^*$.

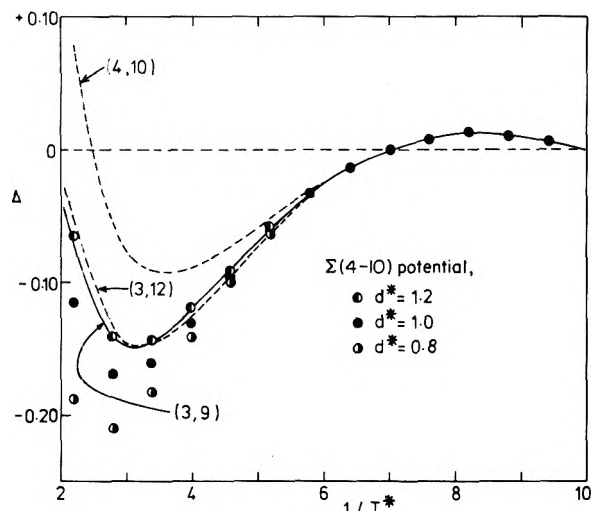


Figure 3. Deviations of the calculated $\ln B_{AS}^*$ from linearity in $1/T^*$ are shown here for several potential functions.

a somewhat better fit to the data than the (4-10), and that variations in m from 9 to 16 with $n = 3$ give a marginally best fit at $m \approx 12$. The preference for a (3- m) potential is surprising at first because the theoretical justification for this model is weak; however, one of the most interesting features of Figure 3 is the indication that the deviations of $\ln B_{AS}^*$ vs. $1/T^*$ from linearity are nearly the same for the $\Sigma(4-10)$ models as for the (3-12) potential, at least for $1/T^* > 4.5$. Thus, one concludes that the $\Sigma(4-10)$ potentials should fit the Kr-gcb data at least as well as the (3-12). It is also clear that the task of refitting the data for Ar, Kr, and Xe on gcb to the $\Sigma(4-10)$ model will be greatly facilitated by this similarity in shape. The simplest method of proceeding is to write

$$\frac{\epsilon_{1s}(\Sigma(4-10))}{\epsilon_{1s}(3-12)} = \frac{a(3-12)}{a(\Sigma(4-10))} \quad (2.5)$$

$$\frac{\sigma_{gs}(\Sigma(4-10))}{s_0(3-12)} = \exp[b(\Sigma(4-10)) - b(3-12)] \quad (2.6)$$

An iterative technique was used to calculate constants for the $\Sigma(4-10)$ potential from the published values for $\epsilon_{1s}(3-12)$ and $s_0(3-12)$. Trial values of $a\{\Sigma(4-10)\}$ and $b\{\Sigma(4-10)\}$ were selected using a reasonable guess for $d^* = d/\sigma_{gs}$. An experimental value of $\sigma_{gs}\{\Sigma(4-10)\}$ was then calculated from eq 2.6; this result was then used to obtain

TABLE II: Well Depths and Size Parameters from the Fit of Data for Rare Gas-gcb Systems to the $\Sigma(4-10)$ Potential Function^a

Gas	ϵ_{1s}/k , K	Experiment		Lorentz-Berthelot	
		σ_{gs} , Å	ϵ_{gs}/k , K	$^{1/2}(\sigma_{gg} + \sigma_{ss})$, Å	$(\epsilon_{gg}\epsilon_{ss})^{1/2}$
He	200-210	2.98	15	2.95	0.87
Ne	348	2.94	26	3.08	0.83
(uncor- rected)	340	3.04	25		
Ar	959	3.38	58	3.40	1.00
	(968)	(3.21)	(65)		
Kr	1255	3.42	75	3.47	1.12
	(1271)	(3.25)	(84)		
Xe	1608	3.78	94	3.66	1.18

^a Values shown in parentheses correspond to $A_{P33} = 12.0$ m²/g; with the exception of helium, other values correspond to $A_{P33} = 11.5$ m²/g.

an improved value of d^* . Two repetitions of this procedure were generally adequate to give convergence to a fixed d^* . In this way, constants for the $\Sigma(4-10)$ potential for the Kr-gcb system were calculated from the values listed by Putnam and Fort for the (3-12) function. In addition, it should be possible to calculate the $\Sigma(4-10)$ parameters for Ne, Ar, and Xe on (P33) gcb by using the values of ϵ_{1s}/k and A_{S0} listed by Sams, Constabaris, and Halsey for the (3-12) law. Of course, this approach is feasible only if the specific area of the (P33) gcb is known. Putnam and Fort¹³ have given a detailed discussion of the results of various types of surface area determinations of gcb, and have argued that the measurement of lattice spacing in diffraction experiments can be combined with isotherm data to give more reliable estimates of surface area than by any other techniques. Since that time, new data have appeared that support this conclusion.¹⁴ Putnam and Fort estimated the surface area of their gcb to be 11.4 ± 0.4 m²/g. They also estimate that the ratio of the area of the P33 gcb used by Halsey and co-workers to that for their sample was 1.04, which gave $A_{P33} = 12.0 \pm 0.5$ m²/g. In order to have some indication of the sensitivity of the results to the value chosen for substrate area, the calculations presented in this paper were carried out for $A_{P33} = 11.5$ and 12.0 m²/g. Table II shows the well depths ϵ_{1s} and ϵ_{gs} and the distance parameters σ_{gs} calculated in this way for the $\Sigma(4-10)$ model. Values in parentheses are for $A_{P33} = 12.0$ m²/g.

The data for the Ne-gcb system were also fitted to the $\Sigma(4-10)$ model after correcting for quantum effects. The correction required is quite small and can thus be estimated from the harmonic oscillator approximation; one has

$$B_{AS}(\text{quantum}) = B_{AS}(\text{classical}) \left[1 - \frac{1}{24} \left(\frac{h\nu}{kT} \right)^2 \right] \quad (2.7)$$

where ν is the frequency of vibration perpendicular to the surface. Estimating ν to be 1.6×10^{12} s⁻¹, eq 2.7 can be rewritten as

$$B_{AS}(\text{classical}) = B_{AS}(\text{exptl}) / \left[1 - \left(\frac{15}{T} \right)^2 \right] \quad (2.8)$$

Table II shows well depths and distance parameters obtained by fitting both the raw Ne-gcb data and the quantum-corrected values to the $\Sigma(4-10)$ model.

Measurements of the Henry's law constants for ³He and ⁴He interacting with gcb at temperatures from 12 to 22 K have also been reported.¹⁵ These gas-solid systems are fully quantized and, consequently, the formal theory appears quite different from that presented here. In

TABLE III: Derivatives of the Potential at Its Minimum

Potential	u''	q
$\Sigma(4-10)$		
$d = 0.8$	46.2	28.6
$d = 1.0$	43.4	28.7
$d = 1.2$	42.1	28.8

TABLE IV: Calculated Vibrational Energies of Rare Gas-gcb Systems for $\nu = 0 \rightarrow \nu = 1$

Gas	$(\Delta\epsilon/k)_{\text{har}}, \text{K}$	$(\Delta\epsilon/k)_{\text{anh}}, \text{K}$	$(\Delta\epsilon/k)_{\text{tot}}, \text{K}$
Ne	64	-8.2	56
^{36}Ar	70	-3.4	67
Kr	52	-1.4	51
Xe	43	-0.8	42

particular, there is no simple way of determining σ_{gs} and ϵ_{gs} from a fit of such data to theory. Nevertheless, theoretical calculations of the Henry's law constants and of the heat of adsorption in the limit of zero coverage were carried out for a $\Sigma(4-10)$ potential using reasonable choices for σ_{gs} and ϵ_{gs} .¹⁵ Moderately good fits between theory and experiment were obtained, and it was estimated that best values for the parameters of the pairwise He-carbon potential required only a slight adjustment to the parameters actually used. The adjusted numbers are also listed in Table II.

Very recently, a study of the inelastic neutron scattering from ^{36}Ar adsorbed on gcb has been reported.¹⁶ This work lead to a number of interesting conclusions which include the finding that the vibrational motion of Ar perpendicular to the surface could be represented as that of an Einstein oscillator coupled to the substrate, with an energy $\Delta\epsilon$ for the $\nu = 0 \rightarrow \nu = 1$ transition of 5.6 Mev or 64 K. Of course, the potential functions determined here allow one to calculate this energy change for Ar as well as the other rare gases. If effects of anharmonicity are included, one can write

$$\left(\frac{\Delta\epsilon}{k}\right)_{0 \rightarrow 1} = \frac{h}{k} \left(\frac{\epsilon_{1s}}{\sigma_{\text{gs}}^2}\right) \left(\frac{u''}{m}\right) - \frac{h^2}{mk} \left(\frac{q}{\sigma_{\text{gs}}^2}\right) \quad (2.9)$$

where the factor q in the anharmonic term is defined as

$$q = \frac{1}{24} \left[5 \left(\frac{u'''}{u''} \right)^2 - 3 \frac{u^{iv}}{u''} \right] \quad (2.10)$$

The derivatives of the potential at its minimum are evaluated in reduced units, for convenience:

$$u^{(n)} = \left[\frac{d^n}{dz^{*n}} \left(\frac{u_s}{\epsilon_{1s}} \right) \right]_{u_s = u_{\text{min}}} \quad (2.11)$$

Values of the force constant u'' and of the factor q are listed in Table III for the $\Sigma(4-10)$ potentials considered in this work, and the calculated vibrational energies are listed in Table IV for the rare gas-gcb systems.

It is notable that the difference between the calculated and the experimental values of $\Delta\epsilon/k$ for ^{36}Ar is well within the combined uncertainty in the numbers. Note also that the correction for anharmonicity is nonnegligible for Ar and becomes quite important for Ne (and He). Clearly, the direct experimental determination of these energies by inelastic neutron scattering (or by other spectroscopic means) is very helpful in testing the accuracy of gas-solid potentials; it is hoped that such studies will soon be carried out for other adsorption systems.

Discussion

One of the long-standing problems in fitting virial coefficient data to theory is that the parameter determined

is the product As_0 (or $A\sigma_{\text{gs}}$) rather than the individual A or s_0 . In the work of Sams et al., a substitution of reasonable choices for s_0 into the experimentally determined products yielded surface areas that differed considerably from the BET area for this gcb. On the other hand, Putnam and Fort could take the areas as known quantities. Since their values for ϵ_{1s} and As_0 are quite close to those obtained by Sams et al., it is not surprising to find that the use of an area close to the BET area by Putnam and Fort gives s_0 for the Kr-gcb system that is unreasonably small [specifically, 2.3 Å for the (3-12) function]. In contrast, the $\Sigma(4-10)$ potential has not only the best theoretical justification and fits the available data as well as the best of the (m, n) functions, it also gives reasonable σ_{gs} and ϵ_{gs} values when the best estimate of the area is used. For example, if it is assumed that the cohesion of basal planes in graphite is due to a sum of pairwise (6-12) power interactions between carbon atoms in different planes, it can be shown that $\sigma_{\text{CC}} = 3.4$ Å and $\epsilon_{\text{CC}}/k = 28$ K.¹⁷ These values can be used together with the combining rules for the parameters of the interaction potentials of unlike atoms to give estimates of σ_{gs} and ϵ_{gs} . Perhaps the best known of these are the Lorentz-Berthelot rules, which consist of an arithmetic mean for σ and a geometric mean for ϵ :

$$\sigma_{\text{gs}} = (\sigma_{\text{gg}} + \sigma_{\text{ss}})/2 \quad (3.1)$$

$$\epsilon_{\text{gs}} = (\epsilon_{\text{gg}}\epsilon_{\text{ss}})^{1/2} \quad (3.2)$$

These expressions have been used previously to estimate the well depths and size parameters for the rare gas-gcb systems.¹⁰ Recalculated values are also shown in Table II (using $\sigma_{\text{CC}} = 3.37$ Å rather than the previous value of 3.40 Å).

The agreement between the calculated and the experimental values of σ_{gs} is as good as one could hope for. The uncertainty in the experimental numbers is at least $\pm 3\%$, due in part to lack of precision in $A\sigma_{\text{gs}}$ obtained from what is essentially a logarithmic fit of data to theory and in part to uncertainty in the area of the substrate. Unfortunately, an error in σ_{gs} leads to an even larger error in ϵ_{gs} , since eq 1.8 shows that a calculation of this parameter from ϵ_{1s} is quadratically dependent upon σ_{gs} .

Although various tests^{18,19} based on properties of bulk mixed rare gases show that the arithmetic mean rule for σ_{ij} is quite accurate, it has been shown that the geometric mean rule for ϵ_{ij} is much less satisfactory. Consequently, a number of combining rules have been proposed as improvements on the Lorentz-Berthelot rule for ϵ_{gs} .²⁰ In most cases, these rules (combined with the arithmetic mean rule for σ_{gs}) give rise to values for the ratio $\epsilon_{\text{gs}}/(\epsilon_{\text{gg}}\epsilon_{\text{ss}})^{1/2}$ which is less than unity by an amount that increases with the size difference between the atoms. Table II shows quite clearly that these extended rules are incapable of predicting the observed behavior for Kr and Xe. In fact, the data seem to indicate that this ratio increases smoothly with increasing size of the gas atom, if one remembers that the ϵ_{gs} have at least 5% uncertainty. A possible explanation for this observation is suggested by the fact that the neglected variations in energy with displacement parallel to the surface vary smoothly with changes in the gas atom/solid atom size ratio. Consequently, the virial coefficients were recalculated without omitting this part of the potential; the results are given in the Appendix (supplementary material), and the slopes and intercepts are shown in Table I. It is readily shown that only the virial coefficient fit for neon is noticeably affected when one uses the refined theory, and that the alterations in this case are a shift in σ_{gs} from 2.94 to 3.00 Å, a shift in ϵ_{gs}/k

from 346 to 344 K and finally, a shift in ϵ_{13}/k from 26 to 27 K, which causes the well-depth ratio listed for neon in the last column of Table II to rise to 0.86. The change in σ_{gs} brings it into better agreement with the arithmetic mean prediction of 3.08 Å, and the change in ϵ_{gs} gives rise to a smoother variation in well-depth ratio with atomic size. However, the inclusion of the parallel variation in energy does not explain the observed deviations from the well-depth combining rules.

Of the various possibilities left as a possible explanation of the values found for the well-depth ratio, it appears that the most likely one is that the gas-solid energy is not exactly equal to a pairwise sum of the gas-solid atom interactions. The presence of delocalized (conduction) electrons in the graphite planes lends some credence to this belief; furthermore, the fact that a large gas atom tends to "see" more of the surface than a small one might lead one to guess that nonlocal interactions would be more important.

The quantum mechanical calculations required to test this hypothesis are not available. Even if such a computation shows that this argument is correct, it should be emphasized that the deviations are small, and that the results of the work presented here are a striking confirmation of the ability of the pairwise additive approximation combined with (12-6) atom-atom potentials to give a good representation of the main features of the rare gas-graphite interactions and of the observable quantities that are directly derivable from this energy.

Acknowledgment. This work was supported in part by a grant from the Petroleum Research Fund, administered by the American Chemical Society.

Supplementary Material Available: An Appendix containing values of B_{AS}^* for the various potentials (2 pages). Ordering information is available on any current masthead page.

References and Notes

- (1) N. N. Avgul and A. V. Kiselev in "Chemistry and Physics of Carbon", Vol. 6, Marcel Dekker, New York, N.Y., 1970.
- (2) W. A. Steele in "The Gas-Solid Interface", Vol. 1, E. A. Flood, Ed., Marcel Dekker, New York, N.Y., 1964.
- (3) R. A. Pierotti and H. E. Thomas in "Surface and Colloid Science", Vol. IV, E. Matijevic, Ed., Wiley-Interscience, New York, N.Y., 1971.
- (4) W. A. Steele and G. D. Halsey, Jr., *J. Chem. Phys.*, **22**, 979 (1954).
- (5) J. R. Sams, Jr., G. Constabaris, and G. D. Halsey, Jr., *J. Phys. Chem.*, **65**, 367 (1961).
- (6) R. Yaris and J. R. Sams, Jr., *J. Chem. Phys.*, **37**, 571 (1962).
- (7) J. R. Sams, Jr., G. Constabaris, and G. D. Halsey, Jr., *J. Phys. Chem.*, **64**, 1689 (1960).
- (8) S. Ross and J. P. Olivier, *Adv. Chem. Ser.*, **33**, 301 (1961); I. D. Morrison and S. Ross, *Surface Sci.*, **39**, 21 (1973).
- (9) F. A. Putnam and T. Fort, Jr., *J. Phys. Chem.*, **81**, 2164 (1977).
- (10) W. A. Steele, *Surface Sci.*, **36**, 317 (1973).
- (11) See, for example, D. L. Freeman, *J. Chem. Phys.*, **62**, 4306 (1975); A. J. Bennett, *Phys. Rev. B*, **9**, 7411 (1974); J. N. Schmit, *Surface Sci.*, in press.
- (12) For example, see, J. A. Venables and P. S. Schabes-Retchkiman, *J. Phys.*, in press.
- (13) F. A. Putnam and T. Fort, Jr., *J. Phys. Chem.*, **79**, 459 (1975).
- (14) Proceedings of the International Conference on Two Dimensional Phases, Marseille, 1977, to appear in *J. Phys.*
- (15) E. J. Derridian and W. A. Steele, *J. Chem. Phys.*, **66**, 2831 (1977).
- (16) H. Taub, K. Camiero, J. K. Kjems, and L. Passell, *Phys. Rev.*, submitted for publication.
- (17) See W. A. Steele, "The Interaction of Gases with Solid Surfaces", Pergamon, New York, N.Y., 1974, section 2.8.
- (18) See, for example, D. Henderson, *Annu. Rev. Phys. Chem.*, **25**, 461 (1974).
- (19) C. H. Chen, P. E. Siska, and Y. T. Lee, *J. Chem. Phys.*, **59**, 801 (1973); C. Y. Ng, Y. T. Lee, and J. A. Barker, *ibid.*, **61**, 1996 (1974).
- (20) See, for example, K. M. Smith, A. M. Rulis, G. Scoles, R. A. Aziz, and V. Nalin, *J. Chem. Phys.*, **67**, 152 (1977).

Raman Spectroscopic Study of Chloroform and Carbon Tetrachloride in 69% Dipalmitoyl Lecithin-31% Water Multilayers

Bernard J. Bulkin* and Nehama Yellin

Department of Chemistry, Polytechnic Institute of New York, Brooklyn, New York 11201 (Received July 5, 1977)

Publication costs assisted by the Polytechnic Institute of New York

The Raman spectrum of 69% dipalmitoyl lecithin (DPL)-31% water multilayers has been studied as a function of addition of CHCl_3 and CCl_4 . The results indicate that a phase transition analogous to that which is thermally induced takes place at constant temperatures below T_c when solute is added. A substantial two phase region is found, although the molecular nature of this two phase region is unclear. The extent of this region is different for CHCl_3 and CCl_4 . By using the solute Raman bands as an internal intensity standard, the intensity changes in various lipid bands, previously measured only as relative changes, can be put on a somewhat more absolute basis. The implications of this for order calculations are discussed.

Introduction

The bilayer structure of phospholipid-water gels and the thermally induced phase transition (at temperature T_c) of gel-liquid crystal of these systems are the subjects of a large number of studies (see, for example, ref 1-5). The gel-liquid crystalline transition exists between two structural states: (1) the rigid crystalline one, $L\beta'$ or $L\beta$, in which the hydrocarbon chains of the phospholipid are in an all-trans extended conformation with some rotational disorder, and (2) the liquid crystalline one ($L\alpha$) in which the chains are fluid, having a liquidlike disorder. Recording, by spectroscopic or calorimetric techniques, thermally induced changes related to the chains in the

bilayer allows one to detect the phase transition of a given gel system.

Small organic molecules can also lead to structural changes of the lipid chains in the bilayer (at constant temperature below T_c). These perturbations, both hydrophobic and hydrogen bonding, have been studied mainly with anesthetic molecules.⁶⁻⁹ It has been found that the effect of the anesthetic molecules is to reduce the order of the bilayer, by partial fluidization of the rigid lipid chains.

The structural changes in the pure bilayers have been studied by most of the modern spectroscopic techniques, including Raman spectroscopy. The Raman spectrum of

TABLE I: Frequency Changes with Phase Transition in 69% DPL-31% H₂O Multilayers

CCl ₄ (26 °C)				CHCl ₃ (26 °C)				CCl ₄ (30 °C)				69% DPL-31% H ₂ O ^c	
Onset		End		Onset		End		Onset		End		T < 30 °C	T > 45 °C
cm ⁻¹	X ^a	cm ⁻¹	X	cm ⁻¹	X	cm ⁻¹	X	cm ⁻¹	X	cm ⁻¹	X		
1094	0.45	1086	1.00	1094	0.25	1085	1.35	1094	<0.14	1085	0.9	1094	1085
1127	0.50	1124	1.00	1127	0.25	1124	1.35	1127	<0.14	1124	0.9	1127	1123
1294	0.45	1298	0.90	1294	0.60	1299	1.40	1294	<0.14	1298	0.8	1294	1298
2844	0.40	2947	0.90	2844	0.25	2848	1.35	2844	<0.14	2848	0.8	2844	2848
												2878	2886

^a X is the mole ratio of solute to DPL. ^b Frequency shift begins below most dilute solution measured. ^c See Figure 4.

1,2-dipalmitoyl-DL-lecithin (DPL) has been assigned¹⁰ and the phase transition of DPL-H₂O multilayers has been found to be manifested very clearly in the Raman spectrum.¹¹⁻¹⁵

In this work, the effect of variable amounts of chloroform and carbon tetrachloride on the structural state of DPL-water multilayers has been studied by Raman spectroscopy. The lipid chains show Raman scattering in several main regions: the C-C stretching region, 1000-1200 cm⁻¹; CH₂ twisting, 1250-1350 cm⁻¹; CH₂ deformation, 1350-1500 cm⁻¹; and the CH stretching region, 2800-3000 cm⁻¹. The 1000-1350- and 2800-3000-cm⁻¹ regions were the object of the present study.

The results show that increasing amounts of chloroform or carbon tetrachloride lead to fluidization of the lipid chains in a very similar manner to the thermally induced fluidization. The order of the fluid state of the bilayer caused by addition of large amounts of CHCl₃ or CCl₄ is almost identical with the order in pure DPL-H₂O multilayers at T > 45 °C (T_c of DPL is 42 °C). Although some differences between the two effects exist, this similarity enables one to compare results between the two systems.

Experimental Section

1,2-Dipalmitoyl-DL-lecithin (DPL) was obtained from Sigma Chemical Co., and was used without further purification. The organic solvents carbon tetrachloride and chloroform were Baker Analyzed Reagents. The DPL-H₂O multilayers were prepared by weighing the appropriate amounts of DPL and H₂O in a 1-mm diameter capillary; the total weight varied from 20 to 30 mg. The sample was mixed thoroughly with a nichrome wire, and was heated to about 70 °C for a few seconds. The procedure of mixing and heating was repeated several times, until a homogeneous gel was established. The multilayers contained 31% (w/w) water, representing full hydration of the polar heads.¹³ To the prepared gel an organic solvent was added, the amount of which was determined by weighing. The sample was mixed thoroughly with the nichrome wire, and then the capillary was sealed.

The spectra were taken with a Spex Model 1401 Raman spectrophotometer equipped with an Ar⁺ laser, which is described elsewhere.¹⁶ The spectral regions studied were 1025-1350 and 2800-3000 cm⁻¹ for lipids as well as 400-500 cm⁻¹ for CCl₄ samples and 620-720 cm⁻¹ for CHCl₃ samples. Laser power of 300 mW and a spectral slit width of 2 cm⁻¹ were used. All spectra were recorded digitally. The interval between two data points was 1 cm⁻¹, with frequency calibration carried out using a Ne lamp, thus giving an accuracy of frequency determination better than the data collection interval. Integration times at each point varied from 5 to 20 s, depending on the signal-to-noise ratio of a given sample.

Absolute frequencies were determined in each run. In addition, the peak area (I) at 1125 and 1295 cm⁻¹, and of a solvent peak, as well as the peak heights (h) at 2878 and

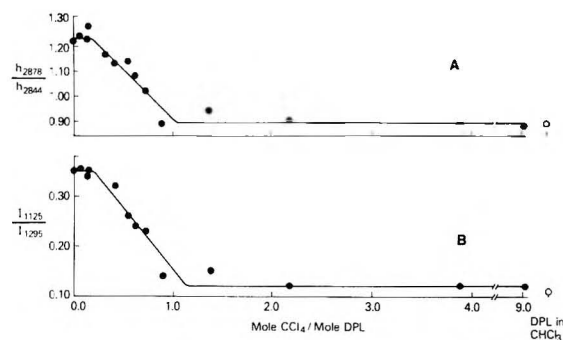


Figure 1. (A) Relative peak heights in CH stretching region spectra of DPL-H₂O-CCl₄ phases as a function of moles of CCl₄ added. (B) Relative areas of peaks in C-C stretch and CH₂ twisting regions of DPL-H₂O-CCl₄ phases as a function of moles of CCl₄ added. Data for micellar solution of anhydrous DPL in CHCl₃ shown at the right. T = 26 °C for all spectra.

2844 cm⁻¹ (without resolving the overlapping peaks) were taken in each run. The changes in frequencies are of the order of 2-8 cm⁻¹. Since the range of error in frequency determination is ± 1 cm⁻¹, the scatter in the frequency change vs T curves is relatively large. However, examples of frequency change are included in the Results section as a comparison to the changes observed in peak area ratio I₁₁₂₅/I₁₂₉₅ and peak height ratio h₂₈₇₈/h₂₈₄₄.

The uncertainties in intensity measurements were computed using counting statistics and propagation of errors theory. The former was taken as the square root of the number of counts collected, while the latter included both subtraction of background and division errors.

Results

On addition of chloroform or carbon tetrachloride in increasing amounts to 69 DPL-31 H₂O multilayer samples, at 26 °C, changes occur in the Raman spectra of the lipid chains. When 1.6 mol of CHCl₃ or CCl₄ per mole of DPL have been added to these gels, the vibrations of the hydrocarbon chains are essentially identical with those seen for the pure gels at 43 °C. Figures 1 and 2 show the changes in relative intensities which occur upon addition of CCl₄ and CHCl₃, respectively, and Table I summarizes some of the frequency changes which occur. As can be seen from the figures, at 26 °C, addition of small amounts of solute to the multilayers does not affect the chain vibrations substantially. Even at mole ratios of 0.1-0.2 mol of solute per mole of DPL the frequencies and intensities are unchanged from the pure gel sample. Similarly, at high mole ratios of solute to DPL, the frequencies and intensities observed are unaffected (with one exception see below) by the amount of solute added, just as in the pure gel they are unaffected by increasing temperature above 45 °C.

There are three important differences between the phase transition of DPL/H₂O multilayers induced by solutes and

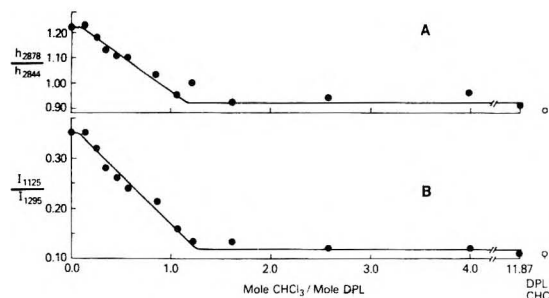


Figure 2. (A) Relative peak heights in CH stretching region spectra of DPL- H_2O - CHCl_3 phases as a function of moles of CHCl_3 added. (B) Relative area of peaks in C-C stretch and CH_2 twisting regions of DPL- H_2O - CHCl_3 phases as a function of moles of CHCl_3 added. Data for micellar solution of anhydrous DPL in CHCl_3 shown at the right. $T = 26^\circ\text{C}$ for all spectra.

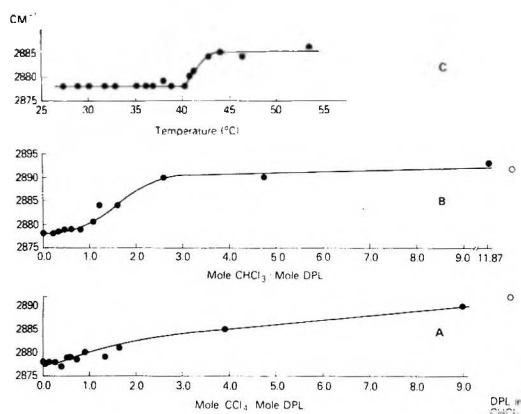


Figure 3. Frequency changes observed in the CH stretching region. (A) Phase transition in 69% DPL-31% water gel induced by CCl_4 at 26°C . Data for micellar solution of anhydrous DPL in CHCl_3 shown at the right. (B) Phase transition induced by CHCl_3 in this gel at 26°C . (C) Thermally induced phase transition of this gel.

that which occurs thermally in the pure multilayers. It has recently been shown^{14,15} that when the parameters plotted in Figures 1 and 2, and summarized in Table I, are plotted for the pure gels, a phase transition occurring at temperatures below the main transition, called the lower transition, can be clearly seen in the spectra. This transition is well known from calorimetric measurements on the gels. This lower transition is not seen in the solute induced phase transition.

The second important aspect of the curves in Figures 1 and 2, relative to the pure gel, is that our most recent spectroscopic data are in accord with calorimetric data in showing that the phase transition induced thermally is truly isothermal, occurring over a temperature range of less than 1°C . When solutes are used to induce the phase transition, the transition occurs over a range of solute concentration. In the region over which the transition occurs, the spectroscopic parameters of the trans and trans + gauche chain segments change in a linear fashion with solute concentration.

The third difference observed between the two liquid crystalline states, the one at $T > 45^\circ\text{C}$ in the pure gel, the other at high solute concentrations, is in the frequency of one peak in the CH stretching region. These results are shown in Figure 3, where they are compared to those of the thermal phase transition. The maximum observed in this region at 2878 cm^{-1} in the low temperature gel shifts to 2885 cm^{-1} at temperatures above the phase transition. Its frequency is then constant as the temperature is raised further. When solutes are added, this frequency change also occurs, but continues to shift after other spectroscopic

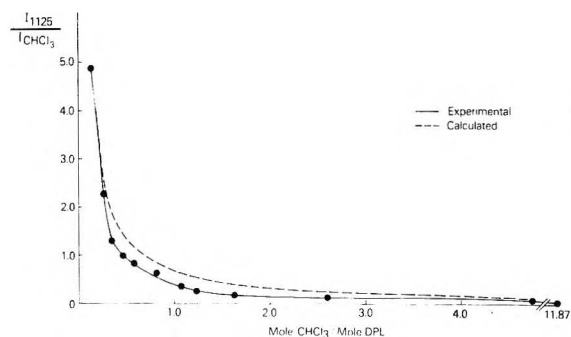


Figure 4. Relative intensity of DPL C-C stretching mode to CHCl_3 band at 669 cm^{-1} . See text for explanation of calculated curve. Data indicate decrease of 1125-cm^{-1} band intensity with increasing CHCl_3 concentration.

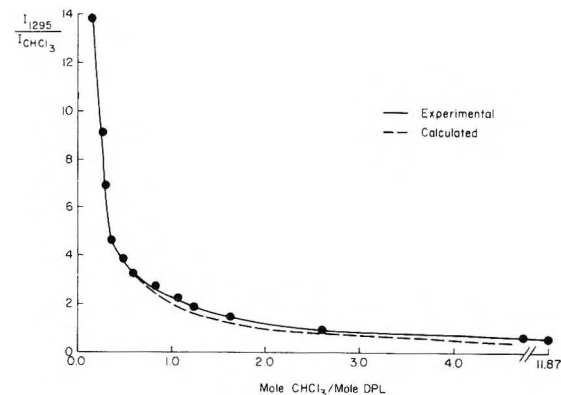


Figure 5. Relative intensity of DPL CH_2 twisting mode to CHCl_3 band 669 cm^{-1} . See text for explanation of calculated curve. Data indicate slight increase in intensity of 1295-cm^{-1} band with increasing CHCl_3 concentration.

parameters indicate that the phase transition is complete. A limiting value is reached at 2892 cm^{-1} only after a micellar solution is present.

The figures show that there is a small but reproducible difference in the CCl_4 and CHCl_3 results. The phase transition in the case of CHCl_3 starts at a lower mole ratio and ends at a higher mole ratio of solute to DPL.

The peak of the solute can be used as a reference peak (ν_1 of CCl_4 at 459 cm^{-1} and ν_2 of CHCl_3 at 669 cm^{-1}) assuming that the only change of the peak area of the solute is due to the change in concentration. The relative change in the peak area I_{1125} with increasing amounts of CHCl_3 is given in Figure 4. The "calculated" values were obtained by computing the relative intensities at the lowest solute concentration, and assuming no other change except solute band intensity due to change in solute concentration. Thus neither the experimental nor calculated values is corrected for change in DPL concentration, and direct comparison is possible. The difference between the experimental and calculated values given (in Figure 4) shows that the absolute value of I_{1125} decreases with increasing amounts of solute.

Figure 5 shows the analogous curve for the band at 1295 cm^{-1} . Here we see that the intensity increases slightly as solute is added. Referring back to Figures 1 and 2, one can conclude that the net changes observed in I_{1125}/I_{1295} are the result of two opposite and somewhat unequal effects, the decrease in I_{1125} and the smaller increase in I_{1295} . In this measurement the CHCl_3 (or CCl_4) has functioned as an internal standard.

In order to study the complementary effect of solute and temperature on the phase transition, an experiment with carbon tetrachloride was carried out at 30°C . The fre-

quency results are shown in Table I. When the temperature is higher, the liquid crystalline state of the bilayer starts at lower mole ratio of CCl_4/DPL and ends at lower mole ratio.

Discussion

Thus far, the majority of investigations of small molecules in bilayers have concentrated on the alcohols, such as benzyl alcohol, because of the importance of these in anesthesia. Our motivation for studying CCl_4 and CHCl_3 is similar. In addition, as will be discussed further below, Martire et al.¹⁷⁻¹⁹ have recently investigated the effects of small spherical molecules on thermotropic liquid crystals. This investigation of a lyotropic liquid crystal complements their work.

Both CCl_4 and CHCl_3 are quite insoluble in the aqueous phase of the bilayers (solubility in water: 0.01 g of $\text{CCl}_4/100$ g of H_2O at 24 °C; 0.072 g of $\text{CHCl}_3/100$ g of H_2O at 23 °C), and we can assume that for spectroscopic purposes they are completely dissolved in the hydrocarbon region. Nonetheless, the greater polarity of CHCl_3 (dipole moment 1.15 D) and its greater dielectric constant (ϵ_{CCl_4} 2.238; ϵ_{CHCl_3} 4.806) may account for some of the differences observed between the two molecules in this study. As no differences were seen in the spectra which would be indicative of any environmental differences between the solutes, no conclusion can be drawn on this point. Neither solute has any Raman bands which overlap with the bands of the lipid used in this study.

The phase transition induced by these solutes is, based on the spectroscopic data, one between the $L\beta'$ phase of the lipid multilayers in which the chains are in an all-trans extended conformation, and one in which there is a high proportion of gauche conformers present. The former conclusion rests on the observation that even at 0.1–0.2 mole ratios of solute/DPL, the spectroscopic parameters are identical with those of the $L\beta'$ phase. The phase existing at high ratios of solute to DPL may or may not be an $L\alpha$ phase, as characterized for the pure bilayers at high temperatures by x-ray methods. While the spectroscopic parameters are quite similar, we do not have enough data to know whether Raman spectroscopy is sufficiently sensitive to distinguish between phases of similar conformation in the disordered chains but different packing symmetry. This point is discussed further at the end of the Discussion.

The phase transition occurs over a range of solute concentration. As the measurements taken here are equilibrium measurements, our discussion must be in that context, not in a kinetic one as is often done for nonequilibrium measurements such as differential scanning calorimetry. Thus the results can be understood in terms of a phase equilibrium between two phases, one in which the lipid chains are highly ordered, and the other in which substantial amounts of gauche conformers are present.

The curves in Figures 1 and 2 indicate that there is a substantial two phase region, the extent of which is different for CCl_4 and CHCl_3 . Such a region is required for a first-order phase transition when spherical impurities are added. In this two phase region, both ordered and disordered chains are present. The fraction of gauche conformers appears to increase linearly with concentration of solute in the two phase region. The curves thus provide us with a portion of the phase diagram for this three component system. It is interesting to note that Martire has also predicted¹⁷ and found¹⁸ a two phase region for the two component system of thermotropic liquid crystal plus spherical solute in the nematic case, but in general this region is very narrow. A similar two phase region is also

found in the case of liquid crystalline solutions of certain polymers in methylene chloride, in which both isotropic and mesophases are present over a range of CH_2Cl_2 concentration.²⁰ McConnell and co-workers²¹ have observed lateral phase separation in related phases. It would be interesting to apply the techniques used by them in their assertion of lateral phase separation to ascertain whether analogous separation is taking place here, or if the fluidization is uniform throughout the multilayer, occurring progressively along the chains from the bilayer center, which would be the alternative reasonable prediction.

The Raman data provide one piece of negative evidence related to this point. In the pure lipid–water gels, the lower phase transition is clearly seen in the Raman parameters.¹⁵ When solute is added, this transition is not seen. In addition, if small amounts of solute (e.g., 0.14 mol of solute/mol of DPL) are added and the transition is induced thermally, the lower transition is still not observed.²² This lower transition occurs between different phases having all-trans, rigid chain conformations. If the two phase region was one in which lateral phase separation occurred, we would expect the region containing all-trans chains to exhibit the lower transition, while the fluidized region would not. As this is not seen, we believe that the fluidization occurs in a statistically random fashion.

Further evidence regarding the phase diagram is obtained from the dependence of the spectroscopic parameters on solute concentration at 30 °C, shown for the case of CCl_4 in Table I. At this temperature, addition of even small amounts of solute already affects the spectroscopic parameters of the lipid chains. Clearly at these temperatures the entropic change caused by the presence of gauche conformers is sufficient to overcome the enthalpic barrier.

The peak area of the solute peaks is linear with concentration, and appears to be unaffected by the phase transition which takes place. We can use this peak area as a reference, and from it derive the absolute change in the peak area of the I_{1125} peak with decreasing order in the bilayer. This latter peak arises from CC stretching modes of the all-trans segments. Its intensity decreases as gauche conformers are introduced.

One can attempt to use this absolute change in intensity to calculate the concentration of trans segments in the system at any given point. If one carries out such a calculation assuming that I_{1125} is directly proportional to the concentration of carbons, the result is that at a 2.5 mole ratio of CCl_4/DPL or CHCl_3/DPL , 55% of the rotatable carbons are in the gauche conformations. This is inconsistent with calculations of Nagle⁴ and others, indicating that even in the vapor phase, no more than 42% gauche conformers exist. Furthermore, transferring our intensity results to the high temperature liquid crystal phase, at 43 °C, we would again conclude that 55% gauche conformers exist, while Nagle's calculations and other measurements would indicate a value of 25% at this point.

The reason for failure of this attempt at using Raman spectra to produce a scale stems from the presence of overlapping modes in the CC region, each of which has a different dependence on concentration of trans segments. Because of the complexity of these modes, there is no way of knowing how many times a particular carbon atom manifests itself in the integrated intensity in any region. Thus we believe that Raman spectra are currently only useful for obtaining an upper limit on the fraction of gauche conformers.

As shown in the Results section, the solute results indicate that I_{1125} decreases while I_{1295} increases. It is

straightforward to explain the former result, as the I_{1125} band is associated with all-trans C-C stretching, and there is a corresponding increase in intensity at 1095 cm^{-1} , corresponding to C-C stretching of gauche segments. The increase in intensity at 1295 cm^{-1} is explained as follows: We note that with the increase in intensity there is a concomitant shift to higher frequency. Referring to force constant calculations for hydrocarbon chain segments, one finds that a number of CH_2 twisting modes are predicted for the $1275\text{--}1325\text{ cm}^{-1}$ region.²³ In the all-trans chains, the selection rules are strict, and certain of these are Raman active, others are infrared active, while some are inactive. In the fluid phase the symmetry is lowered. For example, a trans-gauche segment has no symmetry (C_1 point group). All the CH_2 twisting modes become allowed in this case, leading to an increase in intensity. A similar effect is seen in the CH_2 stretching region, in which an intense infrared band of the all-trans chains at 2930 cm^{-1} , absent from the Raman spectra of the $L\beta'$ phase, appears strongly in the $L\alpha$ phase.¹⁵

The only spectral difference between the liquid crystalline state of DPL- H_2O at $T > 45^\circ\text{C}$ and that of DPL- H_2O -solute at room temperature is in the $2800\text{--}3000\text{ cm}^{-1}$ region. In the second case, the 2878 cm^{-1} peak continues to shift to higher frequency values as more solute is added, although all other measures in the system (including the 2844 cm^{-1} frequency shift and h_{2878}/h_{2844} values) indicate that a liquid crystalline state is already achieved. It seems reasonable to explain this continuous frequency shift with additional amount of solute (as the solute becomes the solvent, in fact) as a result of a gradual change in the long-range organization of the phospholipid molecules, from a bilayer structure to a micellar solution. The Raman spectrum of a micellar solution of DPL in CHCl_3 and that of the highest mole ratio of CHCl_3/DPL in multilayers (or CCl_4/DPL) measured in this study are almost identical. (See Figures 1 and 2, right-hand side.) At a mole ratio of 10 (solute to DPL) one has a 0.036 mole fraction of hydrocarbon in the solvent-hydrocarbon organic phase of the system. At this dilution the existence of micelles cannot be ruled out. The 2878 cm^{-1} frequency shift is not a result of a shift of one peak only, but a consequence of several changes in the $2800\text{--}3000\text{ cm}^{-1}$ region. This region is very difficult to resolve into individual components.

Although the packing is different no other spectral differences exist between the liquid crystalline bilayer and the micellar solution, indicating the same fraction of gauche conformers is present in both cases. The $1000\text{--}1350\text{ cm}^{-1}$ region is apparently not sensitive to packing, only to chain conformational order. This difference in behavior of CH stretches and CC stretches has also been seen in temperature dependence of dilauroyl phosphatidyl ethanolamine spectra.¹²

Further investigations of these systems, particularly temperature dependent studies designed to completely describe the phase diagrams, are in progress and will be reported shortly.

Acknowledgment. This work was supported by a research grant from the U.S. Army Research Office—Durham.

References and Notes

- (1) V. Luzzati and A. Tardieu, *Annu. Rev. Phys. Chem.*, **79** (1974).
- (2) H. J. Hinz and J. M. Sturtevant, *J. Biol. Chem.*, **247**, 6071 (1972).
- (3) D. Chapman, J. Urbina, and K. M. Keough, *J. Biol. Chem.*, **249**, 2512 (1974).
- (4) J. F. Nagle, *J. Chem. Phys.*, **58**, 252 (1973).
- (5) A. Seelig and J. Seelig, *Biochemistry*, **13**, 4839 (1974).
- (6) M. W. Hill, *Biochem. Biophys. Acta*, **356**, 117 (1974).
- (7) J. R. Trudell, W. L. Hebbell, and E. N. Cohen, *Biochem. Biophys. Acta*, **291**, 321 (1973).
- (8) S. J. Paterson, *Biochem. Biophys. Acta*, **266**, 597 (1972).
- (9) S. A. Simon, R. C. McDonald, and P. B. Bennett, *Biochem. Biophys. Res. Commun.*, **67**, 988 (1975).
- (10) R. C. Spiker and I. W. Levin, *Biochem. Biophys. Acta*, **388**, 361 (1975).
- (11) B. J. Bulkin and N. Krishnamachari, *J. Am. Chem. Soc.*, **94**, 1109 (1972).
- (12) R. Mendelsohn, S. Sunder, and H. J. Bernstein, *Biochem. Biophys. Acta*, **413**, 329 (1975).
- (13) K. Larsson and R. P. Rand, *Biochem. Biophys. Acta*, **326**, 245 (1973).
- (14) B. Gaber and W. L. Peticolas, *Biochim. Biophys. Acta*, **465**, 260 (1977).
- (15) N. Yellin and I. W. Levin, *Biochem. Biophys. Acta*, **468**, 490 (1977).
- (16) B. J. Bulkin, E. H. Cole, and A. Noguerola, *J. Chem. Ed.*, **51**, A273 (1974).
- (17) H. T. Peterson and D. E. Martire, *Mol. Cryst. Liq. Cryst.*, **25**, 89 (1974).
- (18) H. T. Peterson, D. E. Martire, and M. A. Cotter, *J. Chem. Phys.*, **61**, 3547 (1974).
- (19) G. I. Agren and D. E. Martire, *J. Phys. (Paris)*, **36**, C1-141 (1975).
- (20) W. A. Hines and E. T. Samulski, *J. Polym. Sci., Symp. No. 44*, 11 (1974).
- (21) E. J. Shimshick and H. M. McConnell, *Biochemistry*, **12**, 2351 (1973).
- (22) B. J. Bulkin and N. Yellin, unpublished data.
- (23) R. G. Snyder, *J. Chem. Phys.*, **47**, 1316 (1967).

Crystal-Field Calculations with Trigonal Bipyramidal Symmetry Potential. 2. Weak-Field Matrices at Nonzero Spin-Orbit Coupling for a $d^{3,7}$ Configuration[†]

F. Palacio

Departamento de Física Fundamental, Facultad de Ciencias, Universidad de Zaragoza, Zaragoza, Spain (Received December 15, 1976)

Trigonal bipyramidal crystal-field energy matrices for a $d^{3,7}$ configuration, at nonzero spin-orbit coupling, in a weak-field scheme are given. Racah algebra has been used for calculating them. The appropriate weak-field basis eigenfunctions are also given and some properties of the group are pointed out in order to describe a quick method for generating those eigenfunctions. All crystal-field matrices calculated here have been fully checked and the checking procedures are also described.

Introduction

Crystal-field and spin-orbit energy matrices have proved to be a valuable tool in the study of the fine structure and

magnetic properties of complex ions. That work has been carried out for all d^n configurations in O_h symmetry¹ and for the majority of those in tetragonal, D_{4h} , and lower "pseudo-cubic" crystal-field symmetries.² In D_{3h} symmetry, however, this calculation has been performed only for d^{13} and d^{24} configurations. The goal of the present

[†] This work was supported in part by Junta de Energía Nuclear, Madrid, Spain.

TABLE I: Compatibility between the Full Rotation Group and the D_{3h} Point Group for Centrosymmetric Half-Odd-Integer Representations

$O(3)$ states	D_{3h} * states
1/2	Γ_7
3/2	$\Gamma_7 + \Gamma_9$
5/2	$\Gamma_7 + \Gamma_8 + \Gamma_9$
7/2	$\Gamma_7 + 2\Gamma_8 + \Gamma_9$
9/2	$\Gamma_7 + 2\Gamma_8 + 2\Gamma_9$
11/2	$2\Gamma_7 + 2\Gamma_8 + 2\Gamma_9$
13/2	$3\Gamma_7 + 2\Gamma_8 + 2\Gamma_9$

paper is to set up complete crystal-field energy matrices from a Hamiltonian that includes also electrostatic repulsion and spin-orbit coupling terms.

We are interested, as pointed out in the first part of this series⁵ (henceforth labeled as CFC-I), in the weak-field, or “free atom”, representation;⁶ therefore the terms of the Hamiltonian

$$\mathcal{H} = \sum_{i>j} \frac{e^2}{r_{ij}} + \sum_i \xi(r_i) \vec{s}_i \cdot \vec{l}_i + V_{D_{3h}} \tag{1}$$

will be treated in the order given in eq 1. The crystal-field

potential, $V_{D_{3h}}$, reduces the spherical symmetry of both Coulombic and spin-orbit terms. Then, in order to obtain the $|d^3\alpha SL\Gamma\rangle$, where Γ denotes an irreducible representation in the point group, eigenfunctions of the Hamiltonian (1), the free ion $|d^3\alpha SLJM\rangle$ states have to be subduced onto the corresponding ones of the crystal-field point group.

We must first discuss some differences in the subduction procedure depending on whether the number of d electrons is even or not. In the first case the subduction of the free ion states can be done as in the zero spin-orbit limit, that is, by considering the $D^J R(\alpha, \beta, \gamma)$ full-rotation group representations, J integer, and restricting them, in the usual form, to the requirements of the point group operations.

In the second case, however, the values of J are half integral numbers and then the elements of the basis of $D^J R(\alpha, \beta, \gamma)$ representations are spinors instead of vectors. Here the homomorphism between the matrices $D^J R(\alpha, \beta, \gamma)$ and the rotations $R(\alpha, \beta, \gamma)$ is a two-to-one homomorphism, that is, there are two $D^J R(\alpha, \beta, \gamma)$ matrices corresponding to each $R(\alpha, \beta, \gamma)$ rotation and, therefore, the representations of $O(3)$ group are double valued.

TABLE II												
d ³ Trigonal Bipyramidal Energy Matrices in the $ d^3\alpha SL\Gamma\rangle$ Representation												
(non-zero elements only; (S) should be understood as 2S+1)												
$\mathcal{H} = \mathcal{H}_{\text{er}} + \mathcal{H}_{\text{so}} + V_{D_{3h}}$												
Matrix Γ_7 (a); $ M = 1/2$												
$\langle \alpha(S)LJ1/2 U_{D_{3h}} \alpha'(S')L'J'1/2 \rangle$	Da	Dt	$\langle \alpha(S)LJ1/2 U_{D_{3h}} \alpha'(S')L'J'1/2 \rangle$	Da	Dt	$\langle \alpha(S)LJ1/2 U_{D_{3h}} \alpha'(S')L'J'1/2 \rangle$	Da	Dt	$\langle \alpha(S)LJ1/2 U_{D_{3h}} \alpha'(S')L'J'1/2 \rangle$	Da	Dt	
3(4)P5/2	3(4)P5/2	-2/3	3	3(2)P5/2	-8/21	6/7	3(2)P5/2	-8/21	6/7	3(2)P5/2	-8/21	6/7
3(4)P7/2	-5/21	6/5/7		3(2)D5/2	10/21	24/7	3(2)D5/2	10/21	24/7	3(2)D5/2	10/21	24/7
3(4)P5/2	1/7	-18/7		3(2)D3/2	0	2/2/3	3(2)D3/2	0	2/2/3	3(2)D3/2	0	2/2/3
3(4)P3/2	0	-2/7		1(2)D5/2	10/21	-4/3/7	1(2)D5/2	10/21	-4/3/7	1(2)D5/2	10/21	-4/3/7
3(4)P5/2	4/27	-2/27		1(2)D3/2	0	-5/4/3	1(2)D3/2	0	-5/4/3	1(2)D3/2	0	-5/4/3
3(4)P3/2	0	-7/6/3		3(2)P3/2	0	1	3(2)P3/2	0	1	3(2)P3/2	0	1
3(4)P1/2	0	-7/6/3		3(2)P1/2	0	-2	3(2)P1/2	0	-2	3(2)P1/2	0	-2
3(4)P7/2	3(4)P7/2	-10/21	-3/7	3(2)D7/2	11/21	-13/14	3(2)D7/2	11/21	-13/14	3(2)D7/2	11/21	-13/14
3(4)P5/2	-13/(15/5)	6/5/7		3(2)D5/2	11/21	-13/14	3(2)D5/2	11/21	-13/14	3(2)D5/2	11/21	-13/14
3(4)P3/2	6/275/35	-11/107/3/7		3(2)P7/2	-2/57/7	1/15/14	3(2)P7/2	-2/57/7	1/15/14	3(2)P7/2	-2/57/7	1/15/14
3(4)P5/2	8/277/5	-1/57		3(2)P5/2	4/5/21	-3/5/7	3(2)P5/2	4/5/21	-3/5/7	3(2)P5/2	4/5/21	-3/5/7
3(4)P3/2	36/273/5	4/157/1/3		3(2)D5/2	2/(21/5)	6/5/7	3(2)D5/2	2/(21/5)	6/5/7	3(2)D5/2	2/(21/5)	6/5/7
3(4)P1/2	0	-1/5/3		3(2)D3/2	3/675/7	11/107/3/7	3(2)D3/2	3/675/7	11/107/3/7	3(2)D3/2	3/675/7	11/107/3/7
3(4)P5/2	3(4)P5/2	-65/175	-13/7	1(2)D5/2	2/105	-11/57/2/3	1(2)D5/2	2/105	-11/57/2/3	1(2)D5/2	2/105	-11/57/2/3
3(4)P3/2	-18/5/175	11/5/7		3(2)P3/2	0	-5/2	3(2)P3/2	0	-5/2	3(2)P3/2	0	-5/2
3(4)P5/2	-24/277/25	3/277		3(2)P1/2	0	5/2	3(2)P1/2	0	5/2	3(2)P1/2	0	5/2
3(4)P3/2	12/277/125	3/277		3(2)P7/2	5/7	9/14	3(2)P7/2	5/7	9/14	3(2)P7/2	5/7	9/14
3(4)P1/2	4/1475/5	0		3(2)P5/2	2/3/35	5/(17/3)	3(2)P5/2	2/3/35	5/(17/3)	3(2)P5/2	2/3/35	5/(17/3)
3(4)P5/2	3(4)P5/2	-65/175	-13/7	3(2)D5/2	-18/3/35	-10/(17/3)	3(2)D5/2	-18/3/35	-10/(17/3)	3(2)D5/2	-18/3/35	-10/(17/3)
3(4)P3/2	-18/5/175	11/5/7		3(2)D3/2	0	2/1/1	3(2)D3/2	0	2/1/1	3(2)D3/2	0	2/1/1
3(4)P5/2	-24/277/25	3/277		1(2)D5/2	0	2/14/11	1(2)D5/2	0	2/14/11	1(2)D5/2	0	2/14/11
3(4)P3/2	12/277/125	3/277		1(2)D3/2	0	-2/271/1	1(2)D3/2	0	-2/271/1	1(2)D3/2	0	-2/271/1
3(4)P1/2	4/1475/5	0		3(2)P3/2	0	4/273	3(2)P3/2	0	4/273	3(2)P3/2	0	4/273
3(4)P5/2	3(4)P5/2	-12/125	0	3(2)P1/2	0	2/1173	3(2)P1/2	0	2/1173	3(2)P1/2	0	2/1173
3(4)P3/2	-4/377/25	4/377		3(2)D9/2	8/15	-1	3(2)D9/2	8/15	-1	3(2)D9/2	8/15	-1
3(4)P1/2	4/27/5	0		3(2)D7/2	2/(21/5)	-5/7	3(2)D7/2	2/(21/5)	-5/7	3(2)D7/2	2/(21/5)	-5/7
3(4)P7/2	3(4)P7/2	-12/125	0	3(2)P7/2	4/(17/3)	-3/3/7	3(2)P7/2	4/(17/3)	-3/3/7	3(2)P7/2	4/(17/3)	-3/3/7
3(4)P5/2	3(4)P5/2	-65/175	-13/7	3(2)D9/2	8/15	-1	3(2)D9/2	8/15	-1	3(2)D9/2	8/15	-1
3(4)P3/2	-4/377/25	4/377		3(2)D7/2	2/(21/5)	-5/7	3(2)D7/2	2/(21/5)	-5/7	3(2)D7/2	2/(21/5)	-5/7
3(4)P1/2	4/27/5	0		3(2)P7/2	4/(17/3)	-3/3/7	3(2)P7/2	4/(17/3)	-3/3/7	3(2)P7/2	4/(17/3)	-3/3/7
3(4)P7/2	3(4)P7/2	-12/125	0	3(2)D9/2	8/15	-1	3(2)D9/2	8/15	-1	3(2)D9/2	8/15	-1
3(4)P5/2	3(4)P5/2	-65/175	-13/7	3(2)D7/2	2/(21/5)	-5/7	3(2)D7/2	2/(21/5)	-5/7	3(2)D7/2	2/(21/5)	-5/7
3(4)P3/2	-4/377/25	4/377		3(2)P7/2	4/(17/3)	-3/3/7	3(2)P7/2	4/(17/3)	-3/3/7	3(2)P7/2	4/(17/3)	-3/3/7
3(4)P1/2	4/27/5	0		3(2)D9/2	8/15	-1	3(2)D9/2	8/15	-1	3(2)D9/2	8/15	-1
3(4)P7/2	3(4)P7/2	-12/125	0	3(2)D7/2	2/(21/5)	-5/7	3(2)D7/2	2/(21/5)	-5/7	3(2)D7/2	2/(21/5)	-5/7
3(4)P5/2	3(4)P5/2	-65/175	-13/7	3(2)D5/2	10/21	24/7	3(2)D5/2	10/21	24/7	3(2)D5/2	10/21	24/7
3(4)P3/2	0	-2/7		3(2)D3/2	0	2/2/3	3(2)D3/2	0	2/2/3	3(2)D3/2	0	2/2/3
3(4)P5/2	4/27	-2/27		1(2)D5/2	10/21	-4/3/7	1(2)D5/2	10/21	-4/3/7	1(2)D5/2	10/21	-4/3/7
3(4)P3/2	0	-7/6/3		3(2)P3/2	0	1	3(2)P3/2	0	1	3(2)P3/2	0	1
3(4)P1/2	0	-7/6/3		3(2)P1/2	0	-2	3(2)P1/2	0	-2	3(2)P1/2	0	-2
3(4)P7/2	3(4)P7/2	-10/21	-3/7	3(2)D7/2	11/21	-13/14	3(2)D7/2	11/21	-13/14	3(2)D7/2	11/21	-13/14
3(4)P5/2	-13/(15/5)	6/5/7		3(2)D5/2	11/21	-13/14	3(2)D5/2	11/21	-13/14	3(2)D5/2	11/21	-13/14
3(4)P3/2	6/275/35	-11/107/3/7		3(2)P7/2	-2/57/7	1/15/14	3(2)P7/2	-2/57/7	1/15/14	3(2)P7/2	-2/57/7	1/15/14
3(4)P5/2	8/277/5	-1/57		3(2)P5/2	4/5/21	-3/5/7	3(2)P5/2	4/5/21	-3/5/7	3(2)P5/2	4/5/21	-3/5/7
3(4)P3/2	36/273/5	4/157/1/3		3(2)D5/2	2/(21/5)	6/5/7	3(2)D5/2	2/(21/5)	6/5/7	3(2)D5/2	2/(21/5)	6/5/7
3(4)P1/2	0	-1/5/3		3(2)D3/2	3/675/7	11/107/3/7	3(2)D3/2	3/675/7	11/107/3/7	3(2)D3/2	3/675/7	11/107/3/7
3(4)P5/2	3(4)P5/2	-65/175	-13/7	1(2)D5/2	2/105	-11/57/2/3	1(2)D5/2	2/105	-11/57/2/3	1(2)D5/2	2/105	-11/57/2/3
3(4)P3/2	-18/5/175	11/5/7		3(2)P3/2	0	-5/2	3(2)P3/2	0	-5/2	3(2)P3/2	0	-5/2
3(4)P5/2	-24/277/25	3/277		3(2)P1/2	0	5/2	3(2)P1/2	0	5/2	3(2)P1/2	0	5/2
3(4)P3/2	12/277/125	3/277		3(2)P7/2	5/7	9/14	3(2)P7/2	5/7	9/14	3(2)P7/2	5/7	9/14
3(4)P1/2	4/1475/5	0		3(2)P5/2	2/3/35	5/(17/3)	3(2)P5/2	2/3/35	5/(17/3)	3(2)P5/2	2/3/35	5/(17/3)
3(4)P5/2	3(4)P5/2	-65/175	-13/7	3(2)D5/2	-18/3/35	-10/(17/3)	3(2)D5/2	-18/3/35	-10/(17/3)	3(2)D5/2	-18/3/35	-10/(17/3)
3(4)P3/2	-18/5/175	11/5/7		3(2)D3/2	0	2/1/1	3(2)D3/2	0	2/1/1	3(2)D3/2	0	2/1/1
3(4)P5/2	-24/277/25	3/277		1(2)D5/2	0	2/14/11	1(2)D5/2	0	2/14/11	1(2)D5/2	0	2/14/11
3(4)P3/2	12/277/125	3/277		1(2)D3/2	0	-2/271/1	1(2)D3/2	0	-2/271/1	1(2)D3/2	0	-2/271/1
3(4)P1/2	4/1475/5	0		3(2)P3/2	0	4/273	3(2)P3/2	0	4/273	3(2)P3/2	0	4/273
3(4)P5/2	3(4)P5/2	-12/125	0	3(2)P1/2	0	2/1173	3(2)P1/2	0	2/1173	3(2)P1/2	0	2/1173
3(4)P3/2	-4/377/25	4/377		3(2)D9/2	8/15	-1	3(2)D9/2	8/15	-1	3(2)D9/2	8/15	-1
3(4)P1/2	4/27/5	0		3(2)D7/2	2/(21/5)	-5/7	3(2)D7/2	2/(21/5)	-5/7	3(2)D7/2	2/(21/5)	-5/7
3(4)P7/2	3(4)P7/2	-12/125	0	3(2)P7/2	4/(17/3)	-3/3/7	3(2)P7/2	4/(17/3)	-3/3/7	3(2)P7/2	4/(17/3)	-3/3/7
3(4)P5/2	3(4)P5/2	-65/175	-13/7	3(2)D9/2	8/15	-1	3(2)D9/2	8/15	-1	3(2)D9/2	8/15	-1
3(4)P3/2	-4/377/25	4/377		3(2)D7/2	2/(21/5)	-5/7	3(2)D7/2	2/(21/5)	-5/7	3(2)D7/2	2/(21/5)	-5/7
3(4)P1/2	4/27/5	0		3(2)P7/2	4/(17/3)	-3/3/7	3(2)P7/2	4/(17/3)	-3/3/7	3(2)P7/2	4/(17/3)	-3/3/7
3(4)P7/2	3(4)P7/2	-12/125	0	3(2)D9/2	8/15	-1	3(2)D9/2	8/15	-1	3(2)D9/2	8/15	-1
3(4)P5/2	3(4)P5/2	-65/175	-13/7	3(2)D7/2	2/(21/5)	-5/7	3(2)D7/2	2/(21/5)	-5/7	3(2)D7/2	2/(21/5)	-5/7
3(4)P3/2	-4/377/25	4/377		3(2)P7/2	4/(17/3)	-3/3/7	3(2)P7/2	4/(17/3)	-3/3/7	3(2)P7/2	4/(17/3)	-3/3/7
3(4)P1/2	4/27/5	0		3(2)D9/2	8/15	-1	3(2)D9/2	8/15	-1	3(2)D9/2	8/15	-1
3(4)P7/2	3(4)P7/2	-12/125	0	3(2)D7/2	2/(21/5)	-5/7	3(2)D7/2	2/(21/5)	-5/7	3(2)D7/2	2/(21/5)	-5/7
3(4)P5/2	3(4)P5/2	-65/175	-13/7	3(2)D5/2	10/21	24/7	3(2)D5/2	10/21	24/7	3(2)D5/2	10/21	24/7
3(4)P3/2	0	-2/7		3(2)D3/2	0	2/2/3	3(2)D3/2	0	2/2/3	3(2)D3/2	0	2/2/3
3(4)P5/2	4/27	-2/27		1(2)D5/2	10/21	-4/3/7	1(2)D5/2	10/21	-4/3/7	1(2)D5/2	10/21	-4/3/7
3(4)P3/2	0	-7/6/3		3(2)P3/2	0	1	3(2)P3/2	0	1	3(2)P3/2	0	1
3(4)P1/2	0	-7/6/3		3(2)P1/2	0	-2	3(2)P1/2	0	-2	3(2)P1/2	0	-2
3(4)P7/2	3(4)P7/2	-10/21	-3/7	3(2)D7/2	11/21	-13/14	3(2)D7/2	11/21	-13/14	3(2)D7/2	11/21	-13/14
3(4)P5/2	-13/(15/5)	6/5/7		3(2)D5/2	11/21	-13/14	3(2)D5/2	11/21	-13/14	3(2)D5/2	11/21	-13/14
3(4)P3/2	6/275/35	-11/107/3/7		3(2)P7/2	-2/57/7	1/15/14	3(2)P7/2	-2/57/7	1/15/14	3(2)P7/2	-2/57/7	1/15/14
3(4)P5/2	8/277/5	-1/57		3(2)P5/2	4/5/21	-3/5/7	3(2)P5/2	4/5/21	-3/5/7	3(2)P5/2	4/5/21	-3/5/7
3(4)P3/2	36/273/5	4/157/1/3		3(2)D5/2	2/(21/5)	6/5/7	3(2)D5/2	2/(21/5)	6/5/7	3(2)D5/2	2/(21/5)	6/5/7
3(4)P1/2	0	-1/5/3		3(2)D3/2	3/675/7	11/107/3/7	3(2)D3/2	3/675/7	11/107/3/7	3(2)D3/2	3/675/7	11/107/3/7
3(4)P5/2	3(4)P5/2	-65/175	-13/7	1(2)D5/2	2/105	-11/57/2/3	1(2)D5/2	2/105	-11/57/2/3	1(2)D5/2	2/105	-11/57/2/3
3(4)P3/2	-18/5/175	11/5/7		3(2)P3/2	0	-5/2	3(2)P3/2	0	-5/2	3(2)P3/2	0	-5/2
3(4)P5/2	-24/277/25	3/277		3(2)P1/2	0	5/2	3(2)P1/2	0	5/2	3(2)P1/2	0	5/2
3(4)P3/2	12/277/125	3/277		3(2)P7/2	5/7	9/14	3(2)P7/2	5/7	9/14	3(2)P7/2	5/7	9/14
3(4)P1/2	4/1475/5	0		3(2)P5/2	2/3/35	5/(17/3)	3(2)P5/2	2/3/35	5/(17/3)	3(2)P5/2	2/3/35	5/(17/3)
3(4)P5/2	3(4)P5/2	-65/175	-13/7	3(2)D5/2	-18/3/35	-10/(17/3)	3(2)D5/2	-18/3/35	-10/(17/3)	3(2)D5/2	-18/3/35	-10/(17/3)
3(4)P3/2	-18/5/175	11/5/7		3(2)D3/2	0	2/1/1	3(2)D3/2	0	2/1/1	3(2)D3/2		

$\langle \alpha S_z \beta \rangle = \langle \hat{L}_z \rangle_{\beta\alpha}$	$\langle \alpha' S_z \beta' \rangle = \langle \hat{L}_z \rangle_{\beta'\alpha'}$	D ₂	D ₂
$\langle 1/2 \hat{L}_z 1/2 \rangle$	$\langle 1/2 \hat{L}_z 1/2 \rangle$	1/2	-3/2
$\langle 1/2 \hat{L}_z 3/2 \rangle$	$\langle 1/2 \hat{L}_z 3/2 \rangle$	1/2	-1
$\langle 3/2 \hat{L}_z 1/2 \rangle$	$\langle 3/2 \hat{L}_z 1/2 \rangle$	-3/2	1
$\langle 3/2 \hat{L}_z 3/2 \rangle$	$\langle 3/2 \hat{L}_z 3/2 \rangle$	-7/2	3
$\langle 3/2 \hat{L}_z 5/2 \rangle$	$\langle 3/2 \hat{L}_z 5/2 \rangle$	-1/2	5
$\langle 5/2 \hat{L}_z 3/2 \rangle$	$\langle 5/2 \hat{L}_z 3/2 \rangle$	3/2	1

$\langle \alpha S_z \beta \rangle = \langle \hat{L}_z \rangle_{\beta\alpha}$	$\langle \alpha' S_z \beta' \rangle = \langle \hat{L}_z \rangle_{\beta'\alpha'}$	D ₃	D ₃
$\langle 3/2 \hat{L}_z 1/2 \rangle$	$\langle 3/2 \hat{L}_z 1/2 \rangle$	1	3
$\langle 3/2 \hat{L}_z 3/2 \rangle$	$\langle 3/2 \hat{L}_z 3/2 \rangle$	-1/3	1/3
$\langle 3/2 \hat{L}_z 5/2 \rangle$	$\langle 3/2 \hat{L}_z 5/2 \rangle$	5/3	1/3
$\langle 5/2 \hat{L}_z 3/2 \rangle$	$\langle 5/2 \hat{L}_z 3/2 \rangle$	-5/3	5/3
$\langle 5/2 \hat{L}_z 5/2 \rangle$	$\langle 5/2 \hat{L}_z 5/2 \rangle$	-1/5	1/5
$\langle 5/2 \hat{L}_z 7/2 \rangle$	$\langle 5/2 \hat{L}_z 7/2 \rangle$	7/5	7/5
$\langle 7/2 \hat{L}_z 5/2 \rangle$	$\langle 7/2 \hat{L}_z 5/2 \rangle$	-7/5	-7/5

It is obvious that their relations with the D_{3h} group operations are

$$\alpha_v(X) = iC_2(Y) \quad \alpha_h = iC_2(Z) \quad S_3^+ = iC_6^-(Z)$$

Therefore, all the operations have in our case $\beta = 0$ or $\beta = \pi$, which simplifies considerably the subduction problem.

As is well-known, the transformation properties of the $|JM\rangle$ states under a pure rotation $R(\alpha, \beta, \gamma)$ are given by the expression^{13,15}

$$R(\alpha, \beta, \gamma)|JM\rangle = \sum_{N=-J}^J |JN\rangle D_{NM}^J \{R(\alpha, \beta, \gamma)\} \quad (2)$$

where $D_{NM}^J \{R(\alpha, \beta, \gamma)\}$ is defined as¹⁶

$$D_{NM}^J \{R(\alpha, \beta, \gamma)\} = \exp(-iM\alpha) d^J(\beta)_{NM} \times \exp(-iN\gamma) \quad (3)$$

and

$$d^J(\beta)_{NM} = \sum_k \frac{(-1)^{k-M+N} [(J+M)!(J-M)!(J+N)!(J-N)!]^{1/2}}{(J-N-k)!(J+M-k)!(k-M+N)!k!} \times (\cos \beta/2)^{2J+M-N-2k} (\sin \beta/2)^{2k+N-M} \quad (4)$$

Then, depending on the values that $D_{NM}^J \{R(\alpha, \beta, \gamma)\}$ takes for all the different values of N , the state $|JM\rangle$ will be transformed onto itself or onto a linear combination of states with different M . Namely, if $\beta = 0$ or π , we have two particularly easy special cases¹⁷

$$\beta = 0 \Rightarrow D_{NM}^J \{R(\alpha, \beta, \gamma)\} = \exp(-iM\alpha) \times \exp(-iN\gamma) \delta_{NM} \quad (5)$$

$$\beta = \pi \Rightarrow D_{NM}^J \{R(\alpha, \beta, \gamma)\} = (-1)^{J-M} \times \exp(-iM\alpha) \exp(-iN\gamma) \delta_{N,-M} \quad (6)$$

So, in the Hamiltonian (1) the absolute values of M will be good quantum numbers. From expressions (5) and (6), therefore, one follows that the $|d^3\alpha SLJ \pm M\rangle$ set of wavefunctions form the basis for Γ_7 , Γ_8 , and Γ_9 representations of the D_{3h} group. The basis of the Hamiltonian (1) and its transformation properties are, finally

$$\begin{aligned} \Gamma_7(a) &\equiv \{|d^3\alpha SLJ \pm 1/2\rangle\} \\ \Gamma_7(b) &\equiv \{|d^3\alpha SLJ \pm 11/2\rangle\} \\ \Gamma_8(a) &\equiv \{|d^3\alpha SLJ \pm 5/2\rangle\} \\ \Gamma_8(b) &\equiv \{|d^3\alpha SLJ \pm 7/2\rangle\} \\ \Gamma_9(a) &\equiv \{|d^3\alpha SLJ \pm 3/2\rangle\} \\ \Gamma_9(b) &\equiv \{|d^3\alpha SLJ \pm 9/2\rangle\} \end{aligned} \quad (7)$$

Calculation of the Crystal-Field Matrices

Using the set of eigenfunctions just described, the Hamiltonian (1) may be reduced to six boxes of the following dimensions

$$\begin{aligned} \Gamma_7(a) &\rightarrow (19 \times 19) \quad \Gamma_8(a) \rightarrow (12 \times 12) \\ \Gamma_9(a) &\rightarrow (17 \times 17) \\ \Gamma_7(b) &\rightarrow (1 \times 1) \quad \Gamma_8(b) \rightarrow (7 \times 7) \\ \Gamma_9(b) &\rightarrow (4 \times 4) \end{aligned}$$

The full representation of the Hamiltonian (1) in the set of basis functions (7) will be, obviously, the sum of three

sets of matrices, one for each term. As the first two sets, which describe respectively the interelectronic repulsion and the spin-orbit coupling, are well known, we are only interested in the calculation of the third. The working out of these crystal-field matrices may be done by using standard tensorial techniques. In expression 3 of CFC-I we gave the form of the electrostatic potential originated on the central cation by a neighborhood of five charges arranged at the corners of a trigonal bipyramid. We supposed there that three charges (q_1) were placed on the XY plane at distances r_1 from the center, and the other two (q_2) along the Z axis at r_2 from the central ion. The potential may be then expressed in a more compact way as a sum of Racah's rationalized spherical harmonics multiplied by appropriate coefficients

$$V_{D,h} = \sum_{k,q} E_{kq} C_q^{(k)}(\theta, \phi) \quad k = 0, 2, 4; q = 0 \quad (8)$$

where

$$C_q^{(k)}(\theta, \phi) = \left[\frac{4\pi}{2k+1} \right]^{1/2} Y_{kq}(\theta, \phi) \quad (9)$$

The magnitude of the E_{kq} coefficients is a function of the charges and their distances from the center of the bipyramid.

Now, on using the Wigner-Eckart theorem we obtain

$$\begin{aligned} \langle d^3\alpha SLJM | V_{D,h} | d^3\alpha' S' L' J' M' \rangle = \\ \delta_{MM'} (-1)^{J-M} \sum_{k=0,2,4} h_{k0} \times \\ \begin{pmatrix} J & k & J' \\ -M & 0 & M' \end{pmatrix} \langle d^3\alpha SLJ || \hat{C}^{(k)} || d^3\alpha' S' L' J' \rangle \end{aligned} \quad (10)$$

where $\hat{C}^{(k)}$ is a tensorial operator the $2k+1$ components of which are the Racah rationalized spherical harmonics, and the h_{k0} radial integrals have been already described in expressions 11-13 of CFC-I.

Let us transform the reduced matrix elements of (10) into the calculated ones given in Appendix II of CFC-I. As the tensorial operators act only upon orbital states, the following tensorial algebra relation can be considered¹⁸

$$\begin{aligned} \langle \alpha_1 j_1 \alpha_2 j_2 J || \hat{T}_2^{(k)} || \alpha_1' j_1' \alpha_2' j_2' J' \rangle = \\ (-1)^{j_1+j_2+J+k} [(2J+1)(2J'+1)]^{1/2} \times \\ \begin{Bmatrix} j_2 & J & j_1 \\ j_1' & J' & j_2' \end{Bmatrix} \langle \alpha_2 j_2 || \hat{T}_2^{(k)} || \alpha_2' j_2' \rangle \delta_{\alpha_1 \alpha_1'} \delta_{j_1 j_1'} \end{aligned} \quad (11)$$

where 1 and 2 are different systems and $\hat{T}_2^{(k)}$ is a tensorial operator acting only on the states of system 2. Transforming the reduced matrix elements in accordance with expression 11, we obtain

$$\begin{aligned} \langle d^3\alpha SLJ || \hat{C}^{(k)} || d^3\alpha' S' L' J' \rangle = (-1)^{S+L'+J+k} \times \\ [(2J+1)(2J'+1)]^{1/2} \times \\ \begin{Bmatrix} L & J & S \\ J' & L' & k \end{Bmatrix} \langle d^3\alpha SL || \hat{C}^{(k)} || d^3\alpha' S' L' \rangle \delta_{SS'} \end{aligned} \quad (12)$$

and by substitution of (12) in (9), we finally have

$$\begin{aligned} \langle d^3\alpha SLJM | V_{D,h} | d^3\alpha' S' L' J' M' \rangle = \\ \delta_{MM'} \delta_{SS'} \sum_{k=0,2,4} h_{k0} (-1)^{2J+S+L'-M-k} \times \\ [(2J+1)(2J'+1)]^{1/2} \begin{Bmatrix} J & k & J' \\ -M & 0 & M' \end{Bmatrix} \times \\ \begin{Bmatrix} L & J & S \\ J' & L' & k \end{Bmatrix} \langle d^3\alpha SL || \hat{C}^{(k)} || d^3\alpha' S' L' \rangle \end{aligned} \quad (13)$$

Expression 13 gives the crystal-field matrix elements as a product of the radial integrals given in CFC-I, expressions 11-14, by a "3 - j " and a "6 - j " coefficients and by the reduced matrix elements already given in Appendix II of CFC-I. It is useful to relate h_{k0} integrals with the more extended ϵ_0 , Ds , and Dt ones by

$$h_{00} = \epsilon_0 \quad h_{20} = 7Ds \quad h_{40} = 21Dt$$

In Table II the complete crystal-field matrices (eq 13) are given for the d^3 configuration in the $[d^3\alpha SL\Gamma\gamma\alpha]$ basis.¹⁹ In order to complete the energy matrices the constant $3\epsilon_0$, deleted from the table for simplicity, should be added to the diagonal elements. Obviously, this amount will cancel for transitions inside the same configuration.

By changing the sign of the crystal-field and spin-orbit parameters the energy matrices for the d^7 configuration can be obtained from those given in Table II.

Check of the Energy Matrices

If in the matrices given in Table II, calculated in the $[d^3\alpha SL\Gamma\gamma\alpha]$ basis, the spin-orbit parameter vanishes, then, the resultant matrices must be equivalent to the previously calculated ones in the $[d^3\alpha S(M_S)L\Gamma\gamma\alpha]$ basis,⁵ because both are basis of the same vectorial space. Namely, both sets of matrices are different representations of the same Hamiltonian

$$\mathcal{H} = \mathcal{H}_{\text{er}} + V_{D_3h}$$

Therefore, both sets of matrices will transform one another by means of a unitary transformation and, after diagonalizing them, the same energy eigenvalues will be obtained.

Each matrix from Table II was checked against the previously published one and, in the zero-spin orbit limit, both gave the same eigenvalues for the same values of parameters. Moreover, accidental errors in all the matrix elements in Table II were avoided by generating them from fully checked subroutines.

Acknowledgment. The author is much indebted to Professor F. Gomez-Beltran for the provision of working facilities and for his help during the author's affiliation with the Inorganic Chemistry Department. I am also grateful to Dr. S. L. Altmann, from Oxford University, for helpful discussions and his critical reading of the paper. A fellowship of the Ministerio de Educacion y Ciencia, which supported the early steps of this work, is also gratefully acknowledged.

Supplementary and Miniprint Material Available. Appendix I (3 pages) and full-size photocopies of Table

II (12 pages). Ordering information is available on any current masthead page.

References and Notes

- (1) See, for example (a) A. D. Liehr, *J. Phys. Chem.*, **64**, 43 (1960); (b) R. N. Euwema, *J. Chem. Phys.*, **42**, 892 (1965); (c) A. D. Liehr and C. J. Ballhausen, *Ann. Phys.*, **6**, 134 (1959); (d) J. C. Eisenstein, *J. Chem. Phys.*, **34**, 310 (1961); (e) *ibid.*, **34**, 1628 (1961) (erratum in *ibid.*, **35**, 2246 (1961)); (f) W. A. Runciman and K. A. Schroeder, *Proc. R. Soc. London, Ser. A*, **285**, 489 (1962); (g) J. Ferguson, *Aust. J. Chem.*, **23**, 635 (1970); (h) H. A. Weakliem, *J. Chem. Phys.*, **36**, 2117 (1962); (i) K. A. Schroeder, *ibid.*, **37**, 2553 (1962); (j) W.-K. Li, *Spectrochim. Acta, Part A*, **24**, 1573 (1968) (this paper has been extensively revised and corrected by E. König, S. Kremer, and R. Schnakig, *ibid.*, **30**, 1347 (1974)); (k) K. A. Schroeder, *J. Chem. Phys.*, **37**, 1587 (1962).
- (2) (a) R. F. Fenske, D. S. Martin, Jr., and K. Ruedenberg, *Inorg. Chem.*, **1**, 441 (1962); (b) M. Flato, *J. Mol. Spectrosc.*, **17**, 300 (1965); (c) J. R. Perumareddi, *Z. Naturforsch. A*, **27**, 1820 (1972); (d) *J. Phys. Chem.*, **76**, 3401 (1972); (e) H. U. Rahman and W. A. Runciman, *J. Phys. C*, **4**, 1576 (1971); (f) J. R. Perumareddi, *Z. Naturforsch. A*, **28**, 1247 (1973); (g) S. Sugano and M. Peter, *Phys. Rev.*, **122**, 381 (1961); (h) F. Carati, A. Sgamellotti, and V. Valenti, *Accad. Naz. Lincei Rend. Cl. Sci. Fis. Mat. Nat., Ser. VIII*, **45**, 76 (1968).
- (3) C. A. L. Becker, D. W. Meek, and T. M. Dunn, *J. Phys. Chem.*, **72**, 3588 (1968).
- (4) C. A. L. Becker, D. W. Meek, and T. M. Dunn, *J. Phys. Chem.*, **74**, 1568 (1970).
- (5) F. Gomez Beltran and F. Palacio, *J. Phys. Chem.*, **80**, 1373 (1976).
- (6) J. Ferguson, *Prog. Inorg. Chem.*, **12**, 159 (1970).
- (7) H. Bethe, *Ann. Phys.*, **3**, 133 (1929).
- (8) W. Opechowski, *Physica*, **7**, 552 (1940).
- (9) H. Kramers, *Proc. Acad. Sci. Amsterdam*, **33**, 959 (1930).
- (10) G. F. Koster, J. O. Dimmock, R. G. Wheeler, and H. Statz, "Properties of the Thirty-two Point Groups", M.I.T. Press, Boston, Mass., 1963.
- (11) C. J. Bradley and A. P. Cracknell, "The Mathematical Theory of Symmetry in Solids", Clarendon Press, Oxford, 1972.
- (12) Although the highest value of J in the d^3 configuration is 11/2, we have extended the subtraction to $J = 13/2$ in order to be able to use the same table for the d^5 configuration which will be studied in one of the following papers.
- (13) S. L. Altmann, *Proc. Cambridge Phil. Soc.*, **53**, 343 (1957).
- (14) In this paper and in the following ones of this series, the most extended active convention as defined by Bradley and Cracknell (loc. cit. p. 52), will be used. This change, nevertheless, does not modify the results of CFC-I.
- (15) E. P. Wigner, "Group Theory and Its Application to the Quantum Mechanics of Atomic Spectra", Academic Press, New York, N.Y., 1959, Chapter 15.
- (16) M. Tinkham, "Group Theory and Quantum Mechanics", McGraw-Hill, New York, N.Y., 1964, Chapter 5.
- (17) See ref. 13. Although this author uses a definition for the rotation matrix that does not follow the Condon-Shortley phase convention, his results are easily transcribed within this convention.
- (18) See, for example, B. W. Shore and D. H. Menzel, "Principles of Atomic Spectra", Wiley, New York, N.Y., 1968, Chapter 6.
- (19) Complete crystal-field matrices should actually contain the representation of the whole Hamiltonian (1). Then, free ion matrices corresponding to the electrostatic repulsion and spin-orbit coupling terms should be added to the matrices given in Table II. Electrostatic matrices have been given by Racah²⁰ and spin-orbit coupling energy matrices can be readily calculated from the Nielson and Koster tables.²¹ The result of that calculation is given in Appendix I (supplementary material).
- (20) G. Racah, *Phys. Rev.*, **62**, 438 (1942).
- (21) C. W. Nielson and G. F. Koster, "Spectroscopic Coefficients for the p^2 , d^2 and f^2 Configurations", M.I.T. Press, Boston, Mass., 1963.
- (22) H. H. Marvin, *Phys. Rev.*, **47**, 521 (1935).
- (23) J. A. Barnes, B. L. Carroll, L. M. Flores, and R. M. Hedges, *At. Data*, **2**, 1 (1970).

Crystal-Field Calculations with Trigonal Bipyramidal Symmetry Potential. 3. $d^{4,6}$ Configurations[†]

F. Palacio

Departamento de Física Fundamental, Facultad de Ciencias, Universidad de Zaragoza, Zaragoza, Spain (Received December 15, 1976)

Trigonal bipyramidal crystal-field energy matrices for a $d^{4,6}$ configuration in a weak-field scheme have been calculated by using Racah algebra both in the zero and the nonzero spin-orbit limit. The appropriate weak-field basis eigenfunctions as well as the reduced matrix elements for the tensor $\hat{C}^{(k)}$ ($k = 0, 2, 4$) in this configuration are also given. All crystal-field matrices calculated here have been fully checked and the checking procedures are also described.

Introduction

In previous papers of this series, hereafter referred to as CFC-I¹ and CFC-II,² complete energy crystal-field matrices in a weak field of D_{3h} symmetry were calculated for the $d^{3,7}$ configuration. Calculations in this symmetry have been previously done for configurations $d^{1,9,3,6}$, $d^{2,8,3,4,6,8}$ and $d^{3,7,9}$ and in order to discuss spectroscopic data of some compounds with $d^{2,3,5,7,8}$ configurations, Norgett, Thornley, and Venanzi¹⁰ and Wood¹¹ have obtained suitable energy level diagrams. As far as we know, not too much has been said about calculations in d^4 and d^5 configurations in spite of the fact that pentacoordinate compounds with this symmetry are well established in these configurations. In $d^{4,6}$ configurations, e.g., high spin pentacoordinate compounds with bipyramidal trigonal symmetry, Cr(II) and Fe(II) have been described.¹²⁻¹⁶ Those cases with trigonal bipyramidal C_{3v} microsymmetry may also be tried with quite good approximation as D_{3h} ones, because the additional perturbation deforming the equatorial plane, necessary to introduce C_{3v} symmetry, does not entail significant modifications in the relative energies.¹¹ Moreover, a large series of high-spin pentacoordinate Mn(III) compounds has recently been prepared.¹⁷⁻¹⁹ All of them have by general formula MnL_2Cl_3 where L is a monodentate ligand such as dioxane, or arsine, phosphine, pyridine, and substituted pyridine oxides. In spite of what would be expected from their stoichiometric formula, they seem to exhibit a distorted C_{4v} symmetry. The only crystal-field energy matrices which are still required for a deeper study of the electronic spectra and magnetic properties of these pentacoordinate compounds are those for D_{3h} symmetry. Matrices for a crystal field of C_{4v} symmetry are easily obtained from those of D_{4h} symmetry already published,²⁰ on considering the isomorphism between the C_{4v} and D_4 groups and the central symmetry of d orbitals.

In the present paper, therefore, we shall calculate the complete crystal field energy matrices for a $d^{4,6}$ configuration in a weak field of D_{3h} symmetry. In the first part of this work the weak-field matrices at zero spin-orbit limit are calculated, and in the second part the case of non-vanishing spin-orbit coupling is also considered. Finally, the third part of the paper deals with a description of the checking procedures that have been used in order to guarantee the reliability of our calculations. The splitting produced in a d^4 configuration under the action of a strong crystal field of D_{3h} symmetry is also considered in that section.

[†] This work was supported in part by Junta de Energia Nuclear, Spain.

Crystal-Field Matrices at Zero Spin-Orbit Limit

We shall obtain in this section the energy matrices of the Hamiltonian

$$\mathcal{H} = \mathcal{H}_{\text{er}} + V_{D_{3h}} \quad (1)$$

in a $\{d^4\alpha SL\Gamma\gamma a\}$ weak-field representation. As in previous papers Γ characterizes the irreducible representation in the D_{3h} group, γ distinguishes the different degenerate states, if any, contained in Γ , and a is a label distinguishing states with equal S and Γ .

The form of the crystal-field potential with D_{3h} symmetry, and the general form of the energy matrices for configuration $d^{3,7}$, was given in expressions 3 and 10, respectively, of CFC-I. After an obvious translation of expressions 10 and 15 of CFC-I to the case of a d^4 configuration, we have

$$\begin{aligned} \langle d^4\alpha SL\Gamma\gamma a | V_{D_{3h}} | d^4\alpha' S' L' \Gamma' \gamma' a' \rangle &= \delta_{\Gamma\Gamma'} \delta_{\gamma\gamma'} \delta_{aa'} \times \\ &\sum_{M_L M_L'} \langle \alpha SL\Gamma a | \alpha S L M_L \rangle \times \\ &\langle \alpha' S' L' M_L' | \alpha' S' L' \Gamma' \gamma' a' \rangle (-1)^{L-M_L} \times \\ &\sum_{k=0,2,4} h_{k0}(3d; 3d) \begin{pmatrix} L & k & L' \\ -M_L & 0 & M_L' \end{pmatrix} \times \\ &\langle d^4\alpha SL || \hat{C}^{(k)} || d^4\alpha' S' L' \rangle \end{aligned} \quad (2)$$

where

$$\begin{aligned} \langle d^4\alpha SL || \hat{C}^{(k)} || d^4\alpha' S' L' \rangle &= \delta_{SS'} 20[(2L+1)(2L'+1)]^{1/2} \begin{pmatrix} 2 & k & 2 \\ 0 & 0 & 0 \end{pmatrix} \times \\ &\sum_{\overline{\alpha} \overline{S} \overline{L}} (-1)^{\overline{L}+k+L} \langle d^4\alpha SL \{ d^3(\overline{\alpha} \overline{S} \overline{L}) d\alpha SL \} \times \\ &\langle d^3(\overline{\alpha} \overline{S} \overline{L}') d\alpha' S' L' \rangle \langle d^4\alpha' S' L' \rangle \times \\ &\left\{ \begin{matrix} \overline{L} & 2 & L \\ k & L' & 2 \end{matrix} \right\} \delta_{\overline{\alpha}\alpha'} \delta_{\overline{S}S'} \delta_{\overline{L}L'} \end{aligned} \quad (3)$$

The radial components, h_{k0} , of relation 2 have been described in eq 11-13 of CFC-I.

The appropriate eigenfunctions to be used in expression 2 may be easily derived with the method given in CFC-II. The explicit form of these functions will be essentially the same as those given in Table I of CFC-I after adequate modifications. It is only necessary to add the eigenstates originated from the subduction of the term 4I . In Table I a compact form of these eigenfunctions is given. Likewise, in Appendix I²¹ the reduced matrix elements

TABLE I: $d^{4,6}$ Eigenfunctions in $\{\alpha SL\Gamma\gamma a\}$ and $\{\alpha SLJ\Gamma\gamma a\}$ Representations^{a,b}

$ \alpha SL(J)A_1'(a)\rangle = \alpha SL(J)0\rangle$	{Even values of $L(J)$ }
$ \alpha SL(J)A_1'(b)\rangle = \sqrt{1/2}(\alpha SL(J)6\rangle + \alpha SL(J)-6\rangle)$	
$ \alpha SL(J)A_2'(a)\rangle = \alpha SL(J)0\rangle$	{Odd values of $L(J)$ }
$ \alpha SL(J)A_2'(b)\rangle = \sqrt{1/2}(\alpha SL(J)6\rangle - \alpha SL(J)-6\rangle)$	
$ \alpha SL(J)A_1''\rangle = \sqrt{1/2}(\alpha SL(J)3\rangle \pm \alpha SL(J)-3\rangle)$	{+ with even values of $L(J)$ }
$ \alpha SL(J)A_2''\rangle = \sqrt{1/2}(\alpha SL(J)3\rangle \pm \alpha SL(J)-3\rangle)$	{+ with odd values of $L(J)$ }
$ \alpha SL(J)E'(a)\rangle = \alpha SL(J) \pm 2\rangle$	
$ \alpha SL(J)E'(b)\rangle = \alpha SL(J) \pm 4\rangle$	
$ \alpha SL(J)E''(a)\rangle = \alpha SL(J) \pm 1\rangle$	
$ \alpha SL(J)E''(b)\rangle = \alpha SL(J) \pm 5\rangle$	

^a In a $\{\alpha SL\Gamma\gamma a\}$ representation (J) must be ignored. In a $\{\alpha SLJ\Gamma\gamma a\}$ representation brackets for J must be suppressed and Bethe's notation²³ followed. ^b Although both doublet components are given, γ is not explicitly included, since we have not used it to distinguish them; a values have been used when necessary.

defined in expression 3 are given for $k = 0, 2, 4$.

The electronic repulsion term in Hamiltonian (1) is diagonal in Γ, γ, a, S , and L so that by adding to the crystal-field matrices from expression 2, the free-ion electronic repulsion ones, complete energy matrices in this Hamiltonian are obtained. Complete crystal-field matrices so calculated are given in Table II as functions of Racah parameters A, B , and C and the ϵ_0, Ds , and Dt crystal-field parameters. The relation between these crystal-field parameters and h_{k0} here used is

$$h_{00} = \epsilon_0 \quad h_{20} = 7Ds \quad h_{40} = 21Dt \quad (4)$$

The energy matrices for the d^6 configuration may be obtained from those of Table II by changing the sign of the crystal-field parameters.

Let us make, before going forward, a useful consideration about the form of the wavefunctions. As it may be realized, we can consider that, in a broad sense, there is in the D_{3h} group a one-to-one relation between $|M\rangle$ and Γ^{22} , therefore we may extend the results discussed in CFC-II for the D_{3h}^* group to our actual case. In order to support this consideration there is, however, a point which needs clarification. We can see from Table I that for values of $|M|$ such that $|M| = 3, 6$ there are, actually, two irreducible representations Γ for each, which destroy the one-to-one relation between $|M|$ and Γ . Owing to the form of the crystal-field potential in this symmetry, however, an accidental degeneracy appears between these states which restores the relation in question. Let us justify this accidental degeneracy.

In the expression of the crystal-field potential in D_{3h} symmetry

$$V_{D_{3h}} = \sum_{k,q} E_{kq} C_q^{(k)}(\theta, \phi) \quad k = 0, 2, 4; q = 0 \quad (5)$$

there are nonvanishing terms only for $q = 0$ when we are interested in the integration over d electrons. It follows then that the "3-j" value, which appears from the application of the Wigner-Eckart theorem, may be reduced to

$$\begin{pmatrix} L & k & L' \\ -M_L & q & M_L' \end{pmatrix} = \delta_{M_L M_L'} \begin{pmatrix} L & k & L' \\ -M_L & 0 & M_L' \end{pmatrix} \quad (6)$$

An immediate consequence from (6) is that the calculation of any matrix element between states of any of these representations will be reduced, at least, to half a sum of two terms, one with $M > 0$ and another with $M < 0$, the equality of which will now be proved.

It follows from the symmetry properties of the "3-j" coefficients that

$$\begin{pmatrix} L & k & L' \\ -M_L & 0 & M_L' \end{pmatrix} = (-1)^{L+L'} \begin{pmatrix} L & k & L' \\ M_L & 0 & -M_L' \end{pmatrix} \quad (7)$$

It is obviously necessary in eq 7 to take into account the two cases in which the parities of L and L' are either equal or opposite. Likewise, the parity of L can be seen from Table I to establish a difference in the form of the wavefunction. In the representation A_1'' , e.g., if L is an even number, the expression of the state is $\sqrt{1/2}(|L3\rangle + |L-3\rangle)$ but, if it is an odd number, the state must be expressed by $\sqrt{1/2}(|L3\rangle - |L-3\rangle)$. So, we always have that

$$\langle L3 | V_{D_{3h}} | L'3 \rangle = \langle L-3 | V_{D_{3h}} | L'-3 \rangle \quad (8)$$

and, finally

$$\begin{aligned} \langle LA_1'' | V_{D_{3h}} | L'A_1'' \rangle &= \langle L3 | V_{D_{3h}} | L'3 \rangle = \\ \langle LA_2'' | V_{D_{3h}} | L'A_2'' \rangle \end{aligned} \quad (9)$$

and accidental degeneracy has been established. The same happens with the A_1' and A_2' states for $|M| = 6$.

After these considerations, eq 2 may be simplified to

$$\begin{aligned} \langle d^4 \alpha S L M_L | V_{D_{3h}} | d^4 \alpha' S' L' M_L' \rangle &= \\ \delta_{M_L M_L'} (-1)^{L-M_L} \times \\ \sum_{k=0,2,4} h_{k0} \begin{pmatrix} L & k & L' \\ -M_L & 0 & M_L' \end{pmatrix} \times \\ \langle d^4 \alpha S L || \hat{C}^{(k)} || d^4 \alpha' S' L' \rangle \end{aligned} \quad (10)$$

Energy Matrices Calculation at Nonzero Spin-Orbit Coupling

In previous calculations the spin-orbit coupling term in the Hamiltonian has been neglected. Let us consider it now and obtain the energy matrices from the Hamiltonian

$$\mathcal{H} = \mathcal{H}_{er} + \mathcal{H}_{so} + V_{D_{3h}} \quad (11)$$

already described in CFC-II, in the $\{d^4 \alpha SLJ\Gamma\gamma a\}$ representation.

Due to the even number of electrons, J is an integer and then the wavefunctions have a form similar to the previous ones. In Table I these eigenfunctions are given. By using this set of wavefunctions the Hamiltonian (11) can be reduced to 10 blocks of the following dimensions²³

$$\begin{aligned} |\Gamma_1(a)| &= 22 & |\Gamma_1(b)| &= |\Gamma_2(b)| = 2 & |\Gamma_2(a)| &= 12 \\ |\Gamma_3| &= |\Gamma_4| = 17 & |\Gamma_6(a)| &= 25 & |\Gamma_6(b)| &= 11 \\ |\Gamma_5(a)| &= 29 & |\Gamma_5(b)| &= 4 \end{aligned}$$

$\langle \alpha(S)LJ\gamma \hat{U}_{D_{3h}} \alpha'(S')L'\gamma' \rangle$	Ds	Dt	$\langle \alpha(S)LJ\gamma \hat{U}_{D_{3h}} \alpha'(S')L'\gamma' \rangle$	Ds	Dt	$\langle \alpha(S)LJ\gamma \hat{U}_{D_{3h}} \alpha'(S')L'\gamma' \rangle$	Ds	Dt			
4(3)05	4(3)05	-4/25	1/2	4(1)P3	4(1)04	-2/11/105	15/2577/2	4(3)P4	4(3)H4	-4/27/11/15	-3/2/22
4(3)04	4(3)04	2/10/11/25	-2/10/11/3		4(1)16	C	-28/(3/11)	4(3)H4	4(3)H5	-4/(5/3)	-3/3/2
4(3)H5	4(3)H5	8/25	3/6	2(1)04	2(1)04	8/21	-11/21	4(3)H4	4(3)H6	-4/25/3	-15/375/2
4(3)H6	4(3)H6	-32/25/5/5	5/10/11/3	4(1)04	4(1)04	8/(21/11)	20/11/21	4(3)04	4(3)04	17/50	-3/2
4(3)H4	4(3)H4	208/625	-2	4(1)16	4(1)16	8/77/85	0	4(3)05	4(3)05	-1/25	3
4(3)H5	4(3)H5	13/4/11/15	2/5/11	4(1)04	4(1)04	-100/231	-17/42	4(3)H4	4(3)H4	-28/5/11/25	-7/2/6
4(3)H6	4(3)H6	-4/7/5/165	0	4(1)16	4(1)16	32/77/11	0	4(3)H5	4(3)H5	-4/25	-1/2
4(3)H5	4(3)H5	5/25	-4/9	4(1)16	4(1)16	10/11	-2/3	4(3)H6	4(3)H6	4/(5/11)	9/(2/11)
4(3)H6	4(3)H6	4/2/5/5	20/10/11/9	Matrix $\Gamma_6(b)_2$ $ M = 4$				4(3)05	4(3)05	4/25	2
4(3)H6	4(3)H6	5/11	4/9	$\langle \alpha(S)LJ\gamma \hat{U}_{D_{3h}} \alpha'(S')L'\gamma' \rangle$	Ds	Dt		4(3)H4	4(3)H4	4/5/11/25	2/2/33
2(1)02	2(1)02	1/7	4/21	4(5)04	4(5)04	2	-1	4(3)H5	4(3)H5	-8/25	1
4(1)02	4(1)02	12/2/7	10/2/21	2(3)P4	2(3)P4	-1/3	-1	4(3)H6	4(3)H6	-32/(5/11)	-1/1/11
4(1)P3	4(1)P3	0	2/35/3	4(3)P4	4(3)P4	-7/3	0	4(3)H4	4(3)H4	-728/825	28/11
2(1)04	2(1)04	-1/(1/3)	10/3/7	4(3)04	4(3)04	-3/3/5	-4/1/3	4(3)H5	4(3)H5	26/25/33/25	-4/6/11
4(1)04	4(1)04	-8/11/3/7	10/3/11/7	4(3)05	4(3)05	-6/3/5	-8/4/3	4(3)H6	4(3)H6	-7/3/55	4/6/11
4(1)16	4(1)16	0	-4/35/11/3	4(3)H4	4(3)H4	-4/27/11/15	2/27/11	4(3)H5	4(3)H5	-8/25	-8/3
4(1)02	4(1)02	6/7	-16/21	4(3)H5	4(3)H5	-4/27/11/15	2/27/11	4(3)H6	4(3)H6	4/(5/11)	-4/(3/11)
4(1)P3	4(1)P3	2/10/7	4/5/4/3	4(3)H6	4(3)H6	-4/(5/3)	2/3	2(1)04	2(1)04	-4/3	2/3
2(1)04	2(1)04	-10/27/3/7	-10/6/7	4(3)P4	4(3)P4	-11/2	3/2	4(1)04	4(1)04	-4/(3/11)	-4/(3/11)
4(1)04	4(1)04	-2/27/3/7	-65/3/22/7	4(3)04	4(3)04	-2/3/10	1/(2/3)	4(1)16	4(1)16	2/27/11	20/27/11
4(1)16	4(1)16	1	2/10/11/3	4(3)05	4(3)05	-2/3/5	1/4/3	4(1)04	4(1)04	50/33	17/33
4(1)P3	4(1)P3	1	7/6					4(1)16	4(1)16	8/27/11	-25/2/11
2(1)04	2(1)04	-4/27/3	0					4(1)16	4(1)16	-2/11	64/11

TABLE IV: Strong Crystal-Field States in a d^4 Configuration

Configuration	$\langle V_{D_{3h}} \rangle$	Splitting after \mathcal{H}_{cr}	Splitting after $\mathcal{H}_{cr} + \mathcal{H}_{so}$
$(e'')^4$	$4e_0 + 4Ds - 16Dt$	$^1A_1'$	Γ_1
$(e'')^3(e')^1$	$4e_0 + Ds - 11Dt$	$^3A_1'', ^3A_2'', ^3E'', ^1A_1'', ^1A_2'', ^1E''$	$\Gamma_1, \Gamma_2, 2\Gamma_3, 2\Gamma_4, 2\Gamma_5, 3\Gamma_6$
$(e'')^3(a_1')^1$	$4e_0 + 5Ds - 6Dt$	$^3E'', ^1E''$	$\Gamma_1, \Gamma_2, 2\Gamma_5, \Gamma_6$
$(e'')^2(e')^2$	$4e_0 - 2Ds - 6Dt$	$^5A_1', ^3A_1', ^2^3A_2', ^2^3E', ^3^1A_1', ^1A_2', ^3^1E'$	$6\Gamma_1, 2\Gamma_2, 2\Gamma_3, 2\Gamma_4, 6\Gamma_5, 6\Gamma_6$
$(e'')^2(a_1')^2$	$4e_0 + 6Ds + 4Dt$	$^3A_2', ^1A_1', ^1E'$	$2\Gamma_1, \Gamma_5, \Gamma_6$
$(e'')^2(e')^1(a_1')^1$	$4e_0 + 2Ds - Dt$	$^5E', ^3A_1', ^3A_2', ^4^3E', ^1A_1', ^1A_2', ^3^1E'$	$3\Gamma_1, 3\Gamma_2, 5\Gamma_3, 5\Gamma_4, 7\Gamma_5, 9\Gamma_6$
$(e')^2(a_1')^2$	$4e_0 + 14Dt$	$^3A_2', ^1A_1', ^1E'$	$2\Gamma_1, \Gamma_5, \Gamma_6$
$(e'')^2(e')^1(a_1')^1$	$4e_0 - Ds + 4Dt$	$^5E', ^3A_1', ^3A_2', ^4^3E'', ^1A_1'', ^1A_2'', ^3^1E''$	$5\Gamma_1, 5\Gamma_2, 3\Gamma_3, 3\Gamma_4, 9\Gamma_5, 7\Gamma_6$
$(e'')^1(e')^3$	$4e_0 - 5Ds - Dt$	$^3A_1'', ^3A_2'', ^3E'', ^1A_1'', ^1A_2'', ^1E''$	$\Gamma_1, \Gamma_2, 2\Gamma_3, 2\Gamma_4, 2\Gamma_5, 3\Gamma_6$
$(e'')^1(e')^1(a_1')^2$	$4e_0 + 3Ds + 9Dt$	$^3A_1'', ^3A_2'', ^3E'', ^1A_1'', ^1A_2'', ^1E''$	$\Gamma_1, \Gamma_2, 2\Gamma_3, 2\Gamma_4, 2\Gamma_5, 3\Gamma_6$
$(e')^3(a_1')^1$	$4e_0 - 4Ds + 9Dt$	$^3E', ^1E'$	$\Gamma_3, \Gamma_4, \Gamma_5, 2\Gamma_6$
$(e')^4$	$4e_0 - 8Ds + 4Dt$	$^1A_1'$	Γ_1

Since accidental degeneracy permits us to use $|M|$ as a good quantum number, the subduction of the $|d^4\alpha SLJM\rangle$ states onto the $|d^4\alpha SLJ\gamma\rangle$ ones will be automatic because we may label the irreducible representations with $|M|$ just as well as with Γ . We may therefore use expression 13 from CFC-II to calculate energy matrices of the crystal-field potential in this representation. So, for a d^4 configuration we have

$$\langle d^4\alpha SLJM | V_{D_{3h}} | d^4\alpha' S' L' J' M' \rangle = \delta_{MM'} \sum_{k=0,2,4} h_{k0} (-1)^{S+L'-M} [(2J+1)(2J'+1)]^{1/2} \begin{pmatrix} J & k & J' \\ -M & 0 & M' \end{pmatrix} \begin{Bmatrix} L & J & S \\ J' & L' & k \end{Bmatrix} \times \langle d^4\alpha SL || \hat{C}^{(k)} || d^4\alpha' S' L' \rangle \quad (12)$$

where the reduced matrix elements appear in Appendix I.²¹

The electronic repulsion and spin-orbit coupling terms in Hamiltonian (11) are diagonal in J and M so that, by adding the crystal-field matrices derived from (12), the free ion electronic repulsion and spin-orbit coupling terms, complete energy matrices of this Hamiltonian will be obtained. In Table III the crystal field matrices (eq 12) are given for the d^4 configuration in the $|d^4\alpha SLJ\gamma\rangle$ representation. Electronic repulsion matrices have been given by Racah²⁴ and are given in the matrices of Table II. Spin-orbit matrices can readily be calculated from the Nielson and Koster tables²⁵ and in order to guarantee the consistency with the wave functions herein used they are given in Appendix II.²¹

In order to complete the energy matrices, the constant $4e_0$, deleted from Table III for simplicity, should be added to the diagonal elements. This amount will cancel if we are considering energetic transitions inside the same configuration.

The energy matrices for a d^6 configuration may be obtained from those of Table III by changing the sign of the crystal-field and spin-orbit parameters.

Check of the Energy Matrices

As previously described, complete crystal field matrices are actually the sum of three matrices, two corresponding to interelectronic repulsion and spin-orbit coupling in the free ion, and the third corresponding to the crystal-field interaction. There is no problem for checking the first two because they may be easily worked out from the Nielson and Koster tables.²³ The problem therefore reduces to the checking of the crystal-field matrices. The same situation arises with the matrices given in Table II for the zero spin-orbit coupling limit.

If both electronic repulsion and spin-orbit terms are neglected in the Hamiltonians given in (1) and (11), the resulting matrices from Tables II and III must give the same energy eigenvalues when the same values of the crystal-field parameters are used. These energy eigenvalues must fit, also in the same parametric conditions, with the resulting ones from a strong-field representation where both electronic repulsion and spin-orbit terms have been ignored. In Table IV expressions for the resulting crystal-field energies in this strong-field representation are given. Successive splitting of crystal-field states produced first by electronic repulsion, and secondly by electronic

repulsion and spin-orbit coupling are also given in this table.

All the matrices from Tables II and III were successfully checked against themselves and against the strong-field states given in Table IV. Moreover, accidental errors in all the matrices elements in Tables II and III were avoided by generating them from fully checked subroutines.

Acknowledgment. The author is much indebted to Dr. S. L. Altmann, from Oxford University, for his critical reading of this paper.

Supplementary and Miniprint Material Available. Appendices I and II (6 pages) and full-size photocopies of Tables II and III (40 pages). Ordering information is available on any current masthead page.

References and Notes

- (1) F. Gomez Beltran and F. Palacio, *J. Phys. Chem.*, **80**, 1373 (1976).
- (2) F. Palacio, *J. Phys. Chem.*, preceding paper in this issue.
- (3) M. Ciampolini, *Inorg. Chem.*, **5**, 35 (1966).
- (4) R. Polak and V. Cerny, *J. Phys. Chem. Solids*, **29**, 945 (1968).
- (5) S. T. Spees, Jr., J. R. Perumareddi, and A. W. Adamson, *J. Phys. Chem.*, **72**, 1822 (1968).
- (6) C. A. L. Becker, D. W. Meek, and T. M. Dunn, *J. Phys. Chem.*, **72**, 3588 (1968).
- (7) M. N. S. Murthy, A. P. B. Sinha, and A. S. Aple, *Indian Pure Appl. Phys.*, **8**, 473 (1970).
- (8) C. A. L. Becker, D. W. Meek, and T. M. Dunn, *J. Phys. Chem.*, **74**, 1568 (1970).
- (9) J. A. Varga and C. A. L. Becker, *J. Phys. Chem.*, **76**, 2907 (1972).
- (10) M. J. Norgett, J. H. M. Thornley, and L. M. Venanzi, *J. Chem. Soc. A*, 540 (1967).
- (11) J. S. Wood, *Inorg. Chem.*, **7**, 852 (1968).
- (12) J. S. Wood, *Prog. Inorg. Chem.*, **16**, 332 (1972).
- (13) M. Ciampolini, *Struct. Bonding*, **6**, 52 (1969).
- (14) M. Ciampolini, *Chem. Commun.*, 47 (1966).
- (15) M. Ciampolini and N. Nardi, *Inorg. Chem.*, **5**, 1150 (1966).
- (16) M. DiVaira and P. L. Orioli, *Acta Crystallogr., Sect. B*, **24**, 1269 (1968).
- (17) M. A. Ciriano, Ph.D. Thesis, University of Zaragoza, Spain, 1974.
- (18) M. Valderrama, Ph.D. Thesis, University of Zaragoza, Spain, 1976.
- (19) R. Uson, V. Riera, M. A. Ciriano, and M. Valderrama, *Transition Met. Chem.*, **1**, 122 (1976).
- (20) J. R. Perumareddi, *J. Phys. Chem.*, **78**, 2678 (1974).
- (21) Available as supplementary material. See paragraph at end of the text regarding supplementary material.
- (22) We are referring to d electrons. In general this consideration would not be valid for $l \geq 3$.
- (23) We are using the convention of labeling the spin-orbital representations with Bethe's Γ notation. For single-valued representations the correspondences between Bethe's and Mulliken's notations is as follows: $A_1' = \Gamma_1$; $A_2' = \Gamma_2$; $A_1'' = \Gamma_3$; $A_2'' = \Gamma_4$; $E' = \Gamma_5$; and $E'' = \Gamma_6$.
- (24) G. Racah, *Phys. Rev.*, **62**, 438 (1942).
- (25) G. W. Nielson and G. F. Koster, "Spectroscopic Coefficient for the p^n , d^n and f^n Configurations", M.I.T. Press, Boston, Mass., 1963.
- (26) J. A. Barnes, B. L. Carroll, L. M. Flores, and R. M. Hedges, *At. Data*, **2**, 1 (1970).

Crystal-Field Calculations with Trigonal Bipyramidal Symmetry Potential. 4. d^5 Configuration†

F. Palacio

Departamento de Física Fundamental, Facultad de Ciencias, Universidad de Zaragoza, Zaragoza, Spain (Received December 15, 1976)

Trigonal bipyramidal crystal-field energy matrices for a d^5 configuration in a weak-field scheme have been calculated by using Racah algebra both in the zero and the nonzero spin-orbit limit. The appropriate weak-field basis eigenfunctions as well as the reduced matrix elements for the tensor $\hat{C}^{(k)}$ ($k = 0, 2, 4$) in this configuration are also given. All crystal-field matrices calculated here have been fully checked and the checking procedures are also described.

Introduction

In previous papers of this series, hereafter referred to as CFC-I,¹ CFC-II,² and CFC-III,³ and in the work of Becker et al.,⁴⁻⁶ complete energy matrices in a crystal-field of D_{3h} symmetry for all d^n configurations except d^5 were calculated. Although pentacoordination in d^5 configurations is not very common, there are enough examples in trigonal bipyramidal symmetry⁷⁻¹³ to allow us to consider this arrangement of ligands as well established. This symmetry is moreover the highest one with coordination number five, so it will be the most suitable for a half-filled spherically symmetric shell such as the d^5 configuration.¹⁴ On the other hand, owing to the fact that the d shell is half filled, crystal-field interaction does not split up in the atomic energy levels in the first order. Thus complete crystal-field energy matrices are required for calculations, and it is probably due to the lack of these energy matrices that there have not been many accurate calculations in d^5 complexes with this symmetry.

The goal of the present paper is to provide complete

crystal-field energy matrices for this configuration in a weak-field of D_{3h} symmetry. In the first part of this work the weak-field matrices in the zero spin-orbit limit are calculated, and in the second part the case of nonvanishing spin-orbit coupling is also considered. Finally, the third part of the paper deals with the checking procedures that have been used in order to guarantee the reliability of our calculations. In order to check these matrices against states calculated in some other representation, the splitting produced in a d^5 configuration under the action of a strong crystal field of D_{3h} symmetry is also considered.

Crystal-Field Matrices at Zero Spin-Orbit Limit

In this section we are interested in working out energy matrices of Hamiltonian

$$\mathcal{H} = \mathcal{H}_e + V_{D_{3h}} \quad (1)$$

in a $\{d^5 \alpha SL \Gamma \gamma a\}$ weak-field representation. As in previous papers of this series Γ characterizes the irreducible representation in the D_{3h} group, γ distinguishes the different degenerate states contained in Γ , if any, and a is a label distinguishing states with equal S and Γ .

† This work was supported in part by Junta de Energía Nuclear, Spain.

TABLE I

d^5 Trigonal Bipyramidal Energy Matrices
in the zero spin-orbit limit

$${}^4A_1'({}^4S_0) = 5c_e + 10A - 35B$$

$${}^4E'({}^4D_0) = 5c_e + 10A - 25B + 5C$$

$${}^4A_1'({}^4G_6) = 5c_e + 10A - 24B + 8C = {}^4A_2'({}^4G_6)$$

${}^4E'$	${}^4E'$
$5c_e + 10A - 18B + 5C$	$5c_e + 10A - 25B + 5C$
${}^4A_1'$	${}^4A_1'$
$5c_e + 10A - 28B + 7C$	$5c_e + 10A - 13B + 7C$
${}^4A_1' = {}^4A_2'$	${}^4A_1' = {}^4A_2'$
$5c_e + 10A - 13B + 7C$	$5c_e + 10A - 25B + 5C$
${}^4E'({}^4G_6)$	${}^4E'({}^4G_6)$
$5c_e + 10A - 18B + 5C$	$5c_e + 10A - 13B + 7C$
${}^4E'({}^4G_6)$	${}^4E'({}^4G_6)$
$5c_e + 10A - 18B + 5C$	$5c_e + 10A - 25B + 5C$

${}^4E'$	${}^4E'$
$5c_e + 10A - 18B + 5C$	$5c_e + 10A - 25B + 5C$
${}^4A_1'$	${}^4A_1'$
$5c_e + 10A - 28B + 7C$	$5c_e + 10A - 13B + 7C$
${}^4A_1' = {}^4A_2'$	${}^4A_1' = {}^4A_2'$
$5c_e + 10A - 13B + 7C$	$5c_e + 10A - 25B + 5C$
${}^4E'({}^4G_6)$	${}^4E'({}^4G_6)$
$5c_e + 10A - 18B + 5C$	$5c_e + 10A - 13B + 7C$
${}^4E'({}^4G_6)$	${}^4E'({}^4G_6)$
$5c_e + 10A - 18B + 5C$	$5c_e + 10A - 25B + 5C$

${}^4E'$	${}^4E'$
$5c_e + 10A - 18B + 5C$	$5c_e + 10A - 25B + 5C$
${}^4A_1'$	${}^4A_1'$
$5c_e + 10A - 28B + 7C$	$5c_e + 10A - 13B + 7C$
${}^4A_1' = {}^4A_2'$	${}^4A_1' = {}^4A_2'$
$5c_e + 10A - 13B + 7C$	$5c_e + 10A - 25B + 5C$
${}^4E'({}^4G_6)$	${}^4E'({}^4G_6)$
$5c_e + 10A - 18B + 5C$	$5c_e + 10A - 13B + 7C$
${}^4E'({}^4G_6)$	${}^4E'({}^4G_6)$
$5c_e + 10A - 18B + 5C$	$5c_e + 10A - 25B + 5C$

${}^4E'$	${}^4E'$
$5c_e + 10A - 18B + 5C$	$5c_e + 10A - 25B + 5C$
${}^4A_1'$	${}^4A_1'$
$5c_e + 10A - 28B + 7C$	$5c_e + 10A - 13B + 7C$
${}^4A_1' = {}^4A_2'$	${}^4A_1' = {}^4A_2'$
$5c_e + 10A - 13B + 7C$	$5c_e + 10A - 25B + 5C$
${}^4E'({}^4G_6)$	${}^4E'({}^4G_6)$
$5c_e + 10A - 18B + 5C$	$5c_e + 10A - 13B + 7C$
${}^4E'({}^4G_6)$	${}^4E'({}^4G_6)$
$5c_e + 10A - 18B + 5C$	$5c_e + 10A - 25B + 5C$

TABLE II

d^4 Trigonal Bipyramidal Energy Matrices in the (d^4S_{22}) Representation
(non-zero elements only; (S) should be understood here as 25×1)

${}^4E'$	${}^4E'$
$5c_e + 10A - 18B + 5C$	$5c_e + 10A - 25B + 5C$
${}^4A_1'$	${}^4A_1'$
$5c_e + 10A - 28B + 7C$	$5c_e + 10A - 13B + 7C$
${}^4A_1' = {}^4A_2'$	${}^4A_1' = {}^4A_2'$
$5c_e + 10A - 13B + 7C$	$5c_e + 10A - 25B + 5C$
${}^4E'({}^4G_6)$	${}^4E'({}^4G_6)$
$5c_e + 10A - 18B + 5C$	$5c_e + 10A - 13B + 7C$
${}^4E'({}^4G_6)$	${}^4E'({}^4G_6)$
$5c_e + 10A - 18B + 5C$	$5c_e + 10A - 25B + 5C$

${}^4E'$	${}^4E'$
$5c_e + 10A - 18B + 5C$	$5c_e + 10A - 25B + 5C$
${}^4A_1'$	${}^4A_1'$
$5c_e + 10A - 28B + 7C$	$5c_e + 10A - 13B + 7C$
${}^4A_1' = {}^4A_2'$	${}^4A_1' = {}^4A_2'$
$5c_e + 10A - 13B + 7C$	$5c_e + 10A - 25B + 5C$
${}^4E'({}^4G_6)$	${}^4E'({}^4G_6)$
$5c_e + 10A - 18B + 5C$	$5c_e + 10A - 13B + 7C$
${}^4E'({}^4G_6)$	${}^4E'({}^4G_6)$
$5c_e + 10A - 18B + 5C$	$5c_e + 10A - 25B + 5C$

${}^4E'$	${}^4E'$
$5c_e + 10A - 18B + 5C$	$5c_e + 10A - 25B + 5C$
${}^4A_1'$	${}^4A_1'$
$5c_e + 10A - 28B + 7C$	$5c_e + 10A - 13B + 7C$
${}^4A_1' = {}^4A_2'$	${}^4A_1' = {}^4A_2'$
$5c_e + 10A - 13B + 7C$	$5c_e + 10A - 25B + 5C$
${}^4E'({}^4G_6)$	${}^4E'({}^4G_6)$
$5c_e + 10A - 18B + 5C$	$5c_e + 10A - 13B + 7C$
${}^4E'({}^4G_6)$	${}^4E'({}^4G_6)$
$5c_e + 10A - 18B + 5C$	$5c_e + 10A - 25B + 5C$

${}^4E'$	${}^4E'$
$5c_e + 10A - 18B + 5C$	$5c_e + 10A - 25B + 5C$
${}^4A_1'$	${}^4A_1'$
$5c_e + 10A - 28B + 7C$	$5c_e + 10A - 13B + 7C$
${}^4A_1' = {}^4A_2'$	${}^4A_1' = {}^4A_2'$
$5c_e + 10A - 13B + 7C$	$5c_e + 10A - 25B + 5C$
${}^4E'({}^4G_6)$	${}^4E'({}^4G_6)$
$5c_e + 10A - 18B + 5C$	$5c_e + 10A - 13B + 7C$
${}^4E'({}^4G_6)$	${}^4E'({}^4G_6)$
$5c_e + 10A - 18B + 5C$	$5c_e + 10A - 25B + 5C$

$\langle \sigma(5) \rangle_{\text{eff}} / \langle \sigma(2) \rangle_{\text{eff}} \langle J_{\text{eff}} \rangle_{\text{eff}}$	$\langle \sigma(1) \rangle_{\text{eff}} / \langle \sigma(2) \rangle_{\text{eff}} \langle J_{\text{eff}} \rangle_{\text{eff}}$	$\langle \sigma_0 \rangle$	$\langle \sigma_1 \rangle$
$\langle \sigma(4) \rangle_{\text{eff}} / 2$	$5(4/1011/2)$	2.4773	5.4773
	$5(4/108/2)$	-2.4773	-5.4773
	$5(4/1017/2)$	-4.9773	-10.4773
	$5(4/105/2)$	4.9773	10.4773
$\langle \sigma(4) \rangle_{\text{eff}} / 2$	$5(4/1011/2)$	-2.4773	-5.4773
	$5(4/105/2)$	$3.4773/1/2$	$2.4773/1/2$
	$5(4/1017/2)$	$-6.4773/1/2$	$-12.4773/1/2$
	$5(4/105/2)$	$-5.4773/1/2$	$-6.4773/1/2$

$\alpha(2)w(1)/2(\gamma)_{0,2n}$	$10^4[8^4(1/2)^{1/2}]^{1/2}$	α_0	β_0
$j(2)j(1)/2$	$1(1205)/2$	$-2\sqrt{2}/5$	0
	$1(1203)/2$	$\sqrt{2}/5$	0
	$5(1205)/2$	$\sqrt{2}$	0
	$5(1203)/2$	$-\sqrt{2}$	0
	$5(2305)/2$	$-24\sqrt{35}/7$	$-5\sqrt{15}/14$
	$5(2115)/2$	$-8\sqrt{17}/5$	$-9\sqrt{5}/7$
	$5(1105)/2$	ϵ	$-5\sqrt{5}/3$
	$5(1103)/2$	ϵ	$5\sqrt{13}/6$

$\alpha(S) \cup \beta(S) \cup \gamma(S) \cup \gamma_{\beta\alpha}$	De	Di
$\{2, 1, 2\}$	$\{2, 1, 0\}$	$\{1, 0, 0\}$
$\{2, 1, 1\}$	$\{2, 0, 1\}$	$\{1, 0, 0\}$
$\{2, 1, 0\}$	$\{2, 0, 0\}$	$\{1, 0, 0\}$
$\{2, 0, 2\}$	$\{2, 0, 0\}$	$\{1, 0, 0\}$
$\{2, 0, 1\}$	$\{2, 0, 0\}$	$\{1, 0, 0\}$
$\{2, 0, 0\}$	$\{2, 0, 0\}$	$\{1, 0, 0\}$
$\{1, 2, 2\}$	$\{1, 1, 1\}$	$\{1, 0, 0\}$
$\{1, 2, 1\}$	$\{1, 1, 0\}$	$\{1, 0, 0\}$
$\{1, 2, 0\}$	$\{1, 1, 0\}$	$\{1, 0, 0\}$
$\{1, 1, 2\}$	$\{1, 1, 0\}$	$\{1, 0, 0\}$
$\{1, 1, 1\}$	$\{1, 1, 0\}$	$\{1, 0, 0\}$
$\{1, 1, 0\}$	$\{1, 1, 0\}$	$\{1, 0, 0\}$
$\{1, 0, 2\}$	$\{1, 1, 0\}$	$\{1, 0, 0\}$
$\{1, 0, 1\}$	$\{1, 1, 0\}$	$\{1, 0, 0\}$
$\{1, 0, 0\}$	$\{1, 1, 0\}$	$\{1, 0, 0\}$
$\{0, 2, 2\}$	$\{0, 1, 1\}$	$\{0, 1, 0\}$
$\{0, 2, 1\}$	$\{0, 1, 0\}$	$\{0, 1, 0\}$
$\{0, 2, 0\}$	$\{0, 1, 0\}$	$\{0, 1, 0\}$
$\{0, 1, 2\}$	$\{0, 1, 0\}$	$\{0, 1, 0\}$
$\{0, 1, 1\}$	$\{0, 1, 0\}$	$\{0, 1, 0\}$
$\{0, 1, 0\}$	$\{0, 1, 0\}$	$\{0, 1, 0\}$
$\{0, 0, 2\}$	$\{0, 1, 0\}$	$\{0, 1, 0\}$
$\{0, 0, 1\}$	$\{0, 1, 0\}$	$\{0, 1, 0\}$
$\{0, 0, 0\}$	$\{0, 1, 0\}$	$\{0, 1, 0\}$

3(4)15/2	5(4)10:11/2	C	-46/211
	5(4)10:9/2	-5(4)12/2/1	-34/107/2/1
	5(4)10:7/2	15(4)3:12/1	-2(4)5/2/1
	5(4)10:5/2	-6(4)12/2/1/1	-11/15/2/1/1
3(4)13/2	5(4)10:12/2	C	2/411
	5(4)10:5/2	C	-1/211
	5(4)10:1/2	-18(4)2/2/1/1	-33(4)2/2/1/1
	5(4)10:1/2	5(4)10/2/1/1	11/10/2/1/1

$3(2)1P1/2$	$1(2)10S1/2$	$2\sqrt{1/5}$	0
$3(2)1D3/2$	$2(2)10S1/2$	$-2\sqrt{2/5}$	0
$5(1)1S1/2$	$5(1)1S1/2$	-2	c
$6(2)1D1/2$	$6(2)1D1/2$	$\sqrt{6}$	0
$5(1)2P3/2$	$5(1)2P3/2$	a	$-\sqrt{5/7}$
$5(1)2P5/2$	$5(1)2P5/2$	$-1/\sqrt{5}$	c
$5(2)10P1/2$	$5(2)10P1/2$	0	$\sqrt{1187/5}$
$5(1)3D7/2$	$5(1)3D7/2$	0	$-\sqrt{1178/5}$

5(2)25/2	5(2)25/2	$8\sqrt{2}/35$	$20\sqrt{2}/71$
5(2)20/2	5(2)20/2	$2\sqrt{5}/35$	$10\sqrt{5}/73$
5(2)17/2	5(2)17/2	$-11\sqrt{5}/7$	$-11\sqrt{5}/73$
5(2)15/2	5(2)15/2	$-8\sqrt{5}/7$	$22\sqrt{5}/21$
5(2)10/2	5(2)10/2	$4\sqrt{55}/7$	$-12\sqrt{55}/17$
5(2)10/2	5(2)10/2	$4\sqrt{55}/7$	$-15\sqrt{55}/7$
5(2)113/2	5(2)113/2	c	$10\sqrt{107}/25$
5(2)111/2	5(2)111/2	0	$8\sqrt{71}/5$

$5(2^1 51/2$	$3(2^1 05/2$	$-8\sqrt{5}/5$	c
$3(2^1 03/2$	$5(2^1 03/2$	$-8\sqrt{5}/5$	d
$1(2^1 09/2$	0	0	$20/(3\sqrt{5})$
$3(2^1 07/2$	0	0	$8\sqrt{5}/3$

3(2)23/2	3(6)77/5	-10(2)22
3(2)17/2	-4(6)77/5	-10(2)77
3(2)25/2	8(1)57/7	20(1)77
3(2)29/2	20(1)37/7	-8(7)77
3(2)107/2	4(1)37/5	-2(5)77
3(2)181/2	n	-4(5)77/7,3
3(2)189/2	o	4(5)77/3

5(2)01/2	2/5	0
5(2)07/2	-6/27/1	11/27/1
5(2)09/2	8/27/1	-11/27/1
5(2)09/2	0	-10/11
5(2)07/2	14/27/15	-5/27/1
5(2)11/2	0	2/27/11

$\langle \sigma_1(2) \sigma_2(2) \int_0^{1/2} u^2(5^+ 1L_2^+ 2^+ 1/2) \rangle$	G_2	G_4
$5(2) D5/2$	$3(2) P7/2$	0
$3(2) P5/2$	$3(2) P5/2$	0
$3(2) D3/2$	$-4(2) F7/2$	0
$3(2) D1/2$	$-8(2) F5/2$	0
$3(2) 1h11/2$	n	n
$3(2) 1h5/2$	0	0

$ \alpha \beta \frac{1}{2} \frac{1}{2} \frac{1}{2} \frac{1}{2} \rangle \langle \mathcal{O}_{\beta \frac{1}{2} \frac{1}{2}} \alpha' \frac{1}{2} \frac{1}{2} \frac{1}{2} \frac{1}{2} \rangle$	\mathcal{E}_α	\mathcal{O}_1
$\langle 2 \frac{1}{2} \frac{1}{2} \frac{1}{2} \frac{1}{2} $	$\frac{1}{2} (1 + 3\sqrt{2})$	$\frac{1}{2} \sqrt{\frac{2}{5}}$
$ \frac{3}{2} \frac{1}{2} \frac{1}{2} \frac{1}{2} \rangle$	$-\frac{1}{2} (1 + \sqrt{2})$	$-\frac{1}{2} \sqrt{\frac{2}{5}}$
$\frac{1}{2} (1 + \frac{1}{2} \sqrt{2})$	$-\frac{1}{2} \sqrt{\frac{2}{5}}$	$\frac{1}{2} \sqrt{\frac{2}{5}}$

$\alpha(3) \cup 1/2 (\sum_{j=1}^n \alpha_j(3) \cup 1/2)$	α	β
$5(2)111/2$	$5(2)111/2$	$6(2)111/1$
$5(2)111/2$	$5(2)111/2$	$7(1)111/3$
$5(2)111/2$	$5(2)111/2$	$8(1)111/3$
$5(2)111/2$	$5(2)111/2$	$6(2)785/1$
$5(2)111/2$	$5(2)111/2$	$7(1)785/1$
$5(2)111/2$	$5(2)111/2$	$8(1)785/1$

$5(2)03/2$	$3(2)07/2$	0	$5/2$
	$3(2)05/2$	0	$-5/2$
	$3(2)09/2$	0	$1/2(1/3)$
	$3(2)07/2$	$-14\sqrt{3}/9$	$14\sqrt{3}/9$
	$3(2)11/2$	0	$1/5\sqrt{3}$
	$3(2)09/2$	0	$-1/5\sqrt{3}$

$3(2)09/2$	$4\sqrt{2}/5\sqrt{7}$	$9\sqrt{5}/22\sqrt{7}$
$3(2)09/2$	$-3\sqrt{11}/2\sqrt{5}$	$-6\sqrt{5}/7$
$3(2)07/2$	$8/21$	$15/7$
$3(2)011/2$	0	$4/11\sqrt{11}$
$3(2)05/2$	$0\sqrt{6}/5\sqrt{7}$	$16\sqrt{6}/55\sqrt{7}$

	Os	De
$5(2;11;1/2) \cup_{23h} (2^2; 8^2; 1) L^{(1)}(11; 2^2)$		
$5(2;11;1/2)$	$2\sqrt{13}$	$2\sqrt{13}$
$5(2;11;1/2)$	$1/\sqrt{13}$	$10/\sqrt{13}$

312177/2	5(2)67/2	-5/5/1	-5/5/14
	5(1)65/2	-2/5/5/1	-5/5/5/1
	5(2)109/2	0	3/5/7/7
	5(2)07/2	0	-15/1/2/5/7
	5(2)113/2	0	5/5/5/2/6/6

5(2109)/2	8/5/75	-1/5/75
5(2113)/2	2/5/75/7	+15/3/75/7
5(2115)/2	-12/1/75/15	8/7/75/15/2
5(2117)/2	-8/1/75/15	5/5/75
5(2109)/2	2/5/75/7	-15/3/75/7

acids $\{_3\{2\}$; $M = 3/2$

$3(2; 15)/2$	$5(218)/2$	$-2\sqrt{35}/7$	$-5\sqrt{33}/7$
$5(2185)/2$	$5(2185)/2$	$-2\sqrt{17}/5$	$-11\sqrt{5}/11$
$5(2169)/2$	$5(2169)/2$	ϵ	$-2\sqrt{15}/11$
$5(2169)/2$	$5(2169)/2$	ϵ	$5\sqrt{3}/11$
$5(2113)/2$	$5(2113)/2$	ϵ	$-5\sqrt{10}/22$

[illegible]

$\alpha(2) \omega(2) \downarrow \uparrow_{C_2}$	$\alpha(2) \omega(2) \downarrow \uparrow_{C_2}$	D ₂	D ₁
$\omega(1) \omega(2)$	$5/4 \times 3/2$	$2/3 \times 5$	C
$\omega(1) \omega(2)$	$5/4 \times 3/2$	$3/2 \times 5$	C
$\omega(1) \omega(2)$	$5/4 \times 3/2$	D	$-2/3 \times 5$
$\omega(1) \omega(2)$	$5/4 \times 3/2$	C	$-2/3 \times 5$

$\langle \sigma \hat{S}_1 \sigma \rangle$	$\langle \hat{S}_1 \rangle$	$\langle \hat{S}_2 \rangle$	$\langle \hat{S}_3 \rangle$
$5/4 + 10/7\sqrt{2}$	$3/4 + 5\sqrt{2}/2$	$20\sqrt{2}/3\sqrt{7}$	$-3(5\sqrt{2}/7)$
	$3/4 + 5\sqrt{2}/2$	$8\sqrt{2}/23\sqrt{3}$	$-110/17\sqrt{2}$
	$3/4 + 5\sqrt{2}/2$	$-12\sqrt{2}/35\sqrt{7}$	$-10\sqrt{2}/7\sqrt{7}$
$5/4 + 10/7\sqrt{2}$	$3/4 + 5\sqrt{2}/2$	$5\sqrt{2}/3$	$-15/17\sqrt{2}$

$\alpha(3)LF5/2(\bigcup_{D_H} \alpha'(3)LF5/2)$	De	De
$1(2)05/2$	$3(2)01/2$	$2(\sqrt{10}/3)$
	$3(2)11/2$	0
	$3(2)09/2$	$-2(\sqrt{5}/11)$

$\langle \sigma(\mathbf{r}) \omega S(2) \hat{T}_{\mathbf{r}} \sigma(\mathbf{r}) \omega S(2) \rangle$	$\Delta \sigma$	$\Delta \pi$
$1(1: 15/2)$	$5(1: 17/2)$	$5(1: 17/2)$
$5(1: 15/2)$	$6(1: 17)$	$1(1: 17/2)$
$5(1: 104/2)$	π	$5(1: 17/2)$
$1(1: 16/2)$	π	$5(1: 17/2)$

$3(4:17)/2$	$32/2(17)/1$	$-36/2(17)/1$
$3(4:19)/2$	$32/2(19)/1$	$-5/5(19)/1$
$3(4:19)/2$	$5(4:21)/2$	$4/5(21)/2$
$5(4:29)/2$	$-7/3(29)/2$	$85/1(6/33)$
$5(4:31)/2$	$-5/5(31)/2$	$-120/10(31)/21$

3(2)05/2	5(2)05/2	-2(2)1/1	10(2)1/1
	9(2)11/2	2(5)3/1	11(10)7/1
	5(2)15/2	2(5)1/1	11(5)1/1
	5(2)09/2	2(11)2/1	15(13)1/1
	5(2)10/2	2(22)1/1	15(22)1/1
	5(2)113/2	3	1(15)1/1

	$5(2;111)/2$	a	$-2\sqrt{15}/3$
	$5(2;121)/2$	c	$35\sqrt{3}/72$
$5(2;1^3)/2$	$3(2;105)/2$	$6\sqrt{21}$	$5\sqrt{21}$
	$3(2;107)/2$	$4/3\sqrt{3}$	$65/14\sqrt{7}$
	$1(2;111)/2$	$6\sqrt{21}/5$	$-5\sqrt{16}$

20180122	51410122	-477355	2435735
	51410973	3537355	103573173
	51410773	637357	113573121
	51410542	-75413731	50377317
20180512	514102242	0	407373

$5(2)113/2$	C	$8/35/34/3$
$5(2)105/2$	C	$4/\sqrt{3}$
$3(2)115/2$	C	$5/13\sqrt{2}$
$3(2)109/2$	$-4\sqrt{6}/7/1$	$-15/14$
$3(2)103/2$	$-6\sqrt{6}/7$	$-\sqrt{6}/7$
$3(2)101/2$		$-\sqrt{6}/7/1$

5(2)P5/2	3(2)109/2	-8/(15) ²	15/(2) ²
	1(2)16/2	20/5 ²	-15/2 ²
	1(2)11/2	2	5/35 ² /3
	3(2)149/2	2/5579/5	-65/105
3(2)109/2	5(2)109/2	2/575	12/575/2

	$5(2)09/2$	$-55/577/2$	$13/577/2$
	$5(4)01/2$	$95/(1/48)$	$2/67/1$
	$5(1)05/2$	$15/1577/30$	$-11/1577/10$
$3(2)05/2$	$3(2)05/2$	$-6/7$	$+5/(3/7)$
	$3(2)P7/2$	$-2/77$	$10/377$
	$3(2)03/2$	$-2/7$	$10/(3/7)$

3(2)109/2	ϵ	$-2\sqrt{5/33}$
3(2)107/2	5(2)109/2	ϵ
5(2)105/2	5(2)107/2	$-1/2\sqrt{5/1}$
5(2)103/2	ϵ	$5\sqrt{5/17}$
5(2)101/2	ϵ	$65/6\sqrt{5/11}$
5(2)111/2	0	$5\sqrt{5/133}$
5(2)109/2	0	$-10\sqrt{5/11}$

	$\xi(2)07/2$	$\sqrt{10777}$	$-5\sqrt{10777}/1$
	$\xi(2)11/2$	$-144/(5\sqrt{1331})$	$-14/(1/\sqrt{1331})$
	$\xi(2)17/2$	$-16/(1/\sqrt{1331})$	$5\sqrt{1331}$
$1(2)07/2$	$\xi(2)08/2$	$\sqrt{10777}$	$-5\sqrt{10777}/1$
	$\xi(2)07/2$	$-\sqrt{1331}/1$	$169\sqrt{5773}/14$
	$\xi(2)12/2$	0	$5\sqrt{1331}/2$

$$\langle n(S)1L2J/2 | \hat{U}_{2,3n} | n'(S')1L'2J'/2 \rangle$$

	D ₀	D ₁
5(2)105/2	3(2)101/2	16/575/11
	3(2)105/2	-2/575/11
5(2)107/2	3(2)101/2	-4/575/11
	3(2)105/2	0/575/11
5(2)109/2	3(2)101/2	30/111/55
	3(2)105/2	-12/111/55
5(2)111/2	3(2)101/2	-12/575/11
	3(2)105/2	14/575/11

$$\langle n(S)1L2J/2 | \hat{U}_{2,3n} | n'(S')1L'2J'/2 \rangle$$

	D ₀	D ₁
5(4)107/2	3(4)103/2	8/575/11
	3(4)107/2	8/575/11
5(4)109/2	3(4)103/2	14/575/11
	3(4)107/2	0/575/11
5(4)111/2	3(4)103/2	14/575/11
	3(4)107/2	0/575/11

$$\langle n(S)1L2J/2 | \hat{U}_{2,3n} | n'(S')1L'2J'/2 \rangle$$

	D ₀	D ₁
5(4)107/2	3(4)103/2	8/575/11
	3(4)107/2	8/575/11
5(4)109/2	3(4)103/2	14/575/11
	3(4)107/2	0/575/11
5(4)111/2	3(4)103/2	14/575/11
	3(4)107/2	0/575/11

$$\langle n(S)1L2J/2 | \hat{U}_{2,3n} | n'(S')1L'2J'/2 \rangle$$

	D ₀	D ₁
5(2)105/2	3(2)101/2	16/575/11
	3(2)105/2	-2/575/11
5(2)107/2	3(2)101/2	-4/575/11
	3(2)105/2	0/575/11
5(2)109/2	3(2)101/2	30/111/55
	3(2)105/2	-12/111/55
5(2)111/2	3(2)101/2	-12/575/11
	3(2)105/2	14/575/11

$$\langle n(S)1L2J/2 | \hat{U}_{2,3n} | n'(S')1L'2J'/2 \rangle$$

	D ₀	D ₁
5(2)105/2	3(2)101/2	16/575/11
	3(2)105/2	-2/575/11
5(2)107/2	3(2)101/2	-4/575/11
	3(2)105/2	0/575/11
5(2)109/2	3(2)101/2	30/111/55
	3(2)105/2	-12/111/55
5(2)111/2	3(2)101/2	-12/575/11
	3(2)105/2	14/575/11

$$\langle n(S)1L2J/2 | \hat{U}_{2,3n} | n'(S')1L'2J'/2 \rangle$$

	D ₀	D ₁
5(4)107/2	3(4)103/2	8/575/11
	3(4)107/2	8/575/11
5(4)109/2	3(4)103/2	14/575/11
	3(4)107/2	0/575/11
5(4)111/2	3(4)103/2	14/575/11
	3(4)107/2	0/575/11

$$\langle n(S)1L2J/2 | \hat{U}_{2,3n} | n'(S')1L'2J'/2 \rangle$$

	D ₀	D ₁
5(2)105/2	3(2)101/2	16/575/11
	3(2)105/2	-2/575/11
5(2)107/2	3(2)101/2	-4/575/11
	3(2)105/2	0/575/11
5(2)109/2	3(2)101/2	30/111/55
	3(2)105/2	-12/111/55
5(2)111/2	3(2)101/2	-12/575/11
	3(2)105/2	14/575/11

$$\langle n(S)1L2J/2 | \hat{U}_{2,3n} | n'(S')1L'2J'/2 \rangle$$

	D ₀	D ₁
5(2)105/2	3(2)101/2	16/575/11
	3(2)105/2	-2/575/11
5(2)107/2	3(2)101/2	-4/575/11
	3(2)105/2	0/575/11

$$\langle n(S)1L2J/2 | \hat{U}_{2,3n} | n'(S')1L'2J'/2 \rangle$$

	D ₀	D ₁
5(4)107/2	3(4)103/2	8/575/11
	3(4)107/2	8/575/11
5(4)109/2	3(4)103/2	14/575/11
	3(4)107/2	0/575/11
5(4)111/2	3(4)103/2	14/575/11
	3(4)107/2	0/575/11

$$\langle n(S)1L2J/2 | \hat{U}_{2,3n} | n'(S')1L'2J'/2 \rangle$$

	D ₀	D ₁
5(2)105/2	3(2)101/2	16/575/11
	3(2)105/2	-2/575/11
5(2)107/2	3(2)101/2	-4/575/11
	3(2)105/2	0/575/11
5(2)109/2	3(2)101/2	30/111/55
	3(2)105/2	-12/111/55
5(2)111/2	3(2)101/2	-12/575/11
	3(2)105/2	14/575/11

$$\langle n(S)1L2J/2 | \hat{U}_{2,3n} | n'(S')1L'2J'/2 \rangle$$

	D ₀	D ₁
5(2)105/2	3(2)101/2	16/575/11
	3(2)105/2	-2/575/11
5(2)107/2	3(2)101/2	-4/575/11
	3(2)105/2	0/575/11
5(2)109/2	3(2)101/2	30/111/55
	3(2)105/2	-12/111/55
5(2)111/2	3(2)101/2	-12/575/11
	3(2)105/2	14/575/11

TABLE III: Strong Crystal-Field States in the d^5 Configuration

Configuration	$\langle V_{D_{3h}} \rangle$	Splitting after H_{cr}	Splitting after $H_{cr} + H_{so}$
$(e'')^4(a_1')^1$	$5\epsilon_0 + 6Ds - 10Dt$	${}^2A_1'$	Γ_7
$(e'')^4(e')^1$	$5\epsilon_0 + 2Ds - 15Dt$	${}^2E'$	Γ_8, Γ_9
$(e')^4(a_1'')^1$	$5\epsilon_0 - 6Ds + 10Dt$	${}^2A_1''$	Γ_7
$(e')^4(e'')^1$	$5\epsilon_0 - 7Ds$	${}^2E''$	Γ_7, Γ_9
$(e'')^3(a_1'')^2$	$5\epsilon_0 + 7Ds$	${}^3E''$	Γ_7, Γ_9
$(e'')^3(e')^2$	$5\epsilon_0 - Ds - 10Dt$	${}^4E', {}^2A_1'', {}^2A_2'', {}^3E''$	$5\Gamma_7, 3\Gamma_8, 4\Gamma_9$
$(e'')^3(a_1')^1(e')^1$	$5\epsilon_0 + 3Ds - 5Dt$	${}^4A_1'', {}^4A_2'', {}^4E'', {}^2A_1'', {}^2A_2'', {}^2E''$	$4\Gamma_7, 7\Gamma_8, 5\Gamma_9$
$(e'')^3(a_1'')^2$	$5\epsilon_0 - 2Ds + 15Dt$	${}^3E'$	Γ_8, Γ_9
$(e')^3(e'')^2$	$5\epsilon_0 - 4Ds - 5Dt$	${}^4E', {}^2A_1', {}^2A_2', {}^3E'$	$3\Gamma_7, 5\Gamma_8, 4\Gamma_9$
$(e')^3(a_1')^1(e'')^1$	$5\epsilon_0 - 3Ds + 5Dt$	${}^4A_1'', {}^4A_2'', {}^4E'', {}^2A_1'', {}^2A_2'', {}^2E''$	$4\Gamma_7, 7\Gamma_8, 5\Gamma_9$
$(e'')^2(a_1')^2(e')^1$	$5\epsilon_0 + 4Ds + 5Dt$	${}^4E', {}^2A_1', {}^2A_2', {}^3E'$	$3\Gamma_7, 5\Gamma_8, 4\Gamma_9$
$(e'')^2(a_1'')^1(e')^2$	$5\epsilon_0$	${}^6A_1, {}^2A_1', {}^2A_2', {}^2E', {}^4A_1', {}^3A_2', {}^5E'$	$14\Gamma_7, 10\Gamma_8, 12\Gamma_9$
$(e')^2(a_1')^2(e'')^1$	$5\epsilon_0 + Ds + 10Dt$	${}^4E'', {}^2A_1'', {}^2A_2'', {}^3E''$	$5\Gamma_7, 3\Gamma_8, 4\Gamma_9$

In Table I of CFC-III the eigenfunctions of Hamiltonian (1) are given in a compact form, and if the accidental degeneracy pointed out there is considered, the form of the crystal-field matrix elements will be given by the expression

$$\langle d^5\alpha SLM_L | V_{D_{3h}} | d^5\alpha' S' L' M_L' \rangle = \delta_{M_L M_L'} (-1)^{L-M_L} \times \sum_{k=0,2,4} h_{k0} \begin{pmatrix} L & k & L' \\ -M_L & 0 & M_L' \end{pmatrix} \langle d^5\alpha SL || \hat{C}^{(k)} || d^5\alpha' S' L' \rangle \quad (2)$$

as was proved in CFC-III. In expressions 11–13 of CFC-I the radial components h_{k0} of (2) have been given and in Appendix I of the present paper the reduced matrix elements for the tensor $\hat{C}^{(k)}$ ($k = 0, 2, 4$) are also given. (Available as supplementary material. See paragraph at end of text regarding supplementary material.)

The crystal-field eigenfunctions given in Table I of CFC-III are eigenfunctions of the Hamiltonian (1) then, by adding the free-ion electronic repulsion matrices to those given in (2) a complete representation of the Hamiltonian (1) will be obtained. In Table I complete weak-field matrices so obtained are given as functions of the Racah parameters A, B , and C and the ϵ_0, Ds , and Dt crystal-field parameters. The relation between these crystal-field parameters and the h_{k0} used here is

$$h_{00} = \epsilon_0 \quad h_{20} = 7Ds \quad h_{40} = 21Dt \quad (3)$$

Energy Matrices Calculation at Nonzero Spin-Orbit Coupling

We shall consider in this section the spin-orbit coupling term in the Hamiltonian

$$\mathcal{H} = \mathcal{H}_{cr} + \mathcal{H}_{so} + V_{D_{3h}} \quad (4)$$

obtaining the energy matrices in a weak-field representation as it has already been described in CFC-II.

Owing to the odd number of electrons in the d^5 configuration, only half integral values of J are possible hence it will be necessary to use the double valued representations of both the full rotation and the D_{3h} groups. In Table I of CFC-II the results of the subduction onto the point group D_{3h} of the $D^J R(\alpha, \beta, \gamma)$ representations are given. Eigenfunctions of the Hamiltonian (4) may easily be set up following the method given in CFC-II. It can be proved that the basis of the eigenfunctions of this Hamiltonian and their transformation properties are

$$\begin{aligned} \Gamma_7(a) &\equiv \{ |d^5\alpha SLJ \pm 1/2\rangle \} & \Gamma_7(b) &\equiv \{ |d^5\alpha SLJ \pm 11/2\rangle \} \\ \Gamma_8(a) &\equiv \{ |d^5\alpha SLJ \pm 5/2\rangle \} & \Gamma_8(b) &\equiv \{ |d^5\alpha SLJ \pm 7/2\rangle \} \\ \Gamma_9(a) &\equiv \{ |d^5\alpha SLJ \pm 3/2\rangle \} & \Gamma_9(b) &\equiv \{ |d^5\alpha SLJ \pm 9/2\rangle \} \\ \Gamma_7(c) &\equiv \{ |d^5\alpha SLJ \pm 13/2\rangle \} \end{aligned}$$

By using this set of wavefunctions the Hamiltonian (4) can be reduced to seven blocks of the following dimensions

$$\begin{aligned} |\Gamma_7(a)| &= 37 & |\Gamma_8(a)| &= 26 & |\Gamma_9(a)| &= 33 \\ |\Gamma_7(b)| &= 4 & |\Gamma_8(b)| &= 16 & |\Gamma_9(b)| &= 9 \\ |\Gamma_7(c)| &= 1 \end{aligned} \quad (5)$$

where every block matrix is formed by adding the electronic repulsion and spin-orbit coupling free-ion matrices to the crystal-field one given by the expression

$$\langle d^5\alpha SLJM | V_{D_{3h}} | d^5\alpha' S' L' J' M' \rangle = \delta_{MM'} \delta_{SS'} \times \sum_{k=0,2,4} h_{k0} (-1)^{2J+S+L'+k-M} [(2J+1) \times (2J'+1)]^{1/2} \begin{pmatrix} J & k & J' \\ -M & 0 & M' \end{pmatrix} \begin{Bmatrix} L & J & S \\ J' & L' & k \end{Bmatrix} \times \langle d^5\alpha SL || \hat{C}^{(k)} || d^5\alpha' S' L' \rangle \quad (6)$$

In Table II crystal-field energy matrices (eq 6) are given in the $[d^5\alpha SLJ\Gamma\gamma\alpha]$ representation. Electronic repulsion matrices have been given for the free ion by Racah¹⁵ and are included in the matrices of Table I. Free-ion spin-orbit matrices for this configuration have been given by Mehra.¹⁶ By adding the free ion electronic repulsion and spin-orbit coupling matrices and the crystal-field ones complete crystal-field energy matrices of the Hamiltonian (4) are obtained. In order to complete these energy matrices the constant $5\epsilon_0$, deleted for simplicity from Table II, should be added to the diagonal elements. Obviously, this quantity will cancel for transitions inside the same configuration.

Check of the Energy Matrices

The procedure for checking the crystal-field matrices in both Tables I and II has been described in CFC-III. In order to perform these checks crystal-field energy expressions in a strong-field representation for this d^5 configuration are necessary and are given in Table III. Successive splittings of these crystal-field stages produced first by electronic repulsion and second by spin-orbit coupling are also given there.

All the matrices from Tables I and II were fully checked one against the other and against the strong-field states given in Table III. Moreover, accidental errors in all the matrix elements in both Tables I and II were avoided by generating them from fully checked subroutines.

Acknowledgment. The author is much indebted to Dr. S. L. Altmann, from Oxford University, for his critical reading of this paper.

Supplementary and Miniprint Material Available: Appendix I (reduced matrix elements of tensor C^k , $k = 0$,

2, 4) (2 pages), and full-size photocopies of Tables I and II (27 pages). Ordering information is available on any current masthead page.

References and Notes

- (1) F. Gomez Beltran and F. Palacio, *J. Phys. Chem.*, **80**, 1373 (1976).
- (2) F. Palacio, *J. Phys. Chem.*, preceding paper in this issue.
- (3) F. Palacio, *J. Phys. Chem.*, preceding paper in this issue.
- (4) C. A. L. Becker, D. W. Meek, and T. M. Dunn, *J. Phys. Chem.*, **72**, 3588 (1968).
- (5) C. A. L. Becker, D. W. Meek, and T. M. Dunn, *J. Phys. Chem.*, **74**, 1568 (1970).
- (6) J. A. Varga and C. A. L. Becker, *J. Phys. Chem.*, **76**, 2907 (1972).
- (7) L. Sacconi, M. Ciampolini, and G. P. Speroni, *J. Am. Chem. Soc.*, **87**, 3102 (1965).
- (8) P. L. Orioli, M. DiVaira, and L. Sacconi, *Chem. Commun.*, 103 (1965).
- (9) J. S. Wood and J. Drummond, *Chem. Commun.*, 1373 (1967).
- (10) M. DiVaira and P. L. Orioli, *Acta Crystallogr., Sect. B*, **24**, 1269 (1968).
- (11) N. M. Karayannis, J. V. Minkiewicz, L. L. Pytlewski, and N. M. Labes, *Inorg. Chim. Acta*, **3**, 129 (1969).
- (12) B. Chiswell and K. W. Lee, *Inorg. Chim. Acta*, **6**, 567 (1972).
- (13) B. Gonzalez, J. Kouba, S. Yee, C. A. Reed, J. F. Kirner, and W. R. Scheidt, *J. Am. Chem. Soc.*, **97**, 3247 (1975).
- (14) B. F. Hoskins and F. D. Williams, *Coord. Chem. Rev.*, **9**, 365 (1972-1973).
- (15) G. Racah, *Phys. Rev.*, **62**, 438 (1942).
- (16) A. Mehra, *J. Chem. Phys.*, **53**, 2125 (1970).

COMMUNICATIONS TO THE EDITOR

Modification of Benzophenone Phosphorescence by Molecular Complexation. A Reversible Process

Sir: The ability to modify molecular luminescence by forming EDA complexes is an interesting concept which has both theoretical and applied implications. The excited state properties of EDA complexes have been recently reviewed by Nagakura.¹ Luminescence induced by complexation of nonluminescing molecules could, in principle, assist in locating the energy of a nonemitting state. In an earlier study we showed that the photochemistry of nitrobenzene can be modified by forming an EDA complex with boron trichloride.²

In this report we demonstrate the effect of an electron acceptor such as boron trichloride on the phosphorescence of benzophenone, which together are known to form a stable 1:1 EDA complex at room temperature.³ The formation of the EDA complex between benzophenone as an electron acceptor and aromatic amines as electron donors has been observed at 77 K to exhibit a phosphorescence peak in the vicinity of 500 nm.⁴ In the present study benzophenone, which possesses a nonbonding pair of electrons and whose phosphorescence spectrum is well known, has been used as an electron donor. The UV spectrum of its EDA complex with BCl₃ does not exhibit any distinctly new absorption bands, however, an approximate 2.4-fold enhanced absorption in the 310-380-nm region, relative to that of free benzophenone, suggests that the complex absorbs in this wavelength range, since the ¹n,π* band of benzophenone should move to higher energy upon complexation. This relatively weak interaction is most likely a reflection of the weak donor properties of benzophenone. Irradiation at 77 K of 6.6 × 10⁻³ M benzophenone in methylcyclohexane with 366 nm yields the recorded phosphorescence shown in Figure 1, which decreases in intensity upon the addition of BCl₃. No emission is observed when BCl₃ in methylcyclohexane glass is irradiated, nor are there any low lying states in BCl₃ absorbing at the excitation wavelength. With regard to the specificity of the effect in terms of solvents, the same phosphorescence behavior is observed in cyclohexane and methylcyclohexane. Alcoholic as well as many other solvents had to be excluded from this investigation since they react with BCl₃. The phosphorescence decrease arises from removal of free benzophenone due to complex formation in the ground state, and at sufficiently high concentrations of BCl₃ a new unstructured emission becomes evident with a wavelength maximum appearing at 505 nm, which is readily assignable to the triplet state of

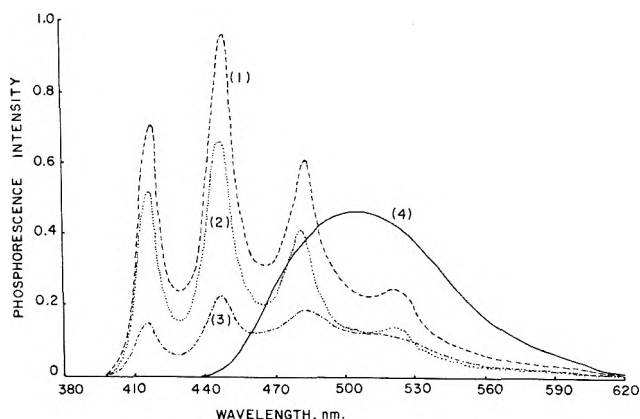


Figure 1. Variation of phosphorescence emission from 6.6×10^{-3} M benzophenone in methylcyclohexane upon addition of BCl₃: (1) no BCl₃, (2) 4.4×10^{-3} M BCl₃, (3) 5.5×10^{-3} M BCl₃, and (4) 6.7×10^{-3} M BCl₃ (366-nm excitation, 77 K).

the charge-transfer complex, (Ph₂CO⁺...⁻BCl₃). No fluorescence was observed from the complex. With the benzophenone concentration constant at 6.6×10^{-3} M, a steep growth of molecular complex phosphorescence occurs when the concentration of BCl₃ exceeds 5.5×10^{-3} M. Continued increase in the concentration of BCl₃ eventually results in precipitation of the complex, which limited the range of concentrations studied. Since the process involves an EDA complex, stable in the ground and excited state, a nonlinear Stern-Volmer plot was observed for the disappearance of benzophenone phosphorescence. In spectrum (3) of Figure 1 it can be seen that most of the benzophenone phosphorescence based on the 413-nm band is gone, and evidence for the EDA complex emission is apparent in the inverted ratio of intensities of the first and third peaks in the phosphorescence spectrum. It should be noted that the weak 413-nm phosphorescence intensity of benzophenone in spectrum (3) reflects a smaller fraction of light absorption relative to spectrum (1), where only benzophenone absorbs. Similarly the small contribution of complex emission in spectrum (3) is due to a smaller fraction of light absorption relative to spectrum (4) where only the molecular complex is absorbing. A small but discernible contribution of benzophenone phosphorescence is still evident at 6.4×10^{-3} M BCl₃.

The phosphorescence maximum of the EDA complex corresponds to an energy of 56.5 kcal/mol, which is clearly lower than the energy of the localized benzophenone triplet, suggesting that it is charge transfer in character.

The phosphorescence quantum yield of the complex was determined to be 0.16 ± 0.02 relative to the value of unity

for benzophenone phosphorescence in EPA and 0.50 in methylcyclohexane. In order to estimate the formation constant of the EDA complex an average half concentration value of $5.5 \pm 1.0 \times 10^{-3}$ M BCl_3 , corresponding to 50% complexation and 50% free BCl_3 was determined by plotting the phosphorescence area of the complex, after graphically subtracting out the benzophenone contribution from the total phosphorescence, as a function of BCl_3 concentration and determining the concentration value of BCl_3 at which the steepest growth in the EDA complex phosphorescence occurs. In a second approach the concentration of BCl_3 at which 50% complexation and 50% free benzophenone occurs was estimated from a plot of the intensity of the 413-nm phosphorescence band of benzophenone, after normalizing the data for the same number of photons absorbed by benzophenone, vs. BCl_3 concentration. The equilibrium constants calculated by the two methods are in satisfactory agreement with each other. From the above half-concentration value the formation constant of the 1:1 complex is $2.6 \pm 1.0 \times 10^2 \text{ M}^{-1}$. This value, which is an apparent equilibrium constant, most likely represents the system at the setting temperature of the glass (-126°C), and is indicative of a relatively weak EDA complex with BCl_3 since benzophenone is an inefficient electron donor.

It is noteworthy that the unstructured phosphorescence of the complex can be converted back to that of benzophenone by simply adding ethyl alcohol, which reacts with boron trichloride to generate a trialkyl borate.³ Neither the BCl_3 nor trialkyl borate contributes to the observed emission. The recovery of benzophenone phosphorescence is quantitative, when correction is made for dilution due to ethyl alcohol addition and the higher phosphorescence yield of free benzophenone in the identical alcohol-methylcyclohexane mixed solvent system. Consequently, the new emission originates from the 1:1 EDA complex, which absorbs at 366 nm, and the addition of BCl_3 simply removes free benzophenone from solution. In general, the system is well behaved with no evidence of side reactions. Additional experiments are in progress to extend these studies to other functional groups, including molecules which do not luminesce.

References and Notes

- (1) S. Nagakura in "Excited States", Vol. 2, E. C. Lim, Ed., Academic Press, New York, N.Y., 1975, p 321.
- (2) W. Trotter and A. C. Testa, *J. Phys. Chem.*, **75**, 2415 (1971).
- (3) (a) W. Gerrard and M. F. Lappert, *Chem. Rev.*, **58**, 1087 (1958); (b) P. N. Gates, E. J. McLaughlan, and E. F. Mooney, *Spectrochim. Acta*, **21**, 1445 (1965).
- (4) S. Arimitsu and H. Tsubomura, *Bull. Chem. Soc. Jpn.*, **45**, 1357 (1972).

Department of Chemistry
St. John's University, New York
Jamaica, New York 11439

R. Snyder
A. C. Testa*

Received July 11, 1977; Revised Manuscript Received December 27, 1977

The Infrared Spectrum of Adsorbed Carbon Monoxide on a Platinum Surface in the Presence of High Pressure Gas-Phase Carbon Monoxide

Sir: The infrared spectrum of adsorbed CO at monolayer and submonolayer concentrations on a low-area platinum surface has previously been reported.^{1,2} In these experiments ultra-high-vacuum techniques were used to clean the surface and CO doping pressures were of the order of

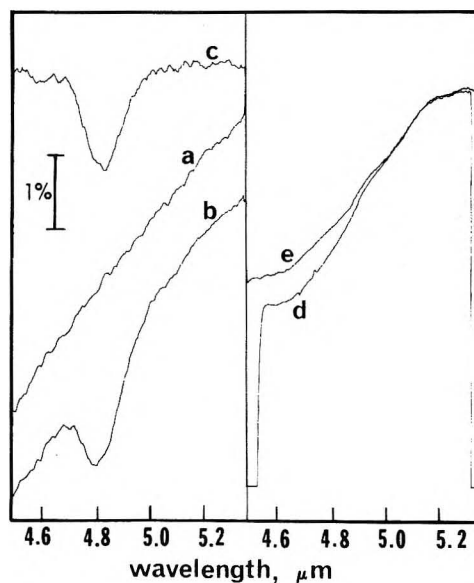


Figure 1. Photograph of the actual spectra of adsorbed CO on a Pt surface. See text for explanation. A transmittance zero is recorded at the beginning and end of curve d.

10^{-6} Torr or lower. Under these conditions the residual gas-phase CO in the vacuum system makes an insignificant contribution to the infrared spectrum.³

In principle one expects to be able to observe the infrared spectrum of an adsorbate layer on a low-area surface in the presence of large quantities of gas-phase adsorbate molecules with a single reflection from the low-area surface. There are, however, practical problems and we believe that this is the first report of such a measurement. In our experience the chief problem has been in the dynamic-range requirement necessary to detect and measure an absorbance of less than 1% due to the adsorbed species against a background signal which changes by factors of 2 or 3 over the spectral range being scanned. This experimental difficulty has been overcome and we have now constructed an instrument which allows us routinely and reproducibly to obtain adsorbate spectra of the quality illustrated in Figure 1 in less than 1 min, even in the presence of gas-phase adsorbate molecules at a pressure of 0.25 atm. The implications are considerable since it is now possible to monitor concentrations of actual surface species in the presence of a gas mixture at pressures of up to 0.25 and therefore we are now in a position to follow surface changes, in both chemical composition and molecular structure, under actual catalytic reaction conditions.

In setting up the particular experiment described in this communication, we deliberately decided not to use clean ultra-high-vacuum techniques but rather to model the relatively dirty conditions under which most real chemical processes occur. The substrate was a piece of polycrystalline Pt foil, about 4 mm \times 15 mm, spot welded to Ni leads so that the strip of foil could be resistively heated. A Pt—Pt—Rh (13% Rh) thermocouple was spot welded to the middle of the foil. The entire assembly was mounted in a glass low-vacuum system (ca. 10^{-5} Torr). The vacuum system was built with greased stopcocks and the infrared windows were sealed on to the sample cell with rubber gaskets. Spectra were recorded with the wedge-filter spectrometer described earlier.⁴ The sample optics were arranged so that radiation from a nichrome wire source was focused on the Pt foil and reflected directly into the spectrometer. The optical aperture at the foil was $f/6$ and the angle of incidence of the axial pencil was about 78° . A double modulation scheme was used to record simul-

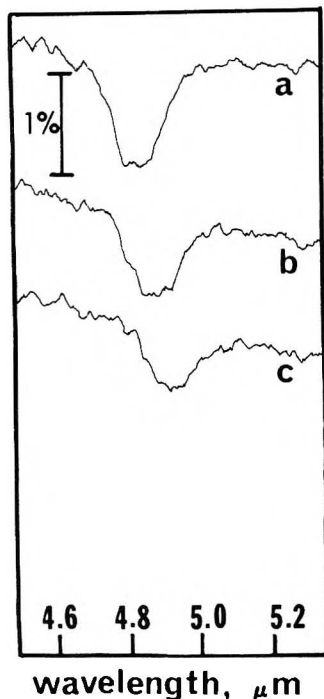


Figure 2. Spectra of adsorbed CO as a function of a pressure of gas-phase CO: (a) $p = 55.0$ Torr; (b) $p = 1.5$ Torr; (c) $p = 5 \times 10^{-3}$ Torr. Note the shift of the absorption maximum.

taneously, and with a single detector, both the total parallel component of radiation transmitted to the spectrometer, I_{\parallel} , and the difference in intensity between the parallel and perpendicular polarized components of the light reflected at the sample surface, $I_{\parallel} - I_{\perp}$. The electronics are arranged to extract two voltages, one proportional to $I_{\parallel} - I_{\perp}$ and the other to I_{\parallel} and the ratio of these voltages is output to the recorder.

The parallel and perpendicular polarized components of the radiation are absorbed to exactly the same extent by the randomly oriented gas-phase molecules but only the parallel component is absorbed by the oriented molecules adsorbed on the metal surface. Thus, in spectral regions in which there is no absorption of radiation by the adsorbate molecules on the surface, the ratio $(I_{\parallel} - I_{\perp})/I_{\parallel}$ is expected to be independent of I_{\parallel} , and hence independent of wavelength. If, however, there is a small absorption, ΔI , of the parallel polarized component by an adsorbate layer, the difference between I_{\parallel} and I_{\perp} is slightly decreased and the output is also decreased by $\Delta I/I_{\parallel}$, i.e., by the fraction of the light absorbed. In practice, it is necessary to ensure that the difference, $I_{\parallel} - I_{\perp}$, is quite small which means that, if the substrate metal is a poor reflector, it is necessary to use some compensating polarizing device to trim the relative intensities of I_{\parallel} and I_{\perp} .

We have used fairly simple techniques to prepare samples; it is apparently quite easy to remove adsorbed CO from the platinum surface by heating to about 450 K in low vacuum or oxygen although this almost certainly leaves the surface contaminated with an oxide layer. Similarly, a CO adsorbate layer may be established by heating the substrate to about 1200 K in an atmosphere of CO. We have found that this technique gives reproducible samples for the spectroscopic experiment, although to date we have not determined the exact surface composition *in situ*.⁵

In Figure 1a we show the spectrum of a surface with no adsorbed CO, in Figure 1b we show the spectrum of the Pt surface with CO adsorbed and with CO at ca. 100 Torr in the cell and in Figure 1c we show the subtraction of 1a

from 1b. Note that the background is not quite flat but is slightly sloping, an artifact which we attribute to residual birefringence in some of the optical components. In Figure 1d we show the curve of the total signal, I_{\parallel} , under the conditions of the experiment with gas-phase CO at a pressure of 100 Torr and in Figure 1e the total signal with the cell evacuated. In Figure 2c we show the spectrum of the adsorbed CO after the CO gas had been pumped out of the cell. Spectrum a in Figure 2 was obtained in exactly the same way as spectrum 1c but it is clear from inspection that there is a wavelength shift of the CO absorption maximum from 4.83 to 4.92 μm (~ 2070 to ~ 2030 cm^{-1}) between spectrum a and spectrum c in Figure 2. This shift is reproducible and we plan to investigate it in more detail. Our present findings are that this pressure shift is not enhanced by increasing the pressure of the gas-phase CO, cf. Figure 2. The spectra shown in Figure 1 are photographed directly from the recorder trace; those shown in Figure 2 have been redrawn but no attempt has been made to smooth out noise. Indeed, all the spectra we show were obtained with a time constant of 0.3 s and it will be easy to improve the signal-to-noise ratio should we so desire.

It is clear to us that the technique we have developed could also be applied to discriminate against absorption by randomly oriented liquid-phase molecules, should one, for example, wish to study a catalytic or electrode surface in a liquid.

Acknowledgment. We are grateful to L. D. Schmidt and C. Marcott for helpful discussions and to B. LaCroix and H. Florell for providing some of the essential components for the experiment. The work was supported by the National Science Foundation through Grant No. CHE 76-7307.

References and Notes

- (1) R. A. Shigeishi and D. A. King, *Surface Sci.*, **58**, 379 (1976).
- (2) F. M. Hoffmann and A. M. Bradshaw, *J. Catal.*, **44**, 328 (1976).
- (3) At a pressure of 10^{-6} Torr, and a typical path length through the gas phase of 30 cm, the gas-phase concentration is $\sim 10^{12}$ molecules/ cm^2 , which is comparable with surface concentration.
- (4) J. F. Blanke, S. E. Vincent, and J. Overend, *Spectrochim. Acta, Part A*, **32**, 163 (1976).
- (5) After the experiment the foil was demounted and AES and XPS spectra were determined. The spectra showed O, S and C peaks (and possibly N) in addition to the main Pt peak; there was no evidence of contamination of the surface by any other metal and the identified contaminants were present to the extent of only a few percent.

Department of Chemistry
University of Minnesota
Minneapolis, Minnesota 55455

William G. Golden
Douglas S. Dunn
John Overend*

Received December 22, 1977

Infrared Spectra and Structure of the Argon-Matrix Isolated HF_2^- Anion

Sir: The hydrogen dihalide anions, HX_2^- , have been the subject of a substantial number of experimental and theoretical investigations, due to interest in their extremely strong hydrogen bonds and accordingly high stability.¹⁻⁶ The major thrust of these studies has been directed at the HF_2^- anion, first from the fact that it is comprised of first row elements which allows accurate theoretical calculations for comparison to experimental results, and secondly from its very high hydrogen-bond strength. Early studies of the HX_2^- species were limited to solid and liquid phase studies, while recent ion cyclotron resonance studies have provided

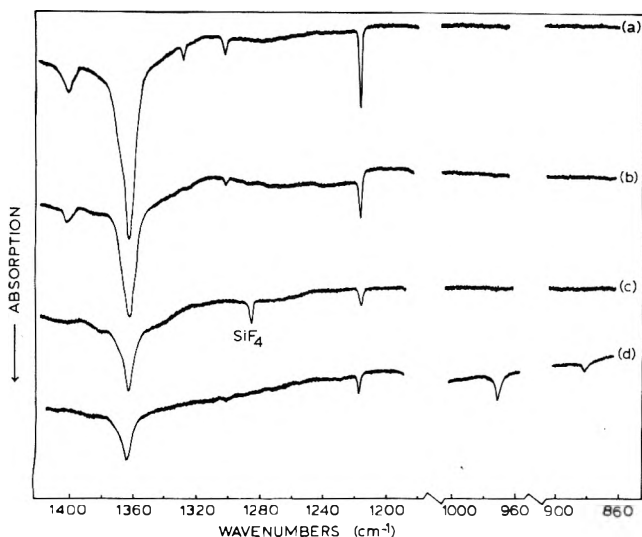


Figure 1. Infrared spectra over the regions 850–900, 950–1000, and 1180–1420 cm^{-1} of the reaction products of CsF with HF and DF in argon matrices. Trace a shows the spectrum of the products of CsF with $\text{Ar}/\text{HF} = 400$, while trace b shows the effect of dilution to $\text{Ar}/\text{HF} = 1000$. Trace c shows an experiment where HF is present only as an impurity (see text), and trace d shows the reaction products of CsF with a mixture of HF and DF in argon, total $\text{M}/\text{R} = 1000$.

gas phase information.⁷ The condensed phase studies have provided infrared spectral data, but under the influence of crystal interactions and possible distortions, while the gas phase studies have only provided thermochemical information. In view of the importance of the first member of this group, HF_2^- , a spectroscopic study in an inert environment appears essential to complete the characterization of the species. The preliminary results of this study are presented here.

The salt/molecule reaction technique has been shown to form ion pairs in argon matrices through the transfer of a halide anion to a Lewis acid, from an alkali halide salt molecule.^{8–10} Several species have been synthesized in this manner, and it is anticipated that the HF_2^- anion can be formed through the reaction of a metal fluoride salt molecule with HF in an argon matrix. The salt molecules are generated through high-temperature evaporation from a stainless steel Knudsen cell, and codeposited with a sample of argon and HF.¹¹

Several experiments were carried out in which CsF was codeposited with a sample of Ar/HF , with M/R ratios between 400 and 1000. A number of bands were observed in the spectrum between 4000 and 200 cm^{-1} which can be assigned to HF and polymeric forms of HF, both in the H–F stretching region, and in the low-frequency deformation region 800–400 cm^{-1} . In addition to these bands, reaction product bands were observed at 1118 (0.08), 1217 (0.13), 1302 (0.03), 1328 (0.02), 1364 (0.46), 1402 (0.05), and 1456 (0.07) cm^{-1} (optical densities given parenthetically). The band at 1364 cm^{-1} was the most intense band, and the broadest band as well, as can be seen in trace a of Figure 1. When a similar experiment was carried out at higher dilution of HF, $\text{M}/\text{R} = 1000$, the same set of product bands was observed with reduced intensity. However, certain bands disappeared at a faster rate than did others. In particular, the bands at 1217 and 1364 cm^{-1} remained relatively intense, with optical densities of 0.07 and 0.26, respectively, while the other five bands were reduced to optical densities of 0.02 or less. Finally, CsF was deposited with a sample of Ar/SiF_4 in one experiment, and this sample subsequently was shown to have a slight HF impurity, on the order of $\text{M}/\text{R} = 2500$. In this same spectral region, only two bands were observed, at 1217 and 1364

cm^{-1} , and the remaining bands were not detected. These results are shown in traces a–c of Figure 1.

The deposition of CsF with a dilute sample of Ar/DF revealed these two bands at 1217 and 1364 cm^{-1} , and also product bands at 970 and 880 cm^{-1} , in about the same intensity ratio, while no intermediate bands were observed in the spectrum between these sets of bands. It should be noted that the parent spectrum of DF showed considerable HF impurity from exchange in the vacuum line and vessel. The spectrum of the experiment is shown in trace d of Figure 1.

The results of these experiments involving CsF and HF in argon can readily be viewed in terms of the formation of the HF_2^- anion in the Cs^+HF_2^- ion pair. Two sets of bands were observed in the various experiments conducted with these reactants. The first set, consisting of the bands at 1217 and 1364 cm^{-1} , maintained a constant intensity ratio of 0.28 throughout all experiments, and persisted even at very high dilution. Consequently, these two bands can be assigned to a 1:1 reaction product. On the other hand, several weaker bands were detected in this same spectral region, but these bands did not show a constant intensity ratio to the 1364- cm^{-1} band. Instead, these bands were more prominent at high reactant levels, and decreased rapidly upon sample dilution. This behavior, coupled with generally low intensity, marks them as due to aggregate species, such as higher H_xF_y^- species, which are known¹ from H_2F_3^- up to H_5F_6^- .

The 1217- and 1364- cm^{-1} bands are attributed to a 1:1 reaction complex, and in view of earlier results using the salt/molecule reaction technique, assignment to the HF_2^- species is reasonable. Both bands show considerable deuterium shift to 970 and 880 cm^{-1} , marking them as hydrogenic vibrations, and both showed no intermediate bands in the deuterium experiment, although D and H were both present, indicating the presence of a single hydrogen atom in the species.

The HF_2^- anion has been studied in solution and in crystals, so that infrared frequencies are available for comparison.¹² ν_3 , the antisymmetric stretching mode and generally the most intense band in hydrogen bonded systems, has been observed from 1450 to 1550 cm^{-1} , depending on the medium and the cation, while the bending mode ν_2 has been observed between 1200 and 1240 cm^{-1} . These numbers are in good agreement with those obtained here, and the assignment of the 1364- cm^{-1} band to ν_3 , and the 1217- cm^{-1} band to ν_2 is straightforward. Several points are worth noting with respect to these assignments. First, the band shapes are much sharper for the respective bands in the argon matrix than in crystals and solution, which might be anticipated for the inert matrix at low temperatures, although ν_3 is slightly broader than ν_2 , as is generally observed for a hydrogen-bonded hydrogen stretching vibration.¹³ Second, the observation of ν_2 of HF_2^- in this study marks the first time that a bending mode of a hydrogen dihalide anion has been observed in an argon matrix through the salt/molecule reaction technique. It has been a question as to whether the presence of the alkali metal counterion in the ion pair might inhibit this mode, but the observation here of the 1217- cm^{-1} band indicates that this is not the case. This is an important step toward obtaining a complete potential function for the HF_2^- anion in inert matrices. Finally, there is no splitting or undue broadening of the 1364- cm^{-1} antisymmetric stretching band, which indicates that the proton is sitting in a broad centrosymmetric single minimum, rather than a symmetric double minimum, in agreement with neutron diffraction and other studies.¹

The sharpness of the ν_3 band in the argon matrix spectrum makes a determination of this type somewhat more substantive than conclusions based on crystalline phase spectra. The hydrogen/deuterium shift ratio for ν_3 of 1.41 is indicative of a nearly harmonic vibration, which also suggests a centrosymmetric potential function. The asymmetric hydrogen bond potential function with cubic anharmonicity generally leads to shifts around 1.35,¹³ while a centrosymmetric potential function contains quartic anharmonicity, and holds this ratio at 1.41 or above.⁹

These results, then, demonstrate that the HF_2^- anion can be synthesized and characterized in a low-temperature argon matrix, free from the perturbations associated with other condensed media. ν_2 and ν_3 were both detected, even at high dilution, and this marks the first time a bending mode has been detected for such an ion pair in an argon matrix. Also these results indicate that the proton feels a single, centrosymmetric minimum in the potential surface, rather than the double minimum postulated for some hydrogen-bonded species. Further studies are in progress to determine the role, if any, of the alkali metal cation; to characterize the higher hydrogen-fluorine anionic species detected here, as they are of considerable interest as well; and to investigate the mixed hydrogen dihalide species FHCl^- under these conditions, where a centrosymmetric potential function is not possible, and a distinct double minimum may be observed. Preliminary studies of this latter species indicate that doubling of levels may

be occurring due to a strongly asymmetric double minimum potential function.¹⁴

Acknowledgment. The author gratefully acknowledges support of this research through Grant No. 8305 from the Research Corporation and the University of Cincinnati Research Council.

References and Notes

- (1) D. G. Tuck, *Prog. Inorg. Chem.*, **9**, 161 (1968).
- (2) D. H. McDaniel and R. E. Valle, *Inorg. Chem.*, **2**, 996 (1963).
- (3) T. C. Waddington, *J. Chem. Soc.*, 1708 (1958).
- (4) J. C. Evans and G. Y.-S. Lo, *J. Phys. Chem.*, **70**, 543 (1966).
- (5) P. A. Kollman and L. C. Allen, *J. Am. Chem. Soc.*, **92**, 6101 (1970).
- (6) H. P. Dixon, H. D. B. Jenkins, and T. C. Waddington, *J. Chem. Phys.*, **57**, 4388 (1972).
- (7) M. S. Foster and J. L. Beauchamp, *Chem. Phys. Lett.*, **31**, 479 (1975).
- (8) B. S. Ault and L. Andrews, *J. Am. Chem. Soc.*, **97**, 3824 (1975).
- (9) B. S. Ault and L. Andrews, *J. Chem. Phys.*, **63**, 2466 (1975).
- (10) B. S. Ault and L. Andrews, *J. Am. Chem. Soc.*, **98**, 1591 (1976).
- (11) For a complete description of the experimental apparatus, see B. S. Ault, *J. Am. Chem. Soc.*, in press.
- (12) K. Nakamoto, "Infrared Spectra of Inorganic and Coordination Compounds", Wiley, New York, N.Y., 1970, p 83.
- (13) G. C. Pimentel and A. L. McClellan, "The Hydrogen Bond", W. H. Freeman, San Francisco, Calif., 1960.
- (14) B. S. Ault, to be published.

Department of Chemistry
University of Cincinnati
Cincinnati, Ohio 45221

Bruce S. Ault

Received August 17, 1977; Revised Manuscript Received
February 23, 1978

PHYSICAL PHENOMENA

spectroscopy,
thermodynamics,
reaction kinetics,
and other areas
of experimental
and theoretical
physical chemistry
are covered
completely in

THE JOURNAL OF PHYSICAL CHEMISTRY

The biweekly JOURNAL OF PHYSICAL CHEMISTRY includes over 25 papers an issue of original research by many of the world's leading physical chemists. Articles, communications, and symposia cover new concepts, techniques, and interpretations. A "must" for those working in the field or interested in it, the JOURNAL OF PHYSICAL CHEMISTRY is essential for keeping current on this fast moving discipline. Complete and mail the coupon now to start your subscription to this important publication.

AVAILABLE IN HARD COPY
OR MICROFICHE.

The Journal of Physical Chemistry American Chemical Society

1978

1155 Sixteenth Street, N.W.
Washington, D.C. 20036

Yes, I would like to receive the JOURNAL OF PHYSICAL CHEMISTRY at the one-year rate checked below:

ACS Member*	<input type="checkbox"/> U.S. \$24.00	<input type="checkbox"/> All Other Countries \$34.00
Nonmember	<input type="checkbox"/> \$96.00	<input type="checkbox"/> \$106.00
Bill me <input type="checkbox"/>	Bill company <input type="checkbox"/>	Payment enclosed <input type="checkbox"/>

Air freight rates available on request.

Name _____

Street _____

Home ☐
Business ☐

City _____

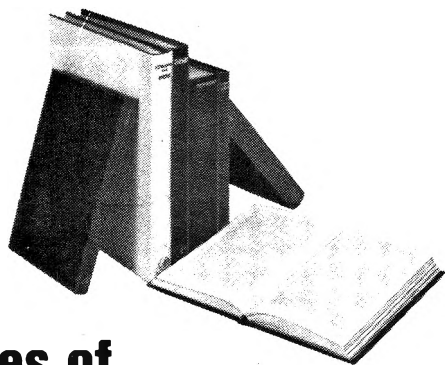
State _____

Zip _____

Journal subscriptions start in January '78.

Allow 60 days for your first copy to be mailed.

*NOTE: Subscriptions at ACS member rates are for personal use only.



Principles of Chemical Kinetics

By GORDON G. HAMMES

Presenting the principles of chemical kinetics together with modern applications, this volume provides the reader with a firm foundation in the basic subject matter as well as exposure to exciting current research.

CONTENTS: Empirical Analysis of Reaction Rates. Theories of Chemical Kinetics. Reactions in the Gas Phase. Unimolecular Decompositions in the Gas Phase. Chemical Reactions in Molecular Beams. Energy Transfer and Energy Partitioning in Chemical Reactions. Kinetics in Liquid Solutions. Fast Reactions in Liquids. Enzyme Kinetics.

1978, 288 pp., \$19.50/£12.65 ISBN: 0-12-321950-7

Theoretical Chemistry VOLUME 3

Advances and Perspectives

Edited by DOUGLAS HENDERSON and HENRY EYRING

CONTENTS: *J. Simons*, Theoretical Studies of Negative Molecular Ions. *F. Weinhold*, Geometrical Aspects of Equilibrium Thermodynamics. *M. S. Jhon and H. Eyring*, A Model of the Liquid State. Three Phase Partition Functions. *R. D. Murphy*, Structure of Fluid ⁴He. *F. H. Stillinger*, Proton Transfer Reactions and Kinetics in Water.

1978, 256 pp., \$25.00/£17.75 ISBN: 0-12-681903-3; also available in Library Edition with Microfiche, \$32.50/£23.05 ISBN: 0-12-681974-2; Microfiche only, \$17.50/£12.40 ISBN: 0-12-681975-0

Advances in Physical Organic Chemistry VOLUME 15

Edited by V. GOLD and D. BETHELL

CONTENTS: *J. Hine*, The Principle of Least Nuclear Motion. *J. M. Thomas et al.*, Topochemical Phenomena in Organic Solid-State Chemistry. *T. E. Hogen-Esch*, Ion-Pairing Effects in Carbanion Reactions. *A. Brändström*, Principles of Phase-transfer Catalysis by Quaternary Ammonium Salts.

1977, 352 pp., \$32.10/£16.40 ISBN: 0-12-033515-8

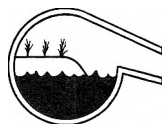
Send payment with order and save postage plus 50¢ handling charge.

Prices are subject to change without notice.

ACADEMIC PRESS, INC.

A Subsidiary of Harcourt Brace Jovanovich, Publishers
111 FIFTH AVENUE, NEW YORK, N.Y. 10003
24-28 OVAL ROAD, LONDON NW1 7DX

Marine Chemistry in the Coastal Environment



Now available—a comprehensive volume containing the most recent advances in this new and increasingly important field.

The collection represents an indispensable source of information for every marine scientist. Emphasis is not merely on describing coastal problems but on showing the potential in applying the tools of modern oceanography and chemistry to solve these problems.

ACS
Symposium
Series No. 18

Thomas M.
Church, *Editor*

A special symposium sponsored by the Middle Atlantic Region of the American Chemical Society.

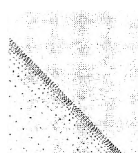
Forty-one chapters cover six major areas:

physical, organic, and tracer marine chemistry; estuarine geochemistry; hydrocarbons and metals in the estuarine environment; ocean disposal forum; applications and resources in marine chemistry; and organic and biological marine chemistry.

710 pages (1975) Clothbound \$35.75
(ISBN 0-8412-0300-8) LC 75-28151

Order from:
Special Issues Sales
American Chemical Society
1155 Sixteenth St., N.W.
Washington, D.C. 20036

Removal of Trace Contaminants from the Air



This important new collection will provide you with critical and in-depth coverage of the latest literature on air pollution characterization and removal.

ACS
Symposium
Series No. 17

Victor R. Deitz,
Editor

A symposium co-sponsored by the Division of Colloid and Surface Chemistry and the Division of Environmental Chemistry of the American Chemical Society.

Order from:
Special Issues Sales
American Chemical Society
1155 Sixteenth St., N.W.
Washington, D.C. 20036

Sixteen chapters focus on several common air pollutants and discuss methods of removing them from different atmospheric situations. The collection stresses the significant interactions among particulates and gas phase contaminants and includes specific information on the following topics:

- precipitation scavenging; persistent pesticides in the atmosphere; hazardous contaminants in the occupational environment
- cigarette smoke filtration; aerosol filtration; sulfur dioxide in stack gases; trace gas adsorption; ozone-hydrogen sulfide reactions
- ambient halocarbons; nitrogen oxides; high ozone concentrations; ozone-olefin reactions; and more

207 pages (September 1975) \$17.25 Cloth-bound (ISBN 0-8412-0298-2) LC# 75-25568